The Role of ARHGAP39 in Cell Migration

INAUGURAL-DISSERTATION

to obtain the academic degree

Doctor rerum naturalium (Dr. rer. nat.)

submitted to

the Department of Biology, Chemistry and Pharmacy

of Freie Universität Berlin

by

CAROLIN BARTH

2018

Carolin Barth
Inaugural-Dissertation
The Role of ARHGAP39 in Cell Migration

Supervision:	Dr. Oliver Rocks
Time period:	June 2011 to September 2018
Institution:	Max-Delbrück-Centrum for Molecular Medicine in the Helmholtz Association, Berlin, Germany

1st Reviewer:	Dr. Oliver Rocks Spatio-temporal Control of Rho GTPase Signaling Max-Delbrück-Centrum for Molecular Medicine Berlin, Deutschland
2nd Reviewer	Prof. Dr. Stephan Sigrist Freie Universität Berlin, Deutschland Department for Biologie Fachbereich Biologie, Chemie, Pharmazie
Date of defense:	22.02.2019

Contents

List of Figures

List of Tables

List of Abbreviations

ARP2/3	Actin-related protein-2/3
Cdc42	cell division cycle 42
cDNA	Complementary DNA
CNKSR2/3	Connector Enhancer of Kinase Suppressor of Ras
CNS	Central nervous system
Comm	Commissureless
DNA	Deoxyribonucleic acid
Dock	Dreadlocks
DOCK	Dedicator of cytokinesis
ECM	Extracellular matrix
EGF	Epidermal grwoth factor
EGFP	Enhanced green fluorescent protein
Ena	Protein enabled
FACS	Fluorescence activated cell sorting
FAK	Focal adhesion kinase
FBP11	formin binding protein 11
FRET	Förster resonance energy transfer
GAP	GTPase activating protein
GEF	Guanine nucleotide exchange factor
GDP	Guanosine diphosphate
GNBP	Small guanine nucleotide binding proteins
GPCR	G protein coupled receptor
GFP	Green fluorescent protein
GST	Gluthathione S Transferase
GTP	Guanosine triphosphate
GTPase	Guanine nucleotide-binding protein
ISV	Intersomitic vessel
LIMK	LIM kinase
mDia	Mammalian diaphanous protein
MENA	Mammalian protein enabled homolog
MLC	Myosin light chain
MLCK	Myosin light chain kinase
MLCP	Myosin light chain phosphatase
MO	Morpholino oligomer

MTOC	Microtubule organizing center
MYO	MYOSIN
NCK	Cytoplasmic protein NCK
Nedd-4	E3 ubiquitin-protein ligase
PAK	p21-activated kinase
PEAK1	Pseudopodium enriched atypical kinase 1
PI3K	Phosphatidylinositol-(4,5)-bisphosphate 3-kinase
$PI(3,4,5)P_3$	Phosphatidylinositol-(3,4,5)-trisphosphate
$PI(4,5)P_2$	Phosphatidylinositol-(4,5)-bisphosphate
PCR	Polymerase chain reaction
PIN1	Peptidyl-prolyl cis-trans isomerase NIMA-interacting 1
Prp40	the Pre-mRNA-processing protein
PTEN	Phosphatase and tensin homolog
PXN	Paxillin
Rac1	ras-related C3 botulinum toxin substrate 1
RhoA	Ras Homology Gene family, Member A
RhoGAP	Rho GTPase activating protein
RhoGDI	Rho guanine nucleotide dissociation inhibitor
RhoGEF	Rho guanine nucleotide exchange factor
ROCK	Rho kinase
RTK	Receptor tyrosine kinase
shRNA	short hairpin RNA
srGAP	Slit-Robo GAP
Sos	Son of sevenless
TANC2	Tetratricopeptide repeat, ankyrin repeat and coiled-coil domain-containing protein 2
TIRF	Total internal reflection fluorescence
VASP	Vasodilator-stimulated phosphoprotein
VEGF	Vascular endothelial growth factor
VEGF-R	Vascular endothelial growth factor receptor
WASP	Wiskott-Aldrich syndrome protein
WAVE	WASP-family verprolin-homologou
YAP65	Yes associated protein, YAP65 homolog YAP1
YFP	Yellow fluorescent protein

1. Abstract

Rho family GTPases are key regulators of cytoskeletal dynamics and control all aspects of cellular morphogenesis, ranging from migration to adhesion. They function as molecular switches that cycle between an inactive GDP-bound state and an active GTP-bound state, in which they can engage with numerous downstream effectors. Rho signalling requires tight spatiotemporal control which is mediated by in total 145 Rho guanine nucleotide exchange factors (RhoGEFs) and Rho GTPase activating proteins (RhoGAPs) in humans. These proteins encode a broad spectrum of targeting and protein interaction domains and thereby contribute specificity to Rho signalling.

During development, wound healing or metastasis, cells must change their positions within organs or the entire body. This is achieved by guided cell migration, where attractive or repulsive signals in the extracellular environment direct cells towards distinct positions. A well-studied class of guidance molecules is the SLIT ligand family that upon binding to their ROBO receptors directs repulsive migration in diverse tissues. The underlying processes are orchestrated by Rho GTPases, however, the downstream RhoGEFs and RhoGAPs that link the receptors to the GTPases are only poorly characterized and also have not been fully identified. Moreover, for the structurally distinct endothelial-specific ROBO4 receptor so far no regulator has been found at all.

In *Drosophila melanogaster* the RhoGAP Vilse/Crossgap, which is the homologue of the novel human RhoGAP ARHGAP39, has been linked to Robo signalling, as its depletion causes misrouting of tracheal ganglionic branches and axons in the central nervous system (CNS). Furthermore in a previous mass spectrometry screen for RhoGEF/GAP interactors (Müller et al., BioRxiv) ROBO4 was identified as binding partner for ARHGAP39. Motivated by the possible interaction of mammalian ARHGAP39 with all human ROBO receptors, I aimed to functionally characterize ARHGAP39 and to investigate its function in guided cell migration.

I could demonstrate that ARHGAP39 is implicated in cell migration by showing that its depletion causes a defect in migratory behavior in a wound healing assay. I provided evidence that the regulator could exert this function by controlling the remodeling of focal adhesion, to which it is recruited by the novel binding partner PEAK1, which itself is a regulator of cell matrix adhesion. Furthermore, ARHGAP39 is also involved in guided cell migration downstream of ROBO1. The regulator directly associates with the receptor and downregulation of

ARHGAP39 increases directed cell migration in a transwell assay in response to SLIT2 stimulation. My data suggests that ROBO1/ARHGAP39 signalling takes place on endocytic vesicles at late time points after receptor engagement. In a third approach, I investigated the role of ARHGAP39 in migration *in vivo* in the zebrafish angiogenesis model system. Morpholino-induced knockdown of *arhgap39* resulted in delayed migration and perturbed development of intersomitic vessels (ISV).

To understand how ARHGAP39 integrates signals from its upstream binding partners I performed structure-function analyses and demonstrated that it binds to all four ROBO receptors. I found that the ARHGAP39/ROBO4 interaction is unique in that it involves additional binding motifs on both proteins. My analysis of the enzymatic properties of ARHGAP39 revealed its substrate specificity for RAC1 and CDC42 and, furthermore, showed that the regulator is subject to auto-inhibition. I found that the N-terminal WW domains of the RhoGAP not only engage in all tested protein interactions but also mediate the backfolding that is responsible for auto-regulation. Also the ARHGAP39 MyTH4 domain, which I could demonstrate to provide structural stability to the protein, can partially release auto-regulation by targeting the protein to the plasma membrane.

Together, my studies yielded insights into the role of ARHGAP39 in cell motility, both in randomly migrating cells and in SLIT2/ROBO-dependent guided migration, and provide the framework for future mechanistic studies.

Zusammenfassung

Rho GTPasen haben eine Schlüsselrolle in der Organisation und dem Umbau des Zytoskeletts und kontrollieren diverse zelluläre Prozesse, von der Zellmigration bis zur Adhäsion. Sie fungieren als molekulare Schalter und wechseln zwischen einem GDP-gebunden inaktiven und einem GTP-gebunden aktiven Zustand, in welchem sie mit einer Vielzahl an Bindepartnern interagieren. Rho GTPasen regulieren komplexe und weitreichende intrazellulare Signalwege. Ihre Aktivität muss daher räumlich und zeitlich beschränkt werden. Dies geschieht durch die insgesamt 145 im menschlichen Genom codierten Rho GTP-Austauschfaktoren (RhoGEFs) und Rho GTPase-aktivierenden Proteine (RhoGAPs). Für diese Proteine ist charakteristisch ein breites Spektrum an Binde- und Protein-Interaktionsdomänen in ihrer Domänenstruktur, wodurch sie die Aktivität der Rho GTPasen lokal und zeitlich regulieren können.

Während der embryonalen Entwicklung, der Wundheilung oder des Krebswachstum bewegen sich Zellen entweder innerhalb eines Organs oder des gesamtem Körpers. Die gerichtete Migration der Zellen wird durch anziehende oder abstossende Signale in ihrer extrazellularen Umgebung erreicht. Gut charakterisierte *Guidance*-Moleküle sind die in verschiedenen Geweben vorkommende SLIT-Liganden, die an ROBO Rezeptoren binden und dadurch die Zellen zur Migration in eine andere Richtung zwingen. Die zugrunde liegenden zellulären Prozesse, die zum Richtungswechsel führen, werden von den Rho-GTPasen kontrolliert, jedoch sind nur wenige RhoGEF und RhoGAP Proteine bekannt und charakterisiert, die Signale von den ROBO Rezeptoren zu den Rho GTPasen weiterleiten. Erstaunlicherweise, konnte bisher kein Rho GTPase regulatorisches Protein identifiziert werden, das an den endothelspezifischen ROBO4 Rezeptor bindet.

Das in *Drosophila melanogaster* endeckte RhoGAP Protein Vilse/Crossgap steht im Zusammenhang mit der Aktivität der ROBO Rezeptoren, da der Verlust von Vilse/Crossgap zur Fehlleitung der Tracheenäste und Axone im Zentralen Nerven System führt. Interessanterweise wurde das humane ARHGAP39, das Homolog zu Vilse/Crossgap, in einem IP-MS Experiment, das der Charakterisierung der Interaktome aller humanen RhoGEF/RhoGAP Proteine diente, als Interaktionspartner von ROBO4 identifiziert . In der Annahme, dass ARHGAP39 mit allen vier humanen ROBO Rezeptoren interagieren könnte, habe ich ARHGAP-39 funktionell charakterisiert und dessen Rolle in der Zellmigration untersucht.

Ich konnte zeigen, dass der Verlust von ARHGAP39 zu einem Defekt in dem Migrationsverhalten der Zellen im Wundheilungs-Experiment führt. Es ist wahrscheinlich, dass das RhoGAP Protein einen Einfluss auf die Zellmigration hat indem es den Auf- und Abbau der Fokalen Adhäsionen kontrolliert, denn es wird durch die Interaktion mit PEAK1, das selbst Fokalen Adhäsionen reguliert, zu diesen Strukturen rekrutiert. Des Weiteren spielt ARHGAP39, in Abhängigkeit von SLIT2-ROBO1 Aktivität, eine Rolle in der gerichteten Zellmigration. Ich konnte beweisen, dass ARHGAP39 an ROBO1 bindet und das die Verringerung der ARHGAP39 Expression die Migration der Zellen unter SLIT2 Stimulation erhöht in Transwell-Migrations Experimenten. Meine Daten suggerieren, dass die ROBO1-ARHGAP39 Signalübertragung mit einer zeitlichen Verzögerung nach der Rezeptorendozytose auf Endosomen stattfindet. Ein weiteres Modelsystem das in dieser Arbeit verwendet wurde, ist die Gefäßbildung während der Angiogenese im Zebrafisch. Der Morpholino-induzierte Knockdown von ARHGAP39 führt zu einer Verlangsamung des Gefäßwachstum und zur fehlerhaften Entwicklung der Gefäße.
Um zu verstehen wie ARHGAP39 Signale von seinen Bindungspartners and die Rho GTPasen weiterleitet, habe ich verschiedene Struktur-Funktions Analysen durchgeführt. Dabei konnte ich zeigen, dass ARHGAP39 an alle vier ROBO Rezeptoren bindet und das die Binding zu ROBO4 mehrere Bindestellen auf beiden Interaktionspartnern benötigt. Die Analyse der enzymatischen Eigenschaften von ARHGAP39 ergab, dass es ein RAC1 und CDC42 spezifisches RhoGAP Protein ist und seine katalytische Aktivität autoinhibiert wird. Ich konnte beweisen, dass die N-terminalen WW Domänen für die Interaktionen zu allen getesteten Bindungspartnern und für das intramolekulare Zurückfalten während der Autoinhibition verantwortlich sind. Des Weiteren kann auch die MyTH4 Domäne, die dem Protein strukturelle Stabilität verleiht, die Autoinhibtion durch die Rekrutierung von ARHGAP39 zur Plasma Membran teilweise aufheben.
Zusammenfassend, geben die Ergebnisse einen Einblick in die Rolle von ARHGAP39 während der Zellmigration, zum Einen ohne Stimulus und zum Anderen in Abhängigkeit von der SLIT2/ROBO1. Für die Zukunft bieten diese Ergebnisse eine Grundlage für fortführende Untersuchungen der Funktion von ARHGAP39 auf der molekularen Ebene während der Migration von Zellen.

2. Introduction

The formation of every multicellular organism, ranging from hundreds of cells in *Cenorhabdytis elegans* to billions of cells in vertebrates, relies on intricate morphogenetic processes that reoccur throughout development. These events involve the proliferation of cells and their differentiation into distinct lineages, their coordinated migration to specific locations and the remodeling of their adhesion to one another to form specific patterns. For each of these processes hundreds of different molecules converge in distinct signalling pathways that have to be precisely orchestrated to ensure the proper cellular response.

A well studied group of signalling molecules central to the control of these morphogenetic processes is the family of small Rho GTPases. They act as molecular switches that can engage numerous downstream effector proteins to diverge incoming signals on many cellular pathways. Rho GTPase activity is modulated by regulatory proteins in a spatiotemporal manner and dependent on the required cellular context. For instance, the migration of commissural neurons or endothelial cells during development depends on similar cellular signalling pathways, including the activity of Rho GTPases, as they are the principle regulators of cell locomotion. At the same time, the strict spatio-temporal control of Rho GTPases activation allows these cells to respond in their very specific signalling context. Thereby enabling commissural neurons to find their track along the midline in the central nervous system and endothelial cells to migrate as a group of connected cells through the tissue to form a vessel sprout.
The importance of Rho GTPases signalling for cell locomotion has become even more evident in studies of the migratory behaviour of cancer cells during tumor growth. The deregulation of Rho GTPase activity leads to constitutively active or inactive downstream signalling and by that tumor growth, aberrant cancer cell migration and invasion during metastasis are facilitated.

2.1. Cell migration

Cell migration is a fundamental process during the development of any organism and also in the adult. During embryonic morphogenesis cells are specified in one location of the organism and then are destined to move over short or long distances to their proper target destination (Aman and Piotrowski, 2010; Kurosaka and Kashina, 2008). In the adult organism guided migration of cells is required for homeostasis, for example during wound repair when fibroblast

and endothelial cells migrate to the damaged areas or the migration of leukocytes to the sites of inflammation. Under pathological conditions, aberrant migration is implicated in diseases such as multiple sclerosis, vascular diseases and chronic inflammation, as well as cancer metastasis when tumor cells migrate in the blood circulatory system and eventually invade into new tissues (Ridley, 2003).

2.1.1. The migration cycle

Cell locomotion is the process of individually migrating cells that first have to polarize and then undergo cycles of membrane extension at the front, adhesion to the substrate, formation of contractile forces and rear retraction (Friedl et al., 2004; Parent and Weiner, 2013).

Cell polarization is the clear distinction between cell front, the leading edge, and the rear of the cell (Lauffenburger and Horwitz, 1996). The cell front is characterized by the formation of active membrane protrusions, which are either lamellipodia or filopodia (Fig. 2.1). Lamellipodia are broad, flat, sheet like structures where actin filaments become cross linked into a "dendritic" network. Filopodia are thin cylindrical structures with actin filaments bundled in a rope like manner (Ridley, 2011). The newly formed protrusions need to be stabilized and to be attached to the substrate at the leading edge.
Central components of focal adhesion structures are integrin proteins that form heterodimeric receptors composed of an α- and a β-chain. Both chains contain a large extracellular region that binds to the ECM and a small cytoplasmic tail, which recruits adaptor proteins to establish the linkage to actin. The interaction with the extracellular matrix (ECM) induces conformational changes in the cytoplasmic domains, which leads to integrin activation and clustering, and thus to the formation of new focal complexes at the leading edge (Ridley, 2003).

The focal complexes mature into larger focal adhesions as the cell migrates over them (Nobes and Hall, 1995; Wehrle-Haller and Imhof, 2003). Over 200 proteins have been identified to be either central part of or associated with focal adhesions allowing this structural organelle to sense and transmit the extracellular stimulus into the cell (Winograd-Katz et al., 2014). Their assembly has been proposed to occur in a sequential manner. First, close to the membrane, proteins that mediate the integrin signalling get recruited, for instance the focal adhesion kinase (FAK) and Paxillin (PXN). Second, an intermediate force transduction layer, containing the cytoskeletal adaptor proteins vinculin and talin, is formed. And lastly, actin regulatory proteins are recruited that establish the link to the actin filaments, such as the vasodilator-stimulated phosphoprotein (VASP), α-actinin and zyxin (Miyamoto et al., 1994; Wozniak et al., 2004; Kanchanawong et al., 2010).

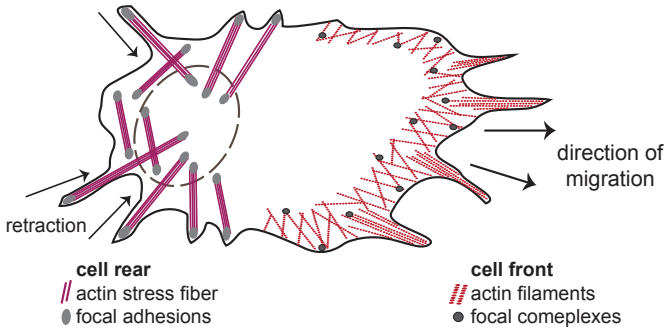

Figure 2.1.: Cytoskeletal alterations during cell migration
During cell migration the cytoskeleton of a cell undergoes drastic changes. Protrusive structures at the leading edge form that are rich in actin filaments, and either form a dendritic network in lamellipodia or align in parallel bundles in filopodia. Moreover, focal complexes are formed to stabilize the extending membrane at the substratum. Simultaneously, at the back the cell retracts its extensions towards its cell body, which is achieved by contractile forces of the actin-myosin filaments. The stress fibers are linked to the extracellular matrix via focal adhesions that are rich in integrins. This way mechanical tension is generated that allow translocation of the cell in the direction of the leading edge. Figure adapted from (Wehrle-Haller and Imhof, 2003).

While the cell extends its membrane protrusions at the front and moves with it cell body forward, it simultaneously retracts at the rear (Fig. 2.1). The forces are generated by the interaction of Myosin II with the actin filaments, which is able to pull two actin filaments past one another (Lauffenburger and Horwitz, 1996). Thus, the contraction of the actomyosin bundles enable the cell to move its cell body forward (Friedl et al., 2004) and applies tension on the adhesive sites, which helps to breakdown the interaction between the integrins and the ECM (Jay et al., 1995). These forces are strongest at the leading edge and the rear of the cell (Beningo et al., 2001).

2.2. The small Rho GTPases

2.2.1. Small guanine nucleotide binding proteins

The small guanine nucleotide binding proteins (GNBPs) present a class of proteins that use the hydrolysis of GTP to regulate their activity status (Sprang, 1997; Nyborg and Clark, 1996). GNBPs regulate processes ranging from cell growth, cell differentiation and migration to vesicular and nuclear transport and are also involved in sensual perception and protein synthesis (Vetter and Wittinghofer, 2001). To the GNBP family belongs, among other protein families, the Ras superfamily with its five subfamilies: Ras, Rho, Rab, Ran and Arf (Wennerberg et al., 2005).

The rat sarcoma (Ras) oncoproteins are the founding members of this family and regulate a variety of signalling pathways, resulting in gene expression, regulation of cell proliferation

and differentiation (Wennerberg et al., 2005). The Ras-like proteins in brain (Rab) GTPases and the ADP-ribosylation factor (Arf) GTPases play an important role in intracellular vesicle transport and the trafficking of proteins (Zerial and Mcbride, 2001; Memon, 2004). The Ras-like nuclear (Ran) protein are responsible for the transport of both proteins and RNA from nucleus to cytoplasm and vice versa (Weis, 2003). The last subfamily are the Ras homologous (Rho) GTPases, which are the central regulators of the actin cytoskeleton and cell shape dynamics (Ridley, 2001).

2.2.2. The small Rho GTPases

The human genome encodes 20 members of the Rho GTPase family, which are subdivided into eight subgroups (Hodge and Ridley, 2016). All Rho GTPase share a Rho insert domain, which forms an additional α-helix in the core G-domain and therefore distinguishes the Rho proteins from the other small GTPases (Valencia et al., 1991). The Rho GTPases RhoA (Ras Homology Gene family, Member A), Rac1 (ras-related C3 botulinum toxin substrate 1) and Cdc42 (cell division cycle 42) are the best characterised members of this family. The first insights into their cellular functions date back to the early 1990s after the discovery of constitutively active (GTPase deficient) mutants of these GTPases. Ridley and Hall could show that a constitutively active RhoA induced the formation of stress fibers and focal adhesions upon growth factor stimulation (Ridley and Hall, 1992), whereas the Rac1 mutant induced the formation of lamellipodia and small focal complexes in fibroblasts (Ridley et al., 1992). A few years later Cdc42 was characterised to induce the formation of filopodia and to contribute to Rac1 activation (Nobes and Hall, 1995).
Since then it has been demonstrated that RhoA, Rac1 and Cdc42 control separate pathways that link transmembrane receptors signalling to the formation of actin-rich structures. The role of Rho GTPases has been further extended to other signal transduction pathways linked to the actin cytoskeleton, for example the regulation of microtubule dynamics and vesicular trafficking or in gene expression and the regulation of enzymatic activities (reviewed in (Jaffe and Hall, 2005; Etienne-Manneville and Hall, 2002)).

2.2.3. Post-translational modifications of Rho GTPases

Most Rho GTPases are prenylated at the cysteine (Cys) residue present in the CAAX tetrapeptide at the C-terminal end of the protein. The CAAX motif is the recognition sequence for the farnesyl- or geranylgeranyltransferases, which attach a farnesyl or a geranylgeranyl moiety, respectively (Cox and Der, 2002). After prenylation the last three amino acids are cleaved and the Cys residue is carboxymethylated (Michaelson et al., 2001). These lipid moieties target the Rho GTPases to distinct membrane compartments within the cell (Katayama et al., 1991; Seabra, 1998).

Other known posttranslational modifications of Rho GTPases are phosphorylation and ubiquitinylation. Phosphorylation has been described to occur either close to the lipid modifications and thereby changing the localisation of the Rho GTPase or at residues of the G-domain, which might affect its GTP/GDP cycling activity or the interaction with effector proteins (Hodge and Ridley, 2016). Ubiquitylation has been proposed to regulate Rho GTPase turnover and activity. However, only the ubiquitylation of RhoA and Rac1 has yet been described in detail (reviewed in (Hodge and Ridley, 2016)).

2.2.4. The Rho GTPase activation cycle

Rho GTPases function as molecular switches. They cycle between an active, GTP-bound conformation and an inactive, GDP-bound conformation (Fig. 2.2). In the active conformation they are able to interact with downstream effector targets to initiate different cellular signal transduction pathways (Schmitz et al., 2000). Both reactions, the exchange of GDP to GTP and the following GTP hydrolysis, are intrinsically slow processes. Therefore, these reactions require guanine nucleotide exchange factors (GEF) and GTPase activating proteins (GAPs), respectively, to be accelerated by several orders of magnitude (Vetter and Wittinghofer, 2001).

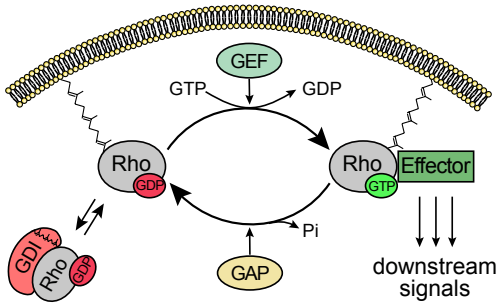

Figure 2.2.: The Rho GTPase activation cycle
Rho GTPases are bimolecular switches that cycle between an active GTP bound and an inactive GDP bound confirmation in the cytoplasm. The Rho GTPase cycle is positively regulated by guanine exchange factors (GEFs) and negatively regulated by GTPase activating proteins (GAPs). In the active confirmation they can bind multiple downstream effector proteins to promote different signalling pathways. RhoGDIs sequester the GDP-bound Rho GTPases from the membrane and keep them inactive in the cytosol. Figure kindly provided by O. Rocks.

GEF proteins bind to the GDP-bound GTPase and deform the nucleotide binding site. This leads to conformational changes in the switch regions and the P-loop, which perturbs the interaction surface with the nucleotide. For that reason the GDP is released from the binding pocket of the GTPase and a new nucleotide can bind (Vetter and Wittinghofer, 2001). Due to the ten times higher concentration level of GTP over GDP in the cytoplasm, GTP binds to the GTPase and displaces the GEF protein (Bos et al., 2007). For the GTP hydrolysis reaction GAP proteins are required to supply a catalytic residue, the so called "arginine finger", into the

active site of the G-domain of the GTPase (Bos et al., 2007). Thus, the GAP protein accelerates the intrinsic slow hydrolysis activity of the GTPase.

This model of activation and inactivation assisted by GEF and GAP proteins can be observed for the twelve "classic" Rho GTPases. However, it does not apply for the atypical members of this family that are constitutively bound to GTP due to amino acid substitutions. These substitutions either increase the affinity for GTP, for example in RhoU, or diminish the GTPase activity completely, as in RhoH. Those proteins are thought to be instead regulated by protein stability, gene expression and phosphorylation (Aspenström et al., 2007).

An additional layer of Rho GTPase regulation is provided by their interaction with the guanine-nucleotide dissociation inhibitors (GDIs). The GDIs bind to most Rho GTPase by burying the prenyl moiety at the C-terminus inside their hydrophobic pocket (Fig. 2.2) Thereby they prevent the recruitment of the small Rho GTPases to the plasma membrane and thus their activation by GEF proteins (Vetter and Wittinghofer, 2001).

2.2.5. The Rho GTPase regulatory proteins

The 12 classical Rho GTPases in humans are outnumbered by 81 RhoGEF proteins (Rossman et al., 2005; Cook et al., 2016) and 66 RhoGAP proteins (Tcherkezian and Lamarche-vane, 2007) (Fig. 2.3). This indicates that the regulatory GEF and GAP proteins are required to precisely regulate the activity of the GTPases in space and time dependent on the distinct cellular context.

To properly exert their functions, the GEF and GAP proteins themselves are regulated in a highly complex fashion. Most of these proteins have a multi-domain architecture to interact with several other proteins or lipids, suggesting that they target the GTPases to specific locations and/or serve as scaffolds to form local protein complexes. Furthermore, the binding of second messengers and posttranslational modifications, such as phosphorylation, have been observed as well. These regulatory mechanisms can alter the ability of the regulators to form protein complexes, can mediate their translocation to a specific compartment or induce allosteric changes in their catalytic domains to promote or release auto-inhibition (Cherfils and Zeghouf, 2013; Bos et al., 2007).

Auto-regulation is a common mechanism for RhoGEF and RhoGAP proteins to regulate their catalytic activity. It is assumed that the terminal regions of the Rho regulatory proteins fold back to another region of the protein. Thereby, the catalytic domain is sterically blocked or masked that prevents the Rho GTPase from accessing it.

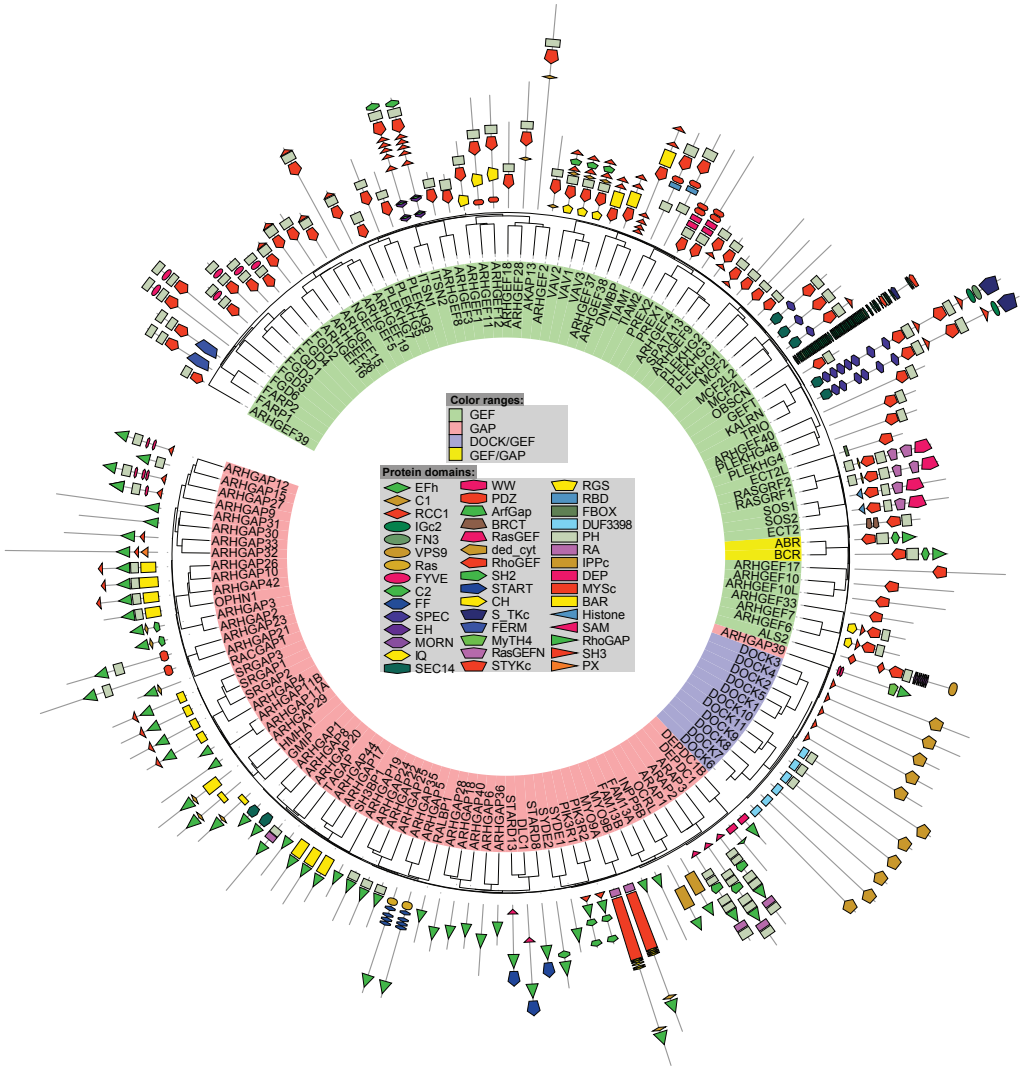

Figure 2.3.: Multi domain architecture of human RhoGAP and RhoGEF proteins
The Rho GTPase activating proteins (GAPs) and guanine exchange factors (GEFs) are multi-domain proteins that serve as scaffolds to target Rho GTPases to specific subcellular targets to link them to diverse signalling pathways. Figure kindly provided by O. Rocks.

Here, I focus on the few known examples of auto-inhibition of RhoGAP proteins. For instance, in RhoGAP proteins of the GRAF family (GTPase regulator associated with Focal adhesion kinase; examples are ARHGAP26, ARHGAP10, ARHGAP42) the N-terminal BAR domain binds to the GAP domain and thereby inhibits its activity (Eberth et al., 2009). In ARHGAP1 two N-terminal peptide sequences bind to the C-terminal GAP domain in a synergistic manner. These intramolecular interactions are prevented by binding of the prenyl-anchor of its substrate Rac1 to the N-terminal peptide seuences. Thus, the self-binding to its GAP domain

is released and ARHGAP1 switches to its open conformation where its catalytic domain binds to the Rac1-GTP (Moskwa et al., 2005). The same regulatory mechanism has been also observed for p190RhoGAP (Molnár et al., 2001). Whereas, a different mechanism applies for the RacGAP β2-Chimerin, which is auto-inhibited by binding of a N-terminal sequence to the diacylglycerol (DAG) binding site in its central C1 domain. Due to the intramolecular folding the GAP domain is sterically blocked. Only the recruitment of β2-Chimerin to membrane bound DAG changes the structural conformation and releases the auto-inhibition (Canagarajah et al., 2004).

2.2.6. Rho GTPases and their effector proteins in cell migration

Cells move through the polarized and dynamic remodelling of the actin cytoskeleton, which includes the formation of membrane protrusions at the front combined with contractile forces in the cell body and the retracting end.

The formation of membrane protrusion requires the assembly of actin filaments. The WASP-family verprolin-homologous protein (WAVE) is a downstream effector of Rac1 and activates the Arp2/3 complex (Miki et al., 2000). Arp2/3 binds to pre-existing actin filaments and induces the formation new daughter filaments that results in a branched actin network at the leading edge (Pollard et al., 2000). Rac1 also activates the p21-activated kinase (PAK) - LIM domain kinase (LIMK) pathway, which results in inhibition of the actin depolymerizing protein cofilin (Stanyon and Bernard, 1999). Filopodia formation depends on active Cdc42 (Nobes and Hall, 1995), which activates the Arp2/3 complex via activation of the Wiskott-Aldrich syndrome protein (WASP) (Fig. 2.4).
The formation of early adhesions in cell migration is associated with Rac1 dependent lamellipodia formation that must be stabilized by attaching them to the extracellular substrate (Nobes and Hall, 1995; Rane et al., 2014). The clustering of integrins on the substratum recruits and stimulates FAK, which phosphorylates Pxn that leads to the recruitment of RAC1 GEFs like β-Pix and DOCK180 (Defilippi et al., 2006) and moreover, the Pxn-β-Pix complex also recruits PAK1 (ten Klooster et al., 2006). All pathways converge on Rac1 activation and promote nascent adhesion assembly in the lamellipodium (Fig. 2.4).

A well known downstream effector protein of RhoA is the Rho kinase (ROCK), which regulates phosphorylation of the myosin light chain (MLC) of Myosin II by inhibiting the myosin light chain phosphatase (MLCP) and activating the myosin light chain kinase (MLCK) (Fig. 1.4). The phosphorylation enhances the assembly of Myosin II with actin filaments (Jaffe and Hall, 2005), and thus increases the contractility of the cell (Etienne-Manneville and Hall, 2002).
Moreover, active RhoA and ROCK contribute to maturation of focal complexes into larger,

more persistent focal adhesions through its ability to activate Myosin II (Ridley and Hall, 1992; Ridley, 2015). RhoA signalling leads to inhibition of cofilin dependent actin depolymerization (Midori Maekawa et al., 1999) and it activates the effector protein diaphanous-related formin-1 (mDia1) that has been shown to stabilize microtubules (Jaffe and Hall, 2005; Watanabe et al., 1999; Ishizaki et al., 2001) and also activates the Arp2/3 complex (Fujiwara et al., 2000) and promotes focal adhesion formation (Watanabe et al., 1999; Palazzo et al., 2001).

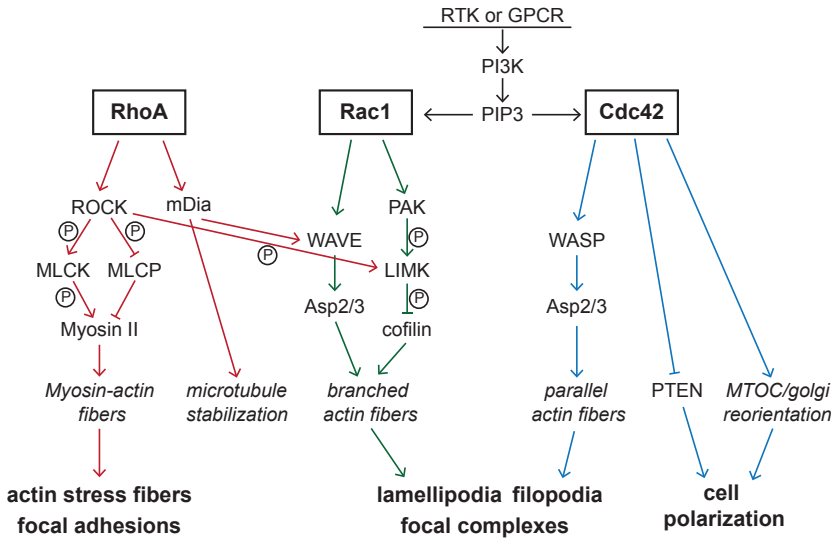

Figure 2.4.: Rho GTPase signalling orchestrates cytoskeletal dynamics during cell migration
Overview of different Rho GTPase dependent signalling pathways at the cell front and back. At the leading edge a phosphatidylinositol 3,4,5-triphosphate gradient (PIP3) is generated by the phosphoinositide 3 kinase (PI3K), that is activated by receptor tyrosine kinases (RTK) or G-protein coupled receptors (GPCR). The PIP3 gradient leads to localized activation of Rac1 and Cdc42 at the cell front. Active Rac1 activates the WAVE/Arp2/3 complex, which results in the formation of a branched actin filament network in lamellipodia. Additionally, Rac1 activates p21 activating kinase (PAK) and LIM domain kinase (LIMK) that inactivate the actin-capping protein cofilin, thus enhancing actin polymerization at the front. GTP-Cdc42 interacts with WASP, which activates the Arp2/3 complex to generate filopodia at the cell front. Cdc42 is also required for cell polarization via re-orientation of the microtubule organizing center (MTOC) between the nucleus and the golgi towards the cell front. Active RhoA is the key regulator of stress fiber formation mainly at the cell back and in the cell periphery via the Rho kinase (ROCK), that leads to phosphorylation of myosin II and thereby increases the formation of actin-myosin fibers. At the same time Rho signalling enhances the formation of focal adhesion sites, thus linking the actin stress fibers to the extracellular substratum. Activation of the formin mDia facilitates actin polymerization and microtubule stabilization. Figure adapted from (Sit and Manser, 2011).

Essential for cells to establish cell polarity is the phosphatidylinositide 3-kinase (PI3K) that produces phosphatidylinositol 3,4,5-triphosphate (PIP3) and phosphatidylinositol 3,4-bisphosphate (PI(3,4)P2), which are enriched at the cell front. It has been shown that PIP3 is required to concentrate active Cdc42 at the cell front, which in turn restricts the regions where protrusions can form by excluding the phosphatase and tensin homolog (PTEN) from the leading edge (Li et al., 2003). Additionally, Rac1 specific GEFs also sense the PI3K products and facilitate

Rac1 activation in the lamellipodium (Welch and Mullins, 2002). Cdc42 is responsible for the re-orientation of microtubule organizing center (MTOC) and the Golgi apparatus in front of the nucleus toward the leading edge (Fig. 1.5) (Etienne-Manneville and Hall, 2002; Rodriguez et al., 2003).

2.2.7. A more complicated model of Rho GTPase activity during cell migration emerges

The simple model of cell migration suggest a conceptual picture of the active Rho GTPases signalling clearly separated within the cell. While Rac1 and Cdc42, at the leading edge, regulate the establishment of lamellipodia and the formation of filopodia, respectively. RhoA mediates cell contractility at the back of the cell (Burridge et al., 2004).

However, a more elaborate model of Rho GTPase signalling during cell migration emerged over the past years. For instance, cells depleted of Rac1 (Wheeler et al., 2006) or Cdc42 (Czuchra et al., 2005) are still able to produce lamellipodia or fiopodia, respectively, and show mild defects in motility. Moreover, RhoA is not only required for cell contractility, but also stabilizes microtubules via activation of mDia at the leading edge. Implying, that RhoA likely performs different functions at the front or back of the cell (Palazzo et al., 2001). Those data contradict the conceptual framework derived from the static model of Rho GTPase signalling.

The use of fluorescence resonance energy transfer (FRET) based biosensors enabled investigators to resolve the spatial and temporal activity patterns of Rho GTPases at the subminutes time scale and micrometer length scale (Pertz, 2010). Two important observations have been made. First, one Rho GTPase can be simultaneously activated at multiple, distinct subcellular locations. It can be assumed that each individual pool of the active Rho GTPase represents a specific interaction with upstream regulators, GEF and GAP proteins, and specific downstream effectors to regulate precise cellular functions required for cell morphogenesis, thereby creating ”spatio-temporal signaling modules” (Pertz, 2010).

Second, overlapping activity zones of multiple Rho GTPases can be found in migrating fibroblasts that require precise crosstalk between Rho GTPases to allow cell migration (Machacek et al., 2009). These activity zones show a characteristic pattern in highly restricted subcellular domains and with precise timing, for instance, the activation of Rho GTPases correlates with protrusion and retraction events during leading edge advancement (Martin et al., 2016).

The future challenge will be to characterize the GEF/GAP proteins that dynamiclly shape the activation patterns of the Rho GTPases in space and time and to decipher the mechanisms of crosstalk between the Rho GTPases that are required to fine tune morphogenetic processes.

2.3. Slit/Robo Signalling and Function

Slit proteins and their corresponding Robo receptors present a well studied guidance system involved in the development of vertebrate and invertebrate organisms. The Slit protein was first discovered as a protein secreted by midline glia cells in *Drosophila melongaster* (Rothberg et al., 1988). Later, in a screen for genes that control midline crossing of commissural axon its receptor Robo was identified (Kidd et al., 1998). Since then, their role in axon guidance has been well characterized. Recently, it has been revealed that Slit/Robo signalling contributes to an increasing number of other developmental processes as well. Numerous studies also indicate an important role of deregulated Slit or Robo expression in tumorgenesis, cancer progression and metastasis.

2.3.1. The family of Slit proteins

Slit proteins are the principal ligands for the Robo receptors (Kidd et al., 1999). Three highly homologues Slit genes can be found in mammals, which are expressed in most organs (Marillat et al., 2002). Slits are large, secreted glycoproteins that contain the following domains: an N-terminal secretion signal peptide, four domains (D1-D4) containing leucine-rich repeats (LRR), several EGF-like sequences, a laminin-G domain and a C- terminal cysteine-rich knot, which is found in several secreted growth factors (Fig. 2.5 A) (Brose et al., 1999). They are proteolytic cleaved by an unknown protease, which is best studied for Slit2. Slit2 is cleaved into a short C-terminal fragment (Slit2-C) of 55-60 kDa and a long N-terminal fragment (Slit2-N) of 140 kDa. For Slit2 full length and Slit2-N their functions as chemorepellant have been shown in *vitro* (Nguyen Ba-Charvet et al., 2001) and in *vivo* (Hu, 1999; Niclou et al., 2000; Wang et al., 1999), however the function of Slit2-C remains unknown.

2.3.2. The family of Robo proteins

In mammals and zebrafish four Robo genes (Robo1/Dutt1, Robo2, Robo3/Rig1, Robo4/Magic Roundabout) are found. They are mainly expressed in the nervous system, whereas Robo4 is specifically restricted to endothelial cells (ECs) (Huminiecki et al., 2002). The Robo receptors belong to the immunoglobulin (Ig) superfamily of cell adhesion molecules (CAMs). Robo1, Robo2 and Robo3 have a highly similar domain architecture containing five immuno-globuline-like C2 motifs (Ig) and three fibronectin type III domains (FN3) in their extracellular region and four conserved cytoplasmic motifs (CC0-CC3) (Dickson and Gilestro, 2006). Robo4 varies in this structure in that it is composed of two Ig motifs and two FN3 domains in its extracellular part. Furthermore, it contains only two of the four conserved cytoplasmic motifs, the CC0 and CC2 motif (Fig. 2.5 B, C). For all Robo receptors the cytoplasmic region is poorly conserved,

except for the four (two in Robo4) conserved linear motifs, thus no regulatory secondary structures have been predicted (Hohenester, 2008).

2.3.3. Slit/Robo binding mechanism

Binding of the Slit proteins to the Robo receptors has been verified for all Robo receptors, except for Robo4, which will be discussed later. It has been demonstrated that the Slit/Robo interaction is evolutionary conserved. For example human SLIT2 binds to cells expressing *Drosophila* Robo or *Drosophila* Slit binds to rat Robo1 or Robo2 (Brose et al., 1999).
There is increasing evidence that heparan sulfate (HS) chains, that consists of repetitive sulfated disaccharide units attached to secreted or membrane-associated core proteins (Heparan Sulfate Proteoglycans, HSPG), are required for the repulsive Slit activity (Fig. 2.5 D) (Ypsilanti et al., 2010). For instance, the removal of HS decreases the affinity of Slit2 for Robo and the enzymatic digestion of HS at the cell surface abolishes Slit/Robo signalling (Hu, 2001; Piper et al., 2013). Moreover, genetic depletion of enzymes required for HS biosynthesis (Lee and Chien, 2004) or of HSPG core proteins (Johnson et al., 2004; Steigemann et al., 2004) prevent Slit/Robo signalling *in vitro*. A model emerged where HS functions as a co-receptor to regulate the distribution of Slit close to Robo and thus the efficiency of Slit binding (Hu, 2001; Johnson et al., 2004), as it was shown that Slit/Robo can form a ternary complex with heparin/HS via the D4 domain of Slit (Fukuhara et al., 2008; Hussain et al., 2006; Seiradake et al., 2009).

As illustrated in Figure 2.5 Robo4 differs in its domain architecture intracellularly as well as extracellularly. Moreover, the conserved amino acids responsible for Slit binding are not present in the Robo4 sequence (Huminiecki et al., 2002). The mechanism of the Slit/Robo4 interaction is still under investigation. On the one hand, there are experimental data showing that Slit2 acts through Robo4. First, in co-immunoprecipitation (Co-IP) experiments the direct binding of Slit2 to Robo4 has been reported (Park et al., 2003). Second, in genetic studies it has been shown that Slit2 acts via Robo4 to mediate its effects on EC motility or vessel growth in mammary glands (Jones et al., 2008; Marlow et al., 2010). Moreover, *in vitro* Slit2/Robo4 signalling has been demonstrated in several ECs migratory assays (Jones et al., 2009a).
On the other hand, many groups failed to replicate these data, for instance using Biocore and surface plasmon resonance (SPR) assays to assess the Slit/Robo4 interaction (Hohenester et al., 2006; Koch et al., 2011; Suchting et al., 2005). It could also not be proved that the extracellular part of Robo4 is able to inhibit the chemotactic effect of Slit2 (Sheldon et al., 2009). To unite the contradicting results it has been proposed that Robo4 requires the binding of a co-receptor to mediate the Slit signal inside the cell. Suggested candidates are syndecans, Robo1 or the Unc5B receptor (Koch et al., 2011; Sheldon et al., 2009).

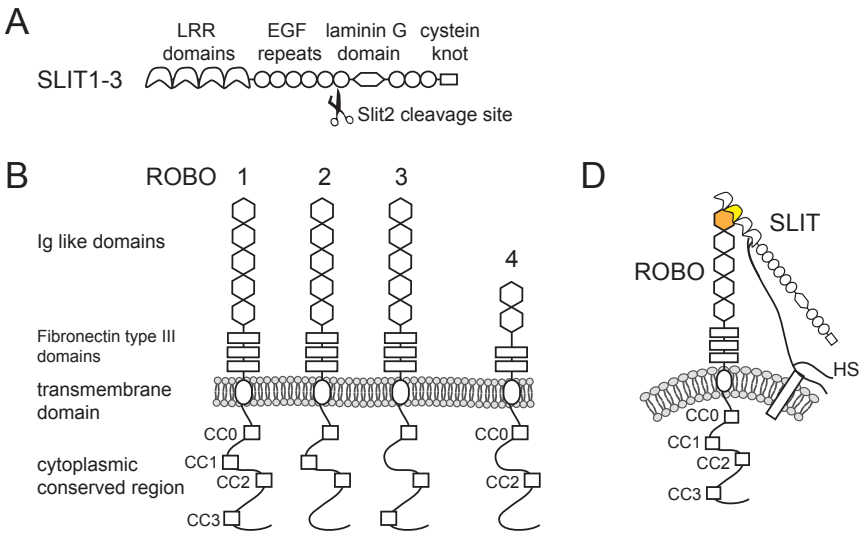

C

	CC0	CC1	CC2	CC3
ROBO1	TVYGDVD	TPYATTQLI	LPPPPAHPPP	PPPPVPPP
ROBO2	AIYSSID	TPYATTQIL	LPPPPVQPLP	
ROBO3	PVYSTID		LPPPPPSCEL	PPPPLPPP
ROBO4	TFYGSLI		LPPAPLFPHE	

Figure 2.5.: Domain architecture of Slit and Robo proteins
A Illustration of the domain architecture of Slit proteins. Human SLIT2 is shown as a representative. The proteolytic cleavage site is indicated. **B** Illustration of the four mammalian ROBO receptors showing the differences in their domain architecture. **C** Comparison of the sequences of CC motifs of the four human ROBO receptors. Sequences for ROBO4 are marked in grey indicating that their identity is still under discussion. **D** Schematic drawing of the Slit/Robo binding mechanism, which has only been demonstrated for Robo1 to 3. The D2 domain of Slit and the first Ig domain of Robo mediate their interaction and are shown in yellow and orange, respectively.

2.3.4. Slit/Robo transmembrane signalling

Once Slits are bound to the Robo receptors the signal has to be transmitted into the cell. It is well known that other transmembrane receptors undergo conformational changes upon ligand binding, which include assembly of oligomers (as intergins (Luo et al., 2007)), dimerization (as receptor tyrosine kinases (RTK) (Hubbard and Miller, 2007)) or clustering at specific locations (as immune receptors (Davis and Merwe, 2006)). Furthermore, various members of the IgCAM family promote neurite outgrowth via a homophilic binding mechanism, which was shown for neural cell adhesion molecule (NCAM), N-cadherin and L1 CAM (Doherty et al., 1991, 1995).

For Robo receptors it can be assumed that they form receptor oligomers as well, which is supported by studies demonstrating the homo- and heterophilic association of the extracellular parts of Robo1 and Robo2 (Hivert et al., 2002) or the interaction of ectopically expressed Robo1 and Robo4 (Kaur et al., 2008; Sheldon et al., 2009). A more recent study suggests

that Robo1 acts as a dimer at the plasma membrane under basal conditions in the absence of Slit2. The authors of this study assume that the dimeric form of Robo1 must be functionally competent, because its dimerization status is not altered upon Slit2 stimulation (Zakrys et al., 2014). If this is true, Robo1 would be a novel example of a transmembrane receptor that exists and functions as constitutive dimer, as it has been shown for the insulin receptor and members of the GPCR class C receptors (Rondard et al., 2011).

2.3.5. Slit/Robo downstream signalling pathways

The cytoplasmic domains of Robo receptors do not contain any catalytic activity. Therefore, it has been assumed that the receptors signal by recruiting adaptor proteins and other signalling molecules (Fig. 2.6).

The control of Rho GTPases downstream of ROBO receptors leading to repulsive migration is not fully understood. Moreover, at present, no Rho GTPase regulatory proteins downstream of ROBO4 are known.
The family of Slit-Robo GAPs (SRGAPs) comprises 3 different members that are similar in their domain structure containing an N-terminal FES-CIP4 homology (FCH) domain, a central RhoGAP domain, followed by a Src homology 3 (SH3) domain (Wong et al., 2001; Bacon et al., 2009; Endris et al., 2002). The three murine srGAP proteins are widely expressed in the mouse nervous system and were identified to interact with Robo in a yeast two-hybrid screen. Based on this study it has been proposed that the SH3 domain binds to the CC3 motif in Robo (Wong et al., 2001; Bacon et al., 2011). This is in line with the observation that srGAP1 and srGAP3 bind to Robo1 and Robo1-2 in mice, respectively (Wong et al., 2001; Bacon et al., 2011). In human the CC3 motif is only encoded by ROBO1 and 3.
In a first analysis srGAP1 was shown to inactivate Cdc42 in HEK 293T cells in the presence of Slit2 (Wong et al., 2001). Recently, it has been proposed that SRGAP1 is Rac1 specific and by that modulates the lamellipodial dynamics and cell motility (Yamazaki et al., 2013). This difference in the SRGAP1 substrate specificity might be due to different experimental set ups with or without Slit2 stimulation. In contrast, both srGAP2 and srGAP3 have been demonstrated to be specific for Rac1 and to negatively regulate cell migration (Wong et al., 2001; Soderling et al., 2002; Guerrier et al., 2009).

So far, Son of sevenless (Sos) has been the only RhoGEF identified to interact with Robo, which was first described in *Drosophila* (Fritz and VanBerkum, 2002). Sos interaction with Robo is mediated by the small adaptor protein Dock in *Drosophila*, Nck in mammals (Hu et al., 1995). The existence of a trimeric complex of ectopic expressed Robo with endogenous Dock and Sos was demonstrated in Co-IP experiments using *Drosophila* embryo lysates (Yang and

Bashaw, 2006). Dock/Nck binds via on of their SH3 domains to a proline rich motif in Robo and thus bridge the Robo-Sos interaction. However, the identified binding sites within the receptors differ between Dock and Nck. For Dock it has been proposed to bind to the CC2 and the CC3 motif of Robo (Fan et al., 2003), whereas the murine Nck/Robo1 interaction requires four PxxP motifs located between the CC2 and CC3 motif (Round and Sun, 2011). Interestingly, ROBO4 also contains five PxxP motifs following its CC2 domain, suggesting that SOS might bind indirectly to ROBO4 via NCK.
In addition of binding Sos, Dock can also recruit Pak1, the main effector of Rac1 and Cdc42, which has been shown in genetic experiments in *Drosohila* and yeast two-hybrid screens (Fan et al., 2003).

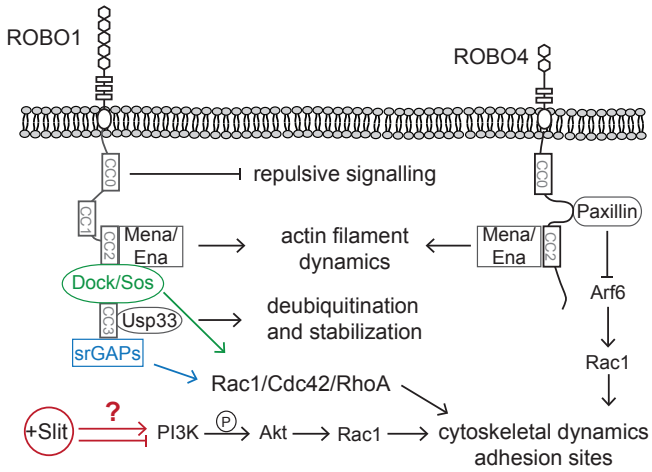

Figure 2.6.: Downstream effector proteins of Slit/Robo
Schematic illustration of Slit/Robo signalling. Interaction of Mena with the CC2 domain and Usp33 with CC3 domain to prevent actin polymerization or to deubiquitinate Robo1 and thus stabilizing its signalling function at the plasma membrane, respectively. Whether Slit2 stimulation inhibits or activates the PI3K/Akt/Rac1 pathway is not clear yet. The Rho regulatory proteins srGAPs (blue) and Sos (green) directly link the Robo receptors to Rho GTPase signalling. Sos interaction with Robo1 occurs indirectly via Dock (Nck in mammals), but the predicted binding sites differ (see text above). Robo4 signalling recruits Paxillin (PXN) to inhibit Arf6 activity, which in turn results in reduced Rac1 activity.

Slit/Robo activity also modulates PI3K signalling. Slit2 has been reported to inhibit PI3K signalling that results in diminished activation of the Ser/Thr kinase Akt leading to suppression of cell locomotion in breast cancer cells (Chang et al., 2012; Prasad et al., 2007). Contradicting results have been obtained in endothelial cells (ECs), showing that Slit2 stimulation enhances PI3K activity and thus cell migration and angiogenic remodelling (Wang et al., 2003; Dunaway et al., 2011).

ARF6 belongs to the family of small Arf GTPases and shows functions in membrane traffick-

ing and transmembrane protein cargo transport (Memon, 2004). Moreover Arf6 can directly activate Rac1 (Nishiya et al., 2005). The link between Slit/Robo and Arf6 came from a study to investigate the role of Robo4 in maintaining vascular stability in ECs. It has been shown that upon Slit2 stimulation Pxn binds and to Robo4 at the plasma membrane. Pxn suppresses Arf6 activation by recruiting the ArfGAP Git, and thus prevents Rac1 signalling in migrating ECs. This signalling pathway is thought to opposes Vefg/Vegfr induced activation of Arf6, which promotes in angiogenesis (Jones et al., 2009b).

Mena belongs to the family of Ena/Vasp homology (EVH) multi-domain proteins that are involved in actin polymerization, protein-protein interactions, axon guidance and cell migration. They localize to the leading edge of lamellipodia and the tips of filopodia (Bear and Gertler, 2009). It has been demonstrated that Ena/Mena binds with its EVH1 domain to the CC2 domain of Robo1 and Robo4 (Bashaw et al., 2000; Jones et al., 2009a; Park et al., 2003). The Robo/Ena interaction is induced by Slit and promotes filopodia formation in the growth cone of axons that are required for repulsion of the growth cone away from Slit (McConnell et al., 2016).

The ubiquitin-specific protease 33 (USP33) is a deubiquitinating enzyme that was found to bind to the Robo1 cytoplasmic CC3 motif (Yuasa-Kawada et al., 2009a,b). With microscopy and biotin labeling experiments it was shown that upon Slit2 stimulation Robo1 is recruited form perinuclear regions to the plasma membrane in an USP33 dependent manner. Therefore, it has been assumed that USP33 is required for Robo deubiquitination and stabilization (Huang et al., 2015)

2.3.6. Biological functions of Slit/Robo

Development of the nervous system

The central nervous system (CNS) receives and integrates signals to coordinate the activity of all parts of the body in bilateral symmetric animals. A long the longitudinal axis of the CNS runs the (virtual) midline, which functions as an organizing center by secreting diffusible molecules. Two different kind of axons exist along the midline. Ipsilateral neurons extend their axons on the same side of the CNS as their cell bodies are located. Commissural neurons have their cell bodies located on one side of the CNS but project their axons across the midline to make contacts with target cells on the other side. The crossing of the midline involves two steps: first the attraction towards the midline to cross it, and second the repulsive guidance to prevent recrossing. Several studies in *Drosophila* and mice demonstrated that Slit/Robo

signalling is a crucial for the axonal steering decision.

The midline cells secrete several diffusible proteins, among them Netrin and Slit2. Netrin is a chemoattractive guidance cue that acts via the receptor deleted in colorectal cancer (DCC). Therefore, the all the axons start migrating towards the midline (Placzek and Briscoe, 2005). Robo receptors are expressed in the growth cones of ipsilateral and commissural neurons, thus making them sensitive to the chemorepellant Slit2. This way, the ipsilateral axons stay away and do not cross the midline (Fig. 2.7 B). However, the commissural axons have to cross the midline (Fig. 2.7 A).

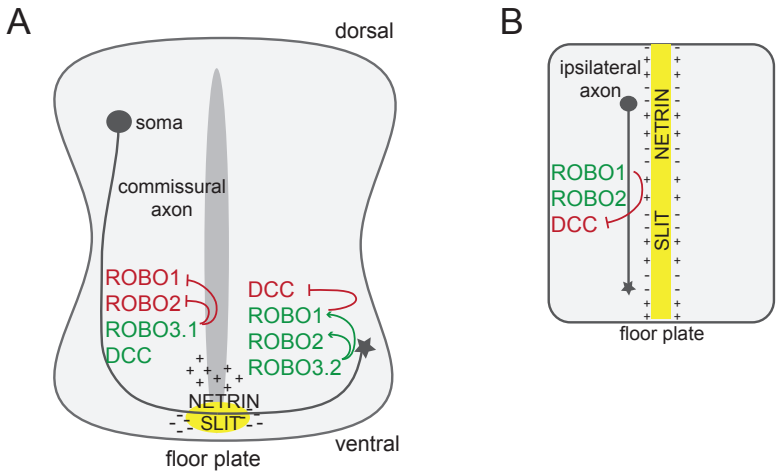

Figure 2.7.: Slit/Robo signalling in axon guidance
A Schematic of cross section of the mouse spinal cord showing the midline in dark grey. The commissural axon (dark grey) grows to the floor plate (yellow) under the attractive action of secreted Netrin (+), which can be sensed by the DCC receptor. Before crossing the midline Robo1/2 expression is repressed by Robo3.1, thus rendering the axon insensitive to secreted Slit (-) at the floor plate. After crossing the midline Robo1/2 are active to mediate Slit repulsive signalling, supported by the expression of Robo3.2. **B** Illustration depicting how ipsilateral neurons stay on the same side of the midline due to the expression of Robo1/2. First, the Robo receptors render the axons sensitive to the repulsive cue Slit at the midline. Second, Robo1 dimerizes with DCC and inhibits the binding of Netrin to DCC, thus preventing the attraction towards the midline.

In *Drosophila* the transmembrane protein Commissureless (Comm) has been found to negatively regulate Robo surface expression levels in the growth cone. Before reaching the midline Comm sorts Robo to late endosomes and lysosomes for degradation, not allowing it to reach the growth cone (Keleman et al., 2002). After crossing the midline a still unknown mechanism inhibits Comm expression. Therefore, Robo receptor levels increase at the plasma membrane making the growth cone reponsive to Slit2 (Keleman et al., 2005). This repels the axons from the midline and prevents recrossing.

In vertebrates no homologue of Comm could be identified. In stead, it has been assumed

that the two differently spliced isoforms of Robo3, Robo3.1 and Robo3.2, regulate Robo responsiveness to Slit2. In this model Robo3.1 prevents Robo1 and Robo2 activation, thereby blocking their repulsive activity. After crossing the midline Robo3.1 is down-regulated and instead Robo3.2 is expressed, which cooperates with Robo1 and Robo2 in mediating Slit repulsion (Fig. 2.7 A) (Sabatier et al., 2004; Chen et al., 2008).
Furthermore, it is thought that upon Slit2 binding Robo1 is able to dimerize with DCC, which prevents the Netrin induced attraction. This might further enhance the repulsion of axons from the midline, thereby preventing the crossing or re-crossing of ipsilateral or commissural axons, respectively (Stein and Tessier-Lavigne, 2001).
After crossing the midline commissural axons turn longitudinally and extend their axons in parallel tracts along midline, in the same way as ipsilateral neurons.

Development of other organs

The Slit and Robo protein expression is not restricted to the nervous system and has been found in a variety of other organs implicating a general guidance role during development. For instance, it has been shown that Slit/Robo activity is important for the correct alignment of myocardioblasts during the formation of the heart chambers in *Drosophila* (Qian et al., 2005). Slit/Robo is also expressed in the epithelium of mammalian lungs and tracheal cells in *Drosophila* (Anselmo et al., 2003). Another example is the formation of mammalian kidneys, that are mainly made of a set of convoluted tubes. Multiple ectopic ureteric buds form in *slit2* and *robo2* deficient embryos that result in the formation and fusion of multiple ureters (Grieshammer et al., 2004).

The vascular system

During embryonic development the vascular network forms, which is crucial to supply all organs with oxygen and nutrients. Robo4 is specifically expressed in EC (Huminiecki et al., 2002; Park et al., 2003). While Robo1, Robo2, Slit2 and Slit3 expression can be found in ECs as well, Slit1 and Robo3 protein levels can be neglected (Liu et al., 2006; Small et al., 2010; Zhang et al., 2009).

Slit2 has been shown to prevent EC migration towards VEGF by binding to Robo4 (Park et al., 2003; Seth et al., 2005). Moreover, Slit2 signalling through Robo4 reduces VEGF induced vascular permeability in *vivo* and in *vitro*, implying that Slit2/Robo4 stabilize existing blood vessels (Jones et al., 2008; London et al., 2010). The interaction of Robo4 with the Unc5B receptor, a vascular Netrin receptor, has been shown to control vascular stability, because inhibition of their association induced vessel hyperpermeability in mice (Koch et al., 2011). Surprisingly, Robo4 has been considered to be dispensable for development, because *Robo4*

deficient mice are viable and fertile (Jones et al., 2008; Koch et al., 2011). However, adult *Robo4*-/- mice show increased corneal neovascularization induced by VEGF (Jones et al., 2008; Koch et al., 2011).
Thus, it has been proposed that Slit/Robo promote anti-angiogenic signalling pathways that prevent EC migration and new vessel formation in order to stabilize the vasculature.

Conflicting reports have been published showing a pro-migratory effect of Slit on ECs by the activation of Robo1 signalling (Wang et al., 2003; Kaur et al., 2008). Moreover, Slit2 has been shown to mediate the association of Robo1 with Robo4 (Kaur et al., 2008; Sheldon et al., 2009), and to facilitate filopodia extensions and thus migration in a Robo1/Robo4 dependent manner (Sheldon et al., 2009). However, it remains unclear which one of the two receptor is responsible for the Slit2 mediated migration of ECs. Kaur and colleagues reported that Robo4 is responsible, whereas Sheldon and colleagues showed that Robo1 mediates cell migration upon Slit2 stimulation. In zebrafish the knock down of *robo4* leads to the delayed outgrowth of the intersomitic vessels, which are then also misdirected along the trunk, arguing that Robo4 is guidance receptor during the early steps of angiogenesis in the vasculature. However, no ligand for Robo4 or any underlying mechanism have yet been suggested (Bedell et al., 2005). These data link Slit/Robo signalling to pro-migratory effects on ECs and pro-angiogenic effect on vessel formation.

A different scenario might be the requirement of diverse Slit/Robo signalling outcomes depending on the stage of development, hence during embryonic development it might act as a pro-angiogenic and in the adult organisms as anti-angiogenic signalling system. Dunaway and colleagues propose a model of cooperative signalling between Slit2 and EphrinA1. If Slit2 is present alone it promotes angiogenesis through the activation of Akt and Rac1 in migrating ECs and vessel remodelling. In the presence of EphrinA1, Slit2 signalling switches to repression of angiogenesis (Dunaway et al., 2011). The precise mechanisms how Ephrin/Eph and Slit/Robo signalling pathways might be connected are unknown, apart from the observation that Vegf stimulates Ephrin synthesis (Cheng et al., 2002). Thus, Vegf might accumulate Ephrin that alters the Slit2/Robo1 system from pro- to anti-angiogenic in order to balance vessel formation.

To conclude, the role of Slit and Robo proteins in angiogenesis has been intensively studied, however fundamental details about their function remain obscure. Specifically, the questions if Slit is the ligand for Robo4, whether Robo4 requires a co-receptor and if there is a role for Robo1 in angiogenesis are still unanswered. Moreover, whether Slit/Robo function contributes to pro- or anti-angiogenic effects during angiogenesis is controversially discussed, as well as its role in EC migration. The diverse outcomes of Slit/Robo signalling obtained in the different

studies might be due to variations in the experimental set ups.

Slit/Robo in Cancer

The importance of Slit/Robo expression for the correct development of the CNS and other organs implicates that under pathological conditions Slit/Robo function might be deregulated. The first link between Slit/Robo and cancer was the finding that deletion of exon 2 of Robo1 results in reduced Robo1 levels in lung and breast cancer cells (Sundaresan et al., 1995; Zabarovsky et al., 2002). Moreover, the promoters of Slit1-3 and Robo1-4 are hypermethylated in a wide range of tumors and cancer cells and thus their expression is repressed (Chang et al., 2012; Mertsch et al., 2008; Shibue and Weinberg, 2011). A recent prognosis model even considers Slit2 and Robo1 expression levels as clinical parameters for predicting brain metastasis in breast cancer patients, where low expression of Slit2 or Robo1 results in poor survival prognosis for the patients with enhanced development of brain metastasis (Qin et al., 2015).
However, it appears that the present data landscape about Slit/Robo activity in cancer cells is controversial. Pro-oncogenic as well as tumor suppressor functions have been reported. Thus, the obtained data need to be analysed dependent on the specific contexts and the potential cross talk between the Robo receptors and also with other receptors should be taken into account.

2.4. Angiogenesis

During embryonic development an extensive endothelial-lined tubular network has to establish that forms the vascular system of the organism. This network is crucial to provide all tissues with oxygen, nutrients and respiratory gases and to allow the circulation of humoral and cellular molecules. These functions are required for the growth of organs during development and early postnatal life, but is also essential to stabilize body temperature and homeostasis and to defend disease in the adult (Carmeliet, 2003). Angiogenesis plays also an important role under pathological conditions, for instance in vessel formation towards cancer cells or is associated with diabetes (Heath and Bicknell, 2009).

2.4.1. Angiogenesis is a multistep process

Angiogenesis, also referred to as sprouting angiogenesis, is the process in which the primary blood vessel network expands by sprouting of new vessels from preexisting vascular tubes.

It is composed of several morphogenic events including spouting of new vessels, branching, lumen formation, establishment of contacts with other vessels and finally their fusion, which results in the formation of a tubular network (Fig. 2.8).

The master signalling molecule during angiogenesis is VEGF-A, which leads to the activation of VEGF-receptor 2 (VEGFR2) in ECs. Few of these ECs differentiate into tip cells that will be the sites of new vessel sprouting based on the fine-tuned feedback loop between VEGF and Notch/DLL4 signalling.

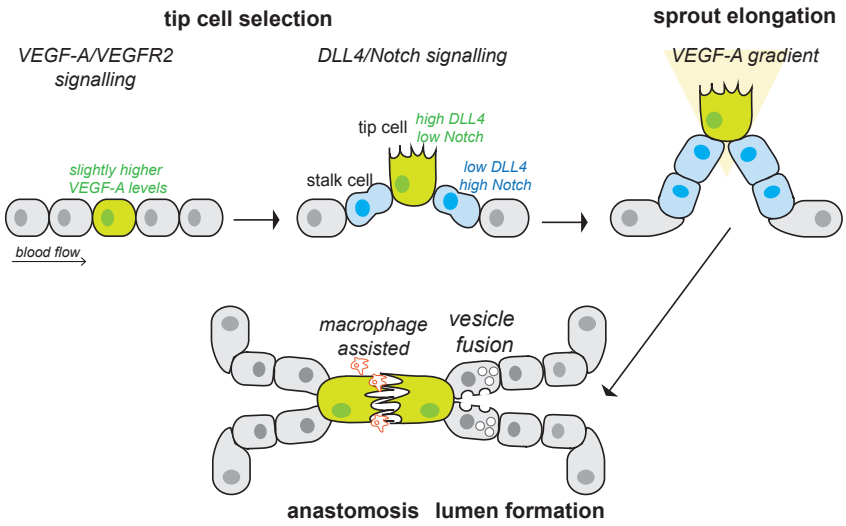

Figure 2.8.: Steps of sprouting angiogenesis
Schematic illustration of processes involved in sprouting angiogenesis. First, the endothelium becomes activated and one cell is selected as tip cell due to a VEGF-A gradient in the extracellular environment. The adjacent cells differentiate into stalk cells due to Notch mediated lateral inhibition of cell specification (see text above). Simultaneously, VEGF-A induces filopodia formation in the tip cell and thus the sprout growth out. Next, the newly formed vessel migrates towards a specific target region, following the VEGF-A gradient. Moreover, stalk cell proliferation, which is dependent on the VEGF-A concentration, contributes to the elongation of the sprout. Lumenisation of the spouts involves the formation of intra- and intercellular vacuoles that fuse across the endothelial cells to form a luminal space. Eventually, two tip cells make contacts with their filopodia and fuse in a process called anastomosis, which has been shown to be assisted by macrophages. (Figure adapted from (Geudens and Gerhardt, 2011))

Briefly, local differences in the extracellular VEGF-A concentration lead to small imbalances in VEGF-A/VEGFR2 signalling that induces slightly higher expression of DLL4 in one cell. The increase in DLL4 expression in this cell dictates the neighbouring cells to activate more Notch signalling and thereby decreasing their own DLL4 levels. This results in high DLL4 and low Notch activity in one cell, which becomes the tip cell, whereas all the adjacent cells have increased Notch and low DLL4 levels and become stalk cells (Fig. 2.8) (Hellström et al., 2007; Lobov et al., 2006; Suchting et al., 2007; Leslie et al., 2007). VEGF-A is also the principle regulator of tip cell filopodia formation and stalk cell proliferation during the sprouting process

(Fig. 2.8). The adjacent stalk cells follow behind the guiding tip cell and form the body of the sprout via proliferation to provide more cells (Gerhardt et al., 2003).

While the sprout grows out of the parent vessel a vascular lumen has to form. In different model systems and even for different vascular systems of the same organism different mechanisms of lumenization have been proposed (Wang et al., 2010). For instance, in the brain vasculature of zebrafish the lumen of a newly sprouting vessel continuous with that of the parent vessel, implicating that stalk cells retain their apical-basal polarity when they bud of from the parent vessel (Huisken and Stainier, 2009). In contrast, for the intersomitic vessels (ISVs) the initial sprouts do not have a lumen when they grow out from the dorsal aorta and thus requires intracellular vesicle formation and fusion to create an lumen (Kamei et al., 2006; Blum et al., 2008).

During elongation and branching of a vessel, its tip cell makes contact with the tip cell of another sprouts, which is followed by the formation of new cell-cell junctions to form a continuous lumen in a process called anastomosis (Fig. 2.8). How the tip cells find each other and how they establish contacts is not yet understood. In recent studies it has been suggested that macrophages assist this process, since they reside at the filopodia that are in contact between two tip cells (Checchin et al., 2006; Fantin et al., 2010; Rymo et al., 2011).

2.4.2. Role of Rho GTPases in angiogenesis

On the molecular level angiogenesis comprises of tight regulation of cell proliferation, migration, matrix adhesion and cell-cell signalling processes to allow the enzymatic breakdown of the basement membrane followed by EC motility and proliferation resulting in vascular tube formation (Merajver and Usmani, 2005; Adams and Alitalo, 2007). Rho GTPases are master regulators of the cytoskeleton and thus their requirement for these angiogenic processes is not surprising (reviewed in (Bryan and D'Amore, 2007; Carmeliet and Jain, 2011; Fryer and Field, 2005)).
Additional, Rho GTPases have been observed to maintain vessel integrity as they can have barrier-protecting and barrier-disturbing functions in ECs depending on the cellular context (van Nieuw Amerongen et al., 2003; Gavard et al., 2008; Beckers et al., 2010). While new vessels form, VEGF-A activates RhoA signalling to increase vascular permeability via the breakdown of endothelial junctions and increased cell migration (Etienne-Manneville and Hall, 2002). After vessel formation Rac1 and Cdc42 are activated at inter-endothelial junctional complexes and stabilize adherens and tight junctions, which results in sealing of ECs to a monolayer and thereby maintaining its barrier function (Braga et al., 1997; Noren et al., 2001; Broman et al., 2007).

The contribution of Rac1 and Cdc42 to vacuole formation and lumenization was first observed when GFP-Rac1 and GFP-Cdc42 targeted vesicles to the intracellular vacuole compartment. Whereas, their dominant-negative mutants failed to induce lumenization in 3D- ECM matrices (Bayless and Davis, 2002). The Rac1/Cdc42 effector proteins Pak2/Pak4 were found to be strongly upregulated during lumen formation. Moreover, the cell polarity proteins Par3/Par6 were detected to establish EC polarity downstream of Cdc42 that allowed the formation of intracellular vacuoles *in vitro* (Koh et al., 2008). Recently, it has been proposed that actin remodelling is required for the formation of lumen. The multi-domain adaptor protein Nck was observed to regulate the activation and localisation of the Cdc42/aPKC polarity complex in ECs. Depletion of *Nck* was shown to impair the actin cytoskeleton and VE-cadherins junctions, that led to the loss of endothelial apical-basal polarity and perturbed lumen formation (Chaki et al., 2015).

Despite the knowledge that Rho GTPases regulate morphogenic processes during vasculature formation, less is known about the upstream regulatory proteins involved. To shed light on how Rho GTPase signalling is modulated in angiogenesis the involved regulatory GEF/GAP proteins have to be identified and characterized.

2.4.3. Zebrafish is model organism to study angiogenesis in vivo

Danio rerio, commonly referred to as zebrafish, has been used as a model system for vertebrate development in many research fields. The advantages of this model organism are the optical clarity to visualize developmental processes of several organs and tissues, the ease to experimentally handle them, the quick generation time, high number of offspring and straightforward strategies for forward and reverse genetic manipulations (Fig. 2.9 A) (Isogai et al., 2001b; Chávez et al., 2016). Furthermore, several transgenic zebrafish lines exist expressing fluorescent proteins in distinct tissues allowing to address developmental questions.

Despite the evolutionary distance between fish and mammals most of the molecular pathways during development are conserved, making zebrafish a well accepted model system to study human diseases. Nevertheless, observations in zebrafish must be complemented with studies in mammalian systems in order to validate the gained knowledge for potential clinical applications. Since gene and protein functions are not 100% conserved and due to physiological differences the outcomes of signalling pathways and morphogenesis might be divergent (Chávez et al., 2016).

2.4.4. Development of vasculature in zebrafish

The transgenic fish line Tg*(fli1:egfp)*^{y1} expresses the green green fluorescent protein (GFP) in all ECs and is a powerful tool to study the development of blood vessels (Lawson and Weinstein, 2002) (Fig. 2.9 A). The focus in this study is on the formation of ISVs that form between each pair of somites, which are blocks of mesoderm that are located on either side of the neural tube. The ISVs sprout out of the dorsal aorta (DA) and migrate along the dorsoventral axis between the intersomitic boundaries. Eventually, they branch into a T-shape structure and join with their anterior and posterior neighbours to form the dorsal longitudinal anastomotic vessel (DLAV) (Fig. 2.9 B).

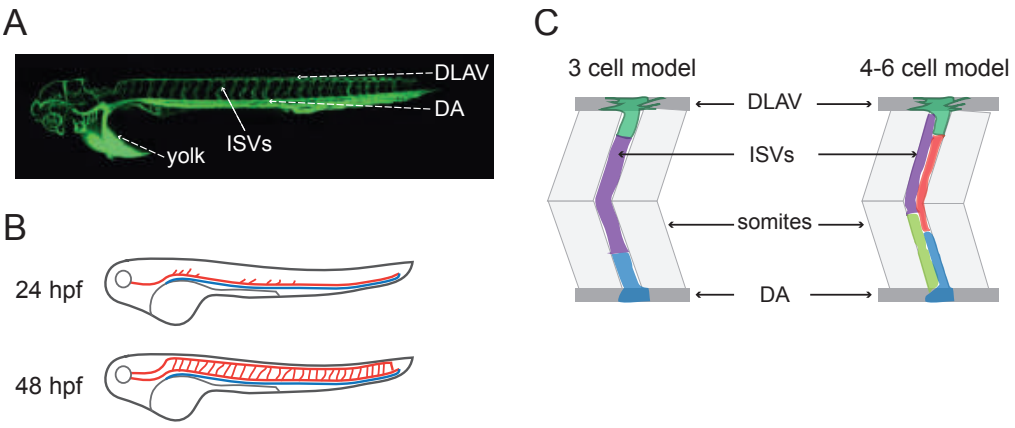

Figure 2.9.: Developing vasculature of the zebrafish embryo
A Development of the vasculature is shown at 48 hours post fertilization (hpf) (pictures from (Isogai et al., 2001a)) . The dorsal aorta (DA), the posterior caudal vein (PCV) and the intersomitic vessels (ISVs) can be easily observed at 48 hpf and are indicated by arrows. **B** Schematic illustration of ISV growth during development in the zebrafish trunk. At 24 hpf sprouting ISVs are detected that start to grow continuously along the somite boundaries. At 48 hpf the tip cells reach the dorsal site of the somites the branch into a T-shape structure and make connections with their anterior- posterior neighbours. **C** A first model assumed that the complete ISV consists of three cells: one leading cell that fuses with the adjacent leading cells, one intermediate cell along the somite boundaries and one cell at the base making contact with the DA, depicted as a green, purple and blue cell, respectively. More recently it has been proposed that the ISVs are composed of four to six cells, with one leading cell but several cells paired along the axis of the ISVs (see text).

First studies suggested that three cells arrange in a strictly choreographed fashion to form one ISV. The lumen has been thought to form via intracellular and intercellular fusion of vacuoles into a seamless tube (Kamei et al., 2006). More recently, the analysis of cell junctions in ISVs revealed that they are composed of four to six cells. While the sprout is growing it contains one leading tip cell and two to three stalk cells that show great overlap and are paired along the axis of ISVs (Fig. 2.9 C). A model has been proposed in which the intracellular vacuoles are released in a common intercellular space between adjacent ECs that is considered as "extracellular" (Blum et al., 2008).

By that, a simple vascular network is established in the zebrafish trunk. Due to their repetitive organization and the simple anatomy, ISVs are a well suited model to follow sprouting angiogenesis.

2.5. Human ARHGAP39

Human ARHGAP39 is a yet uncharacterized RhoGAP protein encoding two N-terminal WW domains, a myosin tail homology (MyTH4) domain and a C-terminal RhoGAP domain.
The ARHGAP39 homologue in *Drosophila* has been initially characterised by two different laboratories which named the protein Vilse or Crossgap (Lundström et al., 2004; Hu et al., 2005). Both studied focussed on developmental guidance processes of axons and ganglionic branches in the *Drosophila* embryo and revealed that Vilse/Crossgap is responsible for correct cell migration at the midline. Specifically the loss of *vilse/crossgap* led to misdirected ganglionic branches (GBs) that stopped at the midline or did not turn correctly to reach their target during development of the respiratory tracheal system (Lundström et al., 2004). In the second study, the guided migration of longitudinal axons along the midline was investigated in *slit-/+,robo-/+* transheterozygous embryos. Both the depletion of *vilse* and its overexpression led to enhanced misguidance of longitudinal axons across the midline (Hu et al., 2005). Furthermore, its gain-of-function phenotype mimics the loss-of-function phenotypes of both *robo* and *rac*, indicating that Vilse might be the regulator linking Robo to Rac1 signalling.
During this thesis work, murine Arhgap39 has been described to regulate spine morphology (Lim et al., 2014), and the rat homologue, also referred to as preoptic regulatory factor 2 (porf-2) to inhibit neural stem cell proliferation (Huang et al., 2016).

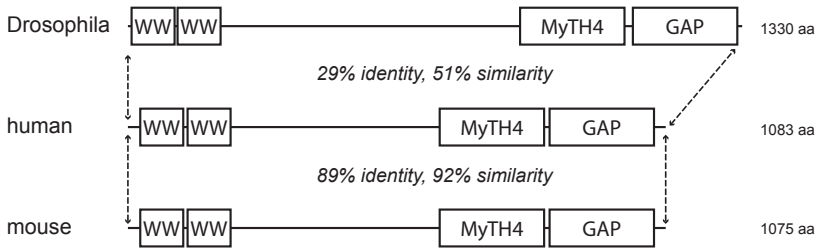

Figure 2.10.: Predicted domain structure of ARHGAP39 and its identified homologues
Two WW domains, one MyTH4 and one C-terminal RhoGAP domain were identified by Pfam protein motif prediction. The degree of identity and similarity is shown for each homologue compared to the human protein. Figure adapted from (**?**).

The human protein and its homologues in *Drosophila* and in mouse share an identical domain

structure with 29% / 89% identity and 51% /92% similarity, respectively (Nagase et al., 2000; Lundström et al., 2004), indicating that the domain functions are evolutionary conserved (Fig. 2.10).
The catalytic activity of the isolated RhoGAP domain of Vilse/CrossGAP was analysed in *in vitro* revealing its substrate specificity for Rac1, and to a lesser extent, for Cdc42 (Lundström et al., 2004). Rac1 specificity was also determined for murine Vilse (Lim et al., 2014), hence it can be speculated that ARHGAP39 exhibits catalytic activity towards RAC1 and presumably towards CDC42.
The putative protein-protein interaction mediating domains of ARHGAP39 are the WW domains. For the murine and fly homologues of ARHGAP39 it was shown that the WW domains associate with the Robo receptor and the neural scaffold protein connector enhancer of KSR-2 (CNKSR2), respectively (Hu et al., 2005; Lundström et al., 2004; Lim et al., 2014). Both studies demonstrated that the WW domains bind to proline-rich sequences in the targeting partners, which are the CC2 motif in Robo and a poly-proline stretch in CNKSR2, thereby establishing a canonical WW domain interaction.
To better understand the action of WW domains and the MyTH4 domain I introduce these two domains in more detail next.

2.5.1. Structure and function of WW domains

WW domains are the smallest and most compact globular protein structures that can be found in nature. They were first identified in Yes-associated protein (YAP) (Chen and Sudol, 1995) and compose only about 35 amino acids. The name was given after the two highly conserved tryptophan (Trp) residues that are separated by 20-22 amino acids in the polypeptide chain, additional there is a strictly conserved proline residue (Pro) at its C-terminus. They mediate protein-protein interaction by recognizing proline rich sequences on binding partners.

WW domains form a stable, triple stranded antiparallel β-sheet module (Fig. 2.11 A). The C-terminus of the WW domain forms a hydrophobic core, where the proline rich ligands can bind to (Jäger et al., 2001, 2007). Two classification systems of WW domains have been proposed. The first depends on the presence of conserved residues: N-terminal Pro and C-terminal Trp (Group 1), only C-terminal Trp (Group 2), only N-terminal Pro (Group 3) (Macias et al., 2000). In the second system the WW domains are divided into 5 classes based on their ligand motif preference (Fig. 2.11 B) (Sudol and Hunter, 2000; Macias et al., 2002; Otte et al., 2003).

A prototype WW domain is depicted in Figure 2.11 C to illustrate which amino acid residues contribute to ligand binding or folding (Macias et al., 2000). The majority of structural studies are based on WW domains that recognize the PPxY motif as described for the Yes-associated

protein YAP65 homolog (YAP1) and the E3 ubiquitin-protein ligase Nedd4 (Ingham et al., 2004; Chen et al., 1997). Crystallization revealed that the central Tyr residue and the last Trp residue bind the prolines, whereas the His resiude makes contact with the tyrosine of the PPxY motif (Macias et al., 2002).

In contrast, the formin binding protein 11 (FBP11) and its homologue in yeast, the Pre-mRNA-processing protein (Prp40), prefer stretches of proline residues as in the PPLP or the (p/f)PPPPP motif (Bedford et al., 1998; Otte et al., 2003), because the presence of three aromatic Tyr residues in the center of the WW domain reduces the space for binding of other aromatic residues (Macias et al., 2002).

A

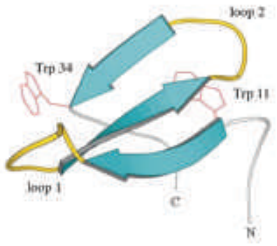

B

Class	recognition motif	examples
I	(L/P) Pp(Y/poY)	YAP, NEDD4
II	PPLPp	FBP11, Prp40
III	(p/f)P(p/g)PPpR / (P/f)PP(R/K)gpPp	FBP21
IV	(poS/poT)P	PIN1
V	(p/f)PPPPP	Prp40

C

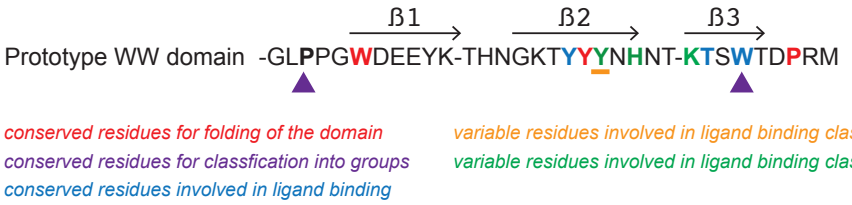

Figure 2.11.: Structure and proline-rich binding motifs of WW domains
A A ribbon diagram of the prolyl-isomerase PIN1 WW domain is depicted. The three β-strands are shown and the loop structures, as well as the side-chains of the two conserved tryptophan residues in red (Figure from (Jäger et al., 2001)). **B** Table of WW domain classes divided after their binding motifs. L: leucine, S: serine, T: threonine, po: phosphorylated residue, lower case: favored residue, upper case: highly conserved residue (adapted (Salah, 2012)) **C** A prototype WW domain is shown, which was generated by (Macias et al., 2000) based on sequence alignment of distinct WW domains. The conserved residues required for the classification into groups are indicated by purple arrow heads. Conserved residues responsible for correct folding of the WW domain are shown in red. Conserved residues and semi-conserved residues (of the individual class) involved in ligand binding are depicted in blue and green/orange respectively. Residues with double function are indicated by an underline in the corresponding color of the second function. UniProt: YAP1 (P46937), Prp40 (P33203), FBP11 (O75400), NEDD4 (P46934), FBP21 (O75554), PIN1 (Q13526). Abbreviations: YAP1: Yes-associated protein YAP65 homolog, Prp40: Pre-mRNA-processing protein, FBP11: formin binding protein 11, FBP21: formin binding protein 21, NEDD4: E3 ubiquitin-protein ligase, PIN1: prolyl-isomerase

The prolyl-isomerase PIN1 and its related proteins exhibit a completely different binding preference by recognizing phosphorylated Ser or Thr residues ahead of a Pro residue. In this case the contacts are established between the phosphorylated residue in the target peptide and the side chains of Ser or Arg residues in the N-terminal sequence of the WW domain (Macias

et al., 2002). Recently more WW domain containing proteins have been identified to recognize phosphorylated proline-rich ligands, even though not all of the Pin1 specific residues are present in their sequence. For instance, the WW domains of YAP1, SMURF1 and NEDD4 recognize very specific phosphorylated residues on SMAD proteins (Aragon et al., 2011).
Surprisingly, the WW domain of ArhGAP9 interacts with none of the predicted proline-rich binding motifs. Its WW domain binds to the common docking (CD) domain in Erk2 and p38α, which contains clusters of complementarily charges residues. Thereby, ArhGAP9 prevents Erk2 and p38α activation and thus inhibits the MAP kinase signalling pathway (Ang et al., 2007).

In most WW domain containing proteins the domain occurs in tandem, thus different binding mechanisms how the WW domains recognize their binding targets are possible.
First, the individual domains of the tandem might recognize the same target motif, albeit with different affinities, as it has been observed for YAP1.2 (Schuchardt et al., 2014), Secondly, each individual WW domain binds a different set of target sequences (Hu et al., 2004). For instance, it has been demonstrated that the first WW domain of YAP1 binds to the PPxY motif in SMAD7, whereas the it recognizes the (poS)P ligand in SMAD1. Third, the two WW domains of the tandem exhibit cooperative binding by chaperoning or stabilization of each other. Chaperoning effects can be explained by structural instability of the interaction of one WW domain with its target, which becomes stabilized through the other WW domain that binds to the first WW domain. And Lastly, the binding of one WW domain to its target sequence induces conformational changes in the neighboring WW domain, which leads to changes in its affinity and structure for its own interaction motif (reviewed in (Dodson et al., 2015; Ingham et al., 2005)).
Thus, the WW domain tandem creates a complex network of specificity and fidelity in cell signalling by providing a platform for multi-protein assembly.

2.5.2. Structure and function of the MyTH4 domain

The Myosin tail homology (MyTH4) domain has been identified in unconvential myosins, plant kinesin (Abdel-Ghany and Reddy, 2000) and in the non-motor protein PLEKHH (pleckstrin homology domain-containig family H) (Huang et al., 2002). In vertebrates it appears in tandem with a FERM (protein 4.1 - ezrin - radixin - moesin) domain (Wu et al., 2011). The MyTH4-FERM domains of unconventional myosins are assumed to have similar functions in the formation of filopodia and related structures such as microvilli and stereocilia (Bohil et al., 2006; Wu et al., 2011; Rzadzinska et al., 2004; Belyantseva et al., 2003; Berg et al., 2000).

The crystal structures of the MyTH-FERM domains of human MYO X-MF, murine Myo VII-MF

and *Dictyostelium discoideum* Myo7 show that the domain tandem organizes into a supramodular structure that is evolutionary conserved (Planelles-Herrero et al., 2016) (Fig. 2.12). Within the supramodule the relative orientations of the FERM and MyTH4 domain are limited due to tight linkage of these two domains. However, variations or sequence insertions exist that might lead to major surface remodelling and thus to functional consequences, for instance in negative or positive cooperativity to bind a target protein (Planelles-Herrero et al., 2016).
The MyTH4 domains consist of 10 helices, with six structurally conserved helices forming a right handed helical core and four more divergent helices at the periphery. The key polar residues involved in forming the inter MyTH4-FERM boundary are highly conserved between different MF domains (Wei et al., 2011).
Recent studies revealed that a positively charged patch on the MyTH4 surface facing the FERM domain of MYO X is crucial for the binding to the C-terminal tail of tubulin, which contains glutamic clusters and is thus negatively charged (Hirano et al., 2011). The interaction with microtubules is a conserved function of MyTH4 domains, even though the interaction can be mediated by different surfaces of the MyTH4 domain in evolutionarily distant MF myosins (Planelles-Herrero et al., 2016).

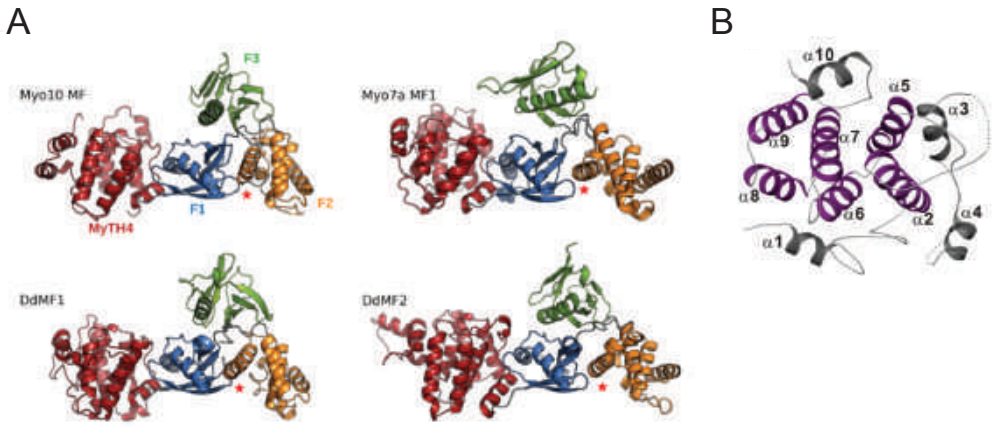

Figure 2.12.: The structure of the MyTH4-FERM domain tandem
A Ribbon diagram depicting the crystal structures of human MYO X-MF (Hirano et al., 2011), murine Myo VII-MF2 (Wu et al., 2011) and DdMyo7-MF1 and DdMyo7-MF2 that are all presented in a similar orientation (from (Planelles-Herrero et al., 2016)). **B** Ribbon diagram showing the helix bundle of the MyTH4 domain of the MyoVII-MF tandem. Conserved helices are represented in purple, divergent helices in grey. Two disordered regions in the MyTH4 domain are shown as dotted lines. (Figure adapted from (Wu et al., 2011))

2.5.3. Putative binding partners of ARHGAP39

The Rocks lab undertook a systematic characterization of all mammalian RhoGEF and RhoGAP proteins, including an analysis of their subcellular localisation, interactome and enzymatic function (BioRxiv). The binding partners were identified by immunoprecipitation of ectopically

expressed Rho regulators and subsequent mass spectrometry. ARHGAP39 was found to associate with actin nucleators, scaffold proteins, adhesion proteins and the endothelial guidance receptor ROBO4 (Fig. 2.13). Selected proteins, in addition to the previously introduced ROBO4, will be briefly presented in the following paragraph.

The Connector Enhancer of Kinase Suppressor of Ras (CNKSR) protein family, originally identified in *Drosophila*, regulates the RAS/ERK pathway at the level of RAF protein kinase (Clapéron and Therrien, 2007). CNKSR2 and CNKSR3 act as multi-domain scaffold proteins, for instance they bind to RAF, Src and Kinase Suppressor of Ras (KSR) (Lanigan et al., 2003; Ziogas et al., 2005).
The following pathway has been elucidated. In the absence of Receptor Tyrosine Kinase (RTK) signalling Raf is inhibited, but upon RTK activation, CNKSRs associates with SRC and RAS to activate RAF, which in turn activates the MEK/ERK pathway (Douziech et al., 2006; Laberge et al., 2005). Therefore, the ability of CNKSRs to regulate RAF activity in the presence/absence of RTK signalling presents a scaffold to temporally and/or spatially modulate the RAF and thus RAS/ERK signalling (Clapéron and Therrien, 2007).
Furthermore, several studies could show that the CNKSR proteins assemble regulatory proteins of different members of the Rho GTPase family namely, Ras, Rho, Rac1, Ral and Arf (Clapéron and Therrien, 2007). Thus, it can be speculated that their function in general is to provide a platform for the individual Rho GTPase and their regulatory proteins. For instance, CNKSR1 contributes to Rho-dependent (Jaffe et al., 2004) and Rac-dependent (Jaffe and Hall, 2005) c-Jun N-terminal kinase (JNK) signalling by assembling different components of theses pathways together.
While working on this project Cnksr2 was found to interact with Arhgap39 in a MS/IP screen in NG108 cells (Lim et al., 2014). Cnksr2 expression is restricted to the postsynaptic density (Ohtakara et al., 2002), where it contributes to synaptic signalling and spine formation (Lim et al., 2014). As a scaffold protein it was shown to recruit proteins involved in Rac signalling, including α-Pix and β-Pix, Git1/2 and Pak3/4 and also Arhgap39 (Vilse) (Lim et al., 2014). Thus, it may act as a spatial modulator of Rac cycling during spine morphogenesis.

PEAK1 (Pseudopodium-enriched atypical kinase 1) was discovered as a cytoskeleton-associated kinase and belongs to the family of non-receptor atypical tyrosine kinases. It localises at actin filaments and focal adhesions, as it was shown to co-localize with Vinculin and Paxillin (Wang et al., 2010). Expression levels of PEAK1 regulate cell spreading and migration, presumingly by modulating focal adhesion dynamics, as it was observed that ectopic expression of PEAK1 leads to increased focal adhesion length (Wang et al., 2010). Moreover, correct assembly and disassembly of focal adhesions depends on the correct phosphorylation status of PEAK1 (Bristow et al., 2013).

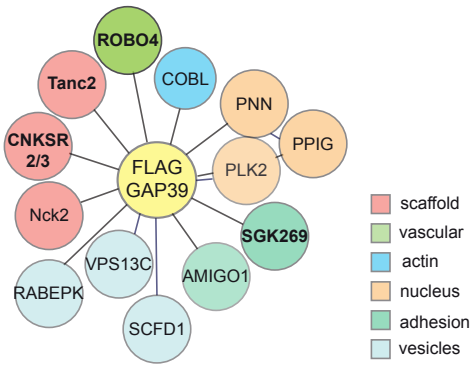

Figure 2.13.: Hairball diagram of predicted interaction partners of ARHGAP39
The different proteins were identified in a co-immunoprecipitation/mass spectrometry (Co-IP/MS) screen with over-expressed Flag-ARHGAP39 as bait in HEK 293T cells. They can be divided into different groups according to their function indicated by different colors. ROBO4: (Magic) roundabout receptor 4; CNKSR2/3: Connector enhancer of kinase suppressor of Ras 2/3; TANC2: tetratricopeptide repeat, ankyrin repeat and coiled-coil containing 2; NCK2: NCK adaptor protein 2; PEAK1: Pseudopodium enriched atypical kinase 1; AMIGO1: adhesion molecule with Ig-like domain 1; PNN: Pinin, 140 kDa nuclear and cell adhesion-related phosphoprotein, Desmosome-associated protein; PPIG:Peptidyl-prolyl cis-trans isomerase G; PLK2: Serine/threonine-protein kinase Polo-like kinase 2; RABEPK: Rab9 effector protein with kelch motifs; VPS13C: Vacuolar protein sorting-associated protein 13C; SCFD1: Sec1 family domain-containing protein 1; COBL: Cordon-bleu

TANC2 (tetratricopeptide repeat, ankyrin repeat and coiled-coil domain-containing protein 2) is a 220 kDa protein that localises in dendritic spines at the post synaptic scaffold together with PSD-95/SAP90 (postsynaptic density-95/synapse-associated protein 90). It encodes several protein-protein interaction domains, including ankyrin repeats, tetratricopeptide repeats (TPRs), and a C-terminal PDZ domain-binding (PB) motif. TANC2 is widely expressed in mouse brain and its overexpression increases dendritic spine density, hence has a positive effect on excitatory synapses (Han et al., 2010).

3. Objective

The previously uncharacterized human RhoGAP ARHGAP39 was identified in a preceding systematic proteomics analysis of all 145 RhoGEFs and RhoGAPs to bind to the ROBO4 guidance receptor (Müller et al., BioRxiv). How ROBO receptors signal to the cytoskeleton to elicit repulsive cell migration is only poorly understood. While for the neuronal ROBO1-3 receptors Rho regulatory proteins have been characterized no such regulators are known for the endothelial-specific ROBO4 receptor. Because of the previously genetic and biochemical interaction of its homologue Vilse/Crossgap with Robo in *Drosophila melanogaster* ARHGAP39 was a good candidate to link all human ROBO receptors including ROBO4 to RhoGTPase signalling and thus to the control of guided cell migration both in neuronal development and angiogenesis.

Therefore, this project aimed to functionally characterize ARHGAP39 and to investigate its function in cell migration, including the following goals:

To characterise the enzymatic activity and substrate specificity of ARHGAP39.
To assess its subcellular localisation and identify potential targeting information.
To investigate if the catalytic GAP function of ARHGAP39 is subject to autoregulation and, if so, to resolve the underlying mechanism.
To analyse the interaction of ARHGAP39 with the ROBO receptors and other binding partners and to detail the binding mechanisms.
To study the role of ARHGAP39 in cell migration, and, specifically, in SLIT2/ROBO signalling-dependent migration.
To investigate *in vivo* in the zebrafish embryo the effect of *arhgap39* knockdown on the migration of the intersomitic vessels during angiogenesis.

4. Materials and Methods

4.1. Materials

4.1.1. Chemicals and Equipment

Table 4.1.: Table of chemicals and consumables/equipment

chemical	company
Acetic anhydride	Sigma, Germany
30 % (w/v) Acrylamide/bisacrylamide (37.5/1)	Roth GmbH, Germany
Agar-Agar, granulated	EMD Chemicals, USA
Agarose	Roth GmbH, Germany
Ammonium persulfate (APS)	Sigma-Aldrich, Germany
Ampicillin sodium salt	Sigma-Aldrich, Germany
Bovine Serum Albumin (BSA) powder	Sigma-Aldrich, Germany
BSA 100x stock solution	New England BioLabs, USA
Bromophenol Blue	Sigma-Aldrich, Germany
Chloramphenicol water soluble	Sigma-Aldrich, Germany
Chloroform	Sigma-Aldrich, Germany
cOmplete Protease Inhibitor Cocktail Tablets	Roche Diagnostics, Germany
Coomassie Brilliant Blue R-250	Thermo Scientififc
Dimethyl sulphoxide (DMSO)	Sigma-Aldrich, Germany
Dithiothreitol (DTT)	Gerbu Biotechnik, Germany
Dry milk powder	Roth GmbH, Germany
Ethanol	Sigma-Aldrich, Germany
Ethidium bromide solution 1 %	Roth GmbH, Germany
Ethylenediaminetetraacetic acid (EDTA)	Sigma-Aldrich, Germany
Ficoll	
Formamide	Sigma-Aldrich, Germany
Glycerol	Roth GmbH, Germany
Glycine	Roth GmbH, Germany
Glycogen	
Goat serum	Sigma-Aldrich, Germany
Hydrochloric Acid	Sigma, Germany
Isopropanol	Roth GmbH, Germany
Kanamycin sulfate	Sigma-Aldrich, Germany
Malic Acid	
Methanol	Roth GmbH, Germany
2-Mercaptoethanol	Sigma-Aldrich, Germany
Nuclease free water	Ambion, USA
Papanicolaou?s solution 2a Orange G	Merck Millipore, Germany

Paraformaldehyde (PFA)	Sigma-Aldrich, Germany
D(+)-Saccharose (Sucrose)	Roth GmbH, Germany
Salmon Sperm DNA	Applied Chemistry
Sigmacote	Sigma-Aldrich, Germany
Sodium chloride (NaCl)	Roth GmbH, Germany
Sodium dodecyl sulfate (SDS)	Roth GmbH, Germany
Sodium hydroxide (NaOH)	
Sodium-Sodium Citrate (SSC), 20x	Roth, Germany
Spectinomycin	LKT
Tetramethylethylendiamin (TEMED)	Roth GmbH, Germany
Tris	Roth GmbH, Germany
Triethanolamine	Sigma-Aldrich, Germany
Triton X-100	Sigma-Aldrich, Germany
Trypan blue solution 0.4 %	Sigma-Aldrich, Germany
consumable/equipment	**company**
Amicon Ultra-15, 100 kDa	Amicon Ultra
CELLview glass bottom dishes, 4 compartments (35mm)	Greiner Bio-One, Austria
Costar flat bottom cell culture plates (24, 12, and 6 well)	Corning, USA
coverslips round 19 mm	VWR, Germany
Falcon centrifuge eppendorf tubes, polypropylene, sterile	Corning, USA
MatTek glass bottom culture dishes (35 mm)	MatTekCorp., USA
Microscopy slides SuperFrost Plus	Thermo Scientific, USA
Tissue culture dishes, polystyrene, sterile (100 mm, 60 mm)	Corning, USA
Transwell Unit, PET membrane clear inserts, 8 µm pore size	Corning-Costar

4.1.2. Antibodies

Table 4.2.: Table of primary and secondary antibodies

antibody	clone/order number	species	WB	IF	IP
ARHGAP39/KIAA1688	Bethyl A302-598	rabbit	1:500	-	4 µg
FLAG	Sigma-Aldrich M2/ F1804	mouse	1:5000	1:500	-
FLAG M2 affinity gel	Sigma-Aldrich A2220	mouse	-	-	20 µl
GFP	abcam ab290	rabbit	1:10000	1:1000	0.5 µl
GFP	abcam ab13970	chicken	1:10000	1:1000	-
GST	CST 26H1	mouse	1:1500	-	-
normal IgG control	Santa Cruz sc-2027	rabbit	-	-	1 µl
Tubulin	Sigma-Aldrich DM1a, T6199	mouse	1:5000	1:500	-
Phalloidin-594	Biotium CF594	-	1:200	-	-
anti-rabbit IgG H+L (Alexa Fluor 488)	Molecular Probes	goat	-	1:1000	-
anti-mouse IgG H+L (Alexa Fluor 647)	Molecular Probes	goat	-	1:1000	-
anti-rabbit HRP coupled	BioRad	goat	1:10000	-	-
anti-mouse HRP coupled	BioRad	goat	1:10000	-	-
anti-chicken HRP coupled	BioRad	goat	1:10000	-	-

WB: Western Blot, IF: Immunofluorescence, IP: Immunoprecipitation. Anti-GFP antibodies recognize YFP, CFP and GFP fluorophores.

4.1.3. DNA constructs

The full length (FL) cDNA of proteins used in this thesis have been assembled by Dr. Oliver Rocks and were kind gifts of the Tony Pawson lab, Samuel Lunenfeld Research Institute (SLRI), Toronto. If not otherwise stated, cDNAs were available as entry clones of the Gateway or donor plasmids of the Creator system. MENA was a kind gift from Akihiro Toyoda, PAXILLIN (HsCD00292821) was purchased from Harvard Medical School (DF/HCC) and zfAhrgap39 was cloned from zebrafish cDNA.

Most fluorescence and FLAG-tag expression constructs were created by recombinatorial Creator and Gateway cloning or required In-Fusion cloning to be introduced in the Creator/Gateway recombination system. Gateway and Creator destination vectors (expression vectors) of Table 4.3 were gifts of the Tony Pawson lab, except for Gateway Cherry/C-terminal from Erich Wanker (MDC) and Gateway Venus/triple Flag C-terminal purchased from addgene (addgene 40999). The vascular specific Gateway expression plasmids pTol*fli1ep:egfp*Dest and pTol*fli1-ep:cherry*Dest were a kind gifts from Ferdinand le Noble (KIT, Karlsruhe). Also the plasmids pCS2+ for *in vitro* RNA synthesis and the Gateway entry plasmid pCR8/GW/TOPO (Invitrogen) were provided by the le Noble lab. The pGEM-T Easy vector was purchased form Promega.

Table 4.3.: Creator and Gateway destination vectors

cloning system	clone number	acceptor plasmid backbone	tag orientation
Creator	v180	triple Flag	N-term
Creator	v3534	Citrine	N-term
Creator	v3535	Cherry	N-term
Creator	v4999	Citrine	C-term
Gateway	v4872	Cherry	N-term
Gateway	v4874	Venus	N-term
Gateway	v4978	triple Flag	N-term
Gateway	v4869	triple Flag	C-term
Gateway	40999	Venus/triple Flag	C-term
Gateway	-	Cherry	C-term
Gateway	pTol*fli1ep:egfp*DEST [1]	EGFP	N-term
Gateway	pTol*fli1ep:cherry*DEST [1]	Cherry	N-term

vascular specifc expression.

Table 4.4.: Creator and Gateway expression vectors

construct name	tag / orientation	species	vector backbone
Cit-ARHGAP39 iso1	Citrine / N-term	human	Creator

Cit-ARHGAP39 iso2	Citrine / N-term	human	Creator
Flag-ARHGAP39	triple Flag / N-term	human	Creator
ARHGAP39-Cit	Citrine / C-term	human	Creator
Cherry-ARHGAP39	Cherry / N-term	human	Creator
Cit-Arhgap39	Citrine / N-term	zebrafish	Creator
ROBO1-Flag	triple Flag / C-term	human	Gateway
ROBO1-Venus/Flag [1)]	Venus/Flag / C-term	human	Gateway
ROBO1-Cherry	Cherry / C-term	human	Gateway
ROBO2-Flag	triple Flag / C-term	human	Creator
ROBO3-Flag	triple Flag / C-term	human	Gateway
ROBO4-Flag	triple Flag / C-term	human	Gateway
ROBO4-Venus/Flag [1)]	Venus/Flag / C-term	human	Gateway
SLIT2-Cherry	mCherry / C-term	human	Gateway
SLIT2-Venus/Flag	Venus/Flag / C-term	human	Gateway
Cit-CNKSR2 iso2	Citrine / N-term	human	Creator
Flag-CNKSR2 iso2	triple Flag / N-term	human	Creator
Cit-CNKSR3	Citrine / N-term	human	Creator
Flag-TANC2	triple Flag / N-term	human	Creator
Cit-PEAK	Citrine / N-term	human	Creator
Flag-PAXILLIN	triple Flag / N-term	human	Gateway
Flag-MENA	triple Flag / N-term	human	p3xFLAG-CMV
Cit-Cherry [2)]	Citrine / Cherry	-	Creator
Flag-Cherry [2)]	Citrine / Cherry	-	Creator

[1)] plasmids used for microscopy

[2)] control plasmids for IPs

The primers used for QuikChange mutagenesis or In-Fusion HD cloning are shown in Table A.1 and Table A.2, respectively (Appendix). Primer sequences are depicted in 5' to 3' orientation. The deletion and truncation constructs of ARHGAP39 were created from isoform2. Primers used for sequencing or standard PCR-based cloning are summarized in Table A.3 (Appendix).

4.1.4. Small synthesized oligomers

Table 4.5.: Sequences of small synthesized oligomers

species	type	target gene	sequence
human	shRNA virus B4	ARHGAP39	CCACCGTGTATAGAGATATAA
human	shRNA virus B5		CCTGGAAAGAAACACTAAGAA
human	shRNA virus B6		CTATGAGATTTACCGGGATTA
human	shRNA virus B7		TCCCGCTTCTACTACTACAAT
human	shRNA virus C8		GAAGAGCAGAAAGCCCTCTTT
zebrafish	morpholino oligomer 1	Arhgap39	CCACCCATTCCAACCTCTCCGCCAT
zebrafish	morpholino oligomer 2		AGATGCGGATGGTGTTTACCTCTCC

4.1.5. Primers for *in situ* hybridization probes

Table 4.6.: Primers to generate *in situ* hybdridization probes

species	targeting transcript	sequence	vector
zebrafish	Arhgap39	Fw: ATGGCGGAGAGGTTGGAATGGGTG Rv: TGGTTTTCGTGCCGGAGAACGATC	pGEM T Easy
mouse	Arhgap39	Fw: GTATGTGGAGCAAGCAGGCTC Rv: GCATTTAGATACCAGCTTCATG	pGEM T Easy

4.1.6. Buffers Biochemistry

Table 4.7 shows recipes of buffers that were prepared in this thesis. PBS and PBS with Ca^{2+} and Mg^{2+} (PBS^{++}) were commercially available (Dulbecco's Phosphate-Buffered Saline (DPBS), Corning).

Table 4.7.: Composition of buffers

Name	Composition
Coomassie Staining solution	0.1 % Coomassie Brilliant Blue R-250, 50 % Methanol and 10 % Glacial acetic acid
Coomassie Destaining solution	40 % Methanol, 10 %G Acetic Acid
NP40 lysis buffer	1 % NP40, 50 mM Tris-HCL pH 8, 150 mM NaCl
Permeabilization buffer	0.2 % Triton X-100, 100 mM Glycine in PBS
SDS running buffer	192 mM Glycine, 25 mM Tris, 0.1 % SDS, pH 8.3
SDS sample buffer 6x	375 mM Tris-HCl pH 6.8, 300 mM DTT, 12 % SDS, 60% Glycerol, 0.06 % Bromophenol Blue, 20 % 2-Mercaptoethanol
Stripping buffer	100 mM 2-Mercaptoethanol, 2 % SDS, 62.5 mM Tris-HCl, pH 6.7
TBST	50 mM Tris, 150 mM NaCl, 0.1 % Tween 20, pH 7.4
Wet Transfer buffer	192 mM Glycine, 25 mM Tris, 20 % Methanol, pH 8.3
6x Orange G loading buffer	50% Glycerol, 25 mM EDTA, 0.5 % Orange G
TAE	40 mM Tris, 20 mM Acetic Acid, 1 mM EDTA, pH 8
TE	10 mM Tris-HCl, 1 mM EDTA, pH 8.0
E3 buffer for zebrafish	5 mM NaCl, 0.17 mM KCl, 0.33 mM CaCl2, 0.33 mM $MgSO_4$
anesthesation buffer	0.16 mg/ml Tricaine /1 % 1-Phenyl-2-Thiourea in E3 buffer

4.1.7. SDS-PAGE gels

Table 4.8.: Composition of SDS-PAGE's

Gel	Composition
Resolving gel	7.5, 10 or 12 % (w/v) Acrylamide/bisacrylamide (37.5/1), 0.1 % (w/v) SDS, 0.1 % (w/v) APS and 0.1 % (w/v) TEMED in 375 mM Tris-HCl (pH 8.8)
Stacking gel	4 % (w/v) Acrylamide/bisacrylamide (37.5/1), 0.1 % (w/v) SDS, 0.1 % (w/v) APS and 0.1 % (w/v) TEMED in 125 mM Tris-HCl (pH 6.8)

4.1.8. Buffers for *in situ* hybridization

Table 4.9.: Ingredients used for *in situ* hybridization buffer

	Name	Composition
cryosections	Acetylation buffer	2 ml Triethanolamine, 0.25 ml 37 % HCl, 0.375 ml Acetic Anhydride, ddH_2O to 150ml
	B1 buffer	0.1 M Tris pH 7.5, 0.15 M NaCl
	Blocking solution	10 % Goat serum in B1 buffer
	Denhart's 50X	5g Ficoll, 5g Polyvinylpyrolidone, 5g BSA, 500 ml ddH_2O (sterile filter)
	Hybridization Buffer	50 % Formamide , 5x SSC pH 5, 5x Denhart's, 150 µg/ml Yeast tRNA, 150 µg/ml Sperm DNA
	In situ staining solution	1 µl NBT/1 ml, 1 µl BCIP/1 ml in NTMT
	NTMT	0.1 M Tris-HCl 1M pH 9.5, 0.1 M NaCl 5M, 0.1 % M Tween 20, 50 mM MgCl
	PBT	100 ml 10x PBS, 10ml 10 % Tween 20
	10 % Tween 20	10ml Tween 20 in 100ml ddH_2O
zf embryos	Boehringer Blocking Reagent	10 % Boehringer Blocking Reagent in MAB
	Hybridization Buffer	50 % Formamide , 5x SSC pH 5, 0.1 % Tween 20, 4.6 mM Citric Acid, 100 µg/ml Yeast tRNA, 50 µ/ml Heparin
	Pre-Hybridization Buffer	50 % Formamide , 5x SSC pH 5, 0.1 % Tween 20, 4.6 mM Citric Acid
	5x MAB (Maleic acid buffer)	58g Malic Acid, 43.5g NaCl, 37.5g NaOH, ddH_2O to 1l, pH 7.5
	MAB-T	1 % Tween 20
	NTMT	0.1 M Tris-HCl 1M pH 9.5, 0.1 M NaCl 5M, 1 % M Tween 20, 50 mM MgCl
	PBT	100 ml 10x PBS, 10ml 10 % Tween 20
	RNAse Buffer	0.1 M Hepes 1M pH 7.5, 0.15 M NaCl, 0.1 % Tween 20

4.1.9. Bacterial strains of *Escherichia coli*

Table 4.10.: *E. coli* strains used in this thesis

E. coli DH5α	F-endA1 glnV44 thi-1 recA1 relA1 gyrA96 deoR nupG φ80dlacZ15 Δ(lacZYA-argF)U169, hsdR17(rK- mK+), λ-
XL10-Gold Ultracompetent Cells	endA1 glnV44 recA1 thi-1 gyrA96 relA1 lac I Δ(mcrA)183 Δ(mcrCB-hsdSMR-mrr)173 tetR F'[proAB lacIqZΔM15 Tn10(TetR Amy CmR)]

4.1.10. Bacterial growth media and agar plates

Table 4.11.: Recipes for bacterial growth media and agar plates

Name	Recipe
LB medium	1 % (w/v) Bacto-Tryptone, 0.5 % (w/v) Yeast extract, 0.5 % (w/v) NaCl
LB agar plates	1.5 % (w/v) agar, 1 % (w/v) Bacto-Tryptone, 0.5 % (w/v)Y extract, 0.5 % (w/v) NaCl, 100 µg/ml Ampicillin or 50 µg/ml Kanamycin or 150 µg/mlSpectinomycin
Sucrose agar plates	1.5 % (w/v) Agar, 7 % (w/v) Sucrose, 1 % (w/v) Bacto-Tryptone, 0.5 % (w/v) Yeast extract, 0.5 % (w/v) NaCl, 30 µg/ml Chloramphenicol

4.1.11. Cell culture media and additives

Dulbecco's Modified Eagle Medium (DMEM)	Gibco, USA
Minimum Essential Medium (MEM)	GE Healthcare, UK
OptiMEM Reduced Serum Medium with GlutaMAX	Gibco, USA
Trypsin/EDTA	Sigma-Aldrich, Germany
Penicillin-Streptomycin (P/S) (10,000 U/mL)	Gibco, USA
Fetal Bovine Serum Albumin (FBS)	Biochrome, Germany

4.2. Molecular Biology

4.2.1. Transformation

Unless otherwise indicated, 100 µl DH5α were briefly thawed on ice before addition of plasmid (20-50 ng) or reaction to be transformed. Bacteria were incubated for 30 min on ice, before heat shock at 42 °C for 45 s. After 2 min on ice, 500 µl of LB medium and 20 mM Glucose was added. Subsequently, bacteria were shaken for 1 h at 37 °C before plating on LB agar plates with the required antibiotic, then left to form colonies overnight at 37 °C. XL10-Gold Ultracompetent Cells were transformed according to manufacturer's instructions.

4.2.2. Plasmid DNA Purification

For Minipreps single colonies were picked from LB agar plates and grown in 5 ml LB medium in presence of the required selection antibiotic overnight at 37 °C shaking. The DNA was purified from pelleted bacteria using the Zymogen Research ZR Plasmid Miniprep Classic kit (D4054), according to manufacturer's instructions. When more DNA was required, Midipreps were performed from 100 ml of bacterial culture, using the Invitrogen Midi kit (K210005). DNA concentrations were then measured using 1 µl of DNA with a NanoDrop 1000 Spectrophotometer (Thermo Scientific, USA).

4.2.3. Glycerol Stock

Glycerol stocks were prepared from the same cultures as those for Minipreps. 700 µl bacteria in LB media was combined with 300 µl glycerol, thoroughly mixed and frozen at -80 °C.

4.2.4. Agarose gel electrophoresis

Agarose gels of 0.8-2 % were prepared by dissolving agarose in TAE. DNA samples were mixed with 6x Orange G loading buffer and then loaded into the gel. The 1 kb DNA Ladder (New England BioLabs, USA) was used as a marker. After running the agarose gels in TAE buffer, they were incubated in an Ethidium bromide bath (0.025 mg/ml) and subsequently visualized under UV light using a transilluminator gel documentation device. For gel extractions, the DNA was excised with a scalpel and purified using the microcentrifuge protocol of the QIAquick Gel Extraction Kit (Qiagen, Germany).

4.2.5. Polymerase chain reaction

Polymerase chain reaction (PCR) was used to amplify selected sequences of DNA during subcloning. Standard PCR reactions were performed using Phusion High-Fidelity DNA Polymerase (New England BioLabs, USA) in a 50 µl reaction that was prepared as shown in Table 4.12. All components were mixed on ice and cycling conditions were chosen as depicted in Table 4.12, bottom part

Additional, PCR was used to verify the presence of a gene of interest after cloning and transformation into bacteria by performing colony-PCR. Here, instead of template DNA a small bit of bacteria from bacterial colonies on agar plates were added to the 50 µl reaction. To the cycling an initial start phase of 5 min at 95 °C was added to break down the bacteria.

Table 4.12.: Standard Polymerase Chain Reaction

Component	Amount
5x Phusion GC Buffer	10 µl
dNTP Mix 10 mM	1 µl
DNA template	10 ? 20 ng
10 µM primer 1 Forward	2.5 µl
10 µM primer 2 Reverse	2.5 µl
DMSO (optional)	1 µl
nuclease free ddH_2O	to 50 µl
Phusion DNA Polymerase	0.5 µl
Total	50 µl

Cycle	Temperature	Time
1x	98 C	60 sec
35x	98 C	10 sec
	65-72 C	30 sec
	72 C	30 sec per kb
1x	72 C	5 min

4.2.6. Gateway recombination

The Gateway system enables recombination of DNA sequences between the Gateway- cassettes, which occurs either between the attB/attP sites or attL/attR sites to create Gateway Entry or Gateway Destination vectors, respectively. Most of the Gateway Entry plasmids used in this study were gifts from the Tony Pawson Lab. The sequences of ROBO1, ROBO4 and PXN had to be introduced into the Entry vector via the respective PCR products containing attB sites to recombine with the attP sites of the Entry vector during BP Clonase reaction. To obtain expression plasmids of a gene of interest LR Clonase reactions were performed to shuffle the gene of interest between the Gateway Entry and Destination plasmids. Both, the Gateway BP Clonase Enzyme Mix and the Gateway LR Clonase II Enzyme Mix (Invitrogen, USA) were carried out following the manufacturer's instructions. Gateway Destination vectors used in this study are listed in Table 4.3.

4.2.7. Creator Recombination

Donor clones with cDNAs of ARHGAP39 and other genes were available as donor plasmids of the Creator recombination system (Tony Pawson lab, Toronto). Subcloning into acceptor expression plasmids with the different epitope tags was then done by Creator recombination

that was described previously (Colwill et al., 2006). The acceptor vectors used are listed in Table 4.3 and the components of the reaction and their amounts used are shown below.

Component	Amount
Donor Plasmid	500 ng
Acceptor Plasmid	500 ng
BSA	1 µl
Cre 10x Buffer	1 µl
Cre Enzyme	0.5 µl
ddH_2O up to	10 µl
Total	10 µl

The reaction was pipetted at room temperature (RT) and incubated for 15 min before heat inactivation of the Cre enzyme for 10 min at 70 °C. After cooling the total reaction was transformed into DH5α and plated onto sucrose chloramphenicol plates. If possible three colonies were picked to be screened. Colonies were then grown overnight in approximately 5 ml LB media containing kanamycin. Purified DNA was digested at 37 °C for 1 h with the restriction enzymes AscI and PacI (New England Biolabs), to cut out the insert from the backbone. Resulting fragments were then assessed by agarose gel electrophoresis. Where necessary clones were sequenced by Source Bioscience with primers O19 and O20.

4.2.8. Site-directed mutagenesis

Subsequent point mutation and deletion/truncation constructs were created by site-directed mutagenesis using the QuikChange II XL kit (Agilent Technologies, USA), following manufacturer's guidelines by using the Pfu polymerase. After PCR reaction the amplified product was incubated with Dpn1 at 37 °C for 4 h, digesting methylated template DNA, leaving the newly made unmethylated mutant DNA. Part of the reaction was transformed into XL10 Gold bacteria according to protocol (Invitrogen).

4.2.9. In-Fusion HD cloning

The In-Fusion Cloning technology (Clontech) is the recombination of DNA fragments with a 15 bp overlap at their ends into any linearized vectors containing the complementary 15 bp at the ends. The advantages are that no restriction digestion, phosphatase treatment, or ligation are required during the cloning process. In-Fusion cloning was performed to obtain ROBO1, ROBO4, SLIT2 and zfARHGAP39 Gateway Entry plasmids and ROBO2 Creator Donor plasmid (see Table 4.4).

According to the manufacturer's protocol gene specific primers were designed with a 15 bp overlap at their ends being complementary to the ends of the linearized vector. Therefore,

the vectors were cut with the required restriction enzyme(s), run on a 0.8 % agarose gel and purified from the gel using the QIAquick Gel Extraction Kit (Qiagen, Germany). Primers for PCR-based amplification of the insert with containing the overlap were designed using the online tool provided by Clontech (at http://bioinfo.clontech.com/infusion/). Phusion polymerase was used for standard PCR to amplify the insert. Part of the PCR product was run on a 0.8 % agarose gel to check its purity and the rest was spin-column purified (Thermo Scientific). Finally, the In-Fusion reaction was pipetted containing the linearized vector, the amplified insert, the In-Fusion enzyme mix and water up to 10 µl. The reaction was incubated for 15 min at 50 ℃ and transformed into XL10 Gold Ultracompetent cells (Agilent) following manufacturer's instruction. Grown colonies on agar plates were tested via colony-PCR.

4.2.10. RNA isolation

Samples for RNA isolation were either whole zebrafish embryos, FACS-isolated endothelial cells of zebrafish embryos or cultured cell lines. To isolate RNA from cells, they were collected in TRIzol reagent (Ambion) according to manufacturer's guidelines. After 5 min of incubation at RT Chloroform was added to the samples, vigorously shaked and centrifuged for 15 min at max. speed at 4 C. The upper phase was transferred into a new eppendorf tube, to which ice cold isopropanol was added. The samples were incubated for 10 min at RT and centrifuged for 10 min at max. speed at 4 C. The RNA pellet was then washed with 75 % ethanol and centrifuged for 5 min at 7.500 g at 4 C. The obtained pellet was then air-dried for 15 min and dissolved in 30 µl of RNAse-free ddH_2O while incubating in a heat block set at 55-60 ℃ for 10-15 minutes. The integrity of the isolated RNA was tested on a 2 % agarose gel and then stored at -70 ℃.
Differences in the RNA isolation protocol for the collected fish embryos were that they were resuspended in 800 µl of TRIzol. Then 200 µg glycogen was added as a carrier molecule to increase the RNA yield. Subsequently, 160 µl Chlorofom was added, vigorously shaked and centrifuged for 15 min at max. speed at 4 C. After phase separation, 400 µl isopropanol was added to the upper phase and incubated for 1 h at -20 ℃. The last steps are identical to the procedure for harvested cells described before.

4.2.11. cDNA synthesis

First strand cDNA was synthesized using RevertAid First Strand cDNA Synthesis Kit (Thermo Scientific) following the manufacturer's guidelines. Oligo (dT)18 primer were used for human RNA, random hexamer primer were added to samples of zebrafish RNA. The reagents RNase free water, template RNA, primer, 5x Reaction Buffer, RNase Inhibitor, dNTP Mix and Revert Aid M-MuIV Reverse Transcriptase were pipetted in the order suggested by the manufacturer. Negative controls contained the same reagents, but the Reverse transcriptase was missing.

4.2.12. Quantitative Real Time PCR

Quantitative real time PCR (qRT-PCR) was performed differently for detection of ARHGAP39 mRNA in human cell lines or in zebrafish tissue. For human cell lines 2x Absolute qPCR SYBR Green Mix (Thermo Scientific) was used according to manufacturer's conditions, using 0.5 µM of primers and 100 ng of cDNA. A three step cycling protocol was chosen, following the guidelines of the manual by using a Bio-Rad C1000 Thermal Cycler to amplify cDNA fragments and the Bio-Rad iQ software to analyse the melting curves. Obtained data of gene expression were normalized against *GAPDH*.
cDNA from zebrafish was subjected to the TaqMan Gene Expression Assay (Applied Biosystems) following the manufacturer's protocol. 25 ng of cDNA and 100 pmol/ µl of each Arhgap39 primer and FAM-5'-Arhgap39-3'-TARA probe were added to the TaqMan Master Mix. Primer probe sets (FAM and TAMRA labels) were obtained from BioTez (Berlin Germany). Amplification was carried out using an ABI Prism 7000 thermocycler (Applied Biosystems), running the PCR cycle 50 times. Gene expression data were normalized against *elongation factor 1-*α (*EF1-*α).

4.2.13. DNA amplification for generation of riboprobes for *in situ* hybridization

Specific DNA fragments of mouse and zebrafish Arhgap39 were amplified from E12.5 or 72 hpf whole embryo cDNA, respectively. Murine cDNA was provided from Dr. Ines Lahmann (Birchmeier lab, MDC), zebrafish cDNA was provided from Katja Meier (Gerhardt lab, MDC). For amplification the Taq polymerase (Thermo Fisher) was used according to the manufacturer's guidlines including 0.5 µM of primers, 200 µM of dNTPs, 1 µl of cDNA and 1 U of Taq polymerase. Cycling parameters were identical to Table x. The purified PCR products (QIAquick Gel Extraction Kit) were cloned into pGEM-T Easy plasmid using T4 DNA ligase (Promega). After transformation into XL10 Gold Ultracompetent cells colonies were applied to colony-PCR to check if the cDNA was inserted into the plasmid. The enzyme SacII was used to linearize 10 µg of plasmid containing the msArhgap39 or zfArhgap39 fragment for 4 h at 37 °C. In vitro transcription of the antisense probe was performed using DIG-RNA labeling kit (Roche) to transcribe 500ng of plasmid for 2h at 37 °C. Labeled cDNA was then purified using RNeasy clean-up kit (Qiagen) and eluted in 50 µl ddH_2O. The probes were stored in 50 % formamide at -80 °C.

4.2.14. Preparation of frozen sections

Frozen mouse embryos were cut in approximately 16 µm thick slices for *in situ* hybridization on a cryostat (Microtom HM560, Walldorf). The sections were collected on glass slides (Marienfeld) and dried for 2h at 37 °C. The slides were stored at -80 °C.

4.2.15. *In situ* hybridization of cryosections

In situ hybridization of cryosections was performed in collaboration with Maciej Czajkowski. Cryosections were postfixed in cold 4 % PFA for 10 min and washed 3 times in PBS. The slides were incubated for 10 min in acetylation buffer, washed 3 times in PBS and prehybridized for 2h at RT in hybridization buffer. The DIG-labeled probes were diluted in hybridization buffer (1µl probe per 100 µl) and denatured for 5 min at 80 ℃ before adding it onto the slides and covering it with Sigmacote (Sigma) coated coverslips coverslips. The hybridization was carried out overnight at 65 ℃ in a humidified chamber. Washing of the slides followed in 5x SSC for 5 min, then in 0.2x SSC for 1h at 70 ℃, followed by 5 min in 0.2x SSC and 5 min in B1 buffer at RT. After incubation with blocking solution for 1h at RT, the slides were then incubated overnight at 4 ℃ with AP-conjugated anti-DIG Fab fragments (Roche) diluted 1:2000 in blocking solution. The next day, the slides were washed three times for 5 min in B1 buffer and one time with NTMT. Then they were incubated at RT in *in situ* staining solution containing NBT (Roche) and BCIP (Roche). After the signal was detected, the reaction was stopped by washes in ddH_2O. The slides were air dried and covered with Shandon Immu-Mount (Thermo Scientific). Images of cryosections were captured using the automated stitching function of the Keyence Fluorescence Microscope BZ-X.

4.2.16. *In situ* hybridization of zebrafish embryos

Zebrafish embryos were dechorinated (removal of the chorion) and then fixed in 4 % PFA for 2 h at RT. After washing three times in PBT they were dehydrated in PBT containing increasing concentrations of MeOH (from 25 %, 50 %, 75 % to 100 %), each step for 5 min at RT and then stored at -20 ℃.

The next day animals were re-hydrated in PBT containing decreasing amounts of MeOH (from 100 % to 25 %) and washed three times in PBT, each step for 5 min at RT. Subsequently, embryos were treated with Proteinase K (10 µg/ml in PBT) at RT for 8 min. The fish were then washed three times in PBT for 10 min and fixed again in 4 % PFA for 20 min, followed by three more washes in PBT for 5min, all steps were performed at RT. The animals were incubated with Pre-hybridization mix (Hybridization mix without heparin and tRNA) for 1 h at 65 ℃ in a humidified chamber. Before hybridization, the probes were denatured for 5 min at 95 ℃, using 500 ng of probe in 500 µl of Hybridization buffer. The Hybridization mix was pre-warmed to 65 ℃, then added to the embryos together with the probes and incubated together over night at 65 ℃ in a humidified chamber.

The following day embryos were washed in Pre-Hybridization mix with increasing concentrations of 2x SSC buffer (from 0 %, 25 %, 50 %, 75 % to 100 %), each washing step was performed for 5 min at 65 ℃ in a humidified chamber. Next, the animals were incubated with 0.2x SSC buffer for 5 min at 65 ℃, followed by 15 min at RT. RNAse digestion followed by

treating the fish with RNase buffer for 5 min at RT before addition of 150 µl of RNAse (stock 10 mg/ml) to 15 ml of RNAse buffer and incubation for 45 min at RT. The fish were then washed twice in MAB-T buffer for 5 min at RT and blocked in 2 % Boehringer Blocking reagent in MAB-T buffer for a minimum of 1 h at RT. The antibody diluted 1:4000 in 2 % Boehringer Blocking reagent/MAB-T (1 ml) was added to the fish and incubated over night at 4 °C while shaking. The next day, the embryos were transferred into new Falcon tubes and washed four times in MAB-T buffer for 30 min at RT. After transferring them into 24 well plates, they were washed twice for 15 min in NTMT buffer at RT and then incubated with BM Purple staining solution (Sigma, Germany) at 65 °C in a humidified chamber and afterwards at 4 °C for varying time points. To stop the reaction the animals were washed twice in NTMT buffer. They were further washed twice in PBT for 5 min at RT and incubated in 70 % EtOH for 1 h at RT. To store them, the embryos were incubated with increasing concentrations of glycerol in PBT (from 20 %, 40 %, 60 % to 80 %), each step for 20 min at RT. Th emebryos were imaged using a Zeiss intravital microscopy (Zeiss Axioscope A1, Carl Zeiss MicroImaging, Jena, Germany) with a 20x (N.A.0.50) water-emersion objective.

4.3. Biochemistry

4.3.1. Cell Lysis

The preparation of protein samples was carried out on ice at all times. Cells were washed in ice cold PBS with Ca^{2+} and Mg^{2+} (PBS^{++}) once and resuspended in 5 ml PBS^{++}. As HEK293T cells easily detach they were harvested by merely pipetting up and down in PBS^{++}. HeLa cell were scraped directly into PBS^{++} with a cell scraper (Nunc, USA). Cells were then pelleted by centrifugation at 400 RCF for 5 min at 4 °C. After aspiration of the supernatant the cells were resuspended in NP40 lysis buffer with cOmplete Protease Inhibitor and incubated 10-15 min on ice. Lysates were then cleared by spinning at 18,000 RCF for 5 min at 4 °C and subsequently transferred to new eppendorf tubes. 10 µl of cell lysate was used for determination of protein concentration if necessary. The rest was mixed with 6x SDS sample buffer and boiled for 5 min at 95 °C. Protein samples were stored at -20 °C for short term and -80 °C for long term storage.

4.3.2. Determination of protein concentration

Overall protein concentration in lysates was measured with Precision Red Advanced Protein Assay (Cytoskeleton) according to manufacturer's instructions. 10 µl of the protein lysate was combined with 1 ml of Precision Red reagent and the absorbance was measured after 1 min at 600 nm. Multiplying the absorbance with 10 equals the total protein concentration in µg/µl.

4.3.3. Immunoprecipitation

Immunoprecipitation (IP) experiments of transiently expressed protein were performed using HEK293T cells, which were transfected when 80 % confluent. For a 100 mm dish up to 25 µg of DNA were transfected using PEI (section 2.4.2). Cells were harvested as described above the following day in 400 µl NP40 lysis buffer with cOmplete Protease Inhibitor. 60 µl of the cleared lysates were kept for blotting controls, combined with 12 µl 6x SDS sample buffer and boiled for 5 min at 95 °C. The rest of the lysates were added to 20 µl of either Flag-M2 affinity gel (Sigma), or Protein G Sepharose beads (Fast Flow, Sigma) coupled with anti-GFP (ab290, Abcam). 20 µl of ProteinG Sepharose bead slurry had been conjugated with 0.5 µl of rabbit anti-GFP for 10 min at 4 °C before, for control IPs 1 µl normal rabbit IgG was used. After minimum of 1 h rotation at 4 °C, beads were washed three times in NP40 lysis buffer and eluted with 2x SDS sample Buffer for 20 min at 37 °C. Samples were again centrifuged at 800 x g for 1 min at 4 °C, subsequently the supernatant was separated from the beads and boiled at 95 °C for 5 min. Lysates and IP samples were analyzed by Western Blot.

For endogenous IP of ARHGAP39, HEK 293T cells grown on 150 mm dish were transfected with 20 µg DNA of ROBO1. The transfected cells were directly lysed in NP40 lysis buffer supplemented with cOmplete protease inhibitor cocktail (Roche) and scraped of the cell culture dish. 4 mg protein was incubated over night at 4 °C with 4 µg of ARHGAP39 antibody or IgG control. 40 µl of beads were then added per sample for 30 min. Samples were centrifuged and the supernatant was kept to check if there is unbound protein in the lysate. Next, the samples were washed three times in NP40 lysis buffer and eluted with 2x Sample Buffer for 20 min at 37 °C.

In the case of stimulation with recombinant SLIT2 (Peprotech), ROBO1 transfected HEK 293T cells were treated with 5 µg/ml of SLIT2 in DMEM– containing 0.2 % BSA for the indicated time points.

4.3.4. SDS-PAGE

Sodium dodecyl sulfate polyacrylamide gel electrophoresis (SDS-PAGE) was used to separate proteins according to their molecular weight. 7.5 %, 10 % or 12 % acrylamide gels with a 1.5 mm thickness and the following composition were prepared as described in Table 2.11. After complete polymerization, samples in 2x SDS sample buffer were heated to 95 °C for 5 min. 1x SDS running buffer was added and samples were first run at 80 V for 10 min anf then up to 200 V until proteins were sufficiently separated. 3 µl of PageRulerTM Prestained Protein Ladder, 10 to 180 kDa (Thermo Fisher Scientific, USA) were used as marker.

4.3.5. Coomassie Brilliant Blue staining

Gels were rinsed briefly with water before staining solution containing Coomassie Brilliant Blue was added for a minimum of 1 h at RT whit gentle agitation. Gels were destained using destaining solution that was replenished several times until background of gels was fully destained.

4.3.6. Western Blotting

Subsequently, gels were transferred onto 0.45 µm Amersham HybondTM ECLT Nitrocellulose (GE Healthcare) using a Mini Trans-Blot Electrophoretic Transfer Cell (BioRad) for 90 min at 100 V in Wet Blot Transfer Buffer. Afterwards, membranes were washed briefly with distilled water before staining with Ponceau S solution (Sigma-Aldrich, Germany) for 5 min. After washing with TBST membranes were blocked with 5 % Milk Powder in TBST for approximately 1 h, before incubating with the primary antibody overnight at 4 °C. They were then washed three times for 5 min in TBST, followed by incubation with HRP-coupled secondary antibodies for 1 h at RT. After washing again three times for 5 min in TBST membranes were incubated with the LumiGlo Peroxide Substrate (Cell Signaling Technology, USA) for 1 min. Super RX X-ray films (Fujifilm, Japan) or for higher sensitivity Amersham Hyperfilm ECL (GE Healthcare Europe GmbH, Germany) films were exposed for varying times before developing.
In some cases the membrane was subjected to staining with another antibody. Bound antibodies were stripped off by incubating the membrane in stripping buffer (Table 2.10) for 30 min at 65 °C. The membranes were washed twice x 10 min in TBST and blocked in 5 % milk for 1 h. For subsequent staining, the same protocol as described above was carried out. Membranes were stored in plastic wrap at -20 °C.

4.3.7. INSTA-BLOT with human tissues

A commercially available INSTA-Blot PVDF membrane (IMB-103, Imgenex) containing 20 µg denatured proteins from human lysates was processed according to manufacturer's instructions using anti-ARHGAP39 antibody.

4.3.8. Peptide Spots

Peptide spot membranes were prepared by the lab of Enno Klussmann, MDC. Peptide spots (Fmoc-protected amino acids, Intavis) were automated SPOT synthesised on Whatman 50 cellulose membranes (amino-modified acid-stable cellulose membrane with PEG-spacer, Intavis) using Fmoc (9-fluorenylmethyloxycarbonyl) chemistry with an AutoSpot-Robot ResPep-SL (Intavis Bioanalytical Instruments). The spots on the membrane are overlapping 25 amino

acid peptides, with each spot shifted by five amino acids. Thereby, the N-terminus of ARHGAP-39 (1-689 aa) and the C-terminus of ROBO4 (494-1003 aa) were spot synthesised.

Membranes were activated with MeOH for 1 min, washed three times for 10 min in TBST and subsequently blocked for at least 2 h in 3 % filtered BSA. Next, membranes were incubated in a sealed plastic bag with 5 ml of 10 µg/ml recombinant purified GST-ARHGAP39 WW domains overnight at 4 ℃. The next day, membranes were washed three times for 10 min in TBST and then incubated with anti-GST primary antibody for 2 h at RT. After three more washes in TBST, membranes were incubated for 1 h at RT with HRP- conjugated anti-mouse secondary antibody and developed as explained for Western blot in 2.3.6.

Cloning, bacterial expression and purification of the recombinant GST-ARHGAP39 WW-domain tandem (1-121 aa) was performed by Anja Schütz, MDC.

4.3.9. SLIT2 purification

To visualize ROBO1 internalization, ROBO1-Venus transfected HeLa cells were stimulated with SLIT2 that was purified from conditioned media. To purify SLIT2 from media, SLIT2-Cherry or -Flag/Venus expression plasmids were transfected in HEK 293T cells plated on 150 mm cell culture dishes. 6h after transfection the medium was changed to 6 ml of DMEM without phenolred containing 2 % FCS. The next day the media was transferred to a 15 ml Falcon tube and centrifuged at 4000 RPM for 5 min to remove cells and cell debris. The supernatant was then added to a concentrator with 100 kDa cut off (Amicon) to concentrate proteins bigger than 100 kDa in the medium. The total protein concentration was measured as described in x. 60 µg of the samples were loaded on a 7.5 % SDS-PAGE together with a BSA standard (100-1000 ng of BSA) to estimated the protein concentration of SLIT2 by Coomassie Brilliant Blue staining (section 2.3.5).

4.4. Cell culture

4.4.1. Cell Lines

All cell lines were cultured at 37 ℃ with 5 % CO2, and split every 2-3 days at the indicated ratios. Cells were washed once with PBS (PAA) before incubation with Trypsin/EDTA (PAA) for the indicated times. Subsequently, cells were resuspended in the indicated media plus additives and replated. Cell lines used in this thesis and splitting ratio, trypsination times and

used media are described in Table 4.14.

Table 4.13.: Cell lines, culturing conditions and splitting ratio

Cell line	Origin	Type	Media	Additives
MDCK	Dog	Madin-Darby canine kidney II	MEM	10 % FBS, 1 % P/S
HeLa	Human	Cervical Cancer	DMEM	10 % FBS, 1 % P/S
HEK 293T	Human	Human Embryonic Kidney	DMEM	10 % FBS, 1 % P/S
NIH 3T3	Mouse	Fibroblast	DMEM	10 % FBS, 1 % P/S

Cell line	Splitting Density	Trypsination Time	DNA Transfection
MDCK	1:8	10-15 min	Effectene
HeLa	1:10	3-5 min	PEI
HEK 293T	1:8	3-5 min	PEI
NIH 3T3	1:10	3-5 min	Lipofectamine 3000

4.4.2. Transient DNA Transfection

For the individual cell lines different transfection methods were used (Table 2.16). Transfections were performed according to manufacturer's instructions of the respective commercially available transfection reagent. For live cell microscopy, cells were transfected the same day as they were seeded, a minimum of 3 h later, after cells had adhered. For Co-Immunoprecipitation (Co-IP), immunofluorescence (IF) and other applications, cells were transfected the day after seeding.

Polyethylenimine (PEI, Polysciences, USA): Stock solution was prepared by dissolving 1 mg/ml PEI in water, pH 7 and sterile filtered before use. OptiMEM was incubated with the DNA and PEI at a ratio of 1:3 (µg:µl) for 15-60 min. The mix was then added dropwise to the cells.

Effectene (Qiagen, Germany): DNA and Enhancer were incubated together in Buffer EC for 5 min. Effectene was added to the DNA:Enhancer mix and incubated for 10 min, before vortexing of the complete mixture for 10 s and adding it to cells. Enhancer and Effectene were both vortexed before use, and were used at a ratio of 3:1:1 (µl:µl:µg) with DNA. Medium on cells was changed to OptiMEM (Invitrogen) before transfection.

Lipofectamine 3000 (Thermo Fisher Scientific, USA): The medium on the cells was changed to OptiMEM before transfection. DNA and p3000 were added to OptiMEM in one eppendorf tube and Lipofectamine was also added to Opti-MEM in a second eppendorf tube. Both mixtures were combined with a final ratio of 1:2:3 (DNA (µg): p3000 (µl): Lipofectamine (µl)) and

incubated for 5 min before the mixture was added dropwise to the cells.

4.4.3. Counting of Cells

A Neubauer Bright-Line Hemocytometer was used to count cells. 10 µl Trypan blue solution (0.4 %) were added to 90 µl cell suspension and 10 µl were loaded into the Hemocytometer. Four squares of 1 mm^2 were counted. The averaged cell number was multiplied by 10^4, which is the cell number per ml of cell suspension.

4.4.4. Virus Infection

Lentiviruses were produced previously in the Pawson laboratory containing shRNA in a pLKO.1 vector and a puromycin selection cassette. The stuffer control virus contains 1.9 kb stuffer sequence in place of the shRNA cassette in the pLKO.1 plasmid. HeLa cells were infected with the lentiviruses and after 24 h puromycin was added to the media at 2 µg/ml. HeLa cells were expanded and cultured in the presence of puromycin.

4.4.5. Scratch Wound Assay

HeLa cell lines containing stuffer shRNA or ARHGAP39 shRNA viruses were seeded with 150,000 cells per well on a 24 well plate and were grown to confluence for the next 12 h, afterwards the medium was changed to starvation medium (DMEM without FCS) for another 12 h. The medium always contained 2 µg/µl Puromycin. Scratches on the cell monolayer were done with 10 µl pipette tips. Subsequently, cells were washed once in PBS and Imaging media containing 10 % FCS and 2 µg/µl Mitomycin C (Sigma), to eliminate the effect of cell proliferation, was added. Mineral oil (Sigma) was added to the wells to avoid evaporation during imaging. Images of the migrating cells were taken every 15 min using a LUCPLFLN 20X / 0.45 NA, long working distance (6.6-7.8 mm) objective of an Olympus Fluoview 1000 Confocal Microscope, equipped with a temperature controlled incubation chamber that was heated to 37 ℃ and set to 5 % CO2 and 65 % humidity.

4.4.6. Transwell Assay

HeLa cell lines containing stuffer shRNA or ARHGAP39 shRNA viruses were seeded on 6 cm cell culture dishes and starved over night in DMEM (without FCS) containing 0.2 % BSA. The next day cells were washed with PBS^{++} before trypsinization and resupension in complete DMEM. Cells were centrifuged for 5 min at 1200 RPM at 4 ℃. The supernatant was aspirated and the cells resuspended in PBS^{++}. Cells were then counted and diluted to $4x10^4$ or $8x10^4$

cells in 200 µl per insert in 0.2 % BSA/DMEM containing 2 µg/µl Mitomycin C (Sigma) to eliminate the effect of cell proliferation.

500 µl DMEM with 10 % FCS were added to the bottom chambers of the 24 well plate. The PET Transwell inserts were assembled ino the chambers and allowed to become moistened with the medium. Inserts had been coated with 1 µg/ml Fibronectin (Sigma) before. SLIT2 arrived as powder (Peprotech) and was dissolved in 20mM Tris-HCl pH 8.8 and 150mM NaCl to a stock concentration of 0.5 µg/µl. If not otherwise stated, 2.5 µg SLIT2 was added to each well to a final concentration of 5 ng/µl. Subsequently, the 200 µl of cell suspension was added into the Transwell inserts. In some cases recombinant human Robo1-Fc (stock 100 µg/ml, RD systems) was added either with 10 µg or with 20 µg to the bottom chambers. After carful shaking forth and back, the plate was left under cell culture hood for 30 min to allow cells to settle, before inserts were incubated for the indicated time points at 37 ℃ and 5 % CO2 in the incubator.

Inserts were then washed gently in PBS several times to remove unattached cells, followed by fixation of inserts in 4 % PFA for 10 min at RT. After trying the inserts up-side down for 10 min, they were washed again three times in PBS^{++}. The inserts were stained with Crystal violet for 20 min. Cells on the upper surface of the insert membranes were removed with a cotton swab by wiping the insert relatively strongly. Next, inserts were washed in distilled water and air dried over night, before their middle regions were imaged in four consecutive rows using an automated stitching function of the Keyence Fluorescence Microscope BZ-X.

4.5. Zebrafish experiments

Care of zebrafish embryos

Zebrafish were kept at 26.5 ℃ and bred under standard conditions. *Tg(fli:egfp)^{y1}*, *Tg(flk1:gfp)*, *Tg(gata1a:Dsred)* and *Tg(flk1:gfp;gata1a:Dsred)* transgenic zebrafish line were used during this thesis. After 24 hpf fish were bleached with 1-phenyl 2-thiourea (PTU), an inhibitor of tyrosinases during melanin formation to stop pigmentation of the embryo and the chorion was opened with forceps to enable imaging of the embryo.

4.5.1. Hemoglobin staining

On order to visualize the circulating blood cells in zebrafish embryos o-dianisidine staining was performed. Fish were dechorinated and incubated with the staining buffer (0.6 mg/ml o-dianisidine, 10 mM sodium acetate (pH 5.2), 0.65 % hydrogen peroxide, and 40 % ethanol) for 15 min in the dark (after (Kawahara and Dawid, 2001)).

4.5.2. Morpholino oligomers

In order to study the function of genes during zebrafish development morpholino oligermers (MO) can be applied to inhibit gene expression that allow to examine effects on the phenotype of the fish. Researchers have intensely employed this antisense RNA technique, which revealed new insight into developmental processes and into gene function (Eisen and Smith, 2008).
MOs typically consist of 25 morpholino bases (morpholino ring and any of the four DNA bases) and a non-ionic phosphorodiamidate backbone (Fig. A.3 A, Appendix). They are designed to target a gene transcript via complementary base pairing. The charged backbone allows the MO to interact with high affinity to the RNA, thereby facilitating steric hindrance of correct transcript processing or translation (Summerton and Weller, 1997; Summerton, 1999). MO are usually injected into the yolk of 1 to 8 cell-staged embryos. During these early embryonic stages cytoplasmic bridges, which connect the cells, allow the rapid diffusion of the hydrophilic MOs. This leads to a ubiquitous delivery throughout the blastocyst (Nasevicius and Ekker, 2000).

Two types of MOs exist that are classified after the target sequence they bind to in the desired mRNA transcript. First, translational blocking MOs bind to 5' untranslated region (UTR) near the translational start of the pre-mRNA and inhibit the initiation of translation by hindering ribosome assembly (Fig. A.3, Appendix) (Summerton, 1999). Second, splice blocking MOs bind to the pre-mRNA at splice binding sites and thus prevent the spliceosomal components from binding. Thereby, it creates spliced mRNAs lacking an exon or with an additionally inserted intron (Fig. A.3, Appendix) (Bill et al., 2009). For this MO Real-time PCR can be used to identify the knock down of mRNA (Morcos, 2007).
When utilizing MOs to investigate early developmental processes scientist have to consider potential drawbacks. One problem is that the efficiency of a MO cannot be estimated without a functioning antibody. Also, the reproducibility of experiments may suffer from the very small volumes of injected MO. Moreover, a commonly known problem of MOs are their potential "off-target" effects. Injected MOs may inhibit the function of non-targeted genes or in addition to the intended gene and thus, the observed phenotype may be only partially the result of the targeted gene. Suggested controls are for instance the usage of a control MO, of different MOs targeting the same gene and rescue experiments (Eisen and Smith, 2008).

4.5.3. Injection of morpholino oligomers and expression constructs

Morpholino antisense oligomers (MOs; Gene Tools) were prepared at a stock concentration of 1 mM according to the manufacturer's instructions and were injected into the yolk of one-cell stage embryos. Two MOs were used targeting *arhgap39*: ATG-blocking morpholino oligomer

M1 and intron-exon splicing morpholino oligomer M2. A MO working solution of 75 µM was prepared in Danieau solution (58 mM NaCl, 0.7 mM KCl, 0.4 mM $MgSO_4$, 0.6 mM $Ca(NO_3)_2$, 5.0 mM HEPES, pH 7.6) and water (up to 10 µl). Approximately 2.4 ng of each MO was injected per egg.
To study the phenotype of Arhgap39 expression and for rescue experiments, poly(A)-capped *arhagp39* mRNA was injected into one-cell stage embryos. Before, *arhagp39* had to be cloned into pCS2+ vector. Sense-capped mRNA was generated by SP6 Message mMachine (Ambion). After purification of poly(A)-capped *arhagp39* mRNA approximately 0.5 nl were injected with 100 ng/ µl.

4.5.4. Zebrafish *arhgap39* cloning

To express *arhagp39* specifically in the vasculature under the control of the *fli* promoter, it was introduced into the Gateway recombination system. *arhagp39* was amplified by PCR using the GoTaq polymerase (Promega) following manufacturer's guidelines and *arhgap39* specific primers: Fw: ATGGCGGAGAGGTTGGAATGGGTGG and Rv: CTATAGCACCCCGTCCATGAAGCTG. For the BP reaction, *arhgap39* PCR product was cloned into the pCR8/GW/TOPO (Invitrogen) plasmid by TOPO cloning. This method exploits the addition of a single deoxyadenosine (A) to the 3' ends of PCR products, which ligates efficiently with the linearized vector pCR8 vector containing an overhanging 3' deoxythymidine (T) residue in the presence of the enzyme Topoisomerase I from Vaccinia virus. Subsequently, the LR reaction was performed to recombine the pCR8 plasmid with pTol*fliep:cherry* and pTol*fliep:egfp* destination vectors. The obtained constructs, pTol*fliep:cherry/egfp-arhgap39* were injected along with Tol2 *transposase* RNA into one-cell stage embryos.

4.5.5. FACS of endothelial cells

To measure *arhagp39* gene expression in the vasculature, ECs were isolated from non-ECs by fluorescence-activated cell sorting (FACS). Approximately 1000 Tg(*fli:egfp)*^{y1} fish were collected in total at 48 hpf. Fish were separated into 200 fish per 15 ml Falcon tube. Pronase (0.5 mg/ml, Roche) in E3 buffer was added to each tube to enzymatically remove the chorion, followed by three washes with E3 buffer. Subsequently, fish were treated with 0.5 % Trypsin (10x, Sigma) for 3 h, with resuspension of the fish every 30 min with a pipette. The last resuspension step was carried out with a syringe to help the dissociation of embryos into individual cells. The obtained fish lysate was poured through a cell strainer and combined in a 50 ml Falcon tube The lysate was centrifuged at 300 g for 10 min at 4 °C. After addition of 500 µlof 0.5 % Trypsin and 100 µl of FCS the lysate was centrifuged again as in the previous step. Next, the lysate was washed in 1 ml of 2 % FCS in PBS. 10 µl of the sample was taken to count the number of cells (section 2.4.3). The remaining lysate was centrifuged again and 0.5 to 2

ml of autoclaved PBS was added to the cell pellet depending on the cell number (maximum of 5x10^7 cells/ml per tube). The cell suspension was then transferred to a FACS tube. After FAC-Sorting the sorted cells were centrifuged at 3000 g for 10 min at 4 °C. The supernatant was aspirated and the cell pellet resuspended in TRIzol and immediately frozen at -80 °C.

4.6. Microscopy

4.6.1. Fluorescence microscopy

Confocal laser scanning microscopy was used for both live and fixed cells, and performed on a Fluoview 1000 confocal laser scanning microscope (Olympus). Cells were observed through a UPLSAPO 60X/1.3 NA silicon immersion oil immersion lens. Images were taken with the following Excitation and Emission settings:

Table 4.14.: Excitation and emission settings

	Exitation	**Emission**
Hoechst	Ex: 405 nm diode laser (50 mW)	Em: 425-475 nm
mCerulean	Ex: 440 nm diode laser (25 mW)	Em: 460-500 nm
GFP, AlexaFluor488	Ex: Multi-Line Argon laser 488 nm (40 mW)	Em: 500-545 nm
mCitrine, Venus	Ex: Multi-Line Argon laser 515 nm (40 mW)	Em: 530-545 nm
AlexaFluor555	Ex: 559 nm diode laser (20 mW)	Em: 570-625 nm
mCherry	Ex: 559 nm diode laser (20 mW)	Em: 575-675 nm
AlexaFluor647	Ex: 635 nm diode laser (20 mW)	Em: 655-755 nm

4.6.2. Immunofluorescence

Cells seeded on glass coverslips in a 12-well tissue culture dish, were washed once with warm PBS^{++}, before fixing with 4 % PFA in PBS for 10 min. Cells were washed twice for 5 min with PBS at RT between every further step. After washing twice with PBS for min, cells were treated with permeabilisation buffer for 10 min at RT. Subsequently, blocked for 20 min in 3 % BSA in PBS. Primary antibodies were incubated in blocking solution for minimum 1 h at RT or at 4 °C over night. Cells were washed again three times for 5min with PBS before incubation with Alexa Fluor secondary antibodies for 30 min in blocking solution. Cells were washed three more times with PBS. The CF568 Phalloidin conjugate (Biotium) was added to the secondary antibody mixture (1:50). Coverslips were mounted using ProLong Gold Antifade Mountant (Molecular Probes).

4.6.3. Live Cell Imaging

Cells were seeded on glass bottom MatTek dishes or CELLview dishes containing 4 compartments and transfected later the same day after having time to adhere. Transfected cells were

imaged the following day in OptiMEM if not otherwise stated.

4.6.4. Time-lapse microscopy of SLIT2 treated cells

For time-lapse microscopy, HeLa cells grown on glass bottom dishes (Matek, CELLview, Ibidi 24 well plate) were transfected the same day after the cells had time to adhere. Cell were transfected with ROBO1 (0.5 µg or 1.5 µg for CELLview and Matek/Ibidi wells, respectively) or co-transfected with ROBO1 and ARHGAP39 in a 1:1 ration with final amount of 0.6-1 µg of DNA. Cells were imaged the next day in Imaging medium (FluoroBrite DMEM, Fisher Scientific). Postions of cells chosen to image were saved with the motorized stage (multi-area time-lapse imaging) of the Olympus Fluoview 1000 Confocal Microscope. Subsequently, SLIT2 purified from conditioned media was added. Amount of SLIT2 in conditioned media was estimated via Coomassie Brilliant Blue staining, comparing the amount of SLIT2 to a BSA standard (section 2.3.9). Imaging started with acquiring images every 5 min for 30-60 min through a 60X silicone immersion oil objective.

4.6.5. Live Imaging of zebrafish embryo

In vivo blood flow was imaged using a Zeiss intravital microscopy setup (Zeiss Axioscope A1, Carl Zeiss MicroImaging, Jena, Germany) with a 20x (0.50 NA) water-emersion objective. Fish were anesthetized with 0.16 mg/ml tricaine /1 % 1-phenyl-2-thiourea (Sigma) diluted in E3 buffer after dechorination at the indicated developmental stages.

To image the development of the vasculature in *Tg(fli:egfp)^{y1}* fish, they were embedded in 0.5 % low melt agarose (Lonza) diluted in E3 buffer after removing of the chorion. Fish were first injected with MOs or synthesised mRNA and anesthetized with 0.16 mg/ml tricaine/1 % 1-phenyl-2-thiourea (Sigma) diluted in E3 buffer. At 48 hpf confocal stack images of the complete fish or the trunk region were acquired using UPLSAPO 20X (0.75 NA, WD 0.6 mm) or 60X UPLSAPO 60XS (1.3 NA, WD 0.3 mm, silicone oil) objectives, respectively, of the Olympus Fluoview 1000 Confocal Microscope.

For confocal time-lapse imaging of ISV sprouting, ISV growth and blood circulation *Tg(fli:egfp)^{y1}* or *Tg(flk1:gfp;gata1a:Dsred)* fish were imaged, respectively. Imaging was done using the HC PL APO CS2 20x (0.75 IMM, WD 0.68 mm) objective of the inverted Leica TSC SP8 confocal microscope, equipped with a tandem resonance scanner and 2 Hybrid detectors (HyD), containing laser lines 488/561/633 nm. Fish were embedded as described before and kept at 37 ℃ and 5 % CO2 in a live cell incubator. Confocal stack mages were acquired of the sprouting/growing ISVs of *Tg(fli:egfp)^{y1}* fish every 1.5 min for 10 h. To visualize blood circulation in *Tg(flk1:gfp;gata1a:Dsred)* fish with or without MO treatment stacks were imaged for various times.

4.6.6. Rho activity sensors

In order to determine the GTPase substrate specificity for ARHGAP39, novel fluorescence resonance energy transfer (FRET) biosensors for RhoA, Rac1 and Cdc42 were used (Fritz et al., 2013, 2015; Martin et al., 2016). All FRET experiments were performed by Paul Markus Müller, MDC (transfection, image acquisition, image analysis).

Experiments were performed in HEK293T cells that were plated on a poly-L-Lysine coated 96 well plate (5.5 x 10^4 cells/well) and transfected with RhoA (pTriEx RhoA-2G WT, Olivier Pertz, Universität Bern), Cdc42 (pTriEx Cdc42-2G WT, Olivier Pertz, Universität Bern) or Rac1 (pTriEx Rac1-2G WT, Olivier Pertz, Universität Bern) FRET sensors, together with mCherry-tagged ARHGAP39 and its truncation constructs in the ratio 1:9 (sensors:ARHGAP39 constructs). Images were taken 48 h post transfection using an IX81 inverted microscope (Olympus, Japan) with a 10x UPlanSAPO Objective and a MT20 150 W xenon arc burner (Olympus, Japan) light source with the following excitation filters, dichroic mirrors and emission filters (Table 2.18).

Table 4.15.: FRET excitation and emission settings

Channel	Exitation	Dichroic mirrors	Emission
Donor	430/25	zt442RDC	483/32
FRET	430/25	zt442RDC	542/27
Acceptor	430/25	zt442RDC	542/27
mCherry	572/23	HC BS 593	623/24

All images were shade- and background corrected and a threshold was set based on the acceptor channel. The FRET ratio is the average intensity of the FRET channel divided by the average intensity of the donor channel. For each condition five different fields of view were recorded. Experiments were carried out at 37 ℃ and always performed in triplicates (three independent transfections).

4.6.7. Image Analysis

To analyse localisation at focal adhesions together with PXN, Fiji software was used to determine fluorescence intensity along a selected line (line scan). The Plot Profile tool was used to analyze pixel intensity along this line.

The Fiji plugin MTrackJ was used to track single cells during woundhealing in the Scratch Wound Assay. Ten cells per scratched well were tracked every 15 min. The cell velocity, migration distance in total and migration distance into the wound were calculated in Excel using

the provided raw data from the MTrackJ plugin.

To analyse the cell number of migrated cells in the Transwell assay the middle of the inserts were imaged in four consecutive rows using the automated stitching function of the Keyence Fluorescence Microscope BZ-X Every second image that did not show border regions of the insert was then automatically analysed with the free software CELLCOUNTER (Li et al., 2014).

Thickness of ISVS of zebrafish embryos were measured in Fiji. Length of filopodia of growing sprouts was measured with the plugin Neurite Tracer in Fiji.

4.6.8. Colocalisation analysis

For the colocalisation analysis of co-expressed ROBO1-mcherry and Venus-ARHGAP39 the JACoP colocalisation analysis toolbox under ImageJ was used (Bolte and Cordelieres, 2006). The Venus channel and the mCherry channel images were background corrected and thresholded. Pearson?s correlation coefficient r was calculated and Manders' coefficients M1 and M2 were calculated as the fraction of mCherry overlapping with Venus (M1) and the fraction of Venus overlapping with mCherry (M2). For the object-based colocalisation approach the option 'Geometricle centre' was chosen with the Costes' automatic threshold in the JACoP colocalisation toolbox. The images shown in this thesis are centres-particles maps showing the centres-particles coincidence.

4.7. Statistics

For statistical analysis of significance between two sets of data an unpaired Student's T-test was used. For comparison of multiple data sets, statistical significance was determined using the One-way analysis of variance (ANOVA), followed by Tukey's multiple comparisons. Values are expressed as the mean (+) standard deviation (SD) or standard error mean (SEM) as indicated. Significance was set at the 95 % confidence level and ranked as * $p<0.05$, ** $p<0.01$, *** $p<0.001$.

5. Results

5.1. ARHGAP39 interacts with all human ROBO receptors

The starting point of my doctoral thesis was the observation of a preceding mass-spectrometry screen that ectopically expressed ARHGAP39 associates with endogenous ROBO4. ARHGAP39 has not been characterized in mammals and nothing was known about its interaction and potential function down stream of ROBO receptors. The only evidence about its involvement in ROBO mediated cell locomotion came from two studies of its *Drosophila* homologue Vilse/Crossgap and its role in axonal pathfinding (Lundström et al., 2004; Hu et al., 2005).

I therefore set out to confirm the interaction of ARHGAP39 with all four ROBO receptors. This was particularly interesting to study, since it would be the first RhoGAP protein described to be able to transmit signals from all ROBO receptors to Rho GTPases, including the endothelial-specific ROBO4.

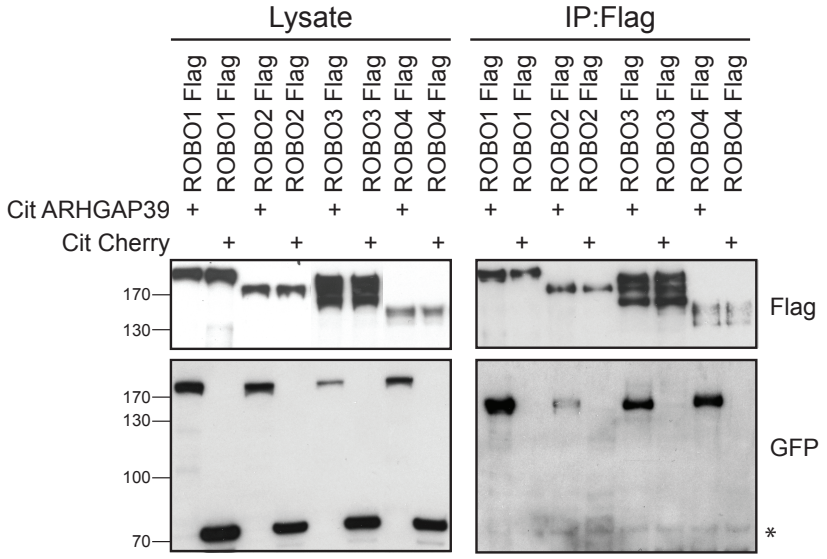

Figure 5.1.: ARHGAP39 binds to all four ROBO receptors
HEK 293T cells transfected with Cit-ARHGAP39 or Cit-Cherry control and Flag-ROBO receptors. Lysates were subjected to immunoprecipitation with Flag-beads and proteins were detected with anti-GFP and anti-Flag antibodies. Asterisk: Fraction of denatured GFP-IgG antibody.

I performed co-immunoprecipitation (Co-IP) experiments of the ROBO receptors co-expressed with Cit-ARHGAP39 or Cit-Cherry control. Indeed, ARHGAP39 specifically bound to all receptors (Fig. 5.1), supporting the hypothesis that ARHGAP39 binds to a sequence motif present in all human ROBO receptors. Overexpressed ROBO3 (MW 150kDa) showed three bands with slightly different MWs in the lysate and in the eluate. Post translational modifications such as phosphorylation or glycosylation might account for these different populations.

5.2. ARHGAP39 is involved in vessel growth during angiogenesis

I demonstrated that ARHGAP39 interacts with the vascular-specific ROBO4 receptor. This implies a novel role of ARHGAP39 in cell guidance in the vascular system. While it has not been convincingly demonstrated whether SLIT/ROBO signalling promotes or inhibits EC migration, or whether it stabilizes or destabilizes the vasculature, it is apparent that deregulation of the SLIT/ROBO pathways dramatically impairs the morphology and function of the vascular system (Park et al., 2003; Seth et al., 2005; Bedell et al., 2005; Jones et al., 2009a).
In order to examine the potential function of ARHGAP39 during angiogenesis the formation of the intersomitic vessel (ISV) in zebrafish was chosen as a model system. The following experiments in this section were conducted in collaboration with the laboratory of Dr. Ferdinand le Noble (now at the Karlsruher Institute of Technology) under the supervision of Katja Meier (MDC).

5.2.1. Identification of *arhgap39* genes in zebrafish

To commence with experiments in zebrafish I had to first confirm the existence of an *ARHGAP-39* homologue in the zebrafish genome. By searching for the human ARHGAP39 protein sequence using the Basic Local Alignment Sequence Tool (BLAST) I found 3 predicted paralogous genes in zebrafish. The appearance of duplicated genes is not uncommon in the zebrafish genome, about 30 % of the mammalian genes have two or more orthologues (Howe et al., 2014). The highest score in the BLAST alignment was obtained for the transcript of the gene si:ch211-218p13.1 (ENSDART00000113684.1) on the forward strand of chromosome 20, which was therefore chosen for gene targeting and further experiments. The other two paralogues were predicted on chromosome 11 and chromosome 23, the genes zgc:92107 and si:ch211-218g4.2, respectively (Fig. 5.2 A, indicated with arrow heads). The transcripts and their putative domain architecture are summarized in the Appendix (Fig. A.1, Appendix).

By PCR I then confirmed the presence of this predicted *arhgap39* transcript ENSDART00000 113684.1 on chromosome 20 in the zebrafish genome. Six sequenced clones showed variations in their nucleotide sequence at the same positions compared to the predicted sequence. However, the only observed change on the protein level was a deletion of two amino acids (Fig. A.2, Appendix). From here on, I refer to this gene as *arhgap39* and its translated protein as Arhgap39. This transcript was cloned into a Cit-expression vector and overexpressed in MDCK cells. Overexpressed Arhgap39 localised at the plasma membrane and basal membrane in MDCK cells (Fig. 5.2 B), similar to the human orthologue, which will be described later in section 5.3.2 (Fig. 5.16), strongly suggesting that its subcellular targeting information is evolutionary conserved.

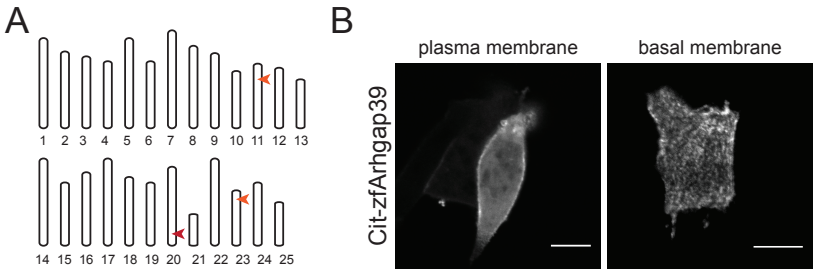

Figure 5.2.: Identification of the predicted arhgap39 paralogous genes in zebrafish
A Illustration of the of the location of the Arhgap39 paralogues on the zebrafish chromosomes, depicted with red arrow heads. Dark red arrow head shows the Arhgap39 transcript (ENSDART00000113684.1) with the highest similarity to the human ARHGAP39 transcript. **B** Overexpression of zebrafish Cit-Arhgap39 (ENSDART00000113684.1) in MDCK cells. Live cells were imaged by confocal microscopy. Abbreviations: zf: zebrafish. Scale bar: 10 µm

I verified the existence the transcript ENSDART00000113684.1 in zebrafish functionally. Surprisingly, the ENSDART00000113684.1 transcript is no longer annotated in the databases at the time of writing. According to Ensemble the entry was retired and replaced by the another transcript (CABZ01087488.1), which is also located on chromosome 20 on the reverse strand (Fig. A.1, Appendix). The new transcript contains the C-terminal half of the ENSDART00000113684.1 transcript and could thus be a shorter isoform. Therefore, it is questionable if the new transcript is functional relevant.

5.2.2. *arhgap39* is expressed in neural and endothelial tissue in zebrafish

Next, I next wanted to investigate where and when *arhgap39* is expressed in the developing fish. I designed *in situ* probes for whole mount hybridisation to detect its expression at different stages during embryonic development.

The onset of *arhgap39* expression was observed at 24 hours post fertilization (hpf), which then increased over time. The signal was restricted to different parts of the brain, whereas the *arhgap39* sense probe, used as a negative control, did not give a signal (Fig. 5.3 A). I could not detect *arhgap39* expression in the vasculature. This might be due to low mRNA transcript levels or insufficient probe sensitivity. By fluorescence activated cell sorting (FACS) GFP labelled ECs of the transgenic fish strain Tg*fli:egfp)*^{y1} (Lawson and Weinstein, 2002) were separated from the remaining cell population and *arhgap39* mRNA levels were determined by TaqMan quantitative real time (qRT-)PCR. This way *arhgap39* mRNA expression was readily detected in EC, albeit at a lower level than in the non-ECs (Fig. 5.3 B).

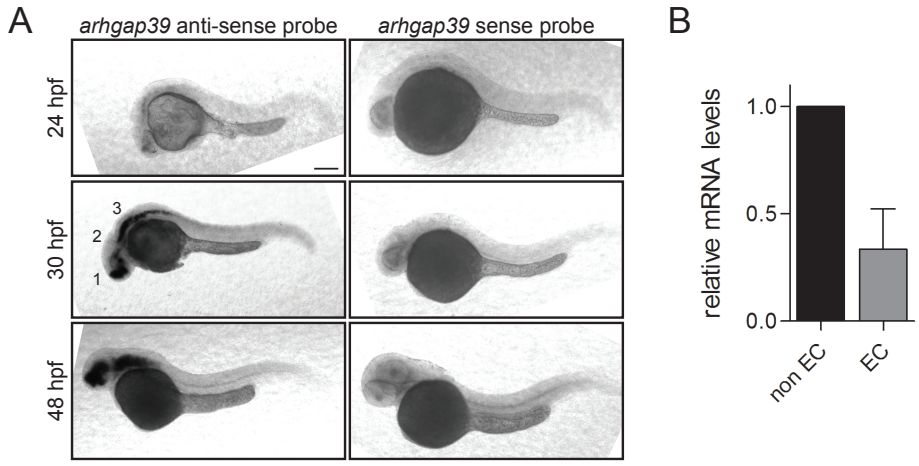

Figure 5.3.: *arhgap39* RNA expression in brain and in EC in zebrafish
A Embryos were fixed at the indicated developmental stages and subjected whole-mount *in situ* hybridisation with *arhgap39* anti-sense or sense riboprobes for 30 h. *arhgap39* expression was only detectable in the brain, appearing at 24 hpf with increasing signal until 48 hpf. Brain structures showing *arhgap39* expression are: 1: the forebrain, 2: the midbrain and 3: the hindbrain. **B** Results of the TaqMan qRT-PCRs show relative *arhgap39* levels in endothelial cells (ECs) compared to non-ECs. Fish were collected from two independent rounds of injection at 48 hpf. Abbreviations: hpf: hours post fertilisation, EC: endothelial cells. Scale bar: 100 µm

5.2.3. *arhgap39* knockdown impairs vessel growth in zebrafish

Robo4 receptor signalling was shown to be required for correct vesssel sprouting and growth of the ISVs (Bedell et al., 2005). I asked if *arhgap39* depletion would also affect the formation of blood vessels, because I speculated that Arhgap39 is a downstream effector of Robo4.

To knock down *arhgap39* gene expression I designed two different morpholino oligomers (MO). One is a translation blocking morpholino (MO1), that binds at the start ATG codon and the sequence upstream in the 5' UTR of the *arhgap39* transcript. The second morpholino is a splice blocking morpholino (MO2) that binds at the exon1-intron1 boundary (Fig. A.3, Appendix)

The first step in using morpholino oligomers is to determine the optimum delivery dose. This provides information regarding phenotypic severity and MO toxicity. For instance with increasing dosage of the MO also morpholino toxicity is enhanced. Critical guidelines for MO use suggest to consider the lethal dose 50 (the dose at which 50 % of the injected fish die) for each MO as the upper limit of injection dose (Bill et al., 2009; Bedell et al., 2011). Tg*(fli:egfp)*^{y1} fish were injected with varying concentrations of MO1 and MO2 (Fig.). At 48 hpf I classified the fish into three groups: without phenotype; with defects in the ISVs (MO phenotype); and dead/severe phenotype ('monster' phenotype showing severe overall deformity, (Bedell et al., 2011)).

I observed that animals injected with 2.4 ng per embryo showed the highest percentage of fish

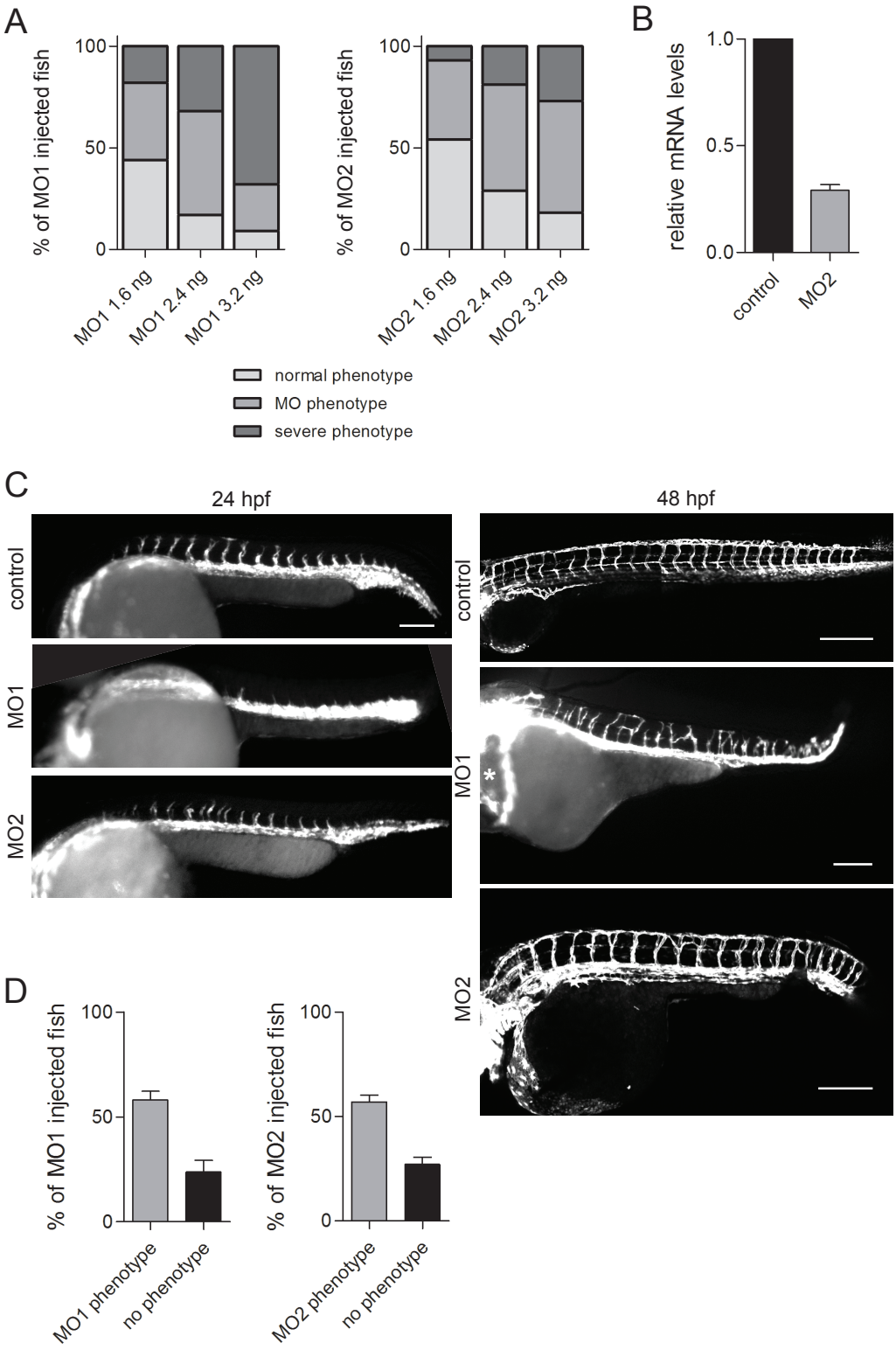

Figure 5.4.: see next page

Figure 5.4.: Delayed and aberrant vessel growth in *arhgap39* knockdown zebrafish
A Diagrams depict the percentage of observed phenotypes of MO1 and MO2 injected embryos at 48 hpf (left and right diagram, respectively) depending on the dosage amount that was injected. Embryos were classified into three groups: no phenotype, fish having defects in ISVs, severe phenotype. **B** TaqMan qRT-PCR results show reduced expression level of *arhgap39* in MO2 injected fish compared to non-injected control fish. Fish were collected from three independent rounds of injection. **C** Control fish and *arhgap39* morphants (MO1 and MO2) were imaged after 24 hpf and 48 hpf with a confocal microscope, respectively. *arhgap39* MO1 injected fish was imaged with normal light microscope after 48 hpf, therefore, the yolk sac gave more background during imaging. MO1 is an ATG translation blocking morpholino and MO2 is an exon-intron splice boundary blocking morpholino. Morphant fish were injected with 2.4 ng of the corresponding morpholino per embryo. Scale bar: 100 µm **D** y-axis depicts percentage of MO1 injected fish (left) and MO2 injected fish (right) that showed the *arhgap39* knockdown phenotype. Injection was repeated in three independent experiments with a total number of 571 fish for MO1 and 281 animals for MO2. Asterisk: indicates enlarged heart. Abbreviation: MO: morpholino, hpf: hour post fertilization.

with defective ISVs and simultaneously the percentage of embryos showing a severe phenotype was relatively low according to the LD50 (Fig.5.4). Therefore, this dose was used in the following experiments. Moreover, this amount is within the recommended range from 1.5 ng to 5 ng of MO, since it was shown that fish injected with 6 ng or more displayed defects that can be considered as off-target effects (Bill et al., 2009).

After determining the working concentration of the morpholino oligomers I analysed the *arhgap39* knockdown phenotype in three independent rounds of injections. The morpholino oligomers were each injected in Tg*(fli:egfp)*^{y1} fish and compared to uninjected control fish. During the first 24 hpf of development I observed a delay in vessel growth in *arhgap39* depleted animals (Fig. 5.4 A). After 48 hpf the knockdown fish showed defects in their ISV compared to the control fish. Furthermore, *arhgap39* embryos were smaller in size, some showed slightly bent tails (Fig. 5.4 B), and frequently enlarged hearts were observed, indicating problems with the blood flow in their ISVs (asterisk in Fig. 5.4 B, middle panel). Of the MO1 and MO2 injected fish approximately 60% were then classified as morphants in three independent rounds of experiments. Whereas, 23% of the injected fish showed no obvious phenotype and the rest were counted as dead or severely damaged fish.
The decrease of the *arhgap39* mRNA in the morpholino injected animal was confirmed by TaqMan qRT-PCR. This approach was only possible for animals injected with MO2, since the mRNA is still properly processed using the translation blocking MO1. The relative levels of *arhgap39* mRNA in the MO2 morphants was reduced by approximately three fold compared to control fish (Fig. 5.4 C).

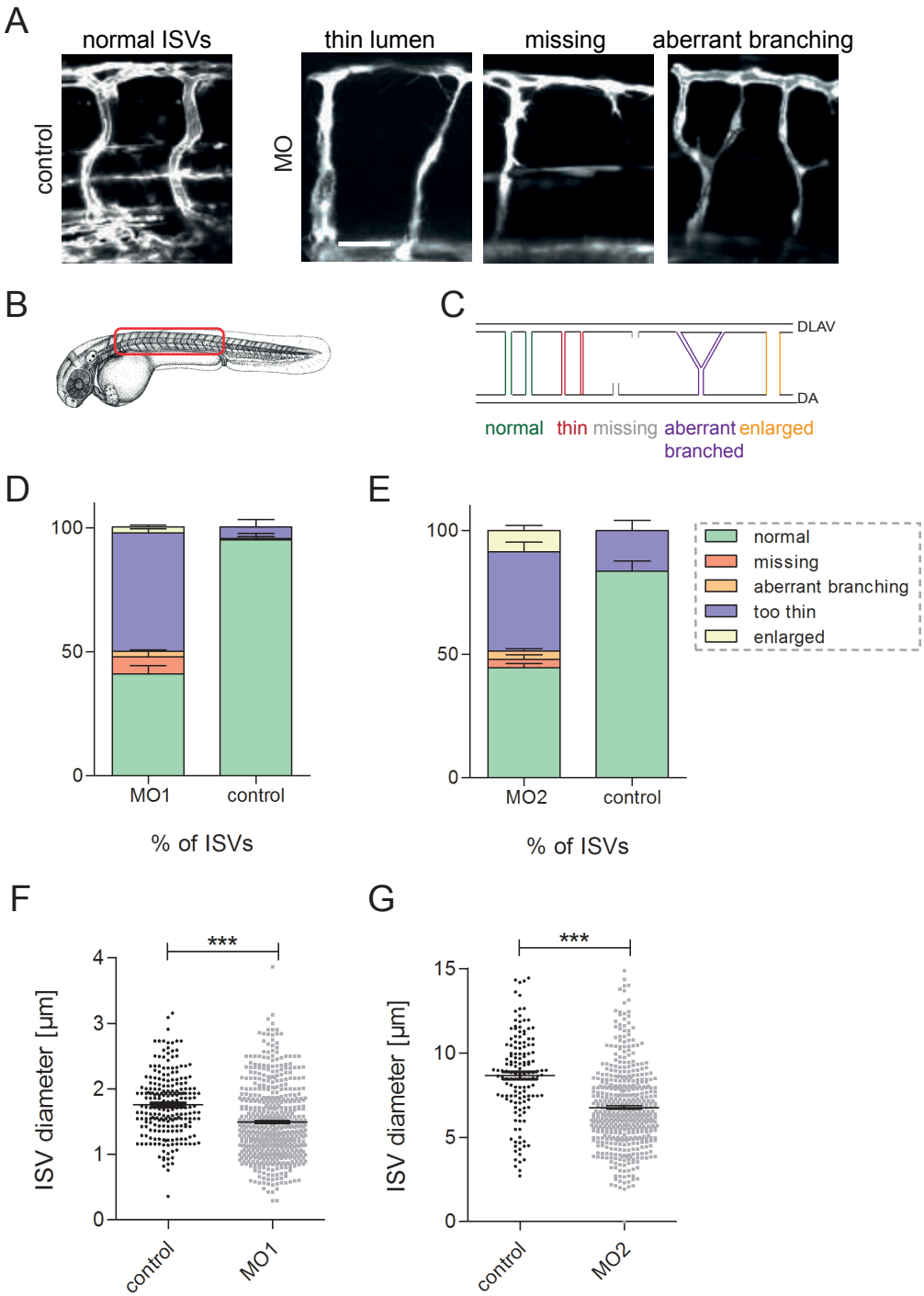

Figure 5.5.: see next page

Figure 5.5.: *arhgap39* knockdown fish show defects in ISVs
A Confocal images of ISVs in control or *arhgap39* knock down fish at 48 hpf. Scale bar: 100 µm **B** Schematic drawing of a zebrafish. Red box indicates the rostral part of the animal, where the ISVs were analysed for the statistics. **C** Illustration depicts ISVs phenotypes used for their classification. **D** Bar diagram showing the percentage of the different vessel phenotypes observed in the rostral region of MO1 and control animals at 48 hpf. **E** Diagram depicting the average vessel diameter of ISVs in the rostral region of MO1 and control fish. For MO1 injected and the control uninjected fish 47 and 18 animals, respectively, were examined. Total numbers of measured ISVs for MO1 morphants and control fish are 601 and 182, respectively. **F** Bar diagram showing the percentage of the different vessel phenotypes observed in the rostral region of MO2 and control fish at 48 hpf. **G** Diagram depicting the average vessel diameter of ISVs in the rostral region of MO2 and control animals. For MO2 injected and the control uninjected fish 27 and 6 animals, respectively, were examined. Total numbers of measured ISVs for MO2 morphants and control fish are 543 and 130, respectively. The difference in the average vessel diameter in F and G is due to imaging wit a light microscope or a confocal microscope, respectively. Both MOs were injected with 2.4 ng per embryo. Asterisks denote statistical significance as calculated by Student's t-test. Significance was ranked as *** $p<0.001$. Abbreviations: MO: morpholino, ISV: intersomitic vessel, DA: dorsal aorta, DLAV: dorsal longitudinal anastomotic vessel.

5.2.4. *arhgap39* morphants exhibit reduced vessel diameter

I then further analysed the defective ISVs in the rostral part of *arhgap39* zebrafish embryos in more detail, because they exhibited various phenotypic changes. For instance, the vessel lumen was defective, the sprouts were incompletely formed or showed aberrant branching. Representative images of the observed defects are depicted in Figure 5.5 A. Each individual vessel along the yolk tube was then classified into the categories: missing vessels, aberrant branching, very thin vessels or with an enlarged lumen (Fig. 5.5 B and C). The analysis was performed in MO1 and MO2 injected fish and compared to uninjected control animals. In the *arhgap39* morphant fish I observed a drastic increase in ISVs showing a very thin lumen, but also missing vessels, vessels with enlarged lumen or branching defects were found. In control animals only a small fraction of very thin ISVs were counted, whereas the other defects could not be found (Fig. 5.5 D: for MO1, E: for MO2).

Since the most frequent phenotype of the impaired rostral ISVs was the reduction in vessel lumen I measured the vessel diameter of all the ISVs included in the analysis in Figure 5.5 E and D. For both morpholinos I found that the vessel diameter of the rostral ISVs was significantly decreased ($p<0.0001$) compared to ISVs of control fish (Fig. 5.5 F: for MO1, G: for MO2).

5.2.5. *arhgap39* mRNA fish show impaired ISV development

After studying the effects of *arhgap39* loss in zebrafish I set out to examine the effect of *arhgap39* overexpression on ISV formation. I therefore generated *arhgap39* mRNA and tested its optimum delivery dose. At 48 hpf the injected animals were categorized into: without phenotype, defects in the ISVs (RNA phenotype), and dead/severe phenotype. The apparent best ratio of fish with no phenotype to RNA phenotype to severe phenotype was obtained at a dose of 50 pg per embryo, which was used in subsequent experiments, if not otherwise stated (Fig. 5.6 B). This dose is in the recommended dose range between 50 pg to 1 ng per embryo (Bill et al., 2009), and thus a good indication that observed defects are due to mRNA expression and not due to toxicity.

The Arhgap39 fish showed a moderate bending of the tail and their ISVs exhibited similar defects as mentioned before for the knockdown fish (Fig. 5.6 A) Approximately 60 % of the *arhgap39* mRNA injected fish were classified as fish with abnormal RNA phenotype, 23 % had no obvious phenotype and a fraction of dead or severely damaged animals was also observed (Fig. 5.6 C). With TaqMan qRT-PCR I measured a three fold increase in relative *arhgap39* mRNA levels in the Arhgap39 animals compared to the uninjected control (Fig. 5.6 D).
Next I examined whether the defects in the ISVs resemble those found in the *arhgap39* knockdown fish, using the same analysis as for the morphants. For the Arhgap39 expressing animals a drastic increase in ISVs showing a very thin lumen was observed. Missing vessels, vessels with branching defects or enlarged lumen were detectable in the Arhgap39 animals with higher frequency compared to control fish (Fig. 5.6 F). The vessel diameter of all ISVs included in the analysis were measured, revealing a significant decrease ($p<0.0001$) of the diameter in the *arhgap39* mRNA fish compared to control animals (Fig. 5.6 E).

Taken together, the phenotypic characterisation revealed the same morphological changes for *arhgap39* knockdown and its ectopic expression. In both conditions ISV formation was impaired during zebrafish development and specifically the vessel diameter was significantly reduced.

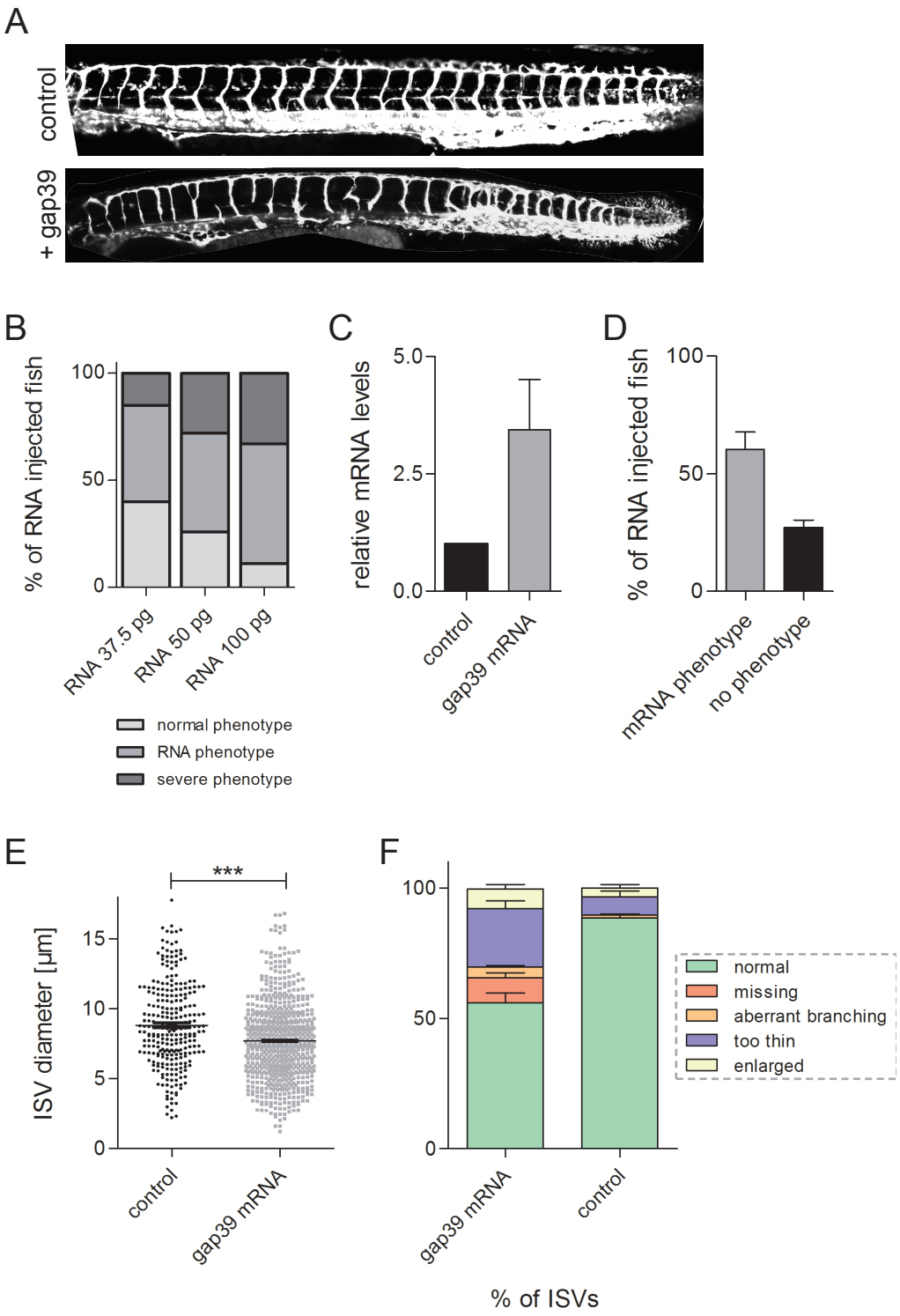

Figure 5.6.: see next page

Figure 5.6.: *arhgap39* mRNA expression causes similar defects in ISVs as the *arhgap39* knockdown
A Confocal images showing Tg*(fli:egfp)*^{y1} fish injected with *arhgap39* mRNA or uninjected control fish at 48 hpf. Scale bar: 100 µm **B** Diagram depicts the percentage of observed phenotypes of *arhgap39* mRNA injected embryos at 48 hpf depending on the dosage amount that was injected. Embryos were classified into three groups: no phenotype, fish having defects in ISVs, severe phenotype. **C** TaqMan qRT-PCR revealed an increase in *arhgap39* mRNA levels in *arhgap39* mRNA expressing fish compared to control animals. Fish were collected from two independent rounds of injection. **D** y-axis shows percentage of *arhgap39* mRNA injected fish that exhibited the abnormal phenotype due to *arhgap39* mRNA expression. Injection was repeated in four independent experiments with a total number of 344 fish **E** Diagram depicting the average vessel diameter of ISVs in the rostral region of *arhgap39* mRNA fish and control fish. Fish were injected with 50 pg of *arhgap39* mRNA. **F** Bar diagram showing the percentage of the different vessel phenotypes observed in the rostral region of the zebrafish at 48 hpf. For *arhgap39* mRNA injected and uninjected control fish in total 37 and 17 fish, respectively, were examined. Total numbers of analysed ISVs in the rostral part of the embryos were 690 and 262 for *arhgap39* mRNA and control animals, respectively. Asterisk denotes statistical significance as calculated by Student's t-test. Significance was ranked as *** p<0.001. Abbreviations: Gap39: Arhgap39, hpf: hours post fertilisation, ISVs: intersomitic vessels, MO: morpholino, DA: dorsal aorta, DLAV: dorsal longitudinal anastomotic vessel.

5.2.6. Functional characterisation of the intersomitic vessels in *arhgap39* morphants

The loss of *arhgap39* led to delayed ISV growth in the zebrafish trunk at 24 hpf and later to the deformation of ISVs. Therefore, it is conceivable that sprouting and/or migration of the ISVs in the knockdown fish is perturbed. I concentrated on the role of Arhgap39 first during the sprouting process and then during growth of the newly formed vessels. Furthermore, I asked if the detected reduction in lumen diameter leads to the functional loss of those vessels in carrying blood.

Impaired growth of newly formed vessels in Arhgap39 morphants

I injected the *arhgap39* MO2 into Tg*(fli:egfp)*^{y1} fish and performed live cell time-lapse imaging of whole mounted zebrafish embryos to follow the growth of the ISVs and compared this to an uninjected control fish. The experiments were carried out with a resonant scanning confocal microscope equipped with a ultrasensitive Hybrid detector. This enabled faster imaging and allowed me to use low laser power, thereby reducing photo-damage of the EGFP signal and sample heating during the 9 h period of imaging acquisition.
In Figure 5.7 the sprouting of vessels in the control and *arhgap39* knock down fish is shown over the time frame of 1 h. At 0 min the sprouts have just emerged from the dorsal aorta. The sprouts of the control fish rapidly formed and retracted filopodia that dynamically probed their environment. This was already seen from the early time points on. In the morphants, in contrast, less filopodia were detectable and the filopodia length was reduced. However, the sprout initiation was not impaired.

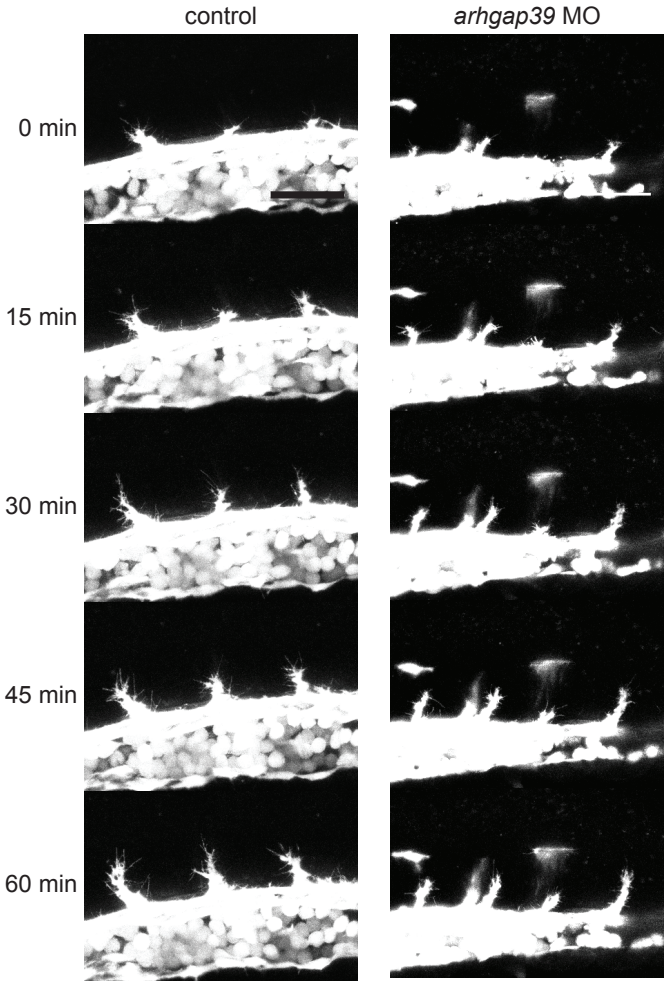

Figure 5.7.: Sprouting of ISVs is not impaired in *arhgap39* knockdown fish
Control and *arhgap39* MO2 injected Tg*(fli:egfp)*^{y1} fish embedded at 22 hpf in low melt agarose. Images were acquired with an inverted Leica TCS SP8 confocal microscope equipped with 2 Hybrid detectors (HyD). Imaging interval was 1.5 min for 1 h. Scale bar: 50 µm

I then assessed the subsequent growth of the sprouts toward the dorsal site of the animals, as well as their branching and fusion. Images are shown from the same fish as presented in Figure 5.7 (Fig. 5.8 and Fig. 5.9). After 1 h the vessels had already grown out of the dorsal aorta in the control (Fig. 5.8) and the *arhgap39* knock down fish (Fig. 5.9).

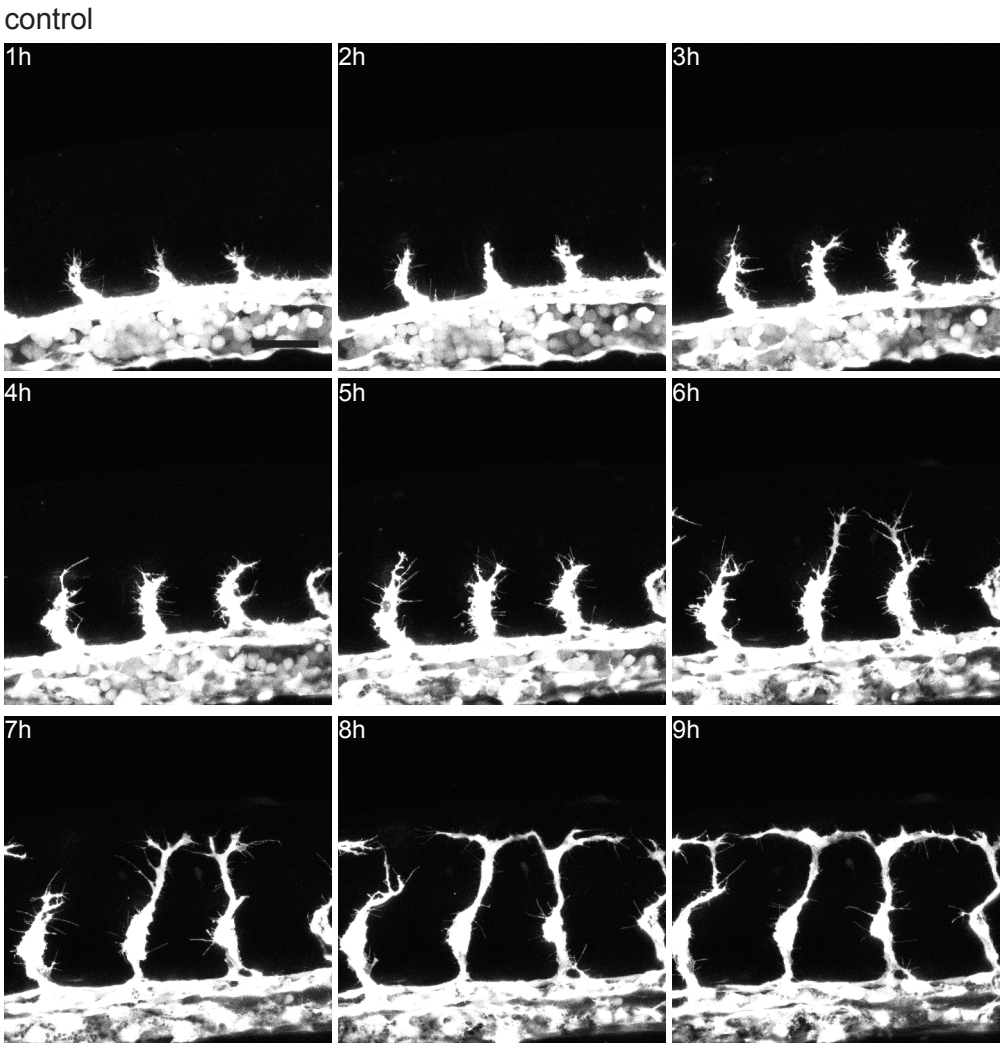

Figure 5.8.: Control fish exhibit dynamic formation and retraction of filopodia along the growing intersomitic vessels
Control Tg*(fli:egfp)*^{y1} fish embedded at 23 hpf in low melt agarose. Images were acquired with a Leica TCS SP8 confocal microscope equipped with 2 Hybrid detectors (HyD). Imaging duration was 9 h, pictures were taken every 1.5 min. Scale bar: 100 µm

In the control fish a rapid appearance and disappearance of the filopodia was very prominent, with elongation and retraction of filopodia at the time scale of minutes (Fig. 5.8). After 7 h the tip of each sprout started to divide into a T-branch. Over the next hours the arms of the T-branch made contact with their neighbours and eventually fused with them. This process is necessary to form the dorsal longitudinal anastomotic vessel (DLAV), enabling blood circulation.

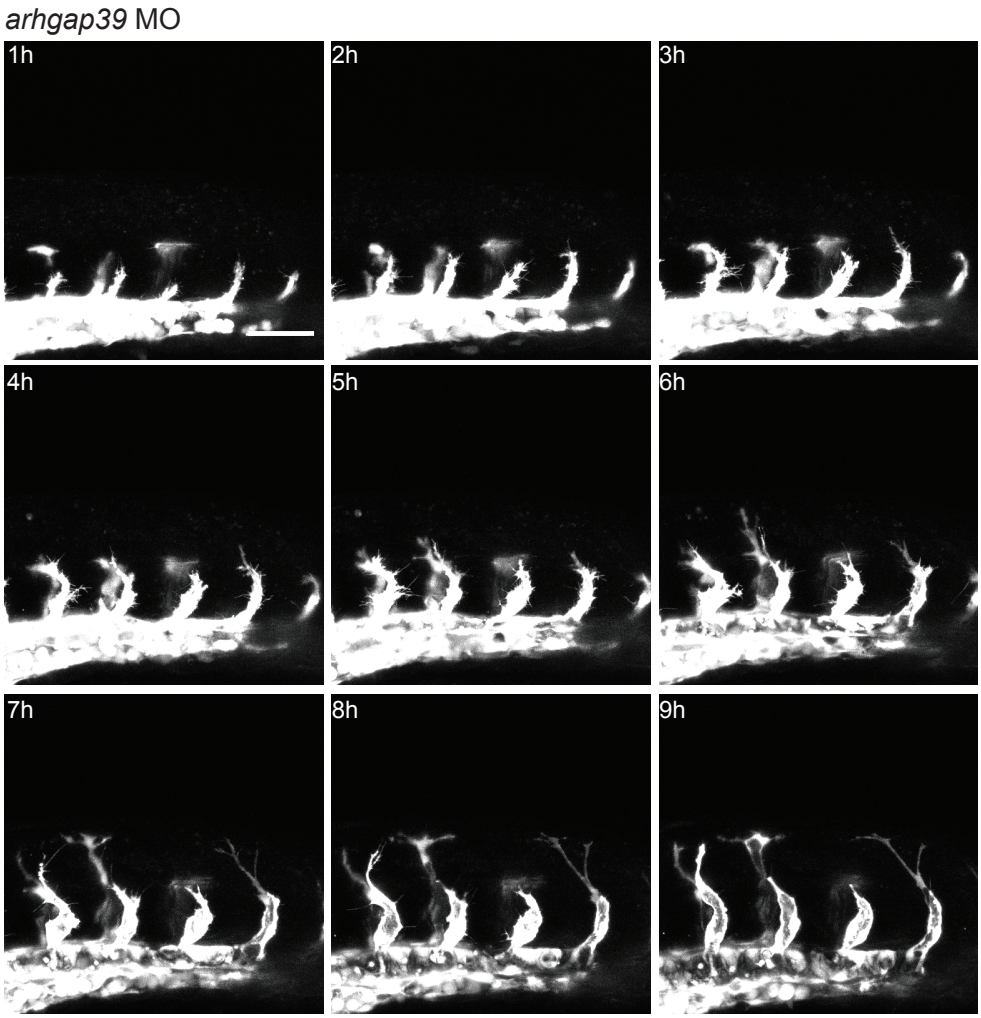

Figure 5.9.: The *arhgap39* morphant shows a delay in intersomitc vessel growth and impaired filipodia dynamics
MO2 injected Tg*(fli:egfp)*^{y1} embedded at 23 hpf in low melt agarose. Images were acquired with a Leica TCS SP8 confocal microscope equipped with 2 Hybrid detectors (HyD). Imaging duration was 9 h, pictures were taken every 1.5 min. Scale bar: 100 µm

In the *arhgap39* morphant the growth of the sprouted vessels was delayed (Fig. 5.9). After 4 h of imaging a reduced sprout size became apparent. I observed the greatest difference after 9 h, when the vessels in the morphant were only two-third the size of the vessels in the control fish. Furthermore, vessels did not exhibit proper T-branching in the *arhgap39* depleted animal and the filopodia density along the vessels was reduced compared to the control fish.

Filopodia are required to sense guidance cues in the environment thereby enabling directed migration towards gradients. The observed reduction of filopodia in *arhgap39* depleted animals was further quantified next. A representative image shows the filopodia of the vessels of uninjected control and *arhgap39* knock down animals (Fig. 5.10 A). The filopodia density is calculated as the total filopodia number divided by the length of the sprout. For the MO2 injected fish a reduced filopodia density was observed for the posterior sprouts along the yolk tube (Fig. 5.10 B).

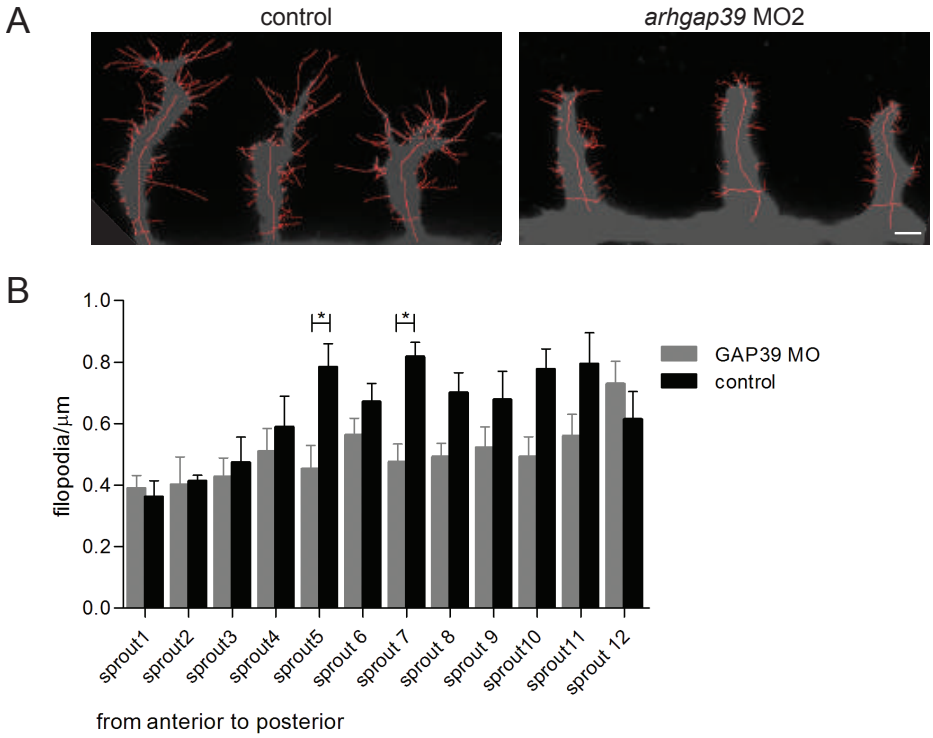

Figure 5.10.: The filopodia density is reduced in *arhgap39* morphants
A Control and MO2 injected animals were imaged at 30 hpf with a confocal microscope. Filopodia were traced using the Simple Neurite Tracer plugin in ImageJ. **B** The growing rostral ISVs of 6 control fish and 10 MO2 morphants were imaged and analysed. Asterisk denotes statistical significance as calculated by Student's t-test. Significance was ranked as * $p<0.05$. Scale bar: 10 µm

Impaired blood flow in newly formed vessels of *arhgap39* morphants

The ISV formation is mostly completed after 48 hpf. By that time most of the vessels in the *arhgap39* morphants had reached the dorsal site of the fish to form the DLAV, however in nearly 50% of the ISVs the lumen was reduced. I therefore investigated if these very thin ISVs are functional to carry blood. In order to study the blood flow in living fish the transgenic fish strain Tg*(gata1a:dsred)*, that has red fluorescent erythrocytes, was mated with the

Tg*(flk:egfp)* strain. Their offspring showed green fluorescent vasculature and red fluorescent erythrocytes. First, I confirmed that the formation of erythrocytes is not compromised in the morphants compared to the uninjected control animals by performing a hemoglobin staining. No obvious changes were detected, neither in the amount of stained erythrocytes nor for the intensity of stained cells (Fig. 5.11 A).

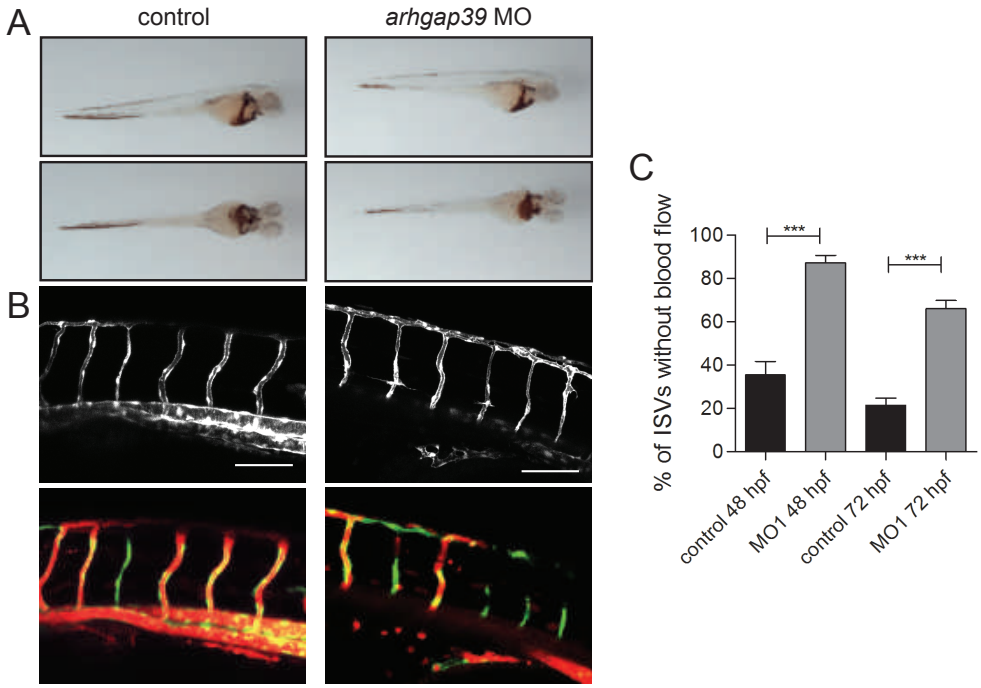

Figure 5.11.: In *arhgap39* morphants have a number of intersomitic vessels with blood
A Tg*(flk:egfp;gata1a:dsred)* fish injected with MO2 or uninjected were stained for hemoglobin at 48 hpf. **B** The blood flow in a control Tg*(flk:egfp;gata1a:dsred)* or MO2 injected animal was imaged by confocal microscopy. The vasculature and erythrocytes are depicted in green and red fluorescence, respectively. MO2 was injected with 2.4 ng per embryo. Confocal stack images were acquired with an inverted Leica TSC SP8 microscope equipped with a tandem resonance scanner and 2 Hybrid detectors (HyD), using a HC PL APO CS2 20x (0.75 IMM, WD 0.68 mm) objective. **C** The ISVs of either control or Tg*(fli:egfp)*^{y1} fish injected with MO1 (2.4 ng per embryo) were analysed if they carry blood. This experiment was repeated three times independently. At 48 hpf in total 17 and 32 fish were analysed for control fish and MO1 morphants, respectively. At 72 hpf 16 and 36 fish analysed for uninjected or MO1 injected animals, respectively. Asterisk denotes statistical significance as calculated by Student's t-test. Significance was ranked as *** $p<0.001$. Abbreviation: MO: morpholino, gap39: arhgap39. Scale bar: 100 µm

In the double transgenic animals I observed then a dramatically reduced blood flow in the ISVs of *arhgap39* morpholino fish compared to control animals. As the blood flow is very fast no individual erythrocyte can be captured in one image-stack, rather a continuous flow can be seen. In the presented examples the *arhgap39* morphant showed proper flow of erythrocytes in only two out of the 6 depicted ISVs. In contrast, in the control animal only 1 out of 7 ISVs was without flow (Fig. 5.11 B).

Additionally, the blood flow in the ISVs can be also easily seen in the bright field channel of a conventional light microscope. I thus quantified the blood flow in the individual ISVs in MO1 injected animals. At both 48 and 72 hpf the percentage of vessels without blood flow was significantly higher ($p<0.0001$) in the morphants compared to control fish. The number of defective vessels without blood flow was reduced in the *arhgap39* depleted animals at 72 hpf compared to 48 hpf (Fig. 5.11 C), indicating that over time more vessels become functional and do have a blood flow.

5.2.7. Experimental set up to rescue effects of the *arhgap39* knockdown

Off-target effects have been described for all gene expression manipulating small molecules. Therefore, control experiments are necessary to establish a clear link between the observed phenotype and the gene target to show that the phenotypes are morpholino specific.
One approach is to use two morpholinos with independent sequence recognition sites, because the chance of the two off-target effects being the same is considerably low (Eisen and Smith, 2008). With the two different morpholinos MO1 and MO2 I observed the same phenotypes in injected fish, which is a first proof that the observed phenotype might be due to the specific targeting of *arhgap39*. Another strategy is to inject RNA in the gene depleted animals to rescue the induced phenotype.

I attempted to conduct rescue experiments by co-injecting MO2 and *arhgap39* mRNA in Tg*(fli:egfp)*y1 animals. The embryos were divided into three experimental groups. The first group was injected only with MO2, in the second and third group *arhgap39* mRNA and MO2 were injected consecutively or simultaneously into the yolk, respectively. Hence, two injection strategies were tested to determine the extent of rescue. With the first, the egg has to be injected twice, whereas only one round of injection is required for the second approach, which makes this strategy technically easier. However, consecutive injections of morpholino DNA and the mRNA are considered to improve the mRNA transcription efficiency, because the mRNA distribution is not as uniform as the morpholino molecules and depends on active transport processes from the yolk into the overlying blastomeres. Therefore, the mRNA should be injected earlier to take advantage of the ongoing transport processes in the developing embryo (Bill et al., 2009).

Figure 5.12 depicts the data of two independent experimental rounds. For the first experiments I used MO2 and the *arhgap39* mRNA with the same dose as used in previous experiments. The co-injection of both components, in either way, did not result in a rescue. Instead, the

percentage of animals without phenotype decreased and the animals observed with a severe phenotype increased (Fig. 5.12 B). Also reduction in mRNA dosage (37.5 pg) resulted in an increased number of fish with a severe phenotype compared to animals injected only with MO2, whereas the percentage of fish without phenotype remained about the same (Fig. 5.12 C). Several further attempts to rescue the *arhgap39* knockdown phenotype with varying concentrations of both MO2 and *arhgap39* mRNA failed. The fact that the co-injection of MO2 and *arhgap39* mRNA increased the amount of fish with a severe phenotype indicates that the two components injected together have an additive effect.

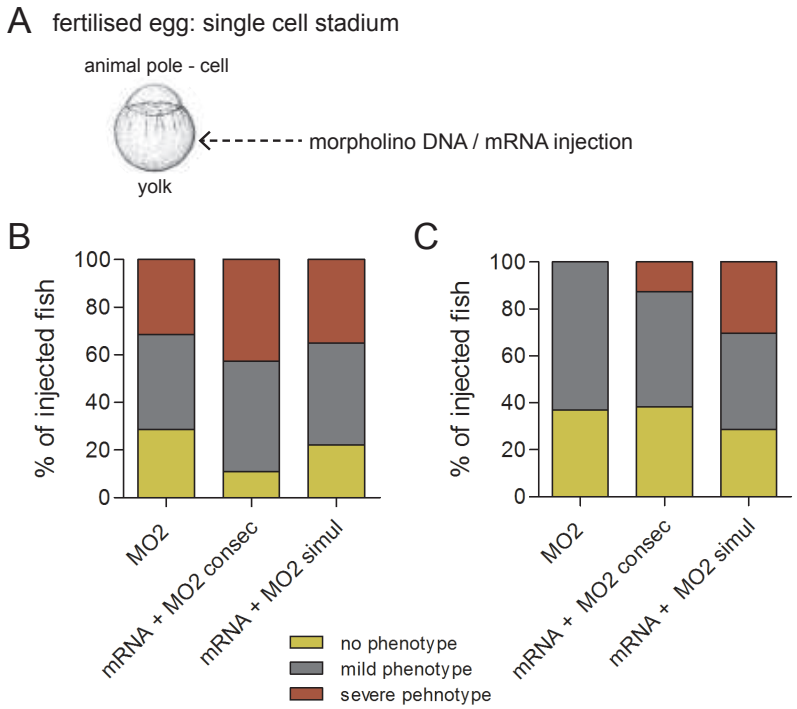

Figure 5.12.: *arhgap39* mRNA did not rescue the *arhgap39* knock down phenotype
A Illustration of a single-cell egg at 1-2 h after post-fertilisation. Arrow depicts where the morpholino DNA and mRNA are injected. **B** Bar diagram of three different groups of injected fish. In the first group only MO2 was injected. The second and third group were injected with MO2 and *arhgap39* mRNA into the yolk consecutively (consec) or simultaneously (simul), respectively. The injected fish were classified as no phenotype, mild phenotype and severe phenotype. Injection of 2.4 ng of MO2 and 50 pg of *arhgap39* mRNA per embryo. **C** Bar diagram of three different groups of injected fish. Everything is the same as in **B**, but 37.5 pg of *arhgap39* mRNA per embryo was injected. Abbreviation: MO: morpholino.

It should be considered that with this experimental set up the *arhgap39* mRNA was ubiquitously expressed, which might affect the formation of the ISVs indirectly. To rule out unwanted developmental defects due to the lack of spatial control of the mRNA expression a tissue specific expression system would be preferable. To this end, *arhgap39* was cloned into Gateway pTol2*fli1:egfp/cherry* destination vectors in order to specifically express *arhgap39* in the developing blood vessels. These plasmids, pTol2fli1ep:egfp-arhgap39 and pTol2*fli1ep:cherry-*

arhgap39, were co-injected with the enzyme Tol2 Transposase, which cuts and randomly integrates the Gateway cassette into the genome. Unfortunately, ectopic expression of pTol2*fli1ep:egfp-arhgap39* and pTol2*fli1ep:cherry-arhagp39* was not apparent in ISVs and thus this vascular specific expression system was not further utilized to establish the rescue of the *arhgap39* morphant phenotype.

Shortly after I performed these experiments the CRISPR gene editing system was established to introduce site-specific modifications in the gene of interest. Nowadays, it is considered as the 'gold standard' to create a CRISPR mutant fish and to validate the corresponding morphant phenotype (Kok et al., 2015). However, due to time limitations this approach was not further pursued.

To conclude, the data suggest a novel role of Arhgap39 in zebrafish angiogenesis. In particular, the growth and lumenization of ISVs is perturbed, as well as filopodia formation of the migrating sprouts. The caveat here is the missing rescue experiment to ultimately prove the detected *arhgap39* knockdown phenotype.
To link the observed defects in ISV growth and migration to Robo signalling I next aimed to understand ARHGAP39 activity on the cellular level. It is conceivable that as a RhoGAP protein it may modulate cell migratory processes, which could then be further studied in the presence of SLIT/ROBO signalling. Moreover, mapping of the ARHGAP39 and ROBO interaction sites would enable me to study Robo defective binding mutants of Arhgap39 in zebrafish for their effect on vessel growth.

5.3. Functional characterisation of ARHGAP39

Two isoforms of ARHGAP39 are annotated in UniProt. These differ only by a 31 amino acid insertion at position 840 in isoform 2 (ENST00000377307.2) compared to the shorter isoform 1 (ENST00000276826.5) and is based on alternative splicing (Fig. 5.13). Ensemble reports an additional isoform (ENST00000528810.1) that cannot be processed into protein.
ARHGAP39 contains its RhoGAP domain at the C-terminus, two N-terminal WW domains and a myosin tail homology (MyTH4) domain just ahead of the RhoGAP domain. Furthermore a proline rich sequence is suggested to be encoded between amino acids 227 and 367 on UniProt. The additional 31 aa insertion in isoform 2 is located inside the MyTH4 domain.

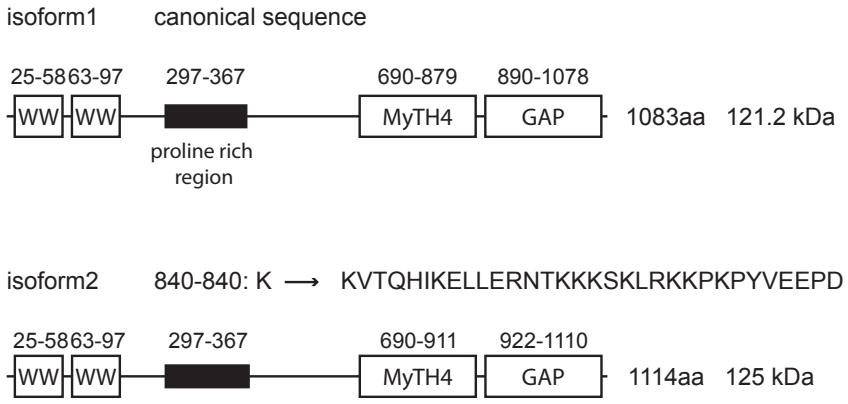

Figure 5.13.: Two isoforms of ARHGAP39 are genetically encoded
Protein architecture of ARHGAP39 (Q9C0H5) isoforms 1 and 2.

5.3.1. Sequence analysis of the ARHGAP39 WW and MyTH4 domain

The WW domains

WW domains mediate protein-interactions by binding to proline rich motifs on partner proteins. In order to predict putative proline-rich recognition motifs of the ARHGAP39 WW domains on binding partners I aligned their sequences with those of different WW domain containing proteins. I chose the WW domains of YAP1, NEDD4, FBP11, its homologue in yeast Prp40, PIN and Arhgap9, which are all well characterized regarding their proline binding motifs, which are summarized in Figure 5.14 A.

A

Class	recognition motif	examples
I	(L/P) Pp(Y/poY)	YAP, NEDD4
II	PPLPp	FBP11, Prp40
III	(p/f)P(p/g)PPpR / (P/f)PP(R/K)gpPp	FBP21
IV	(poS/poT)P	PIN1
V	(p/f)PPPPP	Prp40

B

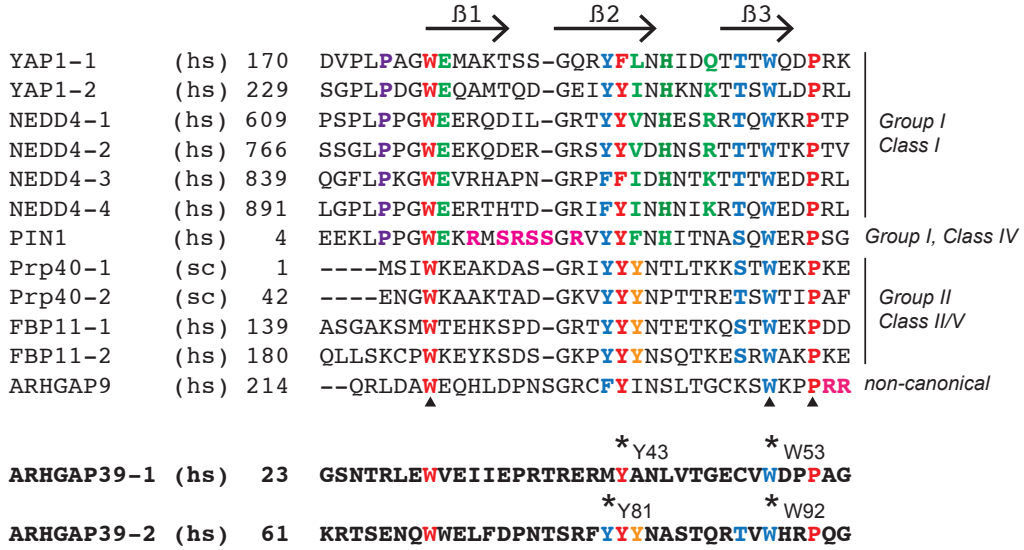

Figure 5.14.: Sequence alignment reveals highly conserved residues in ARHGAP39 WW domains
A Classification of WW domain containing proteins used in sequence alignment. L: leucine, T:Tyrosine, po: phosphorylated residue, lower case: favored residue, upper case: highly conserved residue (adapted (Salah, 2012)) **B** Alignment of representative WW domains generated with Clustal Omega. WW domains are characterised by the presence of two strictly conserved Trp residues and a strictly conserved Pro residue at the C-terminus (indicated by arrows). The strictly conserved Pro residues that is characteristic for group I WW domains is shown in purple. The first Trp, the central Tyr and the last Pro residues (in red) are essential for the structural stabilization of the domain. The central Tyr/Phe, the Thr/Ser and the Trp in the third textbeta-strand (in blue) are conserved for ligand binding. Additional residues involved in ligand binding are shown in green or in orange for class I/IV and class II/V, respectively. The side-chains of the Arg and Ser residues (in pink) are responsible to bind to (pS/pT)P motifs in PIN1. The residues chosen for mutagenesis in the ARHGAP39 WW domains are indicated with an asterisk. UniProt: YAP1 (P46937), NEDD4 (P46934), PIN1 (Q13526), Prp40 (P33203), FBP11 (O75400), ARHGAP9 (Q9BRR9). Abbreviations: YAP1: Yes-associated protein YAP65 homolog, NEDD4: E3 ubiquitin-protein ligase, PIN1: Peptidyl-prolyl cis-trans isomerase NIMA-interacting 1, Prp40: Pre-mRNA-processing protein, FBP11: formin binding protein 11, hs: Homo sapiens, sc: Saccharomyces cerevisiae

Based on the sequence alignment the following assumptions can be made (Fig. 5.14 B).
First, both WW domains contain the two conserved Trp residues and the C-terminal conserved Pro residue that characterize WW domains (indicated by arrows). Furthermore, they can be classified as Group II WW domains because a Pro residue (depicted in purple for Group I) ahead of the first Trp residue is missing (Macias et al., 2000).
Second, the first Trp residue, the Tyr residue in the center and the C-terminal Pro residue, which have all been described to be essentially required for proper folding of the domain, are present in both WW domains (in red) (Wiesner et al., 2002).
Third, while the first WW domain contains the conserved Trp residue in the third β-strand, it misses the Ser/Thr residue ahead and the Tyr/Phe residue in the center. These two residues together with the last Trp are strictly conserved residues for ligand binding (in blue) (Macias et al., 2002; Otte et al., 2003). In contrast, these three residues are present in WW2.
And fourth, the numbers of the aromatic residues in the central region of the second β-strand are different between the two ARHGAP39 WW domains. In WW1 there is only one Tyr residue (Y43) present, as in YAP1, NEDD4 and PIN1, whereas in WW2 there are three consecutive Tyr residues (Y81-Y83) similar to Prp40 and FPB11.

WW2 thus aligns well with the class II WW domains of FBP11 and PrP40 and should preferably bind to stretches of proline in the PPLP or (p/f)PPPPP motifs.
The sequence aligment of WW1, in contrast, is inconclusive. It may prefer the PPxY motif and/or the (pS/pT)P ligand because of the single Tyr residue present in the second β-strand. Moreover, the presence of three Arg residues in the center of WW1 might suggest a preference for phosphorylated Pro residues as in PIN1 (Ranganathan et al., 1997). However, besides missing the Tyr/Phe and Ser/Thr residues a highly conserved His residue of class I WW domains (in green), which is also involved in ligand binding, is missing as well (Sudol, 1996; Macias et al., 2002; Wiesner et al., 2002; Otte et al., 2003). Moreover, WW1 has similarity to the WW domain of ARHGAP9 that also misses one of the strictly conserved residues and all of the other class specific residues responsible for ligand binding. ARHGAP9 is one of the few examples that binds in a non-canonical way to its target proteins involving electrostatic interactions (Ang et al., 2007).

During the course of my project I aimed to analyse the specific interaction of the WW domains with potential binding partners. Therefore, I created point mutations in the two WW domains. The residues chosen for site-directed mutagenesis were selected based on this sequence alignment and should impair either the structural stabilization of the domain (Y43) or the binding to proline rich ligands (W53, Y81, W92) (Fig. 5.14, B) (Macias et al., 2002; Wiesner et al., 2002). The effects of the generated mutants will be discussed after.

The MyTH4 domain

The MyTH4 domain is a common domain in unconventional Myosins, where it appears in tandem with a FERM domain. I compared the MyTH4 domains of ARHGAP39 isoform 1 and isoform 2 with the domains of MYO VIIA, MYO X and MYO XV. The ARHGAP39 sequences can be aligned with high confidence in the regions of the conserved helices (Fig. 3.15, purple helices). The sequence similarity is also strong for the N-terminal and C-terminal linker region. Moreover, the strictly conserved motif responsible for the correct folding of the MyTH4-FERM domain interface (Planelles-Herrero et al., 2016) can be found in ARHGAP39 as well. Only for the highly variable insertions between the conserved helices, as illustrated for MYO VIIA, MYO X and MYO XV, no similarity was detected.
This indicates that the ARHGAP39 MyTH4 domain, even without the FERM domain, might fold in the same way as the MyTH4 domain of MF-Myosins. The 31 amino acid long insertion in isoform 2 locates between the conserved helices 8 and 9 and is therefore expected not to effect the structural folding of the domain (Fig. 5.15).

Five highly conserved residues (black star with red border) in the MYO VII MyTH4 domain mutations have been reported to cause deafness in humans (Usher syndrome I (USH1)) (Fig. 3.15, indicated by black stars). I selected these for mutagenesis in the MyTH4 domain of ARHGAP39. It has been assumed that the mutations either disrupt the proper folding of the domain itself, the interaction sites with the FERM domain or the binding with other proteins, however experimental validation is still missing (Wu et al., 2011). These mutant forms of the ARHGAP39 protein were later used for structure-function relation experiments.

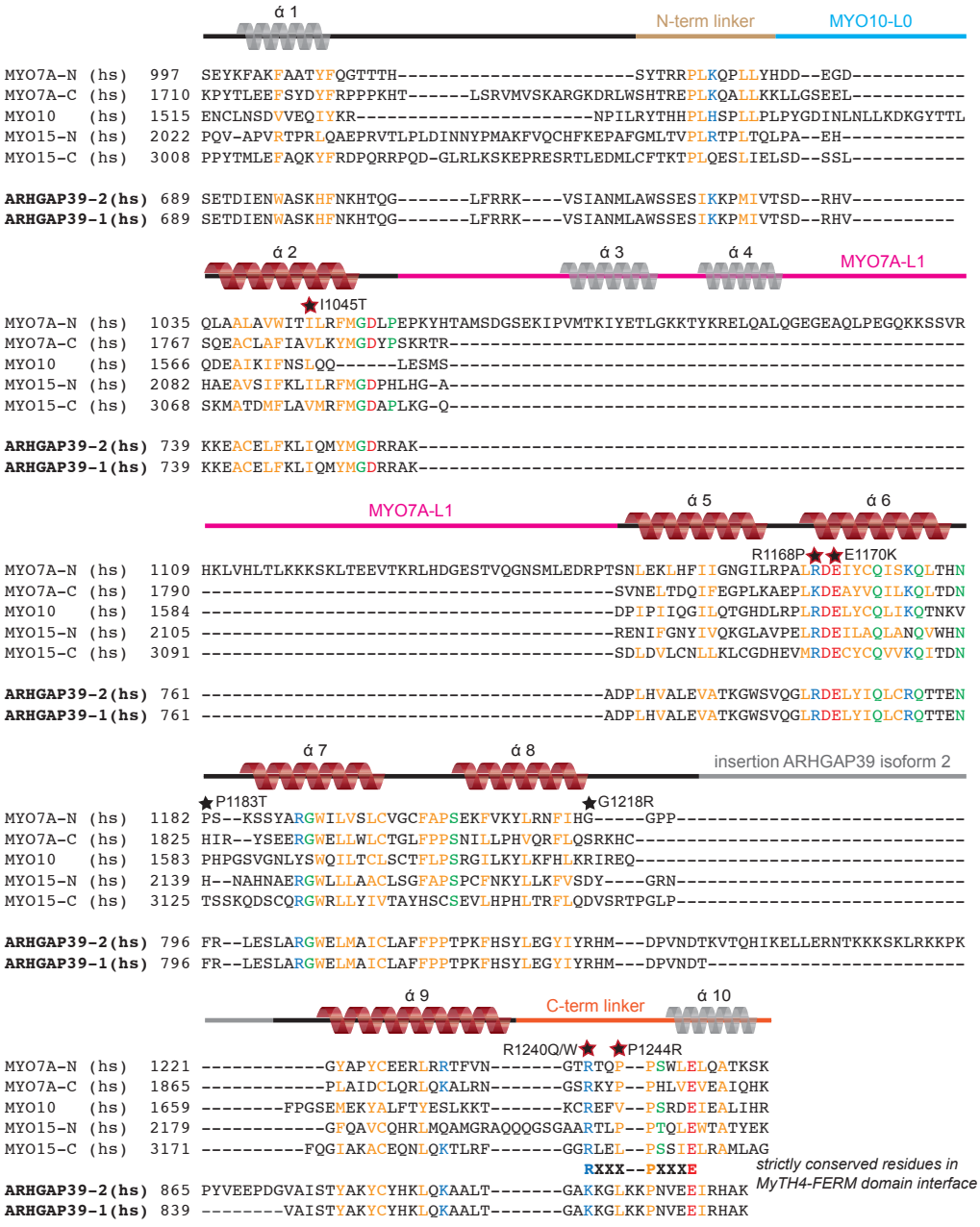

Figure 5.15.: see next page

Figure 5.15.: The ARHGAP39 MyTH4 sequence aligns with the highly conserved helical regions of the MF-MYOSINS
Structure based amino acid sequence alignment analysis using Clustal Omega. The conserved helices refer to the MyTH4 domain nomenclature of MYO VII in this sequence. The 6 conserved α-helices forming the MyTH4 domain of MYO VIIA are colored in red. The α-helices in grey are more variable. The conserved N-terminal and the C-terminal linker region that interact with the MyTH4 core domain on opposing sites are shown in beige and in orange, respectively. Hydrophobic, negatively charged, positively charged and highly conserved residues are shown orange, red, blue and green letters, respectively. Non-conserved insertions of the different MyTH4 domains are represented in indicated colors for MYO VIIA, MYO X and ARHGAP39 isoform 2. The reported seven missense mutations in Usher syndrome I of the N-terminal MyTH4 domain of MYO VIIA are illustrated with black stars. Black stars with a red border show the residues chosen for mutagenesis in the ARHGAP39 sequence. Abbreviations: hs: Homo sapiens, MYO7A: MYOSIN7A, MYO10: MYOSIN10, MYO15: MYOSIN15, -N/C: N/C-terminal MyTH4 domain. UniProt: MYO7A (Q13402), MYO10 (Q9HD67), MYO15 (Q9UKN7) (Figure adapted from (Wu et al., 2011))

5.3.2. ARHGAP39 localises at the plasma membrane and focal adhesions

In order to get an indication of the cellular context where ARHGAP39 operates I determined its subcellular localisation. Therefore, Cit-tagged ARHGAP39 was ectopically expressed in different cells lines. In MDCK and HeLa cells, both ARHGAP39 isoforms localised at the plasma membrane and at the basal membrane (Fig 5.16 A, B). In addition, in a notable fraction of cells, ARHGAP39 was enriched in the cytoplasm and/or in the nucleus. The two isoforms showed no obvious differences in the subcellular localisation and thus I continued working with the longer isoform 2.
To better visualize the basal membrane enrichment, I transfected Cit-ARHGAP39 isoform 2 in NIH 3T3 cells, which are much flatter. Here, ARHGAP39 localised on structures resembling focal adhesions (Fig. 5.16, A).

Next, I generated different truncation and deletion constructs of ARHGAP39 and analysed their subcellular localisation. Like the full length protein the GAP deletion construct also localized at the plasma membrane (Fig. 5.17 A, dGAP). Progressive deletion of the N-terminus in the constructs dWW, dm1, dm2, Cterm1 and Cterm2 had no influence on membrane targeting (Fig. 5.17 A). All these constructs still comprise the MyTH4 domain. The MyTH4 domain only, with the size of 229 amino acids, exhibited the strongest localisation at the plasma membrane (Fig. 5.17 A, MyTH4). The other parts of ARHGAP39 did not show a specific localisation and resided in the cytosol (Fig. 5.17 B). This demonstrates that the Myth4 domain is critical for plasma membrane targeting of ARHGAP39. Moreover, it appeared that the MyTh4 domain is required for correct protein folding of ARHGAP39. Ectopic expression of constructs missing these domains (dMyTH4, Nterm1, Nterm2) led to the formation of protein aggregates (Fig. 5.17 C).

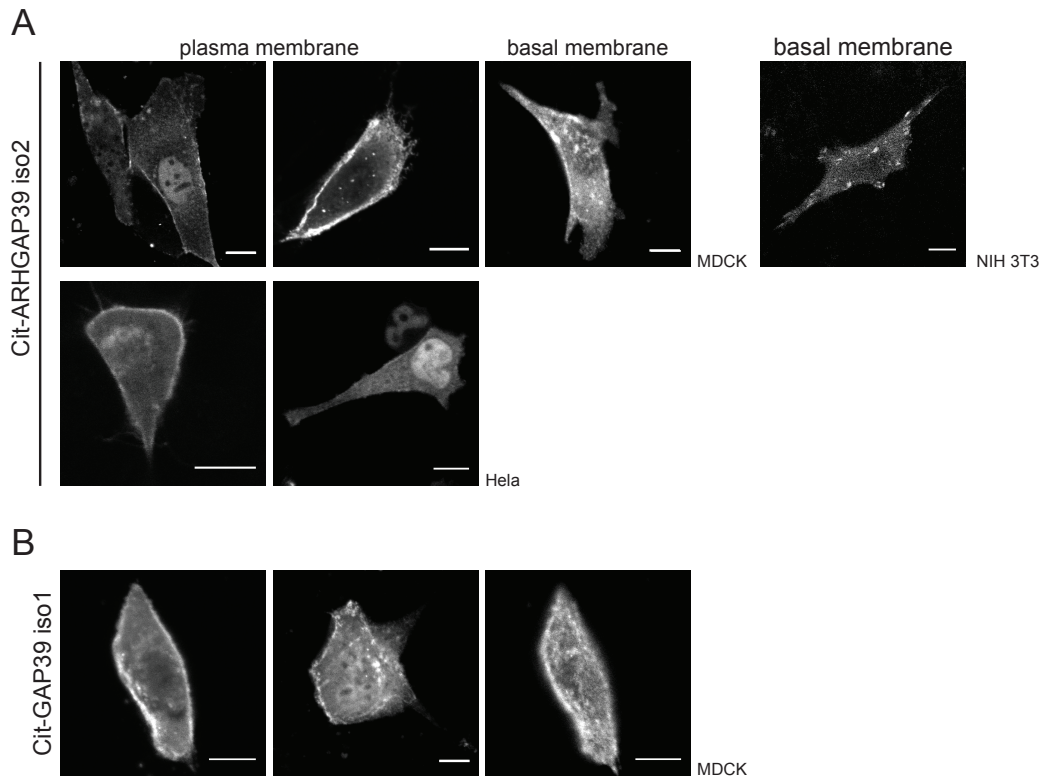

Figure 5.16.: ARHGAP39 localises at plasma membrane and at focal adhesion
A and **B** ARHGAP39 isoform 2 or isoform 1 were overexpressed with a Cit-tag in cells as indicated. Images were obtained in live cells by confocal microscopy. Abbreviations: Scalebar 10 µm

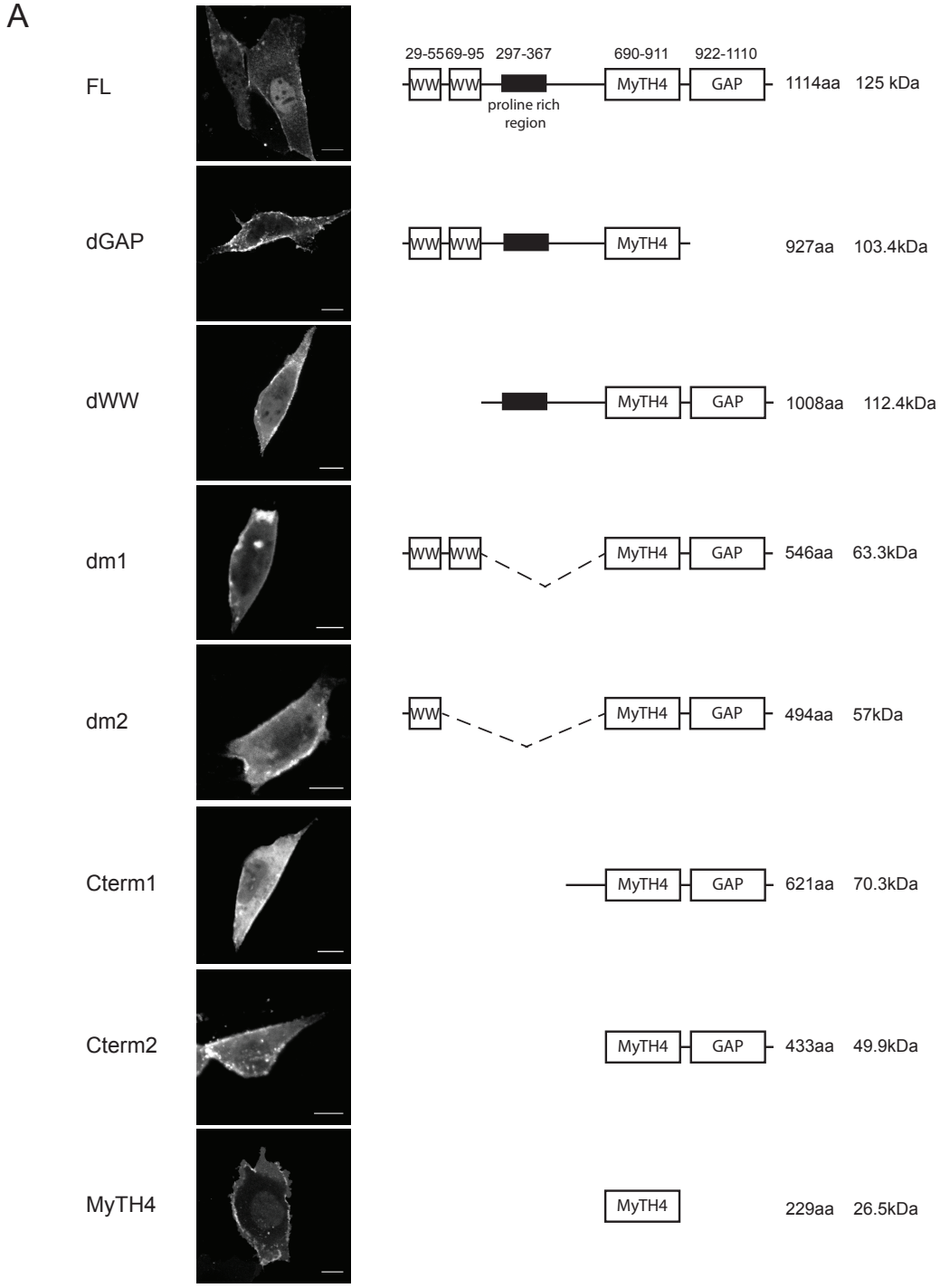

Figure 5.17.: see next page

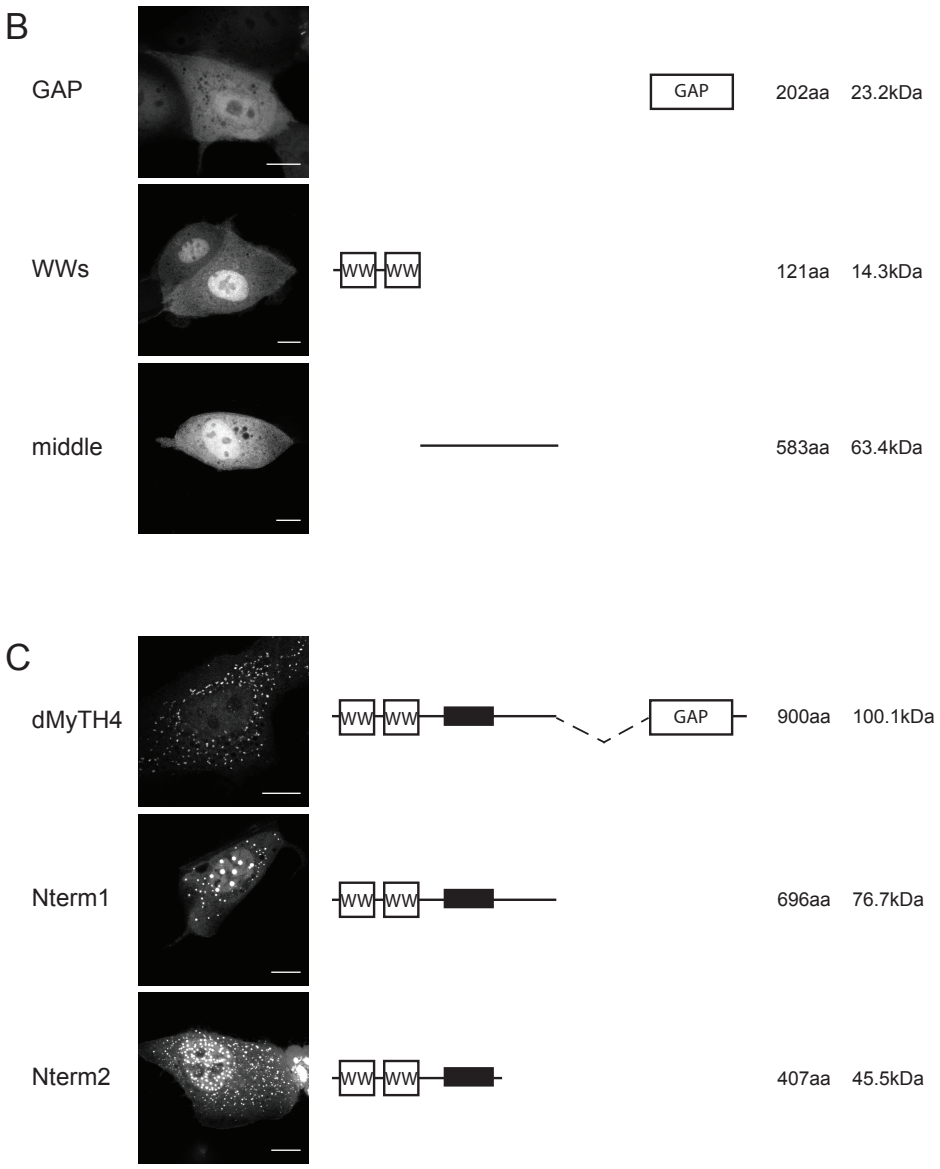

Figure 5.17.: Localisation and domain architecture of ARHGAP39 truncation constructs
A, **B** and **C** ARHGAP39 truncation constructs overexpressed in MDCK cells with an N-terminal Cit-tag. Schematic domain architecture, number of amino acids and predicted size in kDa are shown on the right. Images were acquired by confocal micrcoscopy. Scalebar 10 µm

Furthermore, I observed that ARHGAP39 truncation constructs missing the WW domains do not localize at the basal membrane anymore. To further investigate this, I transfected Cos7 cells stably expressing Cherry-Paxillin, a focal adhesion marker protein, with ARHGAP39 or different truncation or deletion constructs and imaged them by total internal reflection fluorescence (TIRF) microscopy. TIRF is ideally suited for imaging proteins located at the basal membrane of cells due to the low signal to noise ratio compared to confocal microscopy. Cos7 cells are well- suited because of their flat morphology. All images were acquired by Paul Markus Müller (AG Rocks, MDC).

ARHGAP39 clearly colocalised with Paxillin, thus confirming its enrichment at focal adhesions. Both proteins showed the same fluorescence intensity profiles at focal adhesion structures (Fig. 5.18, top panel). In contrast, colocalisation was not detectable for ARHGAP39 dWW missing the WW domains (Fig. 5.18, second panel). While the truncation dm1 containing both WW domains was detected at focal adhesions, truncation dm2, missing the second WW domain, was cytosolic (Fig. 5.18, 3rd and 4th panel, respectively). To further investigate the binding mode of the second WW domain to focal adhesions I examined if point mutations in WW2 could prevent its targeting there. The two mutations were generated based on the WW domain sequence alignment in section 3.3.1 and should be defective in ligand binding. TIRF microscopy revealed that focal adhesion targeting of the ARHGAP39 Y81A mutant was strongly reduced, whereas no effect was observed to the W92A mutant (Fig. 5.18, bottom panels).

In summary, by analysing the structure-function relationship I discovered that the second WW domain located in the N-terminus targets ARHGAP39 to focal adhesions. The MyTH4 domain is required for ARHGAP39 localisation at the plasma membrane and for correct folding of ARHGAP39.

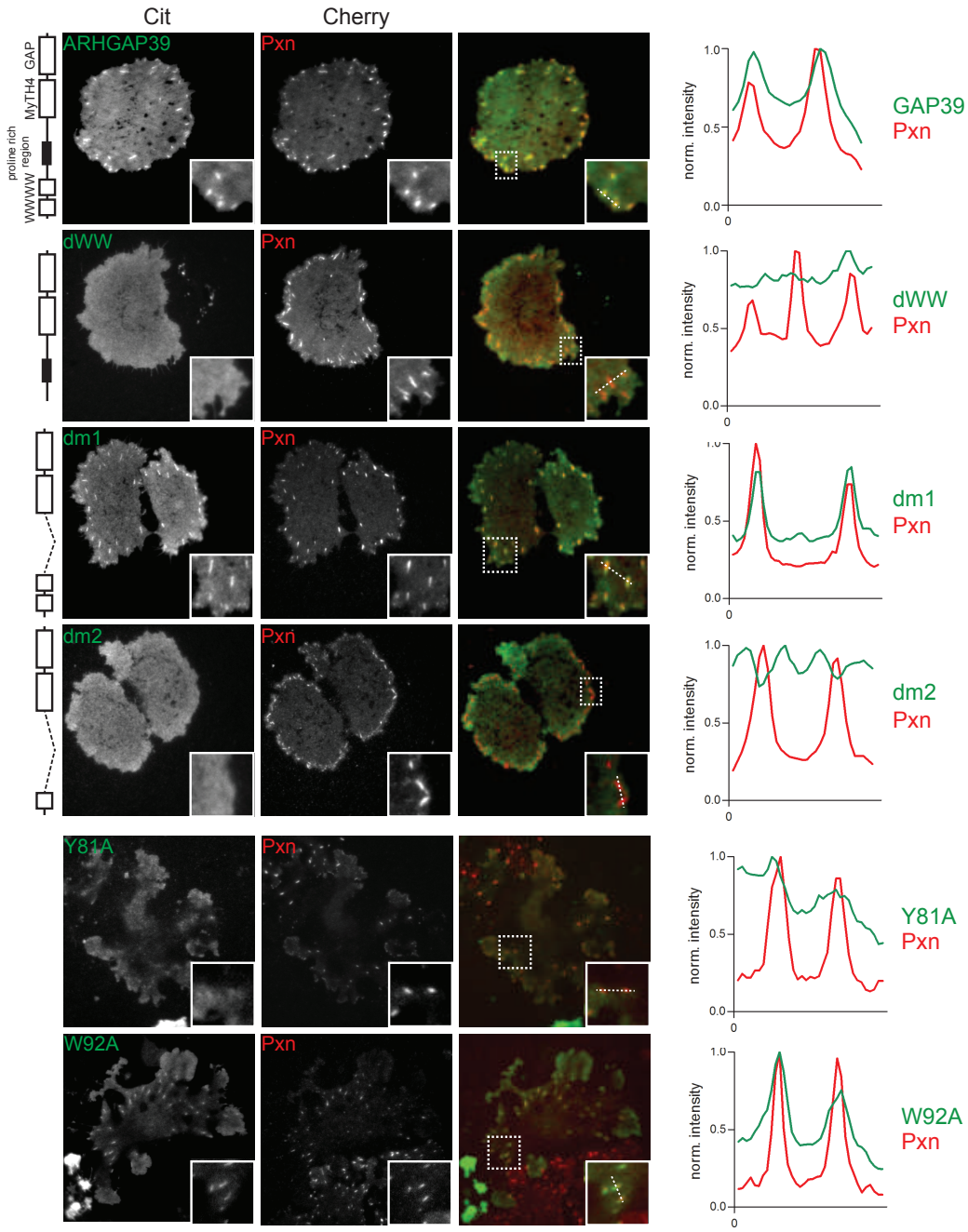

Figure 5.18.: The WW domains are required for binding to focal adhesions
Images of Cit-tagged ARHGAP39, dWW, dm1, dm2 and ARHGAP39 Y81A and W92A mutants ectopically expressed in Cherry-Pxn-Cos7 cells are shown in the first and second column, respectively. The merged image of both channels is depicted in the third column. For the truncation constructs schematic illustrations are shown on the left. For each panel a line scan diagram is shown which represents the intensity profile of both channels, which was measured for as a line through two or more focal adhesions (indicated as white dashed line in the magnified box). All images were acquired after 24 h with a TIRF microscope by Paul Markus Mueller (AG Rocks, MDC). Abbreviations: GAP39: ARHGAP39, Pxn: Paxillin.

5.3.3. ARHGAP39 exhibits substrate specificity for Rac1 and Cdc42

The identification of the substrate specificity of a GAP protein is crucial to understand its potential role in Rho GTPase signalling pathways. Previous work showed that Vilse, the ARHGAP39 homologue in *Drosophila*, is a Rac1/Cdc42 specific RhoGAP. This was shown for the isolated RhoGAP domain in an in vitro GTPase activation assay (Lundström et al., 2004).
To analyse the Rho GTPase specificity of ARHGAP39 I employed a novel Fluorescence Resonance Energy Transfer (FRET) based activity assay (Müller et al., BioRxiv). The advantage of this method over other cell-based assays is that the cellular context of Rho GTPase signalling is maintained, including interacting proteins and subcellular protein distribution. Moreover, the technique is not susceptible to artifacts due to the intrinsic GTPase activity of nucleotide-loaded recombinant Rho proteins used in pulldown assays or to GTP/GDP exchange during cell lysis.

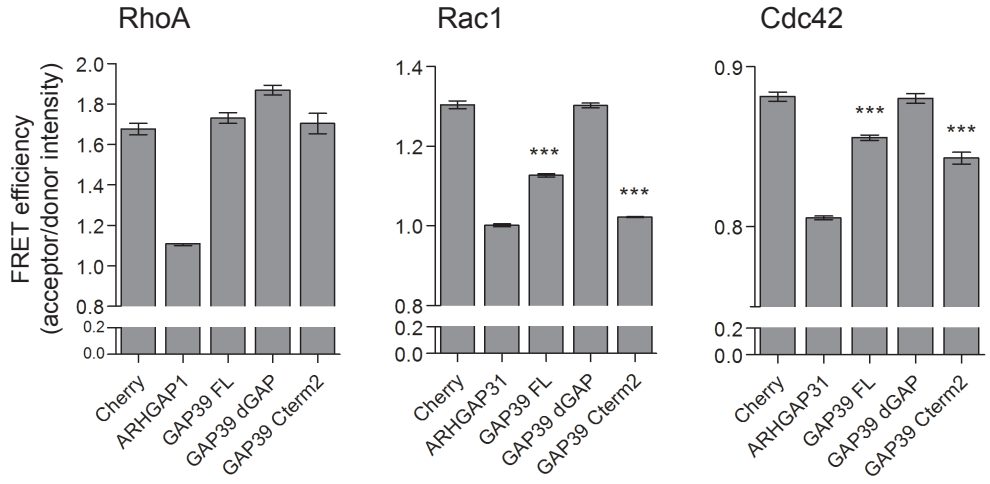

Figure 5.19.: ARHGAP39 is a Rac1 and Cdc42 specific GAP
HEK293T cells were transfected with RhoA, Cdc42 or Rac1 FRET sensors, together with mCherry-tagged ARHGAP39, or indicated truncation constructs or Cherry-Flag alone. Images were taken after 48 h and average FRET ratio was calculated form three independent experiments for which five fields of view were recorded each. Student's t-test was used to determine conditions that were significantly different from Cherry-control. The positive controls, ARHGAP1 or ARHGAP31, were not included in statistical calculations. Error bars represent standard deviation of three independent experiments. Significance was ranked as *** p<0.001, ** p<0.01. Abbreviations: GAP39: ARHGAP39.

This assay uses genetically encoded optimised biosensors for the Rho GTPases RhoA, Rac1 and Cdc42 (Fritz et al., 2013, 2015; Martin et al., 2016). Their domain architecture consists of a donor fluorophore mTealFP1, an effector Rho-binding domain that detects the GTP loaded (active) Rho GTPase, a linker region, the acceptor fluorophore mVenus and the functional Rho GTPase. Upon GTP loading the Rho GTPase binds its effector binding domain, resulting in a conformational change that brings the two fluorophores into close proximity and thereby leads to an increase in FRET efficiency. In cells the exogenously expressed biosensors exhibit an elevated GTP bound state, because the excess GTPase cannot be sufficiently sequestered to the cytosol by the endogenous pool of RhoGDI and thus is activated by endogenous GEF proteins at the membrane (Pertz et al., 2006). Therefore, the biosensors can be readily used to analyse a potential inactivation of Rho GTPases by ARHGAP39 co-expression, as seen by a decrease in FRET efficiency.

mCherry-tagged ARHGAP39 or its truncations were expressed together with the biosensors in HEK 293T cells. mCherry alone was used as a negative control and ARHGAP1 (a known Rho-specific GAP) or a truncation of ARHGAP31 (a Rac1/Cdc42 specific GAP) as positive controls. As anticipated, ARHGAP1 and ARHGAP31 robustly inactivated RhoA or Rac1/Cdc42, respectively. ARHGAP39 FL clearly reduced Rac1 and to a slightly lesser extend also Cdc42 activity, but did not affect the activity of RhoA (Fig. 5.19).
As expected, dGAP lacking the GAP domain did not exhibit catalytic activity towards Rac1 or Cdc42. In contrast, Cterm2 only comprising the RhoGAP domain in tandem with the MyTH4 domain further increased the catalytic efficiency of the GAP, leading to the strongest reduction in Rac1 and Cdc42 activity (Fig. 5.19). This observation implicates that ARHGAP39 is subjected to auto-regulation.

Next, I investigated if the reduction in Rac1/Cdc42 activity levels in ARHGAP39 expressing cells would result in changes in cytoskeletal organisation. ARHGAP39 transfected MDCK cells were immunostained for microtubules (tubulin) and focal adhesions (vinculin) and the actin cytoskeleton was visualised by phalloidin. Ectopic ARHGAP39 expression did not have any obvious effect on any of the mentioned structures (Fig. 5.20). It also did not induce other significant cell morphological changes that could arise from locally confined changes in Rac1 or Cdc42 activities. Since I did not observe any obvious phenotype I did not further examine the impact of ARHGAP39 on cytoskeletal dynamics.

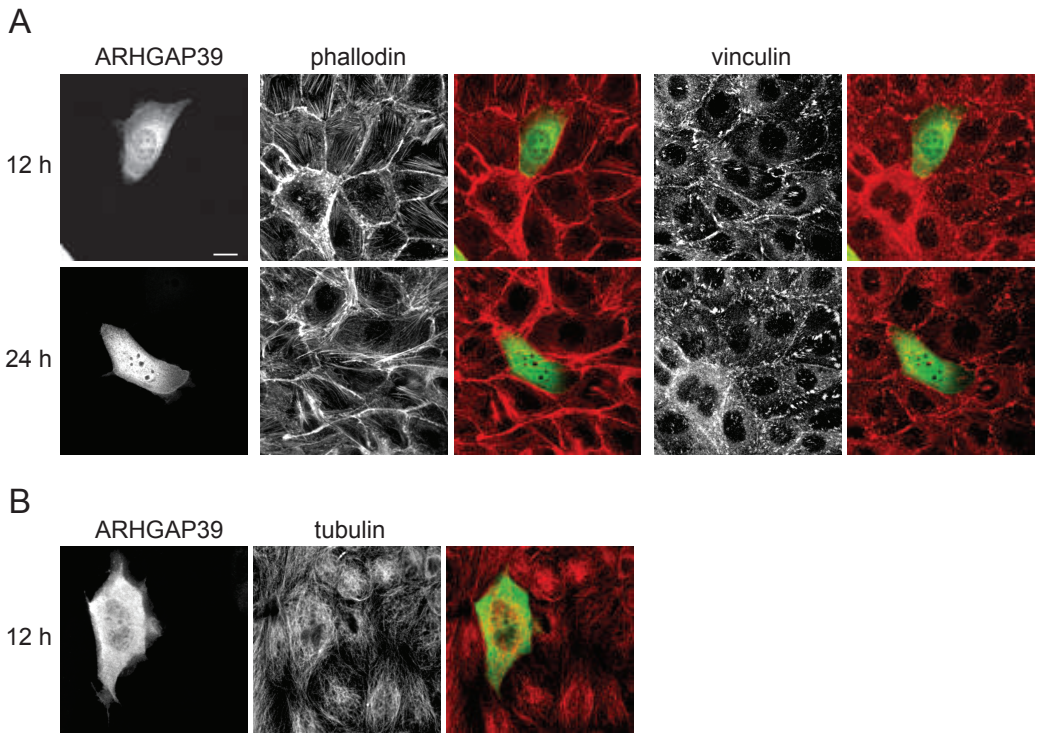

Figure 5.20.: ARHGAP39 overexpression does not obviously influence the cytoskeleton
A MDCK cells were transfected with Cit tagged ARHGAP39, fixed after 12 or 24 h and subjected to IF using rabbit anti-GFP and mouse anti-Vinculin antibodies and phalloidin. **B** Cit-ARHGAP39 was transfected in MDCK cells, fixed after 12 h and and subjected to IF using rabbit anti-GFP and mouse anti-Tubulin antibody.

5.3.4. A single point mutation in the MyTH4 domain disrupts plasma membrane binding of ARHGAP39 and reduces GAP activity

I demonstrated that the MyTH4 domain is responsible for targeting ARHGAP39 to the plasma membrane. In order to examine the functional importance of this domain point mutations were introduced, based on the sequence alignment with the unconventional MF-MYOSINs (Fig. 5.21 A). These mutants were generated in the MyTH4 truncation construct as well as in the ARHGAP39 FL construct and their subcellular localisation was analysed.

Point mutations at amino acids I749T, R781P, K896W and P901R in the MyTH4 domain showed no difference in binding to the plasma membrane. However, the MyTH4 mutant E783K completely lost its ability to bind to the membrane and was only found in the cytoplasm (Fig. 5.21 B). To directly compare the localisation of MyTH4 WT and MyTH4 E783K I co-expressed them in MDCK cells. As shown in Figure 3.21 B , the MyTH4 WT localised at the membrane whereas the E783K mutant was exclusively cytoplasmic, which was also detected for the full length ARHGAP39 E783K (Fig. 5.21 D).

To test if the E783K mutation in the MyTH4 domain would also affect the GAP activity of ARHGAP39 a FRET biosensor activity assay was conducted. The E783K mutant could decrease Rac1 activity, albeit to a significantly lower level than wild type ARHGAP39. This indicates that the plasma membrane localisation of ARHGAP39 enhances the catalytic activity of the GAP domain (Fig. 5.21 E).

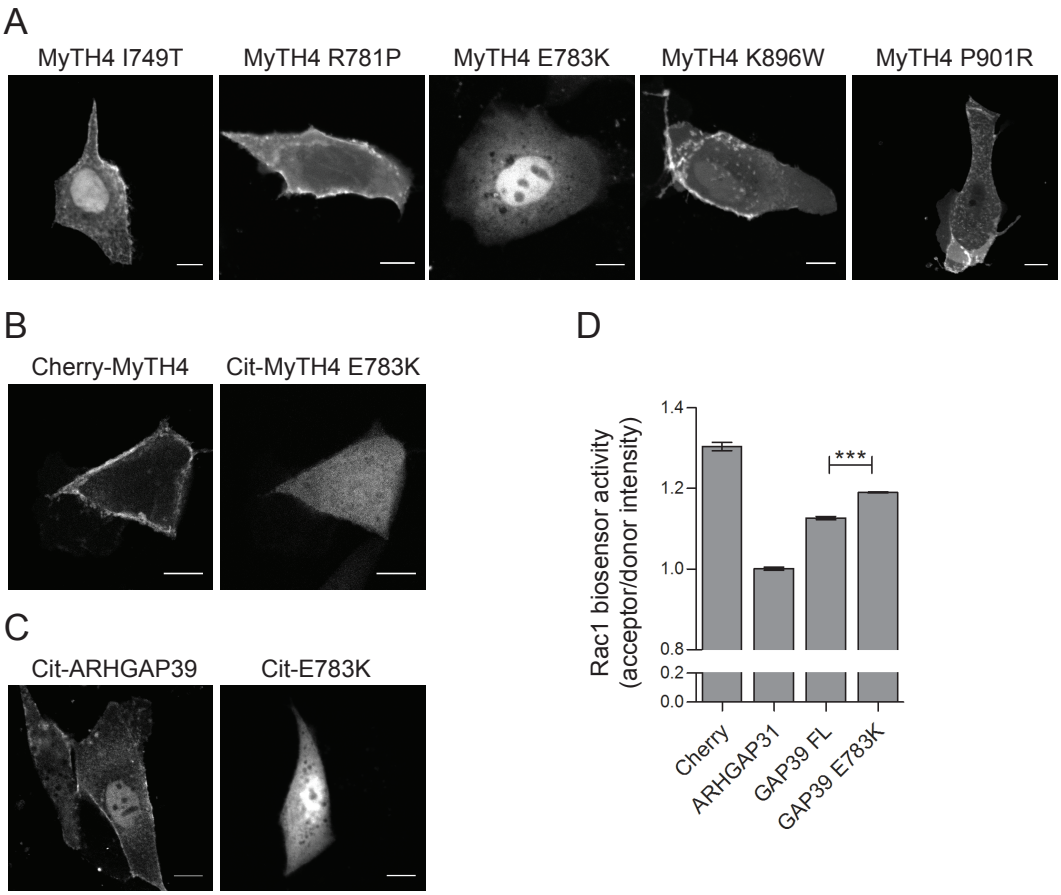

Figure 5.21.: A single point mutaion in the MyTH4 domain abolishes binding to the plasma membrane
A MyTH4-WT or MyTH4 point mutants expressed with an N-terminal YFP-tag in MDCK cells. **B** Co-expression of Cherry-MyTH4 and YFP-MyTH4 E783K in MDCK cells. **C** Overexpression of ARHGAP39 full length or ARHGAP39 E783K mutant with an N-terminal YFP-tag in MDCK cells. All images were acquired in live cells with a confocal microscope. Scalebar 10 µm **D** HEK293T cells were transfected with Rac1 FRET biosensor, together with mCherry-tagged ARHGAP39, or ARHGAP39 E783K or Cherry-Flag alone. Images were taken 48 h after transfection and average Rac1 biosensor activity was calculated from three independent experiments for which five fields of view were recorded each. Student's t-test was used to determine conditions that were significantly different from the GAP39 FL condition. The positive control ARHGAP31 (truncated form) was not included in statistical calculations. Error bars represent standard deviation of three independent experiments. Significance was ranked as *** p<0.001. Abbreviations: GAP39: ARHGAP39.

5.3.5. ARHGAP39 is N-terminally auto-regulated

Auto-regulation is a common mechanism for RhoGEF proteins to regulate their catalytic activity, but has been described for only a few RhoGAPs so far. It is assumed that the Rho regulatory proteins are auto-regulated by intramolecular backfolding of one of their terminal regions. In this "closed" conformation the Rho GTPases are prevented from accessing the catalytic domain. The intramolecular folding is released by specific cues and allows access of the Rho GTPases to the catalytic domains.

ARHGAP39 comprises an N-terminus containing the two WW domains, a structurally disordered central part containing a proline rich region, followed by the MyTH4 domain, which is essentially required for correct folding of ARHGAP39. Due to the location of the GAP domain at the C-terminus of ARHGAP39 it is conceivable that the N-terminal region folds over to establish intramolecular interactions in the central region and/or MyTH4 domain, thereby masking the GAP domain.

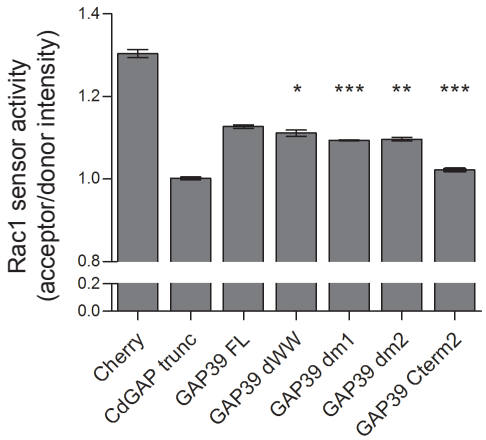

Figure 5.22.: Subsequent deletion of N-terminus increase activity of ARHGAP39
HEK293T cells were transfected with Rac1 FRET biosensor, together with mCherry-tagged ARHGAP39, or ARHGAP39 deletion mutants or Cherry-Flag alone. Images were taken 48 h after transfection and average Rac1 biosensor activity was calculated from three independent experiments for which five fields of view were recorded each. Student's t-test was used to determine conditions that were significantly different from the GAP39 FL condition. The positive control ARHGAP31 (truncated form) was not included in statistical calculations. Error bars represent standard deviation of three independent experiments. Significance was ranked as *** p<0.001. Abbreviations: GAP39: ARHGAP39.

Thus, I set out to examine if deletion of the N-terminal region containing the WW domains (dWW) or deletion of the central region (dm1, dm2) would increase the activity of ARHGAP39. Therefore, Rac1 biosensor activity was measured in the FRET activity assay. I observed a slight increase of GAP activity for the dWW construct and even more for the constructs with-

out the central region (dm1, dm2) (Fig. 5.22) The strongest decrease in Rac1 biosensor activity was detected for the Cterm2 construct, missing both regions. This implies that subsequent deletion of the N-terminal and central regions increases the GAP activity, which is the strongest when both regions are deleted. Thus, both regions are involved in ARHGAP39 auto-inhibition (Fig. 5.23).

Speculating that the N-terminal region binds in *cis* to the central region and/or MyTH4 domain I co-expressed Cit-FL or Cit-dWW with Flag-dm1 and Flag-dm2. The N-terminal region present in dm1 and dm2 should not be able to fold back, because the central region is missing in these deletion mutants (Fig. 5.23 B, C). Moreover, considering a potential association with the MyTH4 domain this might also be prevented due to the lack of flexibility to fold back as the unstructured central region is deleted between the N-terminus and MyTH4 domain. In dWW the central region and /or MyTH4 domain should be unmasked due to deletion of the N-terminal region. Thus, I assume that the N-terminal regions of dm1 and dm2 bind to dWW in *trans*, but not to FL since its central region is masked by its own N-terminus (Fig. 5.23 C) Cterm2 was considered as a negative control that cannot bind to FL and dWW.
Indeed, dm1 and dm2 bound strongly to the dWW mutant, whereas only weak binding to ARHGAP39 FL protein was observed (Fig. 5.23 D). As anticipated, Cterm2 failed to interact with dWW and FL.
Additionally, I used the isolated WW domains as bait to pull down dWW or FL ARHGAP39 and I could show that the isolated WW domains pulled down the co-expressed dWW construct. Moreover, as expected, interaction with the FL construct was dramatically reduced (Fig. 5.23 E, F).

Together, the data strongly implicate that the N-terminal region containing the WW domains is able to bind to ARHGAP39 and thus mediates the intramolecular binding in *cis*. Thus, I aimed next to understand where it would bind to. Due to the presence of the two WW domains in the N-terminal region I assumed that they would recognize proline-rich peptide targets. Furthermore, the WW1 domain was observed to be sufficient to mediate the binding of dm2 to dWW (Fig. 5.23 D). Therefore, it is conceivable that the N-terminus folds back to the central region and/or MyTH4 domain by establishing contacts between WW1 and proline-rich target motifs.

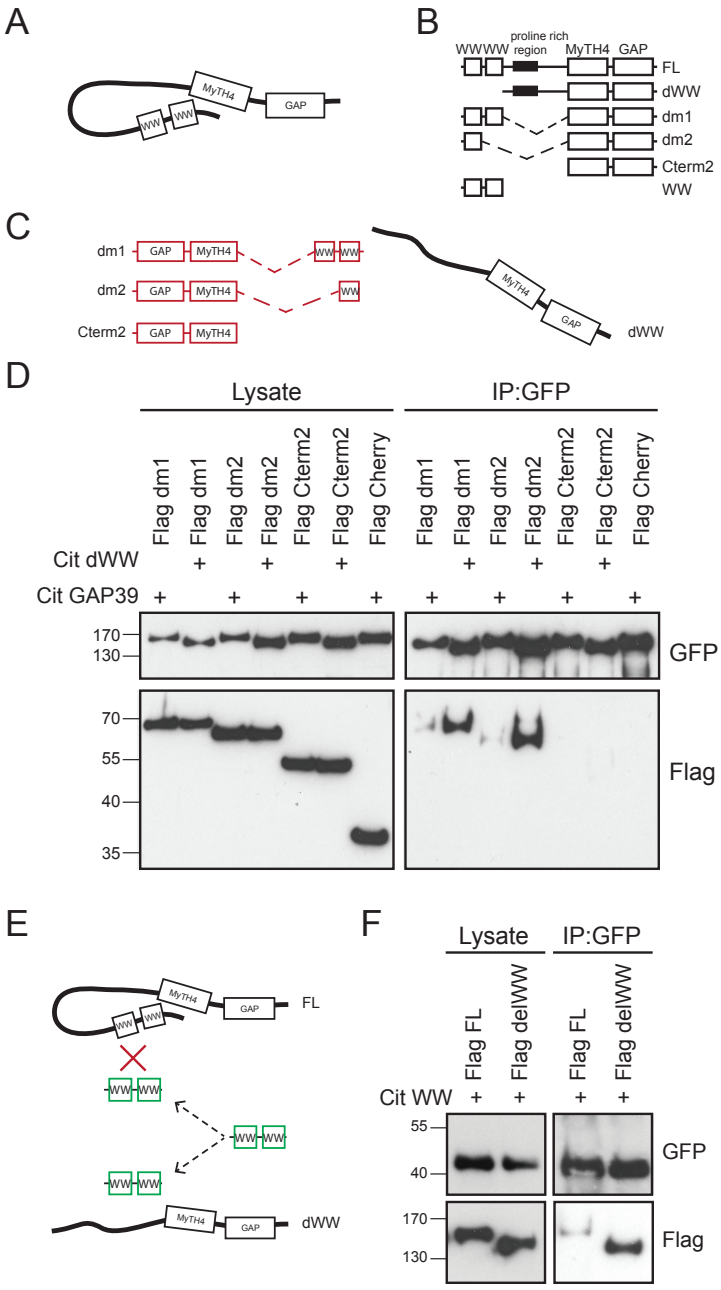

Figure 5.23.: The WW domains mediate the intramolecular folding of ARHGAP39
A Schematic representation of all the ARHGAP39 truncation constructs used in these experiments. **B** Scheme illustrating the backfolding of the N-terminal region of ARHGAP39. Thereby, the central region and/or the MyTH4 domain could be masked. **C** Illustration how the different ARHGAP39 deletion mutants could bind to ARHGAP39 FL or ARHGAP39 dWW. See description in text. **D** HEK 293T cells were transfected with Flag-ARHGAP39 truncation constructs or Flag-Cherry control together with Cit-ARHGAP39, Cit-dWW. Co-IP was performed using GFP-beads and proteins were detected with anti-Flag and anti-GFP antibodies. **E** Illustration of assumed binding mechanism of the WW domains to ARHGAP39 FL and dWW. See description in text. **F** HEK 293T cells were co-transfected with Flag-ARHGAP39 FL (full length) and Flag-dWW and with YFP-WW. Co-IP was performed after 24 h of transfection using GFP-beads and proteins were detected with anti-Flag and anti-GFP antibodies.

Since the central region of ARHGAP39 contains a proline-rich sequence I speculated that the N-terminus would bind there. Peptide spot overlay assays indicate peptide sequences that might be involved in protein-protein interactions. To this end, the N-terminal ARHGAP39 sequence (amino acids 1-690) was spot-synthesized on a cellulose membrane (kindly provided by Dr. Klussmann, MDC), which was then incubated with a recombinant GST-WW fusion protein containing the WW domains of ARHGAP39 (amino acids 2-115, purified by Anja Schütz, MDC).
The strongest signals were observed for the peptides I3 to M3 (amino acids 242-288) that reside in the annotated proline rich region (Fig. 5.24 A, B). Eight single Pro residues are located within this sequence, three of them with a Ser residue ahead that might be potential phosphorylation targets (poSP) (Lu et al., 1999). Two more spots were detected that showed strong interaction with the recombinant WW domains. The spot K1 (amino acids 51-79), a sequence located in the WW domain itself and the spot A7 (amino acids 601-629), an unstructured region in N-terminal proximity of the MyTH4 domain (Fig. 3.24 A). In these two peptide sequences a pair of Pro residues or one single Pro residue can be found, respectively.

To sum up, I demonstrated that ARHGAP39 is subjected to auto-regulation. The backfolding mechanism requires the N-terminal region containing the WW domains. The results of the peptide spot assay implicate that the WW domains recognize two sequence motifs in the central part of ARHGAP39. Interestingly, one peptide sequence contains multiple (pS)P motifs that could be recognized by WW1 (Fig. 5.24 B), however binding to the MyTH4 domain could not be ruled out.

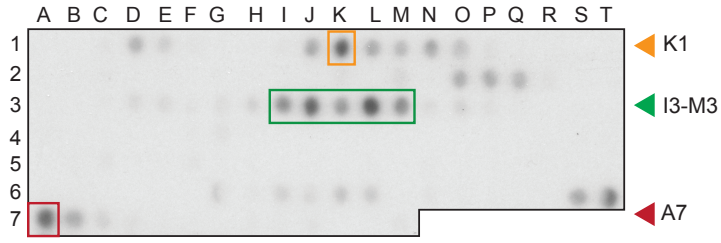

K1: CVWD**PP**AGVRIKRTSENQWWELFDPNTSR

I3-M3: RRPSGSQHS**P**SLQTFA**P**EADGT
IFF**P**ERR**P**S**P**FLKRAEL**P**GSS**P**L

A7: RAFSEDEALAQQENRHWRRGTFEKLGF**P**Q

```
        10         20         30         40         50         60         70
MSQTQDYECR SHNVDLPESR IPGSNTRLEW VEIIEPRTRE RMYANLVTGE CVWDPPAGVR IKRTSENQWW
        80         90        100        110        120        130        140
ELFDPNTSRF YYYNASTQRT VWHRPQGCDI IPLAKLQTLK QNTESPRASA ESSPGRGSSV SREGSTSSSL
       150        160        170        180        190        200        210
EPEPDTEKAQ ELPARAGRPA AFGTVKEDSG SSSPPGVFLE KDYEIYRDYS ADGQLLHYRT SSLRWNSGAK
       220        230        240        250        260        270        280
ERMLIKVADR EPSFLAAQGN GYAPDGPPGV RSRRPSGSQH SPSLQTFAPE ADGTIFFPER RPSPFLKRAE
       290        300        310        320        330        340        350
LPGSSSPLLA QPRKPSGDSQ PSSPRYGYEP PLYEEPPVEY QAPIYDEPPM DVQFEAGGGY QAGSPQRSPG
       360        370        380        390        400        410        420
RKPRPFLQPN KQGPPSPCQQ LVLTKQKCPE RFLSLEYSPA GKEYVRQLVY VEQAGSSPKL RAGPRHKYAP
       430        440        450        460        470        480        490
NPGGGSYSLQ PSPCLLRDQR LGVKSGDYST MEGPELRHSQ PPTPLPQAQE DAMSWSSQQD TLSSTGYSPG
       500        510        520        530        540        550        560
TRKRKSRKPS LCQATSATPT EGPGDLLVEQ PLAEEQPPCG TSLAPVKRAE GEAEGARGAA EPFLAQARLA
       570        580        590        600        610        620        630
WEAQQAHFHM KQRSSWDSQQ DGSGYESDGA LPLPMPGPVV RAFSEDEALA QQENRHWRRG TFEKLGFPQI
       640        650        660        670        680        690
LLEKSVSVQT NLASPEPYLH PSQSEDLAAC AQFESSRQSR SGVPSSSCVF PTFTLRKPS
```

light grey: WW domains
grey: proline rich region

Figure 5.24.: The WW domain bind strongly within in the proline rich region of ARHGAP39
A Peptide spot overlay assay depicting spots were the GST-WW fusion protein (amino acids 2-115) bound to ARHGAP39 (amino acids 1-690) spotted on a cellulose membrane. The strongest spots are highlighted in colored boxes and the corresponding sequences are shown. **B** Sequence of the N-terminal ARHGAP39 protein (amino acids 1-690). The two WW domains and the putative proline rich region are indicated in light grey and dark grey boxes, respectively. The identified sequences in the overlay assay are depicted in bold letters, with the color code corresponding to the identified spots.

5.3.6. ARHGAP39 is broadly expressed in human

In the previous experiments ARHGAP39 was characterized on the molecular level including its subcellular localisation, auto-regulation and its GAP specificity. However, in order to investigate its cellular function on the endogenous level I had to identify a cell line with optimal expression levels to set up cell-based assays.

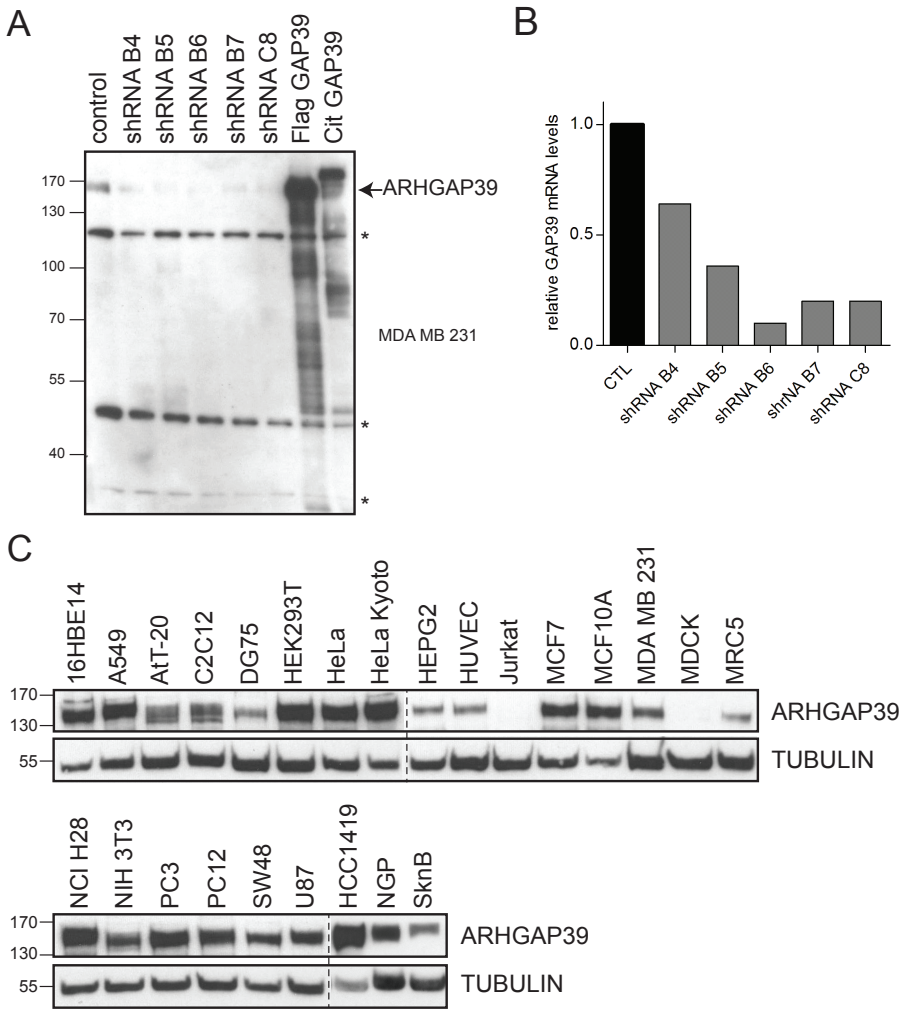

Figure 5.25.: ARHGAP39 is broadly expressed in cell lines
A Detection of ectopically expressed Flag-ARHGAP39, YFP-ARHGAP39 or endogenous ARHGAP39 in MDA MB 231 cells and in *ARHGAP39* shRNA mediated knock down cells with an anti-ARHGAP39 antibody. **B** Detection of *ARHGAP39* knock down by qPCR. **C** Detection of expression levels of endogenous ARHGAP39 in different cell lines with an anti-ARHGAP39 antibody. Asterisks: unspecific bands. Abbreviations: shRNA: small hairpin RNA, qPCR: quantitative PCR

First, I validated the suitability of the commercially available anti-ARHGAP39 antibody from Bethyl (cat. A302-598), which recognized the overexpressed Flag-ARHGAP39 and Cit-ARHGAP39 constructs in MDA MB 231 cells (Fig. 5.25 A). In untransfected control cells a band with a similar molecular weight (MW) to Flag-ARHGAP39 was detected. This band disappeared in MDA MB 231 cells stably transduced with different *ARHGAP39* targeting shRNA viruses.
Notably, the expected MW of endogenous ARHGAP39 is 125 kDa and thus slightly differs from the observed band at 150 kDa (Fig. 5.25 A). This could be due to post translational modifications of the protein or different folding, resulting in different migratory properties in the gel. Additional bands at 120 kDa, 50 kDa and 30 kDa were observed, but were unaffected by the knockdown (Fig. 5.25 A, asterisks). Based on these results, I concluded that the upper band of 150 kDa represents endogenous ARHGAP39. The knockdown of ARHGAP39 in the different shRNA cell lines could additionally be confirmed at the mRNA level by qRT-PCR (Fig. 5.25 B).

Knowing that its homologue Vilse was characterised in axons (Hu et al., 2005; Lundström et al., 2004; Lim et al., 2014) and that zebrafish Arhgap39 is expressed in brain and in ECs (Fig. 5.3) I questioned if its expression would be restricted to neural and endothelial cell lines. Surprisingly, ARHGAP39 was found to be expressed in almost all cell lines tested, apart from Jurkat T lymphocytes (Fig. 5.25 C). No signal was detected in MDCK cells, however these are dog derived cells and therefore the antibody might not recognise the canine homologue. ARHGAP39 was most prominently expressed in commonly used cell lines such as HEK 293T, HeLa, but also in breast cancer cell lines, (MDA MB 231, MCF7, HCC1419), in endothelial cells (HUVEC) and in human glioblastoma (U87) and neuroblastoma cells (NGP, SKNBE2).

Next, I examined if the observed expression pattern of Arhgap39 in zebrafish also applies for the murine and human homologue.
First, the expression of Arhgap39 in mouse tissue was examined. I designed mouse *in situ* probes to detect *Arhgap39* mRNA and tested them on mouse slices from embryonic stage E16. This was done in collaboration with Maciej Czajkowksi (AG Rocks, MDC). Predominant expression was detected in the neural tissue, specifically in the cortex, olfactory bulb, midbrain, hindbrain and in the olfactory epithelium (Fig. 5.26 A), with a similar pattern in E11 and E14 mice (data not shown). I then analysed mouse tissue lysates from adult mice by Western blot. Arhgap39 was found to be strongly expressed in the brain, which is in line with the observation in the mouse *in situ* hybridization experiment, and in testis (Fig. 5.26 B).
I assessed the expression pattern of ARHGAP39 in human tissue lysate. A commercially available PVDF membrane with different human tissues lysates was incubated with anti-ARHGAP39 (Fig. 5.26 C). Again, ARHGAP39 expression was detected in brain and testis.

Figure 5.26.: ARHGAP39 is enriched in neural tissue
A *in situ* hybridization to detect *Arhgap39* mRNA in mouse tissue of E16 embryo. *Arhgap39* mRNA was observed in: 1 cortex, 2 olfactory bulb, 3 midbrain, 4 hindbrain and in 5 olfactory epithelium. In collaboration with Maciej Czaijkowksi (AG Rocks, MDC). Scale bar: 3mm **B** Endogenous Arhgap39 levels in mouse tissue lysates. **C** Endogenous ARHGAP39 expression pattern in human tissue lysates. **D** Endogenous ARHGAP39 levels in human endothelial cell lines. Abbreviations: HPAEC: human pulonary artery endothelial cells (EC), HCAEC: human coronary artery EC, HIAEC: human illiac artery EC, HAEC: human aortic EC, HMVEC-L: human lung microvascular EC, HUVEC: human umbilical cord EC, HUAEC: human primary umbilical artery EC, HMVEC-d Ad: human dermal microvascular EC from derived from adults

Lastly, I confirmed ARHGAP39 expression in various human ECs. Probing of a commercial PDVF membrane containing different human endothelial cell line samples demonstrated a broad expression of ARHGAP39 in endothelial cells (HPAEC, HCAEC, HIAEC, HAEC, HUVEC, HUAEC, HMVEC-d Ad), except for HMVEC- L (Fig. 5.26 D).

To sum up, ARHGAP39 is strongly expressed in the brain and shows robust expression in ECs and testis. The expression pattern of ARHGAP39 applies to the human, the murine and the zebrafish homologue, suggesting a conserved expression pattern.
To study basic cellular functions of ARHGAP39 I decided to use HeLa cells, because endogenous expression levels of ARHGAP39 was among the highest, the cell line is easily transfectable and suitable to create knock down cells by shRNA virus transduction.

5.3.7. Knockdown of *ARHGAP39* impaires cell migration

Since ectopic expression of ARHGAP39 had no effect on the cytoskeleton and showed no cellular phenotype, I aimed to study its function in *ARHGAP39* depleted HeLa cells. A widely used assay to examine the migratory behaviour of cells is the scratch wound assay that can be used to address basic cell migration without stimulation. In this set up an artificial gap is created on a confluent cell monolayer. Then the migration of either the cell monolayer as a whole or individual cells on the edge into the gap is monitored.
Because this assay takes place over multiple hours or even days I decided to stably knock down *ARHGAP39* to avoid problems as transient shRNA mediated knockdown may be lost over the course of the long experiment. arising from different siRNA transfection times. Based on the extend of the shRNA mediated knockdown in MDA MB 231 cells in the previous experiment (Fig. 5.25 A, B) I decided to use the shRNA viruses B6 and B7 for the generation of *ARHGAP39* knockdown HeLa cells. Western blot analysis revealed that ARHGAP39 protein expression is not detectable in shRNA B6 cells and strongly reduced in shRNA B7 cells compared to control HeLa cells and stuffer virus shRNA cells (Fig. 5.27 A). Subsequently, the migratory behaviour of these cells was compared to a non-targeting stuffer virus shRNA cell line. Since HeLa cells tend to migrate as individual cells rather than as a monolayer I analysed single cells.

The migratory activity of *ARHGAP39* shRNA and stuffer shRNA cells was then examined in the scratch wound assay. Briefly, cells were grown until confluency in a 24 well plate and upon wounding they were then allowed to migrate into the wound. After 10 h, I consistently observed slower migration of shRNA B6 and B7 cells into the wound compared to stuffer control shRNA cells, as exemplified in Fig. 5.27 B. This is also illustrated as an overlay of individual tracks of the *ARHGAP39* shRNA B6, shRNA B7 and stuffer shRNA cell lines (Figure 5.27 C).

Next, I analysed the migratory behaviour of individual cells in detail and quantified their total migration distance, velocity and migration distance into the wound (x-axis migration). For both *ARHGAP39* knockdown cell lines I detected a significantly reduced total migration distance (B6: $p<0.0001$, B7: $p=0.0031$) and cell velocity (B6, B7: $p<0.0001$) compared to stuffer shRNA cells (Fig. 5.27 D, E). Moreover, the locomotion into the wound was significantly impaired in the *ARHGAP39* knockdown cells as well (B6, B7: $p<0.0001$) (Fig. 5.27 F).

Taken together, the results implicate a role of ARHGAP39 in cell migration.

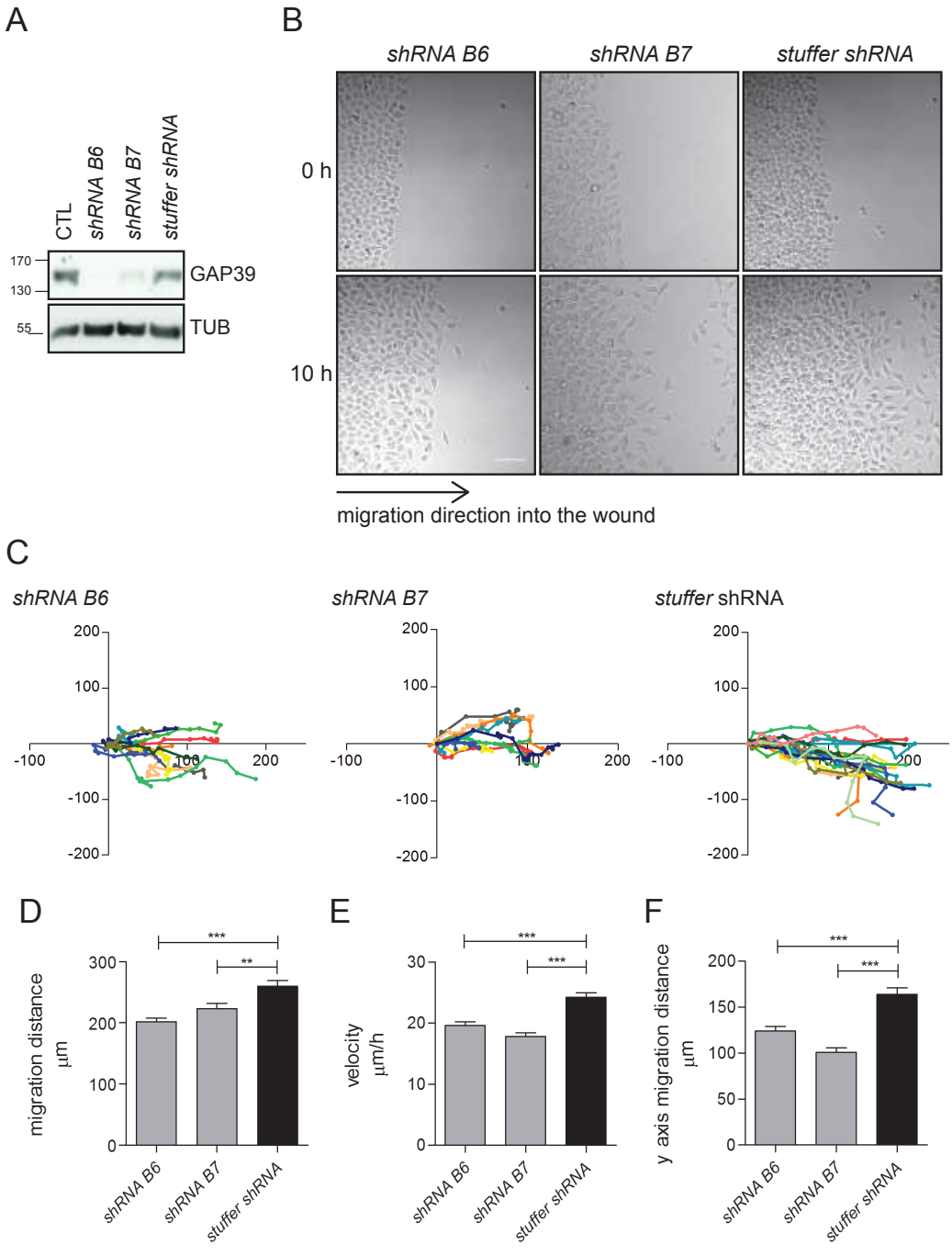

Figure 5.27.: see next page

Figure 5.27.: Impaired migration of *ARHGAP39*
A Endogenous ARHGAP39 expression was tested in HeLa control cells, GAP39 shRNA B6, GAP39 shRNA B7 and stuffer shRNA cells with anti-ARHGAP39 antibody. **B** *ARHGAP39* shRNA B6, B7 and stuffer shRNA cells were cultured in 24 well plate until dense. A scratch was made with a filter tip and cells were imaged with a confocal microscope in 15 min intervals for the next 10 h. Images of HeLa cells stably transfected with shRNA B6, B7 or stuffer lentiviruses taken at 0 h or 10 h after the scratch was made. Cells migrated in the presence of Mitomycin C to inhibit cell division. **C** Scatter plots depicting the migration behaviour of single cells of the indicated cell line during the scratch wound assay. In **D** the total migration distance, in **E** the cell velocity and in **F** the migration into the wound was calculated for individual *ARHGAP39* shRNA B6 and shRNA B7, and stuffer virus shRNA cells after 10 h of migration. Asterisks denote statistical significance as calculated by Student's t-test. Significance was ranked as *** $p<0.001$, ** $p<0.01$. The assay was repeated at least two times with each cell line in duplicates. For each well 10 cells were analysed. Total numbers of analysed cells are: ARHGAP39 shRNA B6: 140 cells, ARHGAP39 shRNA B7: 120 cells, stuffer shRNA: 100 cells. Abbreviations: GAP39: ARHGAP39 Scalebar 100 µm

5.3.8. Validation of ARHGAP39 interaction with binding partners found in a mass-spectrometry screen

One goal of this thesis was to study the function of ARHGAP39 in guided cell migration downstream of SLIT/ROBO signalling. However, apart from the ROBO receptors several other potential binding partners were identified in a previous systematic IP/MS screen (Müller et al., BioRxiv).
Among all of the putative binding partners I could prove the interaction with CNKSR2, CNKSR3, PEAK1 and TANC2. While they are expressed in different tissues and regulate various signalling pathways, they all provide a scaffold for the assembly of multi-protein complexes. Thereby, signalling pathways can be quickly propagated within cells. As ARHGAP39 is a regulatory protein, it is conceivable that it would be recruited by these different scaffold proteins and it has many domains itself that could also contribute a scaffold function.

The interaction of ARHGAP39 with the putative binding partners was first investigated with confocal microscopy. I observed an enrichment of CNKSR3 on cellular structures that resemble the endoplasmatic reticulum (ER) in MDCK cells. When coexpressed, ARHGAP39 completely colocalised with CNKSR3 at these structures (Fig. 5.28 A, top panel), indicating that CNKSR3 sequesters ARHGAP39 from the plasma membrane and suggesting a direct interaction of both proteins. In MDCK cells, overexpressed CNKSR2 localized in puncta and was found in perinuclear aggregates, presumably a consequence of overexpression, The nature of the CNKSR2 punctae was not further characterised here. Upon cotransfection, CNKSR2 and ARHGAP39 strongly colocalised at the plasma membrane and in smaller size punctae that were evenly distributed throughout the cell (Fig. 5.28 A, middle panel).

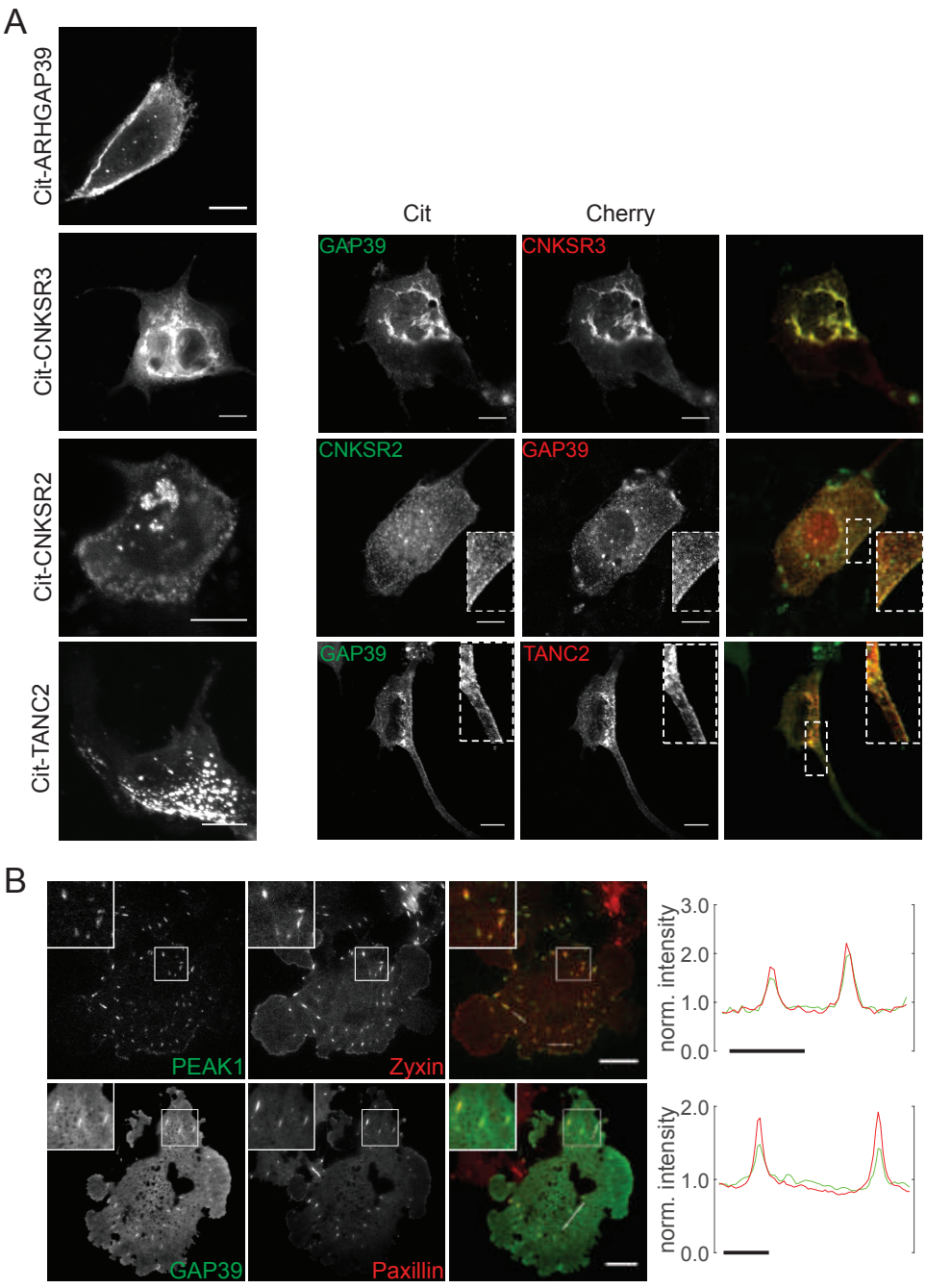

Figure 5.28.: see next page

Figure 5.28.: Colocalisation of ARHGAP39 and its interaction partners
A The left panel shows MDCK cells transfected with Cit-ARHGAP39, Cit-CNKSR2, Cit-CNKSR3 or Cit-Tanc2. The second panel shows MDCK cells co-transfected with ARHGAP39 and CNK2,CNK3 or TANC2 with indicated fluorescence tags. In the last column the merged images are depicted. Insets in images show higher magnification of the boxed region indicated in the merged image for each panel. **B** In the top row Cos7 cells were either co-transfected with Cit-PEAK1 and mCherry-Zyxin. In the bottom row Cos7 cells stably expressing mCherry-Pxn were transfected with Cit-ARHGAP39. Focal adhesion localisation was assessed by live-cell TIRF microscopy. Right panel shows fluorescence intensity profiles of a line scane through focal adhesions, indicated by white lines in the merged images. Intensity plots were normalized to the average intensity over the whole line. Abbreviations: GAP39: ARHGAP39, CNKSR2/3: Connector Enhancer of Kinase Suppressor of Ras, PEAK1: pseudopodium enriched atypical kinase 1, TANC2: Tetratricopeptide repeat, ankyrin repeat and coiled-coil domain-containing protein 2. White scalebars 10 µm, black scalebars 5 µm.

YFP-TANC2 expressed in MDCK cells localised in punctae, again most likely representing protein aggregates (Fig. 5.28 A, bottom panel) A similar expression pattern of exogenously expressed TANC2 has been shown in COS cells (**??**), however the identity of the punctae was not further examined. Low level expression of TANC2 together with ARHGAP39 resulted in co-localisation of both proteins at the plasma membrane, indicating that ARHGAP39 recruited TANC2 to this location.
PEAK1 was shown to localise at focal adhesions (Wang et al., 2010). With total internal reflection fluorescence (TRIF) microscopy the localisation of PEAK1 at focal adhesions could be observed, as determined by colocalisation with the focal adhesion marker Zyxin (in collaboration with Markus Müeller, MDC, www.www.bio.org). The PEAK localisation data are highly identical to the observed recruitment of ARHGAP39 to focal adhesions (Fig. 5.28 B), indicating that PEAK1 recruits ARHGAP39 to focal adhesions.

The microscopic observations were then further validated by Co-IP. Considering the domain architecture of ARHGAP39 the WW domains are the only protein-protein mediating domains present. Moreover, the Vilse/Robo interaction in *Drosophila* was shown to be mediated by the second WW domains that bind to the CC2 motif (Lundström et al., 2004; Hu et al., 2005). Since WW domain interactions require the presence of proline-rich motifs I examined if any proline-rich binding motif can be found in the sequences of CNKSR2, CNKSR3, TANC2 and PEAK1. Indeed, they all contain at least one stretch of poly-prolines. The alignment of these peptide sequences and the proline-rich CC2 motifs of the ROBO receptors revealed a consensus sequences PPPPxxPP. Strikingly, the consensus sequence is in line with the predicted recognition motif for WW2 of ARHGAP39 (Fig. 5.29).

```
ROBO1   1480 aa  -LPPPPAHPPP
ROBO2   1074 aa  -LPPPPVQPLP
ROBO3   1085 aa  -LPPPPP----
ROBO4    714 aa  -LPPAPLFP--

CNKSR2   354 aa  --PPPPAEP--
CNKSR2   702 aa  --PPPP-----
CNKSR3   347 aa  --PPPPAVP--
SGK269   869 aa  PFPPPP-----
SGK269   964 aa  --PPPP-----
SGK269  1152 aa  --PPPLP----
TANC2   1381 aa  --PPPPPQP--
TANC2   1529 aa  -PSPPPSP---

consensus        --PPPPxxP--
```

Figure 5.29.: Identification of a proline-rich consensus sequence
Stretches of Pro residues of identified binding partners of ARHGAP39 are aligned and a revealed a common proline-rich consensus sequence, which is highly similar to the predicted motif PPP(L)Pp for the WW2 domain of ARHGAP39. Abbreviations: SGK269: pseudopodium enriched atypical kinase 1, TANC2: ankyrin repeat and coiled-coil domain-containing protein 2, CNKSR2/3: Connector Enhancer of Kinase Suppressor of Ras 2/3.

Therefore, I then examined if the second WW domain of ARHGAP39 binds to the four putative binding partners by creating two binding deficient mutants, Y81A and W92A. Cit-CNKSR2 and Cit-CNKSR3 pulled down Flag-ARHGAP39, however both proteins did not bind to the Y81A and W92A mutants (Fig. 5.30 A, B).

Cit-PEAK1 was co-transfected with Flag-ARHGAP39 FL, Flag-dWW or Flag-Y81A. I speculated that the mutation at the Tyr residue 81 of WW2 would abolish the interaction, because for this mutant the focal adhesion localisation was impaired (Fig. 5.30 C). Indeed, PEAK1 could only interact with ARHGAP39 FL, but did not bind to the Y81A binding deficient mutant (Fig.). Lastly, Co-IP experiments revealed that Flag-TANC2 bound to YFP-ARHGAP39 (Fig 5.30 D). Unfortunately, the co-expression of TANC2 and the ARHGAP39 mutants was not sufficient to perform Co-IP. Thus, no data regarding the involvement of WW2 was obtained.

Taken together, I confirmed the interaction of ARHGAP39 with the four proteins CNKSR2, CNKSR3, PEAK1 and TANC2. The great extent of colocalisation strongly suggests that all these proteins directly interact with ARHGAP39. Moreover, I identified the requirement of the second WW domain of ARHGAP39 to bind to CNKSR2, CNKSR3 and PEAK1.

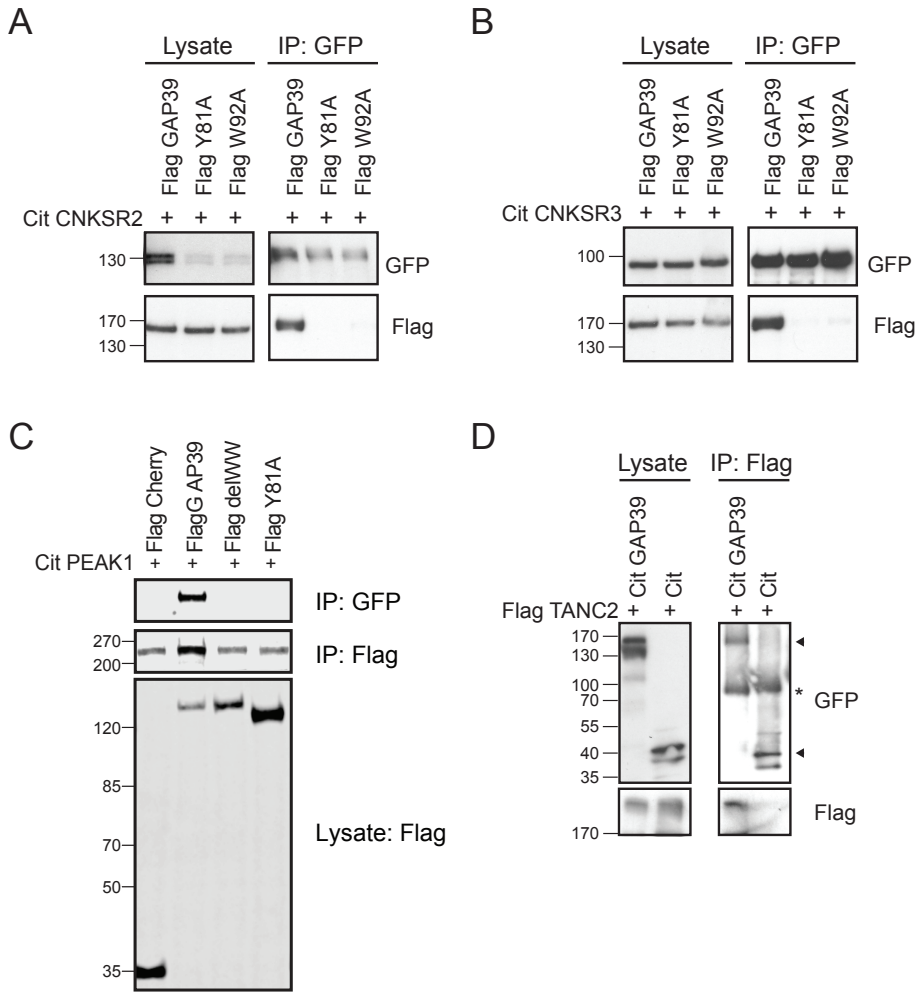

Figure 5.30.: The WW2 domain is required for protein interaction
A HEK 293T cells transfected with Cit-CNKSR2 and Flag-ARHGAP39,Flag-Y81A and Flag-W92A. After 24h lysates were subjected to immunoprecipitation with GFP-beads and proteins were detected with anti-GFP and anti-Flag antibodies. **B** Co-immunoprecipitaion of Cit-CNKSR2 and Flag-ARHGAP39,Flag-Y81A and Flag-W92A mutants with GFP-beads. Proteins were immunoblotted with anti-GFP and anti-Flag antibodies. Note, that the expression levels of Cit-CNKSR2 in lysates was reduced (Fig. 5.30 A, second and third lane), however in the eluate Cit-CNKSR2 levels were comparable. **A** HEK 293T cells overexpressed Cit-PEAK1 and Flag-ARHGAP39, Flag-Y81A, Flag-W92A or Flag-Cherry control. Lysates were subjected to immunoprecipitation with Flag-beads and proteins immunoblotted with anti-GFP and anti-Flag antibodies. **B** Ectopically expressed Flag-TANC2 and Cit-ARHGAP39 or Cit control in HEK 293T cells. Lysates were subjected to Co-IP with GFP-beads and proteins detected with anti-GFP and anti-Flag antibodies. Arrowheads: Indicate the correct size of Cit-ARHGAP39 and Cit. The second band visible might be due to degradation of the proteins. Asterix: Fraction of denatured GFP-IgG antibody used for the IP. Abbreviations: GAP39: ARHGAP39, CNKSR2/3: Connector Enhancer of Kinase Suppressor of Ras, PEAK1: Pseudopodium enriched atypical kinase 1, TANC2: Tetratricopeptide repeat, ankyrin repeat and coiled-coil domain-containing protein 2.

5.4. ARHGAP39 interacts with ROBO receptors

Subsequent to the general characterization of ARHGAP39, I focus here on establishing a link between ROBO receptor signalling and ARHGAP39. I already proved the interaction between all ROBO receptors and ARHGAP39. Here, I created functional mutants of ROBO1, exemplarily for ROBO2 and 3, and of the more divergent ROBO4 receptor in order to analyse the binding mechanism. By confocal time lapse imaging the ROBO1/ARHGAP39 interaction was examined on the subcellular level. To elucidate the role of ARHGAP39 in cell repulsion downstream of ROBO the migratory behaviour of *ARHGAP39* knockdown cells was tested in the presence of SLIT2.

5.4.1. ARHGAP39 WW domains are required for interaction with ROBO1 but not ROBO4

I identified a poly-proline consensus sequence for the WW2 domain, which can be found in the CC2 motifs of ROBO1 and ROBO4 (Fig. 5.29). Thus, I set out to verify that the second WW domain of ARHGAP39 mediates the interaction with ROBO1 and ROBO4.

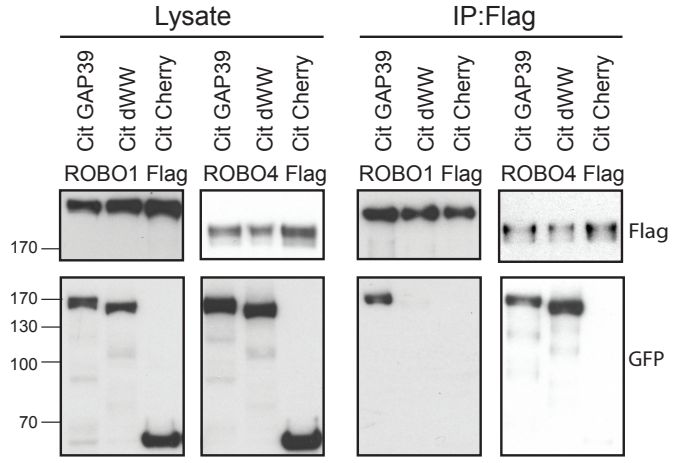

Figure 5.31.: ARHGAP39 dWW does not bind to ROBO1
Ectopic expression of YFP-ARHGAP39, YFP-dWW or YFP-Cherry control and Flag-ROBO1 or Flag-ROBO4 in HEK 293T cells. Lysates were subjected to immunoprecipitation with Flag-beads and proteins were detected with anti-GFP and anti-Flag antibodies.

Co-IP experiments using full length ARHGAP39 and a construct lacking the WW domains (dWW) revealed that the WW domains are crucial for the interaction of ARHGAP39 with ROBO1, but, surprisingly, are dispensable for the interaction with ROBO4 (Fig. 5.31). This was unexpected, since both receptors contain the proline-rich CC2 binding motif, which was

assumed to be critical for the interaction with ARHGAP39 (Hu et al., 2005; Lundström et al., 2004)

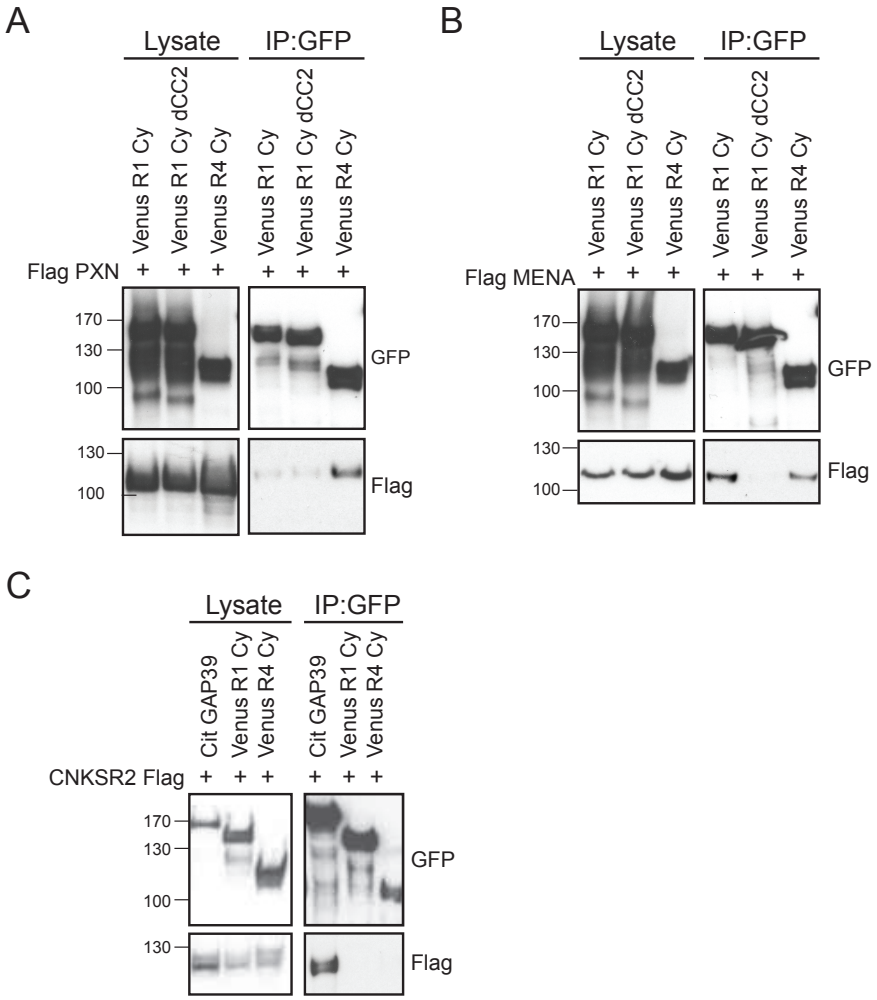

Figure 5.32.: Cytoplasmic truncation constructs of ROBO1 and ROBO4 are functional in Co-IPs
HEK 293T cells expressing PXN, MENA, CNKSR2 together with ROBO4 Cy or ROBO4 Cy dCC2 truncations were harvested after 24h. Lysates were subjected to immunoprecipitation with GFP-beads and proteins immunoblotted with anti-Flag or anti-GFP antibodies. **A** Flag-PXN bound to YFP-ROBO4 Cy, but not to YFP-ROBO1 Cy and ROBO1 Cy dCC2. **B** Flag-MENA co-expressed with YFP-ROBO1 Cy, YFP-ROBO1 Cy dCC2 or YFP-ROBO4 Cy could interact with YFP-ROBO1 Cy and YFP-ROBO4 Cy. **C** Co-expression of Flag-CNKSR2 with Cit-ARHGAP39, YFP-ROBO1 Cy, or YFP-ROBO4 Cy yielded in interaction of Flag-CNKSR2 with Cit-ARHGAP39. Abbreviations: GAP39: ARHGAP39, R1 Cy: ROBO1 cytosolic fragment, R4 Cy: ROBO4 cytosolic fragment, PXN: PAXILLIN, MENA: protein enabled homolog, CNKSR2: Connector Enhancer of Kinase Suppressor of Ras 2

To further investigate the molecular mechanism of interaction, I engaged truncation constructs of ROBO1 and ROBO4 that encode only the cytosolic portion of the proteins (Cy). These constructs were previously used in other studies for IP experiments and demonstrated not

to affect the protein binding properties (Bashaw et al., 2000; Wang et al., 2003; Lundström et al., 2004; Jones et al., 2009a). All truncated versions of ROBO1 and ROBO4 created in this work were tested for their subcellular localisation by microscopy (Fig. A.4 and A.5, Appendix). I performed control Co-IPs with two established ROBO binding partners to confirm their functionality.
MENA is an actin-associated protein and has been shown to bind to the CC2 motifs both in ROBO1 and to ROBO4 (Park et al., 2003; Jones et al., 2009a). The focal adhesion protein Paxillin was reported to bind murine Robo4 via a binding motif C-terminal of the CC0 domain (Jones et al., 2009a), which is not present in ROBO1. CNKSR2, the ARHGAP39 interactor (see Fig.xx), was chosen as negative control that should not bind to the ROBO receptors. As expected, PAXILLIN selectively bound ROBO4 Cy but not ROBO1 Cy (Fig 5.32 A). MENA associated both with ROBO1 Cy and ROBO4 Cy, but not with a ROBO1 Cy construct missing the CC2 motif (Fig 5.32 B). CNKSR2 bound to ARHGAP39, but could not interact with either of the receptors (Fig 5.32 C). ROBO1 Cy and ROBO4 Cy are thus fully functional proteins capable of binding known interaction partners and were therefore used for further experiments to analyse the interaction with ARHGAP39.

5.4.2. ARHGAP39 binds the CC2 motif of ROBO1 via its second WW domain

The initial experiment with the ARHGAP39 dWW construct revealed that its WW domains are required for the ROBO1 interaction (Fig. 5.31). In a complementary Co-IP experiment I could validate this observation by showing that the isolated WW domains could pull down ROBO1 Cy, but did not interact with the control (Fig. 5.33 A).
Next, I aimed to prove that WW2 mediates the binding to ROBO1, since the CC2 motif contains the predicted consensus sequence of WW2. Therefore, the binding deficient mutants of ARHGAP39 WW2, Y81A and W92A, were co-expressed with ROBO1. Indeed, ROBO1 bound to ARHGAP39, but not to the binding deficient mutants (Fig. 5.33 B).

Conversely, I could show that the CC2 motif of ROBO1 is required for the interaction, since the ROBO1 Cy CC2 deletion mutant did not interact with Flag-ARHGAP39 anymore (Fig. 5.34 B). Furthermore, Flag-ROBO1 Cy was also able to precipitate endogenous ARHGAP39, but not the ROBO1 Cy CC2 mutant (Fig. 5.34 C).
To sum up, the binding of ROBO1 to ARHGAP39 involves the CC2 motif and the WW2 domain, respectively, and thus constitutes a canonical WW domain interaction.

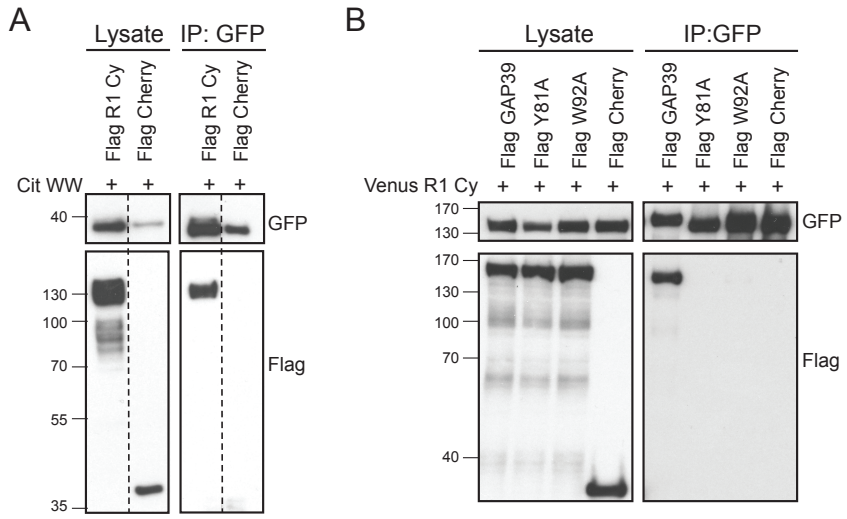

Figure 5.33.: ARHGAP39 binds to ROBO1 via the second WW domain
A HEK 293T cells transfected with YFP-WW and Flag-ROBO1 Cy or Flag-Cherry. Cells were harvested after 24 h of transfection. Lysates were treated with GFP-beads and proteins were detected with anti-GFP and anti-Flag antibodies. **B** Co-transfection of YFP-ROBO1 Cy and Flag-ARHGAP39 or its mutants in HEK 293T cells. Lysates were treated with GFP-beads and proteins were detected with anti-GFP and anti-Flag antibodies. Blots are representative of three similar experiments.

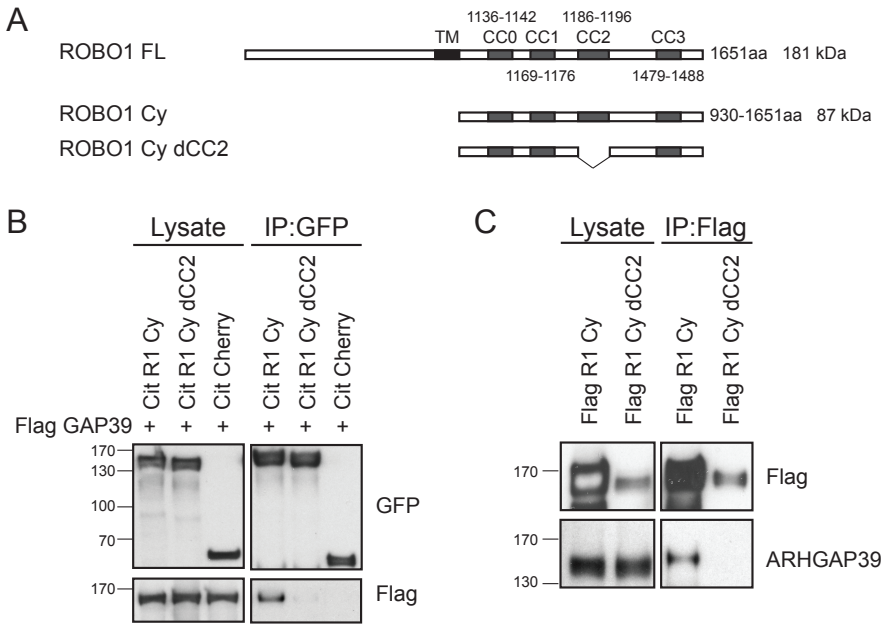

Figure 5.34.: The CC2 motif in ROBO1 is required for interaction with ARHGAP39
A Schematic illustration of ROBO1 constructs used in this thesis. **B** HEK 293T cells transfected with YFP-ROBO1 Cy, YFP-ROBO1 Cy dCC2 or YFP-Cherry and Flag-ARHGAP39. Lysates were subjected to immunoprecipitation with GFP-beads and proteins were detected with anti-GFP and anti-Flag antibodies. **C** Endogenous ARHGAP39 was detected with anti-ARHGAP39 antibody in lysate of HEK 293T cells, transfected with Flag-ROBO1 or Flag-ROBO1 Cy dCC2. Blots are representative of three similar experiments.

5.4.3. ARHGAP39 interacts with ROBO4 in a complex binding mode

I next aimed to understand the binding mechanism between ARHGAP39 and ROBO4. It was already demonstrated that deletion of the WW domains did not abolish the binding to ROBO4 (Fig. 5.31). Thus, the binding must involve other or additional regions on ARHGAP39.

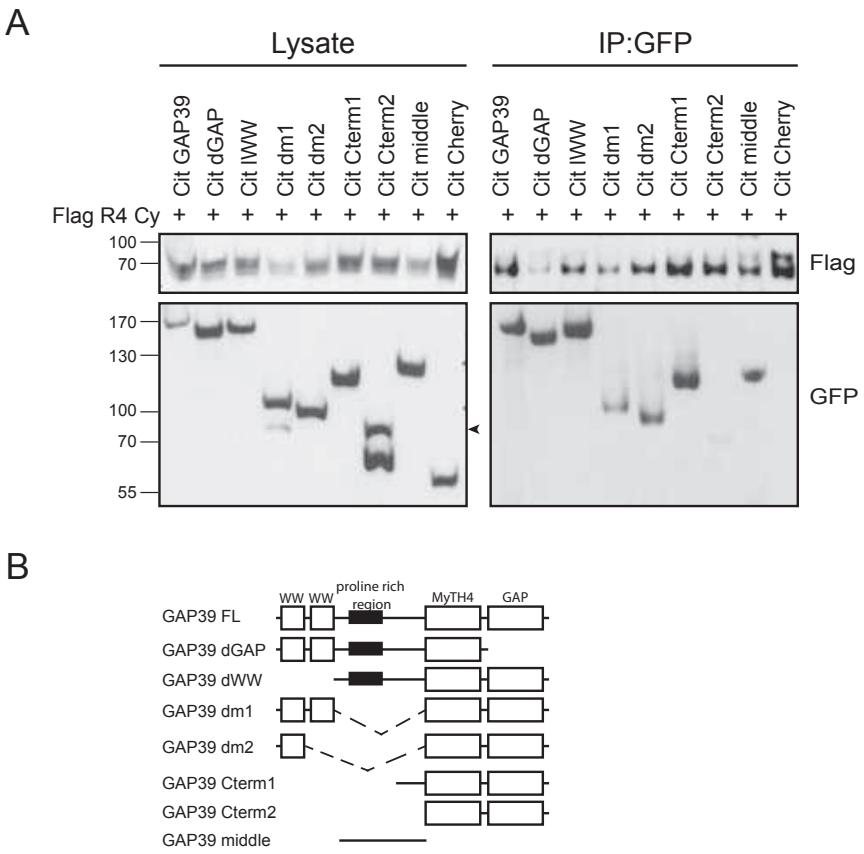

Figure 5.35.: The WW domains are dispensable for binding to ROBO4
A HEK 293T cells transfected with YFP-ROBO4 Cy and Flag-ARHGAP39 or Flag-ARHGAP39 truncations. Lysates were subjected to immunoprecipitation with GFP-beads and proteins were detected with anti-GFP and anti-Flag antibodies. **B** Illustration of truncation and deletion constructs of ARHGAP39 used in this Co-IP. **C** Overexpressed Flag-ROBO4 and Cit-ARHGAP39 or YFP-truncation construct were immunoprecipitated with Flag-beads and proteins immunoblotted with anti-GFP or anti-Flag antibodies. Arrowhead: Indicates band for Cit-Cterm2 in lysate. The second band visible depicts a different MW due to the loss of the YFP-tag. Blots are representative of two similar experiments.

Different ARHGAP39 truncation constructs were therefore subsequently tested by Co-IP. Only the ARHGAP39 C-terminus comprising the MyTH4 and GAP domain (Cterm2) could be excluded to bind to ROBO4 Cy. Surprisingly, all other truncation constructs interacted. In more detail, the constructs dWW, middle and Cterm1, which have in common a 190 amino acid stretch N-terminal of the MyTH4 domain, bound to ROBO4 Cy. But also dm1 and dm2, which

both contain the first WW domain, but lack this sequence of 190 amino acids, were able to interact with ROBO4 Cy, albeit to a lesser extent (Fig 5.35 A).
These results suggest a more complex mode of association of ARHGAP39 and ROBO4. Two binding sites may exist in the N-terminal half of ARHGAP39. One of them in the first WW domain and one adjacent to the MyTH domain.

Subsequently, I tried to pinpoint the critical binding site on ROBO4. First, I examined the role of the ROBO4 CC2 motif in ARHGAP39 binding. A Co-IP of Cit-ROBO4 Cy with or without the CC2 motif and Flag-ARHGAP39 revealed that the deletion of this motif did not completely abolish the interaction with ARHGAP39 and implicates the existence of additional binding sites (Fig. 5.36 A).
Next, a panel of ROBO4 Cy truncation constructs was analysed. Surprisingly, most of them interacted with ARHGAP39. Two representative Co-IP experiments are shown in Figure 5.37 B and C. The smallest construct that bound to ARHGAP39 comprises the amino acids 494 to 543, a sequence adjacent to the transmembrane domain.
Only ROBO4 Cy d593-713, missing the amino acids between the CC0 and CC2 motif, did not bind to ARHGAP39 anymore (Fig. 5.36 B, C). In contrast, ROBO4 Cy d593-662 did interact, indicating that the amino acids 663 to 713 contribute to binding ARHGAP39. Moreover, Flag-ARHGAP39 pulled down the deletion construct ROBO4 Cy d713-794, which misses the CC2 motif, but contains the potential binding region between 663 and 713 amino acids is present (Fig. 5.36 B). This corroborates the relevance of the amino acids between 663 to 713 and the hypothesis that the CC2 motif is not exclusively involved in the association with ARHGAP39 and the amino acids between 663 to 713 are required as well.

The fact that almost all truncation constructs interacted with ARHGAP39 may theoretically be an artifact due to incorrect folding of the truncated proteins, which may facilitate unspecific binding. However, I could demonstrate that ROBO4 Cy correctly binds MENA and Paxillin (Fig. 5.32) and that expressed ROBO4 Cy fragments did not form obvious aggregates (Fig. A.5, Appendix). Assuming that all constructs function properly the data together suggests the existence of at least two ARHGAP39 binding sites also on ROBO4.
Together the Co-IP data suggest the existence of multiple binding sites on ARHGAP39 and on ROBO4 as well.

The ROBO4/ARHGAP39 interaction data implicate that the WW domains of ARHGAP39 contributes to the binding to ROBO4 (Fig. 5.35 A). Therefore, I aimed to identify a WW domain target motif within the ROBO Cy sequence and continued with a peptide spot overlay assay with the sequence of the cytoplasmic tail of ROBO4 (amino acids 493-1003) spot-synthesized on a cellulose membrane (kindly provided by Dr. Enno Klussmann, MDC). The membrane

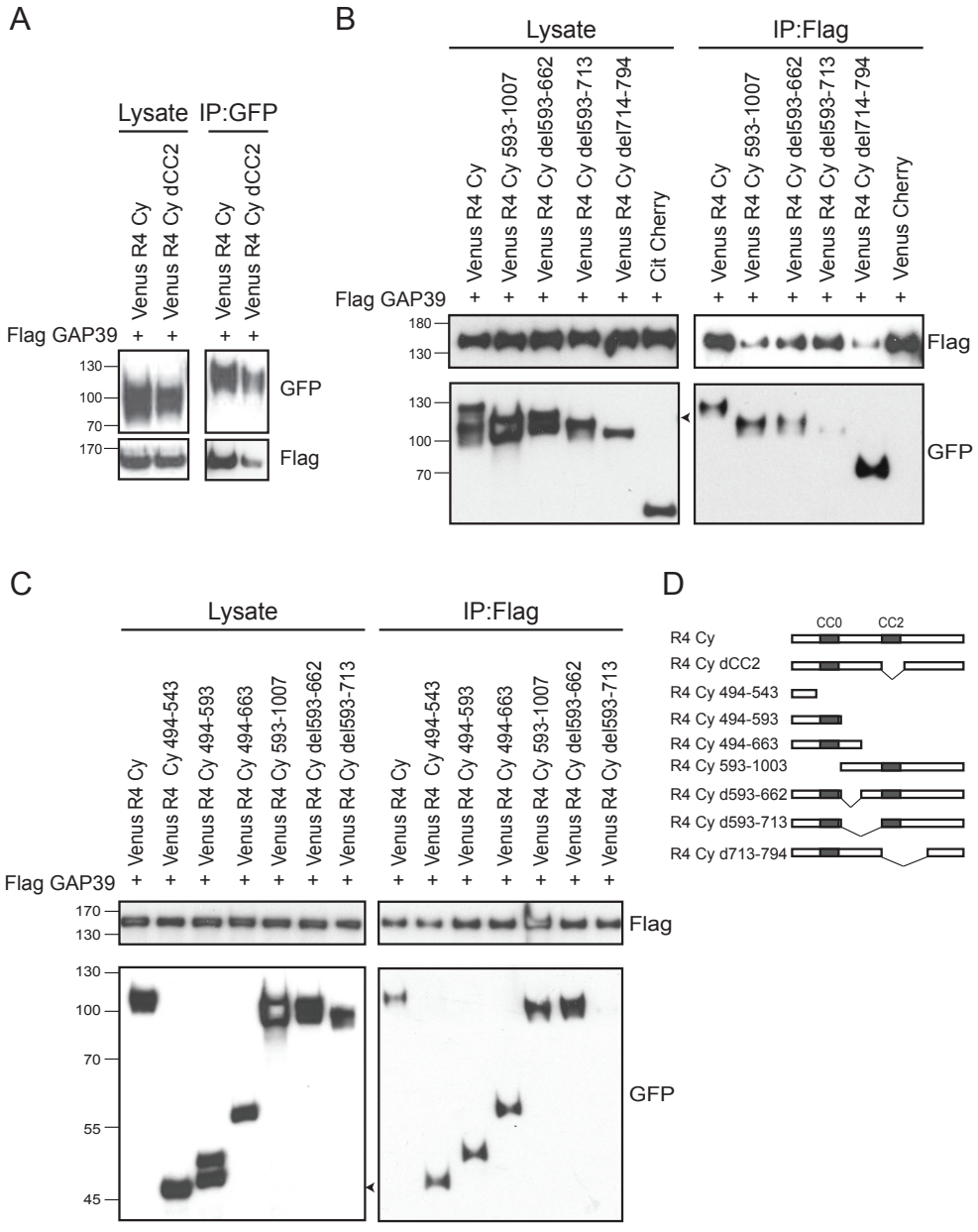

Figure 5.36.: see next page

Figure 5.36.: CC2 motif in ROBO4 not exclusively required for interaction with ARHGAP39
A HEK 293T cells expressing Flag-ARHGAP39 together with YFP-ROBO4 Cy or YFP-ROBO4 Cy dCC2 were harvested after 24h. Lysates were immunoprecipitated with GFP-beads and proteins immunoblotted with anti-Flag or anti-GFP antibodies. **B** and **C** HEK 293T cells were co-transfected with Flag-ARHGAP39 and YFP-ROBO4 Cy or YFP-ROBO4 Cy truncation constructs. Lysates were harvested after 24h and immunoprecipitated with Flag-beads. Proteins were detected with anti-Flag or anti-GFP antibodies. Arrowheads indicate unspecific band for the expressed YFP-constructs in the lysate. Blots are representative of three similar experiments. **D** Schematic drawing of truncation constructs used in the presented Co-Ip experiments. Abbreviations: GAP39: ARHGAP39, R1 Cy: ROBO1 cytosolic fragment, R4 Cy: ROBO4 cytosolic fragment.

was then incubated with the recombinant GST fusion protein of the ARHGAP39 WW domains (amino acids 2-115, purified by Anja Schütz, MDC).
The GST-WW domains bound to the peptide spots O3 to Q3 with the corresponding amino acid sequence from 694 to 731, which includes the CC2 motif PPAPLFP (Fig. 5.37 A, spots highlighted in green). Another array of peptides from D2 to G2 was identified. The corresponding sequence, amino acids 537 to 581, is located just ahead of the CC0 motif and contains only single prolines (Fig. 4.37 A, spots highlighted in orange). The strongest spots detected correspond to the peptides from B6 to G6 with the amino acid sequence 932 to 981 that resides at the very C-terminus of ROBO4 (Fig. 5.37 A, spots highlighted in red). This region contains 3x double prolines in its sequence.
Combining the observations of the peptide spot overlay assay with the Co-IP results reveals that the identified spots O3 to Q3 (amino acids 694-731) are in agreement with binding of the construct ROBO4 Cy d714-792; and the amino acid sequence 537-581 (in spots D2 to G2) partly overlaps with sequence of the construct ROBO4 Cy 494-543 that bound to ARHGAP39.

Taken together, the binding of ARHGAP39 to ROBO4 does not critically involve a WW domain CC2 motif interaction, unlike the association with ROBO1. Two regions in the ARHGAP39 N-terminus, the WW domains and a sequence adjacent to the MyTH4 domain, are involved the binding to ROBO4. In turn, I identified also three binding sites on the ROBO4 sequence, a region following the transmembrane domain, one including the CC2 motif and one C-terminal region. It is conceivable that the multiple binding sites are involved in a complex binding mechanism of ARHGAP39 and ROBO4.

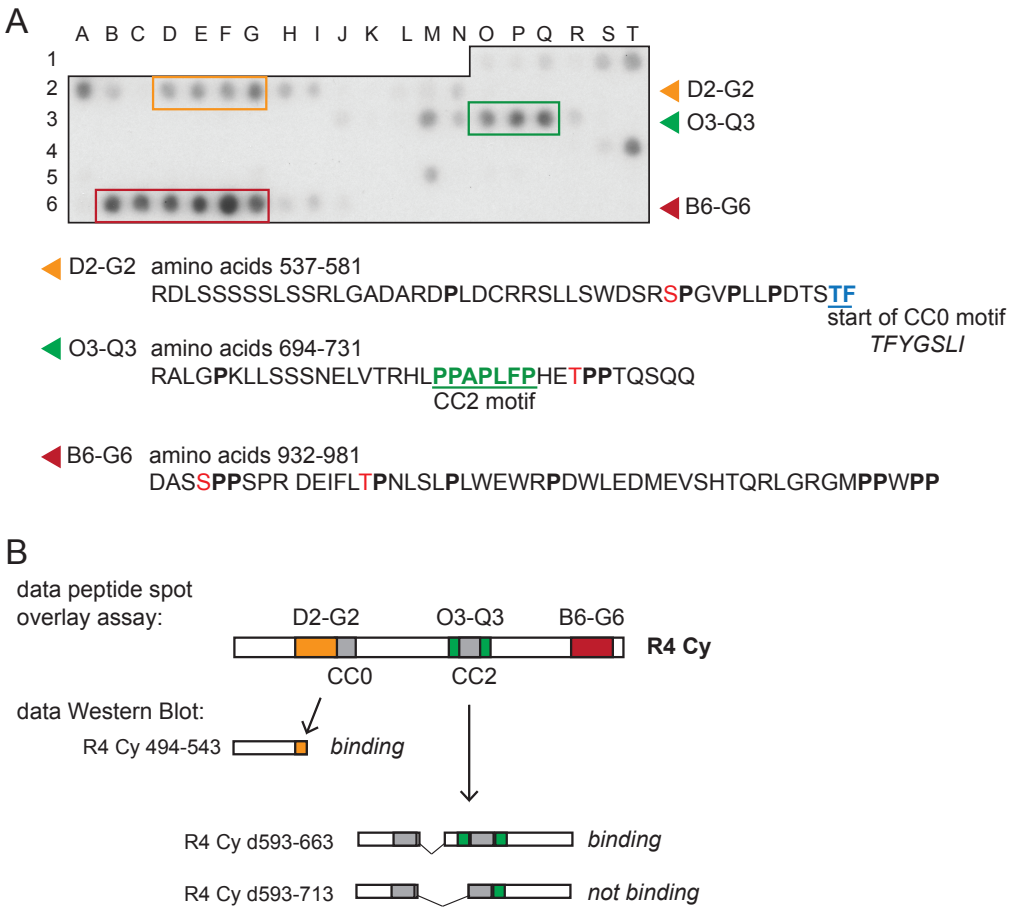

Figure 5.37.: GST-WW fusion protein recognizes three Pro residues containing peptide sequences
A Peptide spot overlay assay depicting spots were the GST-WW fusion protein (amino acids 2-115) bound to ROBO4 Cy (amino acids 494-1003) spotted on a cellulose membrane. The strongest spots are highlighted in colored boxes and the corresponding sequences are shown. Pro residues are highlighted in bold. Red amino acid residues can be modified by phosphorylation. **B** Illustration where within the ROBO4 Cy sequence the peptide stretches were identified by binding of the GST-WW domains. And the corresponding results of the Co-IP experiments are shown.

5.4.4. ROBO1 is internalized upon SLIT2 stimulation

In the previous section I verified the direct interaction of human ARHGAP39 and the ROBO receptors that was detected in the absence of a stimulus, in particular SLIT2. However, many transmembrane signalling receptors engage with downstream effectors once they have been activated upon ligand binding. Therefore, I aimed to examine how SLIT2 stimulation would affect the ROBO/ARHGAP39 interaction. Here, I continue with ROBO1 only, because SLIT2 is known to bind and activate ROBO1, whereas this is not clear for ROBO4.

I set up a cell based system involving ROBO signaling in which the implication of ARHGAP39 can be tested by confocal microscopy. First, I studied the effect of SLIT2 stimulation on trans-

membrane bound ROBO1 in cells. HeLa cells were chosen to ectopically express ROBO1 and then treated either with SLIT2 or with mock conditioned media. Before, SLIT2 treatment ROBO1 expression was observed at the plasma membrane and in the perinuclear region. Using live cell microscopy, no obvious changes in phenotype was detected in control cells treated with SLIT2 for 60 min or in ROBO-YFP cells treated with mock conditioned media for the same time period (Fig 5.38 A, B). In contrast, ROBO1-YFP expressing HeLa cells acquired a more rounded morphology, indicating that ROBO1 transfection drastically increases the cells sensitivity to SLIT2 treatment. Moreover, striking re-localsation of ROBO1 was observed upon SLIT treatment from the plasma membrane into intracellular vesicles (Fig. 5.38 C).

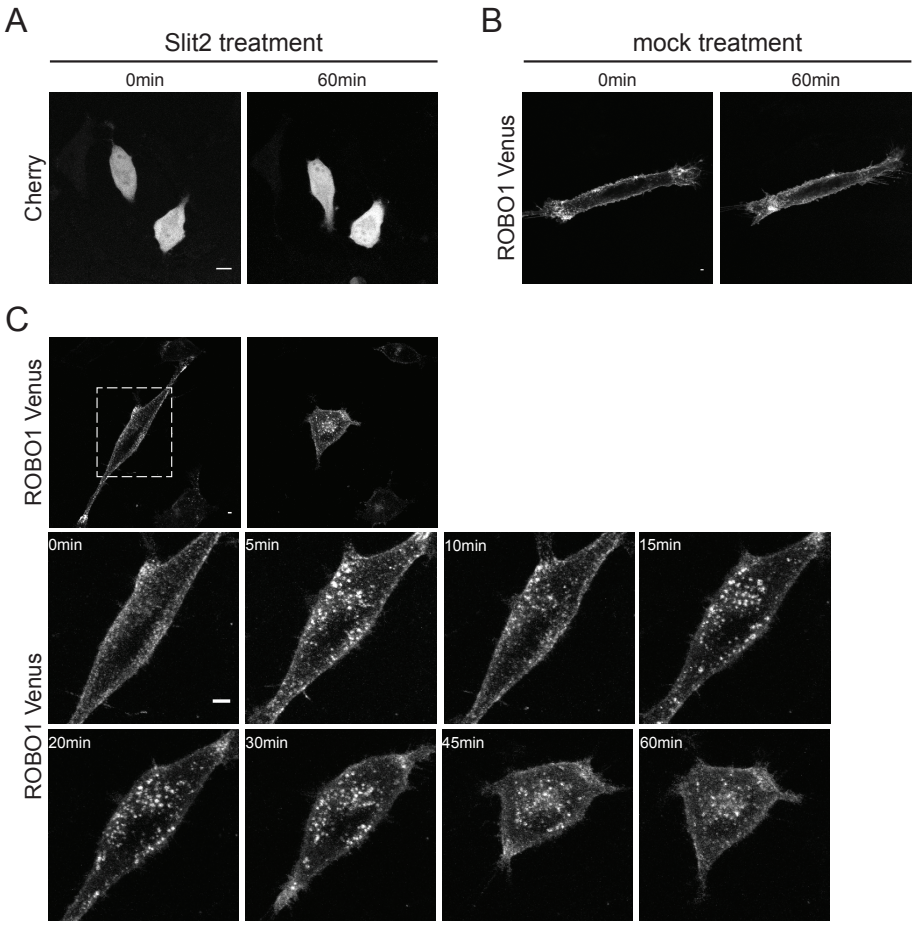

Figure 5.38.: Slit2 induces ROBO1 internalisation
A HeLa cells transfected with Flag-Cherry were treated with SLIT2 media and images were acquired after 60 min. **B** ROBO1-YFP transfected cells were treated with mock media for 60 min. Images were captured with a confocal microscope. **C** ROBO1-YFP transfected cell treated with SLIT2 shown in detail over the time course of 60 min. Images were captured every 5 min with a confocal microscope. Scale bar 10 µm

5.4.5. ARHGAP39 potentially co-internalizes with ROBO1 in the presence of SLIT2

Encouraged by these observations I next asked whether SLIT2 treatment affects the ARHGAP39/ROBO1 interaction. First, the extent of interaction between endogeneous ARHGAP39 and Flag-ROBO1 in the presence of SLIT2 was assessed biochemically by Co-IP. A clear increase in ARHGAP39 binding to ROBO1 was observed after 30 min of SLIT2 stimulation (Fig. 5.39), implicating a delayed recruitment of ARHGAP39.
This observation implies that ROBO1 recruits ARHGAP39 and thus I asked whether ARHGAP39 would also localise in intracellular vesicles. This observation would be particularly interesting since it may provide a means to investigate a direct interaction of ARHGAP39 and ROBO1 in cells. It would be otherwise difficult to study since both proteins expressed alone already localise at the membrane.

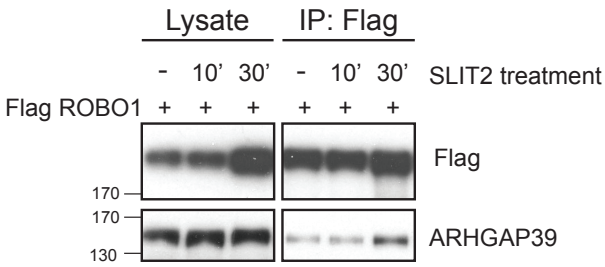

Figure 5.39.: SLIT2 enhances the ARHGAP39 - ROBO1 interaction
HEK 293T cells transfected with Flag-ROBO1and treated with SLIT2 media for the indicated time points. endogenous ARHGAP39 was pulled down with Flag antibodies and detected with the anti-ARHGAP39 antibody.

In Figure 5.40, A the co-localisation of ARHGAP39 and ROBO1 at t= 0 min and t= 30 min of SLIT2 stimulation is depicted. While at t= 0 min the two proteins can be mainly observed at the membrane, but also in the cytoplasm and in few vesicles, at t= 30 min they mainly localise in vesicles along the membrane. Further validation of these observations requires the use of image analysis approaches to quantitatively assess changes in protein localization.
The reduction in plasma membrane staining could be quantified by a line scan analysis that measures the intensity values of both proteins along this line before and after 30 min of SLIT2 stimulation (Fig. 5.40 B). This approach revealed that the pixel intensities decreased by half compared to untreated conditions (Fig. 5.40 C). A caveat here is that for intensity measurements at the plasma membrane the formation and disappearance of membrane ruffles has to be considered, as well as the movement of the membrane during the time course of the experiment and potential photobleaching. This issue needs to be addressed in future experiments by using a plasma membrane marker, which could serve as a reference to create a mask for the membrane to be quantified.

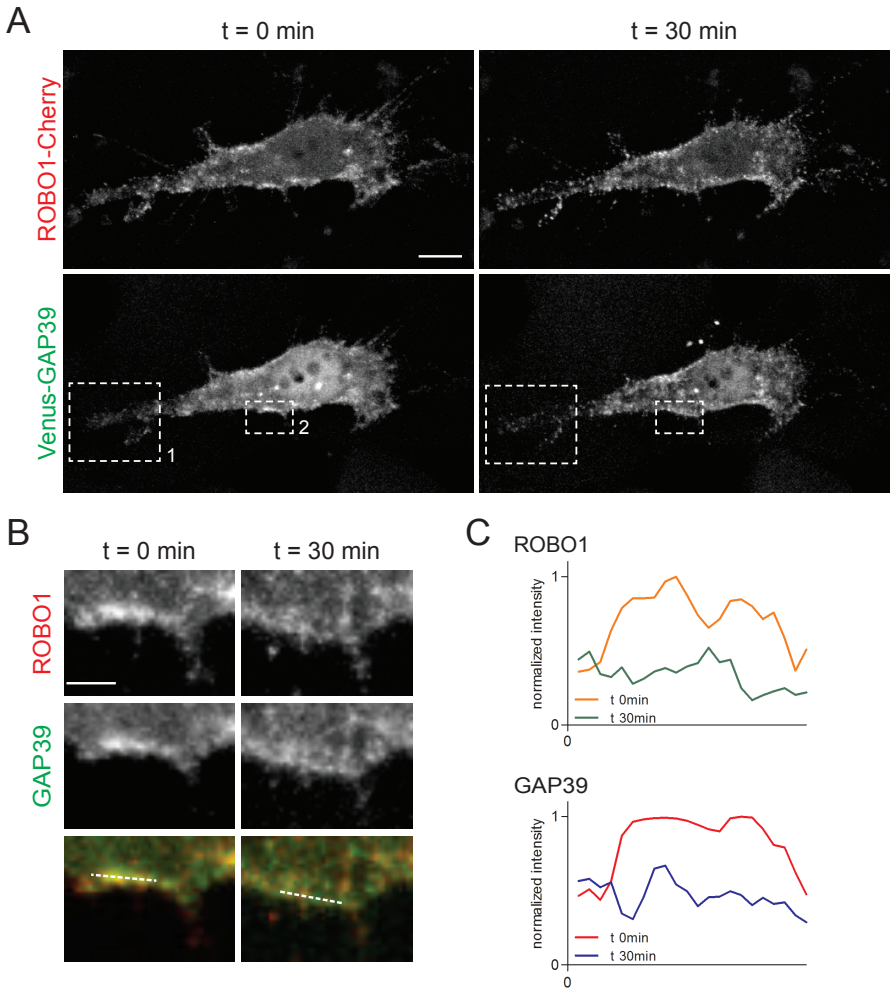

Figure 5.40.: Decrease of ROBO1 and ARHGAP39 localisation at the plasma membrane
A HeLa cells transfected with ROBO1-Cherry and YFP-ARHGAP39 were treated with SLIT2 conditioned medium for 30 min. Images were captured every 3 min with a confocal microscope. Boxed regions represent the depicted magnifications in **B** and **Fig. 3.42**. Scale bar 10 µm.. **B** Images are the magnification of the boxed region in **1**, showing fluorescence signals at the plasma membrane. Images show fluorescent signal of ROBO1 and ARHGAP39 after 0 min and after 30 min of SLIT2 stimulation. The dashed lines at t= 0 min and at t= 30 min show the area chosen for the line scans. **C** Line scans depicting the normalized intensity along the indicated dashed line. Results are depicted for either protein at t= 0 and t= 30 min of SLIT2 stimulation in indicated colors. Scale bar 5 µm. Abbreviation: GAP39: ARHGAP39

Another way to quantify the re-localisation of ARHGAP39 and ROBO into vesicles is to analyse the co-localisation correlation coefficients. The easiest way to measure the colocalisation is by calculating the Pearson's coefficient (r) and Manders' coefficients (M1= fraction of ROBO1-mCherry overlapping with Venus-ARHGAP39, M2= fraction of Venus-ARHGAP39 overlapping with ROBO1-mCherry). I used the public domain tool JACoP (Just Another Co-localization Plugin) in Fiji (Fiji Is Just ImageJ) to measure the correlation coefficients of ARHGAP39 and ROBO1 at t= 0min and t= 30 min in Figure 5.41 A. This revealed that at both time points the Pearson's and Manders' coefficients have similar values (Fig. 5.41), which implicates that ROBO1 and ARHGAP39 partially colocalize independent of SLIT2.

In addition, an object-based colocalisation approach could be included, which measures the coincidence of discrete structures. Objects of the green and red channel co-localise if the centroid of an object of the green channel falls into the area covered by an object of the red channel and vice versa. Co-localisation can be then quantitatively expressed as the percentage of positive couples divided by the overall number of structures for the current channel. For the images shown here in Figure 5.41 centers-particles overlap maps show the spatial overlap of objectives of the ARHGAP39 and the ROBO1 channel at t= 0 min and t= 30 min (Fig. 5.41 B). This correlation method could visualise the appearance of vesicles containing ROBO1 and ARHGAP39 upon SLIT2 treatment.

The data sets so far were compromised by an inconvenient signal-to-noise ratio and therefore colocalisation of ROBO1 and ARHGAP39 could not be quantitatively assessed. To obtain better quality images in the future I first have to overcome problems regarding the transfection efficiency of both proteins in HeLa cells and define the optimal time point with maximal internalisation.

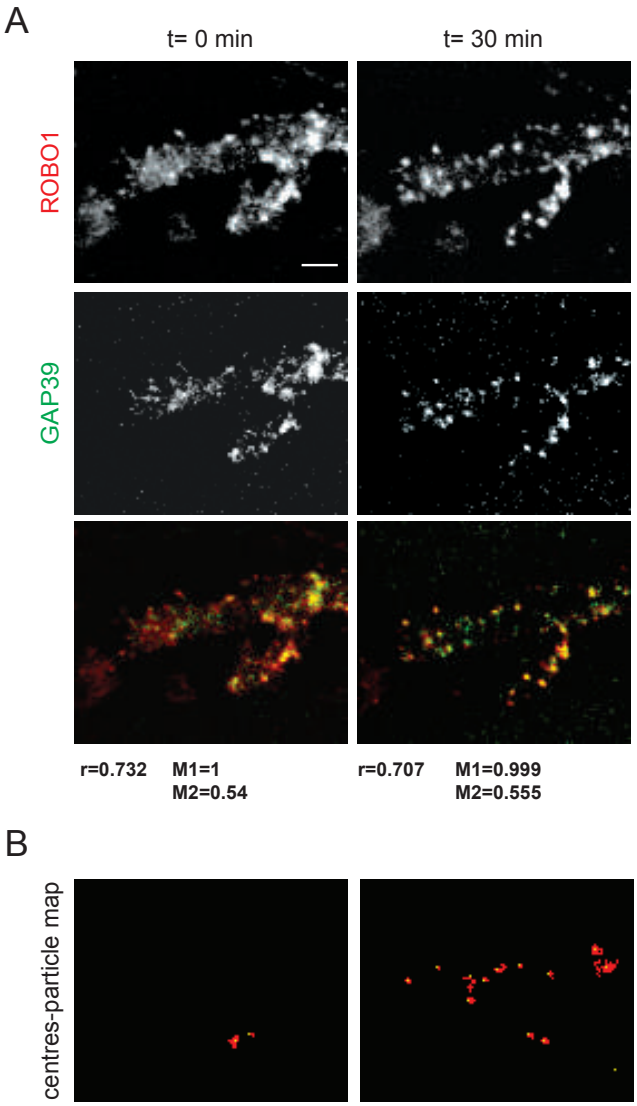

Figure 5.41.: Partial colocalisation of ROBO1 and ARHGAP39 estimated by Pearson's and Mander's coefficients

A HeLa cells transfected with ROBO1-Cherry and YFP-ARHGAP39 were treated with SLIT2 conditioned medium for 30 min. Images were captured every 3 min with a confocal microscope. Boxed regions represent the depicted magnifications in Figure 5.40 A, **2**. Scale bar 5 µm. The Pearson's and Mander's coefficients were calculated using the Fiji plugin JACoP (http://rsb.info.nih.gov/ij/plugins/track/jacop.html). Blue lines drawn on top of the scatter plot indicate the automatic threshold levels that were used by JACoP to calculate the threshold based Mander's coefficients M1 and M2. **B** Centers-particles overlap maps are shown that present the the event of colocalisation of centers of the green image (ARHGAP39) and particles of the red image (ROBO1). The images of ARHGAP39 and ROBO1 in A were used to create the centers-particles maps at t= 0 min and t= 30 min of SLIT2 conditioned media stimulation. Scale bar 5 µm. Abbreviation: GAP39: ARHGAP39

5.4.6. *ARHGAP39* knock down has no effect on ROBO1 internalisation

I next asked whether ARHGAP39 is involved in SLIT2 mediated ROBO1 internalisation. To this end, ROBO1-YFP was transfected into ARHGAP39 shRNA B6 knockdown or control HeLa cells and treated either with mock media or SLIT2 conditioned media. By confocal imaging in live cells, I did not observe any obvious difference in the extent of ROBO1 endocytosis upon SLIT2 stimulation between HeLa shRNA B6 and stuffer virus cells (Fig. 3.42). ROBO1 rapidly and extensively internalised in both cell lines. These results indicate that ARHGAP39 is not essentially required for ROBO1 endocytosis upon SLIT2 treatment in this cell line.

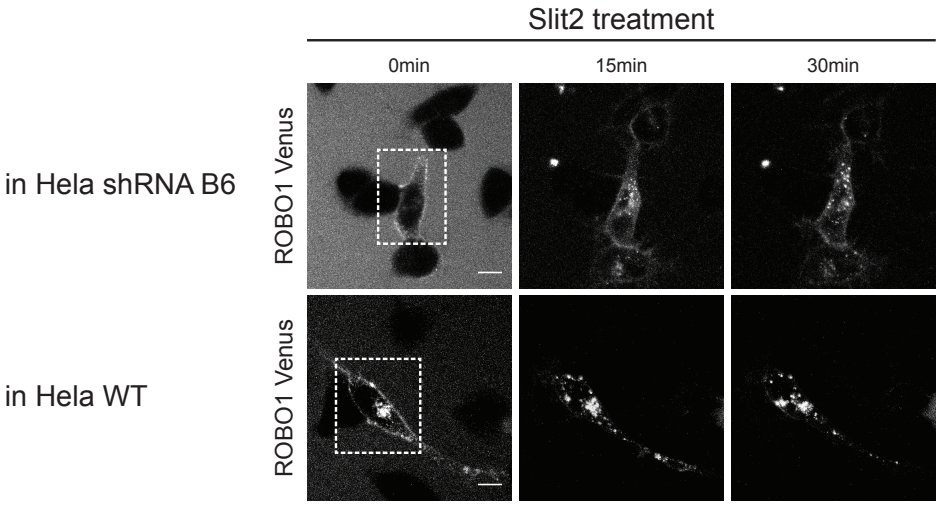

Figure 5.42.: Slit2 induced ROBO1 internalisation is unchanged in ARHGAP39 shRNA cells
The indicated HeLa cells were transfected with ROBO1-YFP and treated with mock or SLIT2 conditioned media for 30 min. Images were captured every 3 min with a confocal microscope. Scale bar 5 µm.

5.4.7. *ARHGAP39* knock down reduces SLIT/ROBO induced cell repulsion

Finally, I aimed to explore a functional link between ARHGAP39 and ROBO1 in directed cell migration. Therefore, the transwell migration assay, a well-established technique to quantify cell migration in response to attractive or repulsive cues, was employed.
First, I optimized the assay by determining the cell density and incubation time that should be used for HeLa cells. The average numbers of cells that migrated through the membrane for *ARHGAP39* knockdown cells and stuffer virus control cells were about the same for both the initial cell numbers seeded and the incubation time (Fig. 3.43 A, B). These experiments revealed that the transwell migration of *ARHGAP39* depleted cells in the presence of serum, but absence of SLIT stimulus, is not impaired.

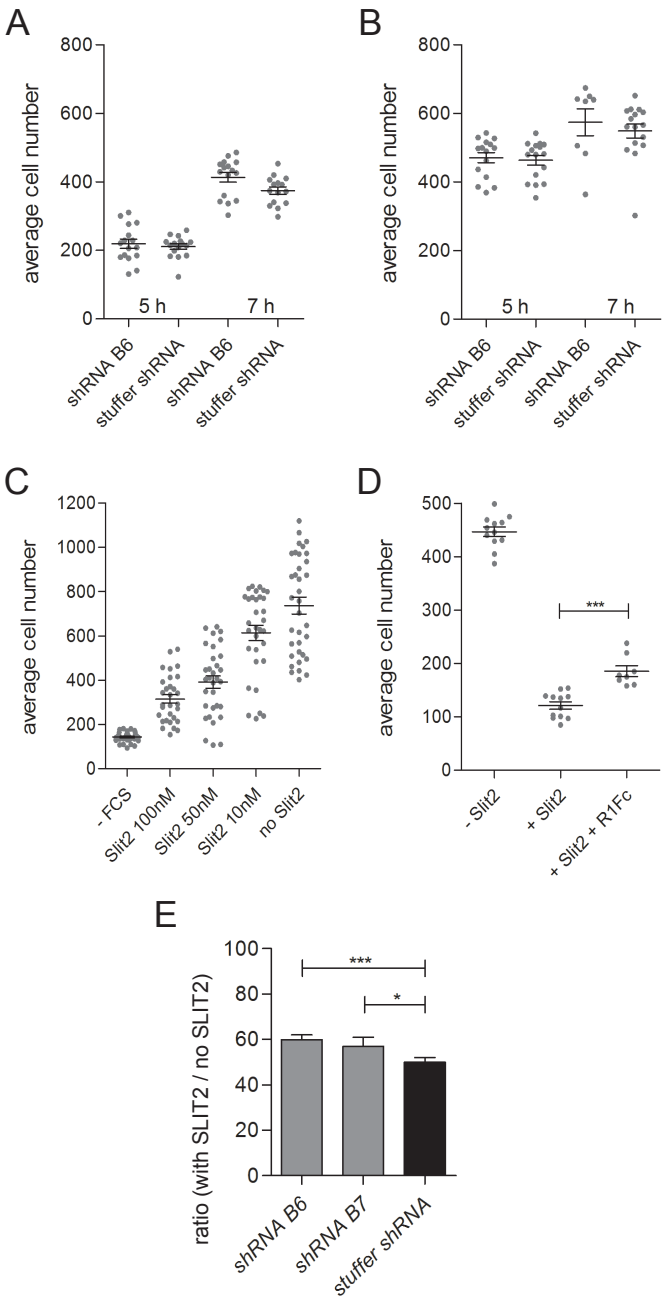

Figure 5.43.: see next page

Figure 5.43.: ARHGAP39 knock down increases cell migration in the presence of SLIT2
In **A** 40,000 and in **B** 80,000 cells were treated the in the same way: GAP39 shRNA B6 and stuffer shRNA cells were seeded and were allowed to migrate for the indicated periods of time. Afterwards the insert membranes were fixed and stained with crystal violet. Between 8 and 15 fields of view were imaged per transwell insert. **C** 40,000 HeLa cells were seeded. In the bottom chamber media was present either without serum or with serum plus SLIT2 at 100 nM, 50 nM, 10 nM to 0 nM concentration. **D** 40, 000 HeLa cells were seeded per insert. Media in the bottom chamber contained either no SLIT2 or 50 nM SLIT2 plus 400 nM ROBO1 Fc. Afterwards the insert membranes were fixed and stained with crystal violet. Between 10 and 12 fields of view were imaged per transwell insert. One insert per condition was analysed. **E** 80,000 cell seeded per insert and incubated for 6 h in presence or absence of SLIT2 50 nM. The migration index was measured as the ratio the ratio of cells migrated in presence of SLIT2 divided by the average cells migrated in the absence of SLIT2. The average cell number of cells migrated without SLIT2 was set to 100%. For each transwell insert between 8 and 15 fields of view were imaged. Two inserts per condition were analysed, the experiment was repeated in two independent rounds. Cell counting was done with the free software CELLCOUNTER (https://bitbucket.org/linora/cellcounter/downloads)(Li et al., 2014). Asterisks denote statistical significance as calculated by Student's t-test. Significance was ranked as * $p<0.05$, *** $p<0.001$. Abbreviations: GAP39: ARHGAP39, FCS: fetal calf serum, ROBO1Fc: ROBO1 extracellular region linked to Fc fragment of IgG antibody.

I next determined the minimal SLIT2 concentration required to detect impaired cell movement. In the absence of SLIT2 and presence of serum, the maximum transwell migration was observed. In contrast, without serum and SLIT2, cell migration was reduced to the greatest extent. With increasing concentrations of SLIT2 in presence of serum fewer cells migrated through the insert into the bottom compartment (Fig. 3.43 C). 50 nM SLIT2 was chosen for further experiments, as it resulted in a substantial change in migratory behaviour.

To show that the effect of SLIT2 on HeLa cells occurs via ROBO1 binding I used a ROBO1-IgFc chimeric protein, which contains the extracellular part of ROBO1 linked to the IgG-Fc fragment. By adding the ROBO1-IgFc to the media it should neutralise the SLIT2 molecule in the media, thereby preventing the activation of the ROBO1 receptor on HeLa cells. The media in the bottom chamber contained serum with or without SLIT2 plus ROBO1 Fc. As shown before, the average cell number of migrated cells was dramatically reduced in the presence of SLIT2. I observed an significant increase in average cell number when ROBO1 Fc was added to the media ($p<0.0001$) (Fig. 3.43 D). This shows that the decrease in cell migration in the presence of SLIT2 partially requires ROBO1 activation.

Subsequently, I asked whether knockdown of *ARHGAP39* affects the repulsive migratory behaviour of cells in the presence of SLIT2. I observed that upon depletion of ARHGAP39 significantly more cells migrated through the membrane in the presence of SLIT2 compared to stuffer virus cells (Fig. 3.43 E). The ratio of the cells migrated in presence of SLIT2 divided by the cells migrated in the absence of SLIT2 is shown in Figurexx. The migration of *ARHGAP39* depleted HeLa cell is increased (60% / 57%) compared to shRNA stuffer HeLa cells (50%) in the presence of SLIT2. This result indicates that the loss of *ARHGAP39* makes

the cells less sensitive to SLIT2, as they do not respond as strongly as wildtype cells.

To sum up this chapter, I could demonstrate a functional link between ROBO signalling and ARHGAP39 by showing that *ARHGAP39* depletion renders the cells less responsive to SLIT2. I proved a canonical binding mechanism for the ARHGAP39 WW2 domain and the ROBO1 CC2 motif. ROBO4, however, binds by a different binding mechanism to ARHGAP39 that potentially requires multiple binding sites. Furthermore, I provided evidence that ARHGAP39 is co-recruited to ROBO1 in endocytosed vesicles upon SLIT2 stimulation and is therefore implicated in the signalling pathways downstream of ROBO1.

6. Discussion

6.1. ARHGAP39 interacts with all four human ROBO receptors

This thesis aimed to functionally characterize ARHGAP39 and to study its role in cell migration. The protein was previously found in the Rocks lab to interact with the vascular-specific ROBO4 receptor (Müller et al., BioRxiv). This observed ROBO4/ARHGAP39 interaction was interesting for two reasons. First, the link between ROBO receptors and the control of repulsive cell migration is not fully established. The only other reported Rho regulatory proteins downstream of ROBO receptors are the RAC1GEF SOS and the Cdc42/Rac1-specific SRGAPs1-3 (Wong et al., 2001; Fan et al., 2003; Yang and Bashaw, 2006; Yamazaki et al., 2013). And second, no GEF/GAP protein has so far been identified to associate with ROBO4, which lacks some of the bindings motifs present in the other ROBO family members. ARHGAP39 may thus connect ROBO4 signaling to the control of angiogenesis.

I could indeed demonstrate that ARHGAP39 binds to all four ROBO receptors (Fig. 5.1) and that it is predominantly a Rac1- and to lesser extend a CDC42-specific GAP (Fig. 5.19). Thus, for the first time one RhoGAP protein links all ROBO receptors to RAC1/CDC42 signalling
The observed substrate specificity is in agreement with the previously reported specificity of Vilse/Crossgap for Rac1 and Cdc42. This was analysed *in vitro* by performing a GTPase activation assay using a GST-fusion protein of the purified RhoGAP domain of Vilse (Lundström et al., 2004) and also *in vivo* by examining whether Vilse/Crossgap can rescue the Rac1 overexpression phenotype in *Drosophila* eyes (Hu et al., 2005).
It was nevertheless important to investigate the catalytic activities of human ARHGAP39 in an independent manner, given the controversial data landscape on substrate specificities in the literature in general (Müller et al, BioRxiv). Conflicting results are frequently observed when the GTPase substrate specificity is analysed with different assay systems and, especially, when *in vitro* or *in vivo* methods are compared. *In vitro* studies utilize truncated versions of GEF/GAP proteins containing only the catalytic domain but lacking potential regulatory regions and measure activities in a non-physiological context. Potential regulation by post-translational modifications, protein interactions and the subcellular protein distribution is not taken into account. In this study, I used a novel robust and reliable screening assay based on FRET biosensors that allows the investigation of full length Rho regulatory proteins in their

native cellular environment (Müller et al, BioRxiv).

The molecular characterization of the ROBO1/ARHGAP39 interaction revealed a canonical binding mechanism involving the second WW domain of ARHGAP39 and the proline-motif containing the CC2 region of ROBO1 (Fig. 5.32, 33). This binding mode very likely applies to interactions with ROBO2 and 3, since their poly-proline sequences in the CC2 motif are highly similar. Moreover, the same domains in Vilse/CrossGAP and Robo are engaged during their interaction in Drosophila, implying that this is an evolutionary conserved mechanism (Lundström et al., 2004; Hu et al., 2005).
Unexpectedly, the association of ARHGAP39 with ROBO4 does not follow the same mechanism. In both proteins I identified additional regions implicated in binding. The involvement of more than one interaction site might be due to the divergent domain architecture of ROBO4 as its extracellular domain and the cytoplasmic tail are shorter, the latter containing only two of the four CC motifs.

The cytoplasmic portions of the ROBO receptors can be considered as intrinsically disordered. A substantial fraction (30-40 % (Olsen et al., 2017)) of the proteome contains larger disordered regions lacking a clear defined three-dimensional structure. Examining the binding mechanisms and kinetics of such intrinsically disordered proteins (IDPs) is an emerging field in structural biology research, as they can engage in diverse biological functions ranging from signal transduction, scaffolding, cell cycle progression to transcription (see reviews (van der Lee et al., 2014; Mollica et al., 2016; Olsen et al., 2017).
IDPs are characterized by the enrichment of modification sites that are freely accessible for post-translational modifications; the presence of small binding sites that fold upon binding of a partner proteins (coupled folding and binding) and a high degree of flexibility and access to binding sites that facilitates the assembly of complexes (Tompa and Fuxreiter, 2007). One mode of interaction of IDPs is 'fuzzy binding', in which the disordered regions largely remain unstructured even in the bound state of the protein (Tompa and Fuxreiter, 2007). IDPs and their binding partner can have a number of interaction sites and during binding the individual interactions between the IDP and its partner protein can be short-lived compared to the overall life-time of the complex. Additionally, one binding site on the IDP might recombine with several sites on the interactor within the life-time of the complex. Thus, the unstructured regions of IDPs are dynamic in the bound state and occupy several conformational states (reviewed in (Olsen et al., 2017)).
The engagement of multiple phosphorylated binding sites of the cyclin-dependent kinase inhibitor Sic1 with one single binding motif on its receptor Cdc4 exemplarily illustrates the "fuzzy" binding model (reviewed in (Mollica et al., 2016; Wright and Dyson, 2015; Schlessinger et al., 2007)). The interaction of the individual Sic1 binding sites with Cdc4 exhibit fast associa-

tion/dissociation with weak binding affinities. It is assumed that these multiple weak-binding motifs of Sic1 may synergize and lead to an over-all high affinity of the Sic1-Cdc4 interaction (Mittag et al., 2008). The binding sites in Sic1 are post-translationally phosphorylated, which might enhance the specificity of the binding or further fine tune the binding affinity to Cdc4.
My results suggest that besides the CC2 motif on ROBO4 additional binding sites must exist to mediate the binding to ARHGAP39. The CC2 motif, which was assumed to be the binding motif for ARHGAP39, differs between ROBO4 and the other receptors (Fig. 5.29) Therefore, the multiple binding sites in the cytoplasmic portion of ROBO4 might be required to increase the affinity of the ROBO4/ARHGAP39 interaction, as the CC2 motif alone may not be sufficient.

The important question arises why the interaction of ARHGP39 with ROBO1 follows a canonical WW domain-mediated mechanism, whereas the association with ROBO4 requires multiple binding sites, even though the cytoplasmic portions of both receptors are disordered. The ROBO4 receptor emerged later in evolution, contains simpler domain architecture and its expression is restricted to endothelial tissue (Huminiecki et al., 2002). Moreover, ROBO4 receptor activation and signalling might also differ from ROBO1. Whether ROBO4 can be activated by SLITs is still controversially discussed leading to the hypothesis that ROBO4 might be activated through ROBO1 as its co-receptor (Koch et al., 2011; Sheldon et al., 2009). Therefore, one can speculate that a different binding mechanism has evolved also for the recruitment of cytosolic partner proteins .
Thus, I hypothesise that while the generic function of ROBO receptor downstream signalling is to induce cytoskeletal rearrangements they might exploit different binding mechanisms to elicit these responses. Activation of ROBO4 downstream pathways in the vasculature might involve and require other regulatory mechanisms than ROBO1 receptor signalling in neurons, which might be due to tissue specific expression of effector proteins and/or guidance cues. It will be interesting in the future to compare the interactomes of ectopically expressed ROBO4 in neuronal cells with those in endothelial cells in order to identify differences in the signaling and regulatory networks in the different tissue contexts. For instance the interaction with Ena/Mena was shown to differ between fly Robo and murine Robo4. In *Drosophila* the binding of Ena to Robo is described to occur via the CC2 and CC1 motif (Bashaw et al., 2000). Whereas the interaction of Mena (mammalian Ena) with the Robo4 receptor involves the CC0 and CC2 motifs(Park et al., 2003).

Interestingly, the requirement of more than one binding motif of the cytoplasmic region of Robo has been observed also for Dock (the homologue of Nck), which has been mapped to associate with the CC2 and the CC3 motif of Robo. Removal of one or the other domain reduced the binding of Dock to Robo, but only deletion of both domains completely abolished

the binding (Fan et al., 2003). Moreover, Nck2 recognizes four PxxP motifs between the CC2 and CC3 motif of murine Robo1, which all contribute to this interaction (Round and Sun, 2011) and resembles the "fuzzy binding" mechanism of an IDP. Therefore, the here observed multiple binding sites of the ARHGAP39/ROBO4 interaction is not a exceptional observation. Moreover, the established binding sites of ROBO1 and its downstream effectors should be revised in the light of IDP interactions.

To further analyse the GAP39/ROBO4 interaction experimental approaches are required that meet the demands of structurally disordered proteins. The thorough characterization of IDPs is a an emerging research field in structural biology that is addressed by nuclear magnetic resonance (NMR) spectroscopy, small-angle X-ray scattering (SAXS) or single-molecule fluorescence resonance energy transfer (smFRET) (van der Lee et al., 2014). For instance, the NMR spectrum of the ROBO4 cytoplasmic portion reveals information about its degree of disorder in its unbound conformation and could be compared to the ROBO4/ARHGAP39 spectrum. Additionally, transferred cross-saturation (TCS) NMR could be employed to map the binding interface of the ROBO4/ARHGAP39 complex.

6.2. The ARHGAP39 WW2 is a class II domain that mediates interactions

The WW domains are important for the interaction of ARHGAP39 with its binding partners. In this thesis, I demonstrated that they are required for the interaction with ROBO1 and ROBO4, but also with CNKSR2, CNKSR3 and PEAK1. Analysing the molecular binding mechanism revealed that the association with these interaction partners is solely mediated by the WW2 domain, with the exception of the ROBO4 interaction.

From sequence alignment of the two WW domains I concluded that the WW2 is a class II domain that recognizes stretches of poly-prolines (Fig. 5.14). Strikingly, at least one poly-proline stretch was found in all binding partners and alignment of these stretches revealed a consensus sequence PPPPxxP, which is in agreement with the predicted target motif for class II domains. Moreover, I could then show that point mutations in WW2 abolished the binding to the CNKSR proteins, PEAK1 and to ROBO1 (Fig. 5.28, 30).

The WW domain sequence alignment for the WW1 domain was not entirely conclusive. The presence of only one Tyr residue in the center of the WW1 domain sequence suggests that it favours a PPxY motif. However, a His residue that is possibly required for ligand specificity is

missing (Otte et al., 2003).
Alternatively, the motif (poS/poT)P may be recognized due to the presence of three Arg residues in the central region of WW1 that are capable of interacting with the negatively charged phosphorylated Ser/Tyr residues, as described for PIN1 (Macias et al., 2002).
Another scenario is that WW1 does not act as canonical WW domain at all and instead binds to a yet unidentified motif. WW1 aligns well with the WW domain of Arhgap9, which binds to conserved acidic residues in the common docking (CD) domains of MAP kinases, involving two Arg residues adjacent to the WW domain, thereby forming electrostatic interactions (Ang et al., 2007). Interestingly, the WW1 domain of ARHGAP39 and the ARHGAP9 WW domain both lack most of the conserved amino acid residues responsible for ligand binding.
Lastly, WW1 could provide structural stabilisation for the second WW domain while it is in engaged in binding (Dodson et al., 2015). I observed that point mutations in WW1 decreased the binding of ARHGAP39 to ROBO1 (Fig.). Thus, the first WW domain might strengthen the WW2 domain - CC2 motif interaction, which can be affected by mutations in the WW1 sequence, because both domains are connected by an only four amino acid long linker.

During the course of this thesis it was reported that murine Arhgap39 binds to Cnksr2 to form a multi-protein complex (Lim et al., 2014). This is in agreement with my observation that human ARHGAP39 and CNKSR2 associate with each other. The multi-protein signalling platform established by Cnskr2 includes, besides from Arhgap39, the RacGEFs αPix and βPix, Pak3 and Pak4, and regulates Rac1 cycling during spine morphogenesis in the murine hippocampus (Lim et al., 2014).
Interestingly, TANC2, another ARHGAP39 interactor that I could validate in my work, is expressed in spines as well, where it is implicated to modulate the spine density along dendrites (Han et al., 2010). Thus, I presume that ARHGAP39 and TANC2 can interact in the same physiological environment as they are both present in the post synaptic compartment. Together, this implicates that Arhgap39 activity is spatially and temporary defined within dendrites to allow spine formation and maturation.

In contrast, nothing is known about the association with the atypical kinase PEAK1. This interaction opens up a new cellular context of ARHGAP39 signalling independent of ROBO. PEAK1 was shown to modulate cell spreading and migration by altering the life-time and assembly/disassembly cycle of focal adhesions (Wang et al., 2010; Bristow et al., 2013). I demonstrated that PEAK1 mediates the recruitment of ARHGAP39 to focal adhesions via its WW2 domain. It will be interesting to further elucidate the role of ARHGAP39 in the control of focal adhesion dynamics.
First, it should be addressed how the interaction of both proteins is regulated. The recruitment of ARHGAP39 to focal adhesions could be analysed in the presence and absence of EGF,

which was shown to stimulate the translocation of the PEAK1 signalling complex to focal adhesions (Bristow et al., 2013).
The second question is whether PEAK1 itself can modulate ARHGAP39 activity. It is conceivable that ARHGAP39 could be released from its auto-regulation by phosphorylation. However, PEAK1 shows only weak tyrosine kinase activity (Wang et al., 2010), presumably due to its atypical kinase domain and so far no substrate has been identified. It also possible that binding of PEAK1 releases ARHGAP39 from its auto-inhibited conformation. This question can be addressed using the FRET biosensor activity assay in an experiment where cells are co-transfected with the RAC1 sensor, mCherry-ARHGAP39 and iRFP-PEAK1 and the potential release from auto-inhibition is compared to the absence of cotransfected PEAK1.
Lastly, in order to understand the role of ARHGAP39 in PEAK1 mediated focal adhesion turnover it should be investigated how the knockdown of *ARHGAP39* affects cell migration and focal adhesion dynamics. For instance mCherry-Pxn fluorescence could be monitored in *ARHGAP39* depleted Cos7 cells by TRIF microscopy in live cells. Thereby, the focal adhesion assembly/disassembly and life-time can be analysed.

Lately, PEAK1 gained attention as an oncogene involved in tumor cell migration and proliferation (Wang et al., 2010; Croucher et al., 2013). Its expression is upregulated in a wide range of cancerous cell lines and in tumors, for instance in colon, rectal and in breast cancer (Huang et al., 2018; Croucher et al., 2013), and PEAK1 downregulation in colorectal cancer cells inhibited cell migration, invasion and proliferation (Huang et al., 2018).
This indicates that ARHGAP39 activity might be linked to cancer progression and metastasis. ARHGAP39 is endogenously expressed in MDA-MB-231 and MCF-10A cells (Fig. 5.25), which do also express PEAK1 (Wang et al., 2010; Croucher et al., 2013), thus both proteins can be studied in an endogenous setting. As it was shown that PEAK1 promotes the growth of MCF-10A acini in three-dimensional culture it could be assessed if ARHGAP39 expression leads to the same phenotype in *PEAK1* cells, indicating that ARHGAP39 acts downstream of PEAK1 signalling.

6.3. The MyTH4 domain targets ARHGAP39 to the plasma membrane

The MyTH4 domain is a rare protein module that appears in tandem with a FERM domain and can be found in actin-based motor proteins, in plant kinesin and in unconventional myosins.

In this thesis I made three interesting observations regarding the MYTH4 domain of ARHGAP39. First, ARHGAP39 is the only vertebrate protein characterised that contains an isolated MyTH4

domain (Fig. 5.21). Second, the MyTH4 domain is required for the plasma membrane localisation of ARHGAP39, indicating a new function for MyTH4 domains. And third, it is crucial for the correct folding of ARHGAP39 (Fig. 5.17).

It has been proposed that MyTH4 domains invariably coexist in tandem with a FERM domain in higher organisms (Wu et al., 2011). While isolated MyTH4 domains have been found in MyoIV and in MyoXII of the non-vertebrate organisms *Acanthamoeba* and *Caenorhabditis elegans*, respectively, it is assumed that they were originally paired with a FERM domain, which became unrecognizable as such during evolution (Mooseker and Foth, 2008). Therefore, ARHGAP39 is the first protein characterized containing only the MyTH4 domain.

Structurally it could be argued that correct folding of the MyTH4 domain may require the presence of the FERM domain. By sequence comparison I observed that the ARHGAP39 sequence is highly similar within the conserved helices of the MyTH4 domain, which mediate the folding of the core domain. Additionally, the conserved residues of the N-terminal linker and the C-terminal linker sequences are present in ARHGAP39 MyTH4 as well (Fig. 5.15). Both regions further stabilize the MyTH4 core domain. Therefore, it can be assumed that the ARHGAP39 MyTH4 core domain folds in a similar way as it would do in the MyTH4-FERM tandem.
Surprisingly, ARHGAP39 lacking the MyTH4 domain is not able to properly fold indicating that the globular structure of the MyTH4 domain is essential to confer overall structural integrity of ARHGAP39.

A plasma membrane targeting function of MyTH4 domains has not been reported before. Generally, the membrane localization of MF-Myosins is mediated by the FERM domain via binding to plasma membrane associated binding partners. For instance, the FERM domain of MyoX interacts with β-integrins (Zhang et al., 2004) or the C-terminal FERM domain in MyoVII binds to vazatin, a transmembrane protein at adherens junctions (Küssel-Andermann et al., 2000).
A recent model of MyTH4 domain evolution suggests that insertion and deletion of sequences within the variable regions leads to changes in the exposed surface of the MyTH4 domain, while its overall domain integrity provided by the six core helices is unaffected. Thus, the variable sequences have the potential to define new functions of the MyTH4 domain (Planelles-Herrero et al., 2016), suggesting that the variable sequences in the MyTH4 domain of ARHGAP-39 might be responsible for the interaction with the plasma membrane.
Interestingly, a single point mutation in one of the conserved helices of the MyTH4 domain (E783K) is sufficient to abolish the plasma membrane binding. This implicates that impaired folding of the core domain may affect the surface exposure of residues critical for plasma

membrane binding of MyTH4 and thus its function to bind to the plasma membrane.

Crystallization of the ARHGAP39 MyTH4 domain could reveal information on how the binding to the plasma membrane is established. It may be speculated that the MyTH4 module either binds to other membrane proteins or directly interacts with the lipid bilayer. One emerging question is if an isolated MyTH4 domain of a MyTH4-FERM tandem would also bind to the membrane.

The functional implication of the plasma membrane localisation of ARHGAP39 still needs to be determined. It can be speculated that ARHGAP39 is either constitutively bound to the membrane or it is recruited in a regulated manner. If ARHGAP39 is constitutively membrane bound this would open up the possibility for an additional unction independent of ROBO1 and PEAK1. This would bring ARHGAP39 in close proximity to membrane-associated RAC1 and CDC42 and thus enables ARHGAP39 to locally inactivate them. However, by microscopy I observed that a notable fraction of ectopically expressed ARHGAP39 was present in the cytoplasm and not enriched at the membrane (Fig. 5.16). Thus, it might be assumed that its membrane localisation is temporary regulated, for instance in a cell-cycle or signalling-state dependent manner.

6.4. ARHGAP39 is N-terminally autoinhibited

Auto-regulation is a widespread mechanism that enables signalling proteins to process upstream signals in a spatially and temporally confined manner and allows them to selectively engage their cognate downstream pathways. Many Rho regulatory proteins are subjected to auto-regulation through backfolding of their terminal regions (Cherfils and Zeghouf, 2013). The intramolecular folding can be released by specific cues that mediate an increased accessibility of the catalytic domain for the Rho GTPase substrate.

In this work I could demonstrate that also ARHGAP39 is auto-inhibited and that its regulation is mediated by the N-terminus that comprises the two WW domains.
Using FRET biosensor activity assays I could show that deletion of the N-terminal WW domains or of the central region increases the catalytic activity of ARHGAP39. Truncation of the entire N-terminus in the construct Cterm2, which encodes only the MyTH4 and GAP domain, resulted in the highest GAP activity.
The analysis of the binding site in the N-terminus revealed that the WW1 domain mediates the intramolecular interaction (Fig. 5.23). My results suggest two different modes of action. The WW1 either binds to a putative (pS)P consensus motif as discussed above or in a non-

canonical way involving yet to be determined binding motifs (Section 5.3.1). Evidence for the first assumption is the observed interaction of the purified GST-WW domains with two sequences containing isolated Pro residues in combination with a Ser residue. This (pS)P motif might constitute a recognition motif for the WW1 domain. However, how the two identified peptide sequences, which are separated by more than 300 amino acids, contribute to the binding needs further validation. Alternatively, the sequence homology of WW1 with the WW domain of Arhgap9 also suggests that it may engage in electro-static interactions (Ang et al., 2007). Theoretically, the WW1 could also bind to the MyTH4 domain or the GAP domain directly which both were both not included in the peptide spot assay.

To further decipher the backfolding mechanism a repetition of the peptide-spot overlay assay with purified isolated WW1 and WW2 should be conducted to confirm that only the WW1 domain mediates the intramolecular binding. Moreover, the complete ARHGAP39 sequence, including the MyTH4 and GAP domain, should be spot synthesized in a phosphorylated and non-phosphorylated form (Otte et al., 2003) in order to validate if phosphorylation of the (pS)P motif enhances the interaction with WW1.

An important question is how the auto-inhibited conformation of ARHGAP39 is released. It is conceivable that the interaction with binding partners can release ARHGAP39 from the auto-inhibitory state. This question can be addressed using the FRET biosensor activity assay. An increase in activity detected in the presence of a binding partner indicates that binding to the partner protein releases the intramolecular backdfolding of the N-terminus.

Interestingly, a decrease in ARHGAP39 activity was observed for the plasma membrane binding deficient E783K mutant compared to the wildtype protein. This implies a second mechanism to release the auto-regulation of ARHGAP39. Cytosolic ARHGAP39 may reside in a strongly auto-inhibited conformation, which is partly released upon binding to the plasma membrane. Thereby, the MyTH4 domain-mediated interaction with the membrane could bring ARHGAP39 into a stable conformation and orientation that can be better accessed by its substrates RAC1 and CDC42. To formally exclude that ARHGAP39 GAP activity is not simply impeded due to improper folding of the MyTH4 domain it is necessary to examine if the other mutant MyTH4 domains generated in this work, which still bind to the membrane (Fig. 5.21), also affect the GAP activity.

6.5. ARHGAP39 is implicated in cell migration

Cell migration involves the dynamic regulation of the cytoskeleton and cell adhesions and is tightly coordinated by Rho GTPases in a context-specific manner.

Here, I could show that knockdown of *ARHGAP39* impaired the migratory behaviour of HeLa

cells in a wound healing assay (Fig. 5.27). This assay is a standard method to address basic cell migration independent of a specific tissue context or stimulus. The reduced cell velocity and migration distance in *ARHGAP39* depleted cells (Fig.) therefore, indicate a general role of ARHGAP39 in cell migration.

An interesting question for future studies is which of the many cellular functions of RAC1/CDC42 implicated in the regulation of migration are mainly controlled by ARHGAP39. This could be addressed by reconstitution experiments in which functional mutants or truncations of ARHGAP39 are reexpressed in CRISPR-CAS9 knockdown cells. For instance, a role in the control of focal adhesion turnover could be tested using the WW2 domain point mutants that is incapable of binding to PEAK1 and is thus not recruited to these structures.

6.6. ARHGAP39 plays a role guided cell migration

Having demonstrated that ARHGAP39 is implicated in basic cell motility I aimed next to identify a functional link between SLIT2/ROBO1 mediated cell repulsion and ARHGAP39.
I found that depletion of *ARHGAP39* decreases the repulsive effect of SLIT2, causing cells to continue to migrate towards a SLIT2 gradient. Furthermore, I could verify that the SLIT2-induced repulsive response is ROBO1 dependent (Fig. 5.43).

The observed role of ARHGAP39 in cell repulsion is in line with defects in midline repulsion in *vilse/crossgap* depleted animals. The relatively mild effect on cell repulsion observed in this work resembles the low penetrance of the misguidance phenotype in *vilse/crossgap* Drosophila embryos. This phenotype is further enhanced in animals missing one copy of *slit/robo* (Lundström et al., 2004), indicating a direct function of Vilse/Crossgap downstream of Robo. Functional redundancy is a common phenomenon that confers robustness to signalling systems and could also account for the mild *ARHGAP39* knockdown phenotype in Slit2 mediated repulsion in cells observed here. It is possible that the depletion of ARHGAP39 is compensated by other Rho GTPase regulators, for instance by members of the SRGAP family, which are RAC1-specific.

Surprisingly, data from the literature is inconsistent regarding the question whether RAC1 signalling is enhanced or inhibited in SLIT2/ROBO1 mediated cell migration. Whereas initial studies claimed that RAC1 activity is downregulated during repulsive axonal guidance (Fritz and VanBerkum, 2002) it has been shown that active RAC1 is required in axonal repulsion along the ventral nerve cord in *Drosophila* (Hakeda-Suzuki et al., 2002; Matsuura et al., 2004). RAC1-GTP levels were also increased in MDA-MB-435 cells that ectopically express SLIT2

(Stella et al., 2009) and in Robo expressing HEK 293T cells in the presence of Slit2 (Fan et al., 2003). Moreover, it has never been investigated whether the substrate specificites of the Rho regulators Sos, SrGAP2-3 and also of Vilse, change upon activation of Robo. Therefore, these data have to be reviseted in order to better understand how SLIT stimulation affects Rho GTPase signaling downstream.

6.7. Rapid internalisation of ROBO1/ARHGAP39 upon SLIT2 stimulation

Guidance molecules bind and activate their cognate signalling receptors, which get internalized by endocytosis and are sorted into endosomal compartments to eventually become degraded in lysosomes or to be recycled to the plasma membrane. The processes of regulated endocytosis, receptor trafficking and regulated proteolysis are general mechanisms to modulate the amplitude and duration of receptro signalling.

By live-cell microscopy I demonstrated the rapid and efficient internalisation of ROBO1 upon SLIT2 stimulation and, furthermore, could show its colocalisation with ARHGAP39 on vesicles at late time-points after stimulation (Fig. 5.41). This result strongly suggests that both proteins interact in stimulated cells and are co-internalized. Whether this interaction already occurs at the plasma membrane cannot be concluded from microscopy data since both proteins localise at the cell periphery independent of each other.
The biochemical examination of the binding of endogenous ARHGAP39 to ROBO1 revealed a basal interaction independent of SLIT2. However, after 30 min of SLIT2 treatment a strong increase in ROBO1/ARHGAP39 interaction could be observed (Fig. 5.39). Combining the biochemical data with the observed colocalisation in endosomes could hint at a delayed recruitment and consequently signalling response of ARHGAP39.

A recent study discovered a similar delayed engagement of the downstream effector Sos which was shown to be recruited to the endocytosed Robo receptor upon Slit2-stimulation (Chance and Bashaw, 2015). It was therefore proposed that the internalization of Robo into the cell is necessary to activate the receptor and to transmit repulsive signals. While it was assumed in the past that guidance receptor endocytosis upon ligand binding solely causes the attenuation of receptor signalling in order to desensitize the growth cone or to spatially restrict the response to guidance cues (Winckler and Mellman, 2010; Bashaw and Klein, 2010), these data suggest that endocytosed Robo receptors continue to signal on endosomes (Chance and Bashaw, 2015). How Robo is signalling is terminates is not fully understood yet. It was shown that Robo resides on early and late endosomal compartment and might thus be targeted for

degradation (Chance and Bashaw, 2015), however Robo receptor reclycing to the plasma membrane can not be excluded.

Such receptor signalling from endosomes has been studied intensively for other signalling receptors such as Notch, EGFR and VEGF-R2 or GPCRs (Vaccari et al., 2008; Jékely et al., 2005; Lanahan et al., 2010; Tsvetanova and Irannejad, 2015). Here, it has been observed that different signalling environments exist at the plasma membrane and the endosomal compartment allowing for different signalling responses of the same receptor. Modulation of the transport kinetics of ligand-bound receptors to lysosomes alters the time duration of the signal before it is terminated. Moreover, it has been observed that a first, acute response of the ligand-bound receptor at the plasma membrane is followed by a second sustained response on endosomes (Sorkin and von Zastrow, 2009; Villasenor et al., 2016).
Therefore, it is surprising that the specific mechanisms beyond SLIT2 mediated ROBO internalization, ROBO trafficking within the endosomal compartments or continued ROBO signalling on endosomes have not been addressed more thoroughly, though it is crucial to understand how signal transduction occurs downstream of ROBO that lead to dynamic rearrangement of the cytoskeleton.

6.8. Model: A ROBO-independent cellular function of ARHGAP39

After having discussed the main discoveries revealed by the functional characterization of ARHGAP39 here I aim to combine these results with the observed role of ARHGAP39 in cell migration. First, I present a model of ARHGAP39 implicated in basic cell migration.
Focal adhesions couple integrin complexes to actin filaments, thereby creating actomyosin contractility, which in return allows them to sense and transmit mechanical tension to control cell migration. Moreover, they serve as signalling hubs that recruit scaffold proteins, kinases, phosphatases and other signalling effectors that modulate motility or signalling pathways in response to adhesion (Fritz and Pertz, 2016). Active RAC1 is implicated in nascent adhesion formation and turn over in the lamellipodium, maturation to focal adhesions requires RHO A dependent actomyosin contractility (Lawson et al., 2014).

It is assumed that assembling nascent adhesions recruits and activates phospho-regulated scaffold proteins, which in turn generate signals that activate RAC1/CDC42. For instance, FAK and PXN signalling leads to the recruitment of RAC1-specific GEFs at nascent adhesions that activate RAC1 to stimulate actin polymerization and thus the induction of membrane protrusions and the formation of new nascent adhesions (Deramaudt et al., 2011; Parsons et al., 2010). In this context, ARHGAP39 might function to inhibit RAC1 signalling to either allow

the disassembly of nascent adhesions or to ensure proper adhesion turnover at the lamellum-lamellipodium interface by contributing to the protrusion-retraction cycles of the leading edge during cell migration (Machacek et al.,2009).

The signalling function of ARHGAP39 at focal adhesions may be regulated by PEAK1. PEAK1 was shown to function as a phospho-regulated scaffold that recruits several adhesion and signalling proteins (Wang et al., 2010; Bristow et al., 2013). Downstream of PEAK1 the SRC-p130CAS-CRK-PXN signalling axis has been shown to mediate RAC1 activation, for instance via recruitment of the RAC1 specific GEF DOCK180, which induces membrane protrusions and cell migration (Defilippi et al., 2006). Thus, by targeting ARHGAP39 to this complex RAC1 activity can be tightly regulated, allowing for continuous cycling of the activity state of the GTPase.
Moreover, PEAK1 is also implicated in cancer progression via the EGFR-RAS-RAF-ERK signalling pathway, as it was shown that a phosphorylation resistant mutant prevented increased activation of ERK (Croucher et al., 2013). Thus, deregulated PEAK1 phosphorylation levels facilitates proliferation and survival of cancerous cells. In addition, PEAK1 promotes enhanced cancer cell migration and invasion, which is assumed to be due to uncontrolled p130CAS-CRK-PXN pathway activation, which might lead to abnormal focal adhesion dynamics. Therefore, ARHGAP39 might have a tumor suppressor function to inhibit sustained RAC1 activity in cancer cells. It is also conceivable that aberrant phosphorylation or dephosphorylation of PEAK1 might affect the recruitment of ARHGAP39 to the PEAK1 scaffold. It will be interesting to analyse cancer databases such as the Broad Institute Achilles Project for interdependencies of ARHGAP39 and PEAK1 signalling network components.

6.9. Model: ARHGAP39 function downstream of SLIT/ROBO signalling

In the first model a role of ARHGAP39 in cell migration was presented independent of a specific tissue or signaling context. In the following section I discuss a model of ARHGAP39 function in guided cell migration downstream of SLIT2/ROBO1.

In a randomly migrating cell, the membrane protrusions that directly encounter SLIT2 immediately retract. This requires the contraction of actomyosin filaments that are connected to focal adhesions to mediate their disassembly. This process is RHO A dependent and thus requires RHO A-specific GEFs. In additional, local activation of RAC1 and CDC42 specific GAP proteins could prevent the formation of cell protrusions in the retracting area and thereby further

facilitate retraction.
Subsequently, RAC1 and CDC42 are activated either locally at the opposite side of the cell or globally. Active RAC1/CDC42 induces actin polymerization and the formation of membrane protrusions and allows the cell to initiate migration away from the SLIT signal. This requires the engagement of RAC1/CDC42 specific GEFs and, potentially, also of RhoA GAPs to prevent local actomyosin contractility.

How does this model fit into the data landscape?
No RHO A-specific GEFs have so far been identified that are activated upon SLIT2 stimulation. The SRGAPs could prevent further RAC1/CDC42 signalling during retraction of the membrane. However, it has not been mechanistically elaborated how exactly these proteins mediate the repulsive response downstream of ROBO. The only other known regulatory protein downstream of ROBO is the RAC1-specific GEF SOS (Yang and Bashaw, 2006; Chance and Bashaw, 2015), which is engaged on endosomes upon binding to the activated ROBO receptor. SOS activity establishes membrane protrusions and nascent adhesions required for cell migration at the opposite side of the cell. This process does not necessarily have to occur selectively at the opposite side of the cell as long as local RhoA activity at the SLIT stimulated side of the cell overturns SOS-induced protrusion formation and cell anchorage.

In this framework of SLIT2-stimulated cells, ARHGAP39 could represent a novel player contributing to cell repulsion. Two phases of ARHGAP39 action are conceivable. In the absence of SLIT2, a substantial fraction of ARHGAP39 is present at the plasma membrane. My biochemical data suggest that it can already weakly associate with ROBO1 at this stage (Fig. 5.39). ARHGAP39 at the cell surface could be partially active and contribute to a tonic inactivation of RAC1/CDC42. The binding of the Myth4 domain to the membrane thereby may contribute to this GAP activity as it may favour partial release of autoinhibition. Upon SLIT2 stimulation, ROBO1 is internalized on endosomes where it activates RAC1 via SOS to induce migration (Chance and Bashaw, 2015). A population of ARHGAP39 is co-internalized with ROBO1. However, tight binding of ROBO1 to ARHGAP39 is observed only as late as 30 min after receptor engagement. This may cause the complete releases of ARHGAP39 auto-inhibition on a late endocytic compartment.
At this stage, ARHGAP39 GAP activity contributes to the termination of RAC1/CDC42 signalling at the leading edge to restrict protrusion formation. ARHGAP39 would thus function as a timer to confine excessive motility in stimulated cells. This model is based on the observed auto-inhibition of ARHGAP39 involving its N-terminus and the assumption that binding of ROBO1 to the WW2 domain releases the backfolding. The opposite effect of ROBO1 binding, namely the inhibition of ARHGAP39, cannot be formally excluded at this point. A critical experiment to clarify this issue is to use the RAC1 biosensor to investigate how the pres-

ence of ROBO1 affects the catalytic activity of ARHGAP39 in presence of absence of SLIT2. This experiment would also allow to precisely deconvolute the temporal profile of ARHGAP39 activity after SLIT stimulation.

Lastly, the time scale of ROBO1/ARHGAP39 interaction and thus ARHGAP39 activity should be revised. In a recent study in the *Dictyostelium* model organism, attractive and repellent guidance cues were used to analyse induction of rear retraction, breakdown of symmetry (polarization) and establishment of the front after encountering the repellent. These processes were completed in less than two minutes (Cramer et al., 2018).

To more generally shed light on the temporal profile of the distinct cytoskeletal rearrangements induced upon ROBO receptor engagement, morphological changes could be analysed by live-microscopy of single cells to which SLIT2 is applied to one site of the cell. By utilizing marker proteins such as lifeact, cytoskeletal rearrangements within the cells can be monitored and temporally resolved. The initial experiment would include control cells and cells transfected with ROBO1 that are subsequently stimulated with SLIT2. In subsequent experiments the effect of ARHGAP39 on the cytoskeletal alterations could be tested

Furthermore, ROBO1 endocytosis and the presumed co-recruitment of ARHGAP39 requires detailed further investigations. Perturbation of ROBO internalization using different pharmacological or genetic inhibitors of endocytosis such as dynasore, pitstop2 or the dynamin K44A mutant will reveal whether the increased association with ARHGAP39 and consequently also the modulation of its enzymatic activity requires the trafficking to a specific endocytic compartment. The precise compartments where ARHGAP39 and ROBO colocalise should also be determined using immunofluorescence of marker proteins. Finally, the ultimate fate of the endocytosed ROBO receptor, recycling or lysosomal degradation, has never been properly studied. It would be interesting to investigate whether the inhibition of the endolysosomal pathway using bafilomycin or of dominant negative forms of the ESCRT protein complex (Eccles et al., 2016) affect ROBO signaling in general and specifically SOS and ARHGAP39 dependent signals.

6.10. Function of ARHGAP39 in the vasculature

The establishment of the vasculature in vertebrates is a complex process that involves the formation of primary vessels by vasculogenesis and subsequently the sprouting of secondary vessels during angiogenesis. In this work I made use of the zebrafish angiogenesis model system to study the potential role of ARHGAP39 downstream of the ROBO4 receptor, which was shown to be required for the sprouting and directional migration of intersomitic vessels (ISVs) (Bedell et al., 2005).

My work provided evidence for a novel role of ARHGAP39 in vascular development *in vivo*. The loss of Arhgap39 resulted in delayed vessel growth, a reduction in vessel lumen diameter (Fig. 5.4) and a decrease in filopodia density of growing vessels. Both gain- and loss-of-function analyses showed that Arhgap39 plays a role in directional migration and correct morphogenesis of endothelial sprouts.
ARHGAP39 signalling in the context of angiogenesis is in agreement with its expression in zebrafish endothelial cells (Fig. 5.3) and various human endothelial cell lines (Fig. 5.26) and with previously published data showing that Drosophila Arhgap39 mediates axonal repulsion at the midline (Lundström et al., 2004). Together the data suggest a conserved role for ARHGAP39 in guided cell migration across tissues.
I also observed that maintaining proper Arhgap39 activity levels is critical for directional migration of ISVs, since both its knockdown and overexpression resulted in similar phenotypes. This observation is in line with the results of the gain- and loss-of-function experiments of its homologue in Drosophila that both resulted in increased inappropriate axonal midline crossing (Lundström et al., 2004; Hu et al., 2005).

While vessel migration in the *arhgap39* depleted animals was impeded, the sprouting process itself was not perturbed (Fig. 5.7). In addition, a decrease in the number of filopodia and lumen diameter was observed. These three phenotypes have recently been demonstrated to correlate with each other in zebrafish (Phng et al., 2013; Abraham et al., 2015). Inhibition of filopodia formation along the growing ISVs decreased migration velocity. Moreover, is has been concluded that filopodia dynamics positively correlates with vessel width in the developing fish, presumably by guiding the growing sprout along the somite borders and thus establishing a functional vessel (Phng et al., 2013). Another recent study discovered a RAC1/CDC42 exchange factor complex that upon VEGF stimulation leads to consecutive RAC1 and CDC42 activation, which was shown to be required for filopodia formation, tube remodelling and promotes the lumen morphogenesis (Abraham et al., 2015).
Therefore, I assume that the observed reduction in filopodia density of growing sprouts in *arhgap39* knockdown animals is linked to the delay in vessel migration and also to the reduction vessel diameter. The other morphological defects of ISVs such as aberrant branching or aborted vessels formation could be a secondary effect due to loss of function of these vessels.

Interestingly, in *robo4* knockdown animals the ISVs show sprouting defects and misdirected, delayed growth, which ends in aborted vessel formation (Bedell et al., 2005). The delayed migration of ISVs in *robo4* fish is similar to the *arhgap39* knockdown phenotype and ROBO4 has been shown to induce filopodia formation in ECs and in HEK293T cells that either enhanced (Kaur et al., 2006) or prevented cell migration (Sheldon et al., 2009).

In the light of my data I speculate that Arhgap39 might function downstream of Robo4 to mediate the migration of the ISVs. It could be assumed that Robo4 dependent filopodia formation allows the growing vessels to find their path by sensing external cues, which could be extracellular molecules or mechanical stimuli from the surrounding tissue. While depletion of *robo4* impairs the guidance of vessels during sprouting and migration into one specific direction, the loss of *arhgap39* might perturb the migration process itself. The *arhgap39* knockdown phenotype could be attributed to impaired signal transduction downstream of Robo4, although evidences for a genetic or biochemical interaction in zebrafish yet need to be estblished.

An important issue is the validation of the specificity of the *arhgap39* MO induced phenotype in zebrafish that requires complementation experiments. The conducted rescue experiments using either ubiquitous expression or vascular specific expression of *arhgap39* mRNA were not conclusive (Fig. 5.12). Unfortunately, I conducted my experiments at a time when the CRISPR-mediated gene targeting system had not been established as the 'gold standard' to analyse gene knockdown in zebrafish. The method is based on a prokaryotic genetic silencing mechanism, which integrates fragments of foreign nucleic acid into its host genome at one end of a repetitive element, called clustered regularly interspaced short palindromic repeat (CRISPR). In the last years this system has been successfully adopted for application in fish and should now be employed to validate morpholino knockdown fish.

The role of Arhgap39 in angiogenesis is certainly far from being understood and also needs further validation. Several important questions need to be addressed, for instance: does Arhgap39 interact with Robo4 in vivo? What is the stimulus that triggers their association and does this result in activation or inhibition of Arhgap39 activity?
Ideal would be the establishment of a CRISPR/Cas-*arhgap39* knock-out zebrafish. By comparing the phenotype of the mutant fish to the *arhgap39* morphants the specificity of the *arhgap39* MO-induced gene knockdown would be examined. Recently, the development of a tissue specific CRISPR/Cas system was shown to mediate tissue specific expression of the gene-specific target sequences (sgRNAs) and the Cas9 enzyme that yields in spatially restricted downregulation of the gene of interest (Liu et al., 2017). To complement the phenotypic characterization a transgenic CRISPR/Cas-*arhgap39* knock-in fish could be generated (Kimura et al., 2014).
To explore the genetic interaction of *arhgap39* and *robo4*, a *robo4*-specific MO could be injected into the CRISPR/Cas-*arhgap39* knock-in fish and wildtype animals. The rescue of the *robo4* morphant phenotype in the transgenic CRISPR/Cas-*arhgap39* knock-in fish could indicate their genetic interaction.
The analysis of Rac1 and Cdc42 activities in vivo in wildtype fish and arhgap39 morphants is difficult. FRET biosensors have been used in zebrafish, however this requires the generation

of a specific transgenic fish line carrying the biosensor (Zhao et al., 2015; Andrews et al., 2016). Thus at present, the use of the here employed cell based FRET biosensor activity assay in endothelial cell culture should be considered.

Finally, to further investigate the function of ARHGAP39 in angiogenesis in mammalian cells, 3D matrigel assays could be performed which allow the investigation of tube and lumen formation and of filopodia dynamics of growing sprouts by live-cell microscopy. This assay also allows gene targeting by siRNA or shRNA, the transfection with ARHGAP39 and functional mutants thereof, or the addition of soluble cues such as SLIT2 or vascular growth factors, or pharmacological perturbations using drugs or inhibitors. With this system also the potential role of Robo1 as a co-receptor of Robo4 could be addressed.

7. References

Abdel-Ghany, S. E. and A. S. Reddy
2000. A novel calcium/calmodulin-regulated kinesin-like protein is highly conserved between monocots and dicots. *DNA Cell Biol*, 19(9):567–578.

Abraham, S., M. Scarcia, R. D. Bagshaw, K. Mcmahon, G. Grant, T. Harvey, M. Yeo, F. O. G. Esteves, H. H. Thygesen, P. F. Jones, V. Speirs, A. M. Hanby, P. J. Selby, M. Lorger, T. N. Dear, T. Pawson, C. J. Marshall, and G. Mavria
2015. A Rac/Cdc42 exchange factor complex promotes formation of lateral filopodia and blood vessel lumen morphogenesis. *Nature Communications*, 6:1–14.

Adams, R. H. and K. Alitalo
2007. Molecular regulation of angiogenesis and lymphangiogenesis. *Nature Reviews Molecular Cell Biology*, 8(June):464–478.

Aman, A. and T. Piotrowski
2010. Cell migration during morphogenesis. *Developmental Biology*, 341(1):20–33.

Andrews, N., M.-c. Ramel, S. Kumar, Y. Alexandrov, D. J. Kelly, S. C. Warren, L. Kerry, N. Lockwood, A. Frolov, P. Frankel, L. Bugeon, J. Mcginty, M. J. Dallman, and P. M. W. French
2016. Visualising apoptosis in live zebrafish using fluorescence lifetime imaging with optical projection tomography to map FRET biosensor activity in space and time. *Journal of Biophotonics*, 9(4):414–424.

Ang, B. K., C. Y. Lim, S. S. Koh, N. Sivakumar, S. Taib, K. B. Lim, S. Ahmed, G. Rajagopal, and S. H. Ong
2007. ArhGAP9, a novel MAP kinase docking protein, inhibits Erk and p38 activation through WW domain binding. *Journal of Molecular Signaling*, 2.

Anselmo, M. A., S. Dalvin, P. Prodhan, K. Komatsuzaki, J. T. Aidlen, J. J. Schnitzer, J. Y. Wu, and T. B. Kinane
2003. Slit and robo: Expression patterns in lung development. *Gene Expression Patterns*, 3(1):13–19.

Aragon, E., N. Goerner, A.-i. Zaromytidou, Q. Xi, A. Escobedo, J. Massague, and M. J. Macias
2011. A Smad action turnover switch operated by WW domain readers of a phosphoserine code. *Genes and Development*, 25:1275–1288.

Aspenström, P., A. Ruusala, and D. Pacholsky
2007. Taking Rho GTPases to the next level : The cellular functions of atypical Rho GTPases. *Experimental Cell Research*, 3:10–16.

Bacon, C., V. Endris, I. Andermatt, V. Niederkofler, R. Waltereit, D. Bartsch, E. T. Stoeckli, and G. Rappold
2011. Evidence for a role of SRGAP3 in the positioning of commissural axons within the ventrolateral funiculus of the mouse spinal cord. *PLoS ONE*, 6(5).

Bacon, C., V. Endris, and G. Rappold
2009. Dynamic expression of the Slit-Robo GTPase activating protein genes during development of the murine nervous system. *Journal of Comparative Neurology*, 513(2):224–236.

Bashaw, G. J., T. Kidd, D. Murray, T. Pawson, and C. S. Goodman
2000. Repulsive axon guidance: Abelson and Enabled play opposing roles downstream of the roundabout receptor. *Cell*, 101(7):703–15.

Bashaw, G. J. and R. Klein
2010. Signaling from axon guidance receptors. *Cold Spring Harbor perspectives in biology*, 2(5):1–16.

Bayless, K. J. and G. E. Davis
2002. The Cdc42 and Rac1 GTPases are required for capillary lumen formation in three-dimensional extracellular matrices. *Journal of cell science*, 115:1123–1136.

Bear, J. E. and F. B. Gertler
2009. Ena / VASP : towards resolving a pointed controversy at the barbed end. *J Cell Sci*, 122:1947–53.

Beckers, C. M. L., V. W. M. V. Hinsbergh, and G. P. V. N. Amerongen
2010. Driving Rho GTPase activity in endothelial cells regulates barrier integrity. *thrombosis and Haemostasis*, 103:40–55.

Bedell, V. M., S. E. Westcot, and S. C. Ekker
2011. Lessons from morpholino-based screening in zebrafish. *Briefings in Functional Genomics*, 10(4):181–188.

Bedell, V. M., S.-Y. Yeo, K. W. Park, J. Chung, P. Seth, V. Shivalingappa, J. Zhao, T. Obara, V. P. Sukhatme, I. A. Drummond, D. Y. Li, and R. Ramchandran
2005. Roundabout4 Is Essential for Angiogenesis in Vivo. *Proceedings of the National Academy of Sciences of the United States of America*, 102(18):6373–8.

Bedford, M. T., R. Reed, and P. Leder
1998. WW domain-mediated interactions reveal a spliceosome-associated protein that binds a third class of proline-rich motif: the proline glycine and methionine-rich motif. *Proceedings of the National Academy of Sciences of the United States of America*, 95(18):10602–10607.

Belyantseva, I. a., E. T. Boger, and T. B. Friedman
2003. Myosin XVa localizes to the tips of inner ear sensory cell stereocilia and is essential for staircase formation of the hair bundle. *Proceedings of the National Academy of Sciences of the United States of America*, 100(24):13958–63.

Beningo, K. A., M. Dembo, I. Kaverina, J. V. Small, and Y.-l. Wang
2001. Nascent Focal Adhesions Are Responsible for the Generation of Strong Propulsive Forces in Migrating Fibroblasts. *Journal of Cell Biology*, 153(4):881–887.

Berg, J. S., B. H. Derfler, C. M. Pennisi, D. P. Corey, and R. E. Cheney
2000. Myosin-X, a novel myosin with pleckstrin homology domains, associates with regions of dynamic actin. *Journal of cell science*, 113 Pt 19:3439–3451.

Bill, B. R., A. M. Petzold, K. J. Clark, L. a. Schimmenti, and S. C. Ekker
2009. A primer for morpholino use in zebrafish. *Zebrafish*, 6(1):69–77.

Blum, Y., H. G. Belting, E. Ellertsdottir, L. Herwig, F. Lüders, and M. Affolter
2008. Complex cell rearrangements during intersegmental vessel sprouting and vessel fusion in the zebrafish embryo. *Developmental Biology*, 316(2):312–322.

Bohil, A. B., B. W. Robertson, and R. E. Cheney
2006. Myosin-X is a molecular motor that functions in filopodia formation. *Proceedings of the National Academy of Sciences*, 103(33):12411–12416.

Bolte, S. and F. P. Cordelieres
2006. A guided tour into subcellular colocalisation analysis in light microscopy. *Journal of Microscopy*, 224(3):13–232.

Bos, J., H. Rehmann, and A. Wittinghofer
2007. GEFs and GAPs : Critical Elements in the Control of Small G Proteins. *Cell*, 129:865–877.

Braga, V. M. M., L. M. Machesky, A. Hall, and N. A. Hotchin
1997. The Small GTPases Rho and Rac Are Required for the Establishment of Cadherin-dependent CellâCell Contacts. *The Journal of Cell Biology*, 137(6):1421–1431.

Bristow, J. M., T. A. Reno, M. Jo, S. L. Gonias, and R. L. Klemke
2013. Dynamic phosphorylation of tyrosine 665 in pseudopodium-enriched atypical kinase 1 (PEAK1) is essential for the regulation of cell migration and focal adhesion turnover. *Journal of Biological Chemistry*, 288(1):123–131.

Broman, M. T., D. Mehta, and A. B. Malik
2007. Cdc42 Regulates the Restoration of Endothelial Adherens Junctions and Permeability. *TCM*, 17(5):151–156.

Brose, K., K. S. Bland, K. H. Wang, D. Arnott, W. Henzel, C. S. Goodman, M. Tessier-Lavigne, and T. Kidd
1999. Slit proteins bind robo receptors and have an evolutionarily conserved role in repulsive axon guidance. *Cell*, 96(6):795–806.

Bryan, B. A. and P. A. D'Amore
2007. What tangled webs they weave: Rho-GTPase control of angiogenesis. *Cellular and Molecular Life Sciences*, 64(16):2053–2065.

Burridge, K., K. Wennerberg, C. Hill, and N. Carolina
2004. Rho and Rac Take Center Stage Review. *Cell*, 116:167–179.

Canagarajah, B., F. C. Leskow, J. Yew, S. Ho, H. Mischak, L. F. Saidi, M. G. Kazanietz, and J. H. Hurley
2004. Structural Mechanism for Lipid Activation of the Rac-Specific GAP , â¤ 2-Chimaerin. *Cell*, 119:407–418.

Carmeliet, P.
2003. Angiogenesis in health and disease. *Nature Medicine*, 9(6):653–660.

Carmeliet, P. and R. K. Jain
2011. Molecular mechanisms and clinical applications of angiogenesis. *Nature*, 473:298–307.

Chaki, S. P., R. Barhoumi, and G. M. Rivera
2015. Actin remodeling by Nck regulates endothelial lumen formation. *Molecular biology of the cell*, 26(17):3047–60.

Chance, R. K. and G. J. Bashaw
2015. Slit-Dependent Endocytic Trafficking of the Robo Receptor Is Required for Son of Sevenless Recruitment and Midline Axon Repulsion. *PLoS Genetics*, Pp. 1–27.

Chang, P.-h., W. W. Hwang-verslues, Y.-c. Chang, C.-c. Chen, Y.-m. Jeng, K.-j. Chang, J.-y. Shew, H. Lee, and C. G. Hospital
2012. Activation of Robo1 signaling of breast cancer cells by Slit2 from stromal fibroblast restrains tumorigenesis via blocking PI3K/Akt/β-catenin pathway. *Cancer Research*, 72(18):4652–4661.

Chávez, M. N., G. Aedo, F. A. Fierro, M. L. Allende, and J. T. Egaña
2016. Zebrafish as an emerging model organism to study angiogenesis in development and regeneration. *Frontiers in Physiology*, 7(MAR):1–15.

Checchin, D., F. Sennlaub, E. Levavasseur, and M. Leduc
2006. Potential Role of Microglia in Retinal Blood Vessel Formation AND. *Invest*, 47(8):3595–602.

Chen, H. I., A. Einbond, S. J. Kwak, H. Linn, E. Koepf, S. Peterson, J. W. Kelly, and M. Sudol
1997. Characterization of the WW domain of human Yes-associated protein and its polyproline-containing ligands. *Journal of Biological Chemistry*, 272(27):17070–17077.

Chen, H. I. and M. Sudol
1995. The WW domain of Yes-associated protein binds a proline-rich ligand that differs from the consensus established for Src homology 3-binding modules. *Proceedings of the National Academy of Sciences of the United States of America*, 92(17):7819–7823.

Chen, Z., B. B. Gore, H. Long, L. Ma, and M. Tessier-lavigne
2008. Report Alternative Splicing of the Robo3 Axon Guidance Receptor Governs the Midline Switch from Attraction to Repulsion. *Neuron*, 58:325–332.

Cheng, N., D. Brantley, M., H. Liu, Q. Lin, M. Enriquez, N. Gale, T. O. Yancopoulos, George Cerretti, Douglas Pat Daniel, and J. Chen
2002. Blockade of EphA Receptor Tyrosine Kinase Activation Inhibits Vascular Endothelial Cell Growth Factor-Induced Angiogenesis. *Molecular Cell Research*, 1:2–11.

Cherfils, J. and M. Zeghouf
2013. Regulation of small GTPases by GEFs, GAPs, and GDIs. *Physiological reviews*, 93(1):269–309.

Clapéron, A. and M. Therrien
2007. KSR and CNK: two scaffolds regulating RAS-mediated RAF activation. *Oncogene*, 26(22):3143–3158.

Colwill, K., C. D. Wells, K. Elder, M. Goudreault, K. Hersi, S. Kulkarni, W. R. Hardy, T. Pawson, and G. B. Morin
2006. Modification of the Creator recombination system for proteomics applications–improved expression by addition of splice sites. *BMC biotechnology*, 6:13.

Cook, D. R., K. L. Rossman, and C. J. Der
2016. Rho guanine nucleotide exchange factors: regulators of Rho GTPase activity in development and disease. *Oncogene*, 33(31):4021–4035.

Cox, A. and C. Der
2002. Ras family signaling: therapeutic targeting. *Cancer Bio Ther.*, 1(6):599–606.

Cramer, L. P., R. R. Kay, L. P. Cramer, R. R. Kay, and E. Zatulovskiy
2018. Repellent and Attractant Guidance Cues Initiate Cell Migration by Distinct Rear-Driven and Front-Driven Cytoskeletal Mechanisms Report Repellent and Attractant Guidance Cues Initiate Cell Migration by Distinct Rear-Driven and Front-Driven Cytoskeletal Mec. *Current Biology*, 28:995–1004.

Croucher, D. R., F. Hochgräfe, L. Zhang, L. Liu, R. J. Lyons, D. Rickwood, C. M. Tactacan, B. C. Browne, N. Ali, H. Chan, R. Shearer, D. Gallego-Ortega, D. N. Saunders, A. Swarbrick, and R. J. Daly
2013. Involvement of Lyn and the atypical kinase SgK269/PEAK1 in a basal breast cancer signaling pathway. *Cancer Research*, 73(6):1969–1980.

Czuchra, A., X. Wu, H. Meyer, J. V. Hengel, T. Schroeder, R. Geffers, K. Rottner, and C. Brakebusch
2005. Cdc42 Is Not Essential for Filopodium Formation , Directed Migration , Cell Polarization , and Mitosis in Fibroblastoid Cells. *Molecular Biology of the Cell*, 16(October):4473–4484.

Davis, S. J. and P. A. V. D. Merwe
2006. The kinetic-segregation model : TCR triggering and beyond. *Nat Immunol.*, 7(8):803–809.

Defilippi, P., P. D. Stefano, and S. Cabodi
2006. p130Cas : a versatile scaffold in signaling networks. *Trends in Cell Biology*, 16(5).

Deramaudt, T. B., D. Dujardin, A. Hamadi, F. Noulet, K. Kolli, J. De Mey, K. Takeda, and P. Rondé
2011. FAK phosphorylation at Tyr-925 regulates cross-talk between focal adhesion turnover and cell protrusion. *Molecular biology of the cell*, 22(7):964–975.

Dickson, B. J. and G. F. Gilestro
2006. Regulation of Commissural Axon Pathfinding by Slit and its Robo Receptors. *Annu Rev Cell Dev Biol*, 22:651–677.

Dodson, E. J., V. Fishbain-Yoskovitz, S. Rotem-Bamberger, and O. Schueler-Furman
2015. Versatile communication strategies among tandem WW domain repeats. *Experimental biology and medicine (Maywood, N.J.)*, 240(3):351–60.

Doherty, P., L. H. Rowett, S. E. Moore, D. A. Mann, and F. S. Walsh
1991. Neurite Outgrowth in Response to Transfected N-CAM and N-Cadherin Reveals Fundamental Differences in Neuronal Responsiveness to CAMS. *Neuron*, 6:247–258.

Doherty, P., E. Williams, and F. S. Walsh
1995. A Soluble Chimeric Form of the L1 Glycoprotein Stimulates Neurite Outgrowth. *Neuron*, 14:57–66.

Douziech, M., M. Sahmi, G. Laberge, and M. Therrien
2006. A KSR/CNK complex mediated by HYP, a novel SAM domain-containing protein, regulates RAS-dependent RAF activation in Drosophila. *Genes and Development*, 20(7):807–819.

Dunaway, C. M., Y. Hwang, C. W. Lindsley, R. S. Cook, J. Y. Wu, M. Boothby, J. Chen, and D. M. Brantley-Sieders
2011. Cooperative signaling between Slit2 and Ephrin-A1 regulates a balance between angiogenesis and angiostasis. *Mol Cell Biol*, 31(3):404–416.

Eberth, A., R. Lundmark, L. Gremer, R. Dvorsky, K. T. Koessmeier, H. T. M. C. Mahon, and M. R. Ahmadian
2009. A BAR domain-mediated autoinhibitory mechanism for RhoGAPs of the GRAF family. *Biochemical Journal*, 377:371–377.

Eccles, R. L., M. T. Czajkowski, C. Barth, P. M. Müller, E. McShane, S. Grunwald, P. Beaudette, N. Mecklenburg, R. Volkmer, K. Zühlke, G. Dittmar, M. Selbach, A. Hammes, O. Daumke, E. Klussmann, S. Urbé, and O. Rocks
2016. Bimodal antagonism of PKA signalling by ARHGAP36. *Nature communications*, 7:12963.

Eisen, J. S. and J. C. Smith
2008. Controlling morpholino experiments: don't stop making antisense. *Development (Cambridge, England)*, 135(10):1735–43.

Endris, V., B. Wogatzky, U. Leimer, D. Bartsch, M. Zatyka, F. Latif, E. R. Maher, G. Tariverdian, S. Kirsch, D. Karch, and G. a. Rappold
2002. The novel Rho-GTPase activating gene MEGAP/ srGAP3 has a putative role in severe mental retardation. *Proceedings of the National Academy of Sciences of the United States of America*, 99(18):11754–11759.

Etienne-Manneville, S. and A. Hall
2002. Rho GTPases in cell biology. *Nature*, 420(December):629–635.

Fan, X., J. P. Labrador, H. Hing, and G. J. Bashaw
2003. Slit stimulation recruits Dock and Pak to the roundabout receptor and increases Rac activity to regulate axon repulsion at the CNS midline. *Neuron*, 40(1):113–127.

Fantin, A., J. M. Vieira, G. Gestri, L. Denti, Q. Schwarz, S. Prykhozhij, F. Peri, S. W. Wilson, and C. Ruhrberg
2010. Tissue macrophages act as cellular chaperones for vascular anastomosis downstream of VEGF-mediated endothelial tip cell induction. *Blood*, 116(5):829–841.

Friedl, P., Y. Hegerfeldt, and M. Tusch
2004. Collective cell migration in morphogenesis and cancer. *The International journal of developmental biology*, 48(5-6):441–9.

Fritz, J. L. and M. F. VanBerkum
2002. Regulation of Rho Family GTPases Is Required to Prevent Axons from Crossing the Midline. *Developmental Biology*, 252(1):46–58.

Fritz, R. D., M. Letzelter, A. Reimann, K. Martin, L. Fusco, L. Ritsma, B. Ponsioen, E. Fluri, S. Schulte-Merker, J. van Rheenen, and O. Pertz
2013. A Versatile Toolkit to Produce Sensitive FRET Biosensors to Visualize Signaling in Time and Space. *Science Signaling*, 6(285):rs12–rs12.

Fritz, R. D., D. Menshykau, K. Martin, A. Reimann, V. Pontelli, and O. Pertz
2015. SrGAP2-Dependent Integration of Membrane Geometry and Slit-Robo-Repulsive Cues Regulates Fibroblast Contact Inhibition of Locomotion. *Developmental Cell*, 35(1):78–92.

Fritz, R. D. and O. Pertz
2016. The dynamics of spatio-temporal Rho GTPase signaling: formation of signaling patterns. *F1000Research*, 5(0):749–761.

Fryer, B. H. and J. Field
2005. Rho, Rac, Pak and angiogenesis: Old roles and newly identified responsibilities in endothelial cells. *Cancer Letters*, 229(1):13–23.

Fujiwara, T., A. Mammoto, Y. Kim, and Y. Takai
2000. Rho Small G-Protein-Dependent Binding of mDia to an Src Homology 3 Domain-Containing IRSp53/BAIAP2. *Biochemical and Biophysical Research Communications*, 629:626–629.

Fukuhara, N., J. A. Howitt, S.-a. Hussain, and E. Hohenester
2008. Structural and Functional Analysis of Slit and Heparin Binding to Immunoglobulin-like Domains 1 and 2 of Drosophila Robo *. *The Journal of Biological Chemistry*, 283(23):16226–16234.

Gavard, J., V. Patel, and J. S. Gutkind
2008. Article Angiopoietin-1 Prevents VEGF-Induced Endothelial Permeability by Sequestering Src through mDia. *Developmental Cell*, (January):25–36.

Gerhardt, H., M. Golding, M. Fruttiger, C. Ruhrberg, A. Lundkvist, A. Abramsson, M. Jeltsch, C. Mitchell, K. Alitalo, D. Shima, and C. Betsholtz
2003. VEGF guides angiogenic sprouting utilizing endothelial tip cell filopodia. *Journal of Cell Biology*, 161(6):1163–1177.

Geudens, I. and H. Gerhardt
2011. Coordinating cell behaviour during blood vessel formation. *Development (Cambridge, England)*, 138:4569–4583.

Grieshammer, U., L. Ma, A. S. Plump, F. Wang, M. Tessier-Lavigne, and G. R. Martin
2004. SLIT2-Mediated ROBO2 signaling restricts kidney induction to a single site. *Developmental Cell*, 6(5):709–717.

Guerrier, S., J. Coutinho-Budd, T. Sassa, A. Gresset, N. V. Jordan, K. Chen, W. L. Jin, A. Frost, and F. Polleux
2009. The F-BAR Domain of srGAP2 Induces Membrane Protrusions Required for Neuronal Migration and Morphogenesis. *Cell*, 138(5):990–1004.

Hakeda-Suzuki, S., J. Ng, J. Tzu, G. Dietzl, Y. Sun, M. Harms, T. Nardine, L. Lou, and B. J. Dickson
2002. Rac function and regulation during Drosophila development. *Letters to nature*, 416(March):438–442.

Han, S., J. Nam, Y. Li, S. Kim, S.-H. Cho, Y. S. Cho, S.-Y. Choi, J. Choi, K. Han, Y. Kim, M. Na, H. Kim, Y. C. Bae, S.-Y. Choi, and E. Kim
2010. Regulation of dendritic spines, spatial memory, and embryonic development by the TANC family of PSD-95-interacting proteins. *The Journal of neuroscience : the official journal of the Society for Neuroscience*, 30(45):15102–12.

Heath, V. L. and R. Bicknell
2009. Anticancer strategies involving the vasculature. *Nature reviews. Clinical oncology*, 6(7):395–404.

Hellström, M., L.-k. Phng, J. J. Hofmann, E. Wallgard, L. Coultas, P. Lindblom, H. Gerhardt, C. Betsholtz, M. L. Iruela-arispe, and M. Kale
2007. Dll4 signalling through Notch1 regulates formation of tip cells during angiogenesis. *Nature*, 445(February):2–6.

Hirano, Y., T. Hatano, A. Takahashi, M. Toriyama, N. Inagaki, and T. Hakoshima
2011. Structural basis of cargo recognition by the myosin-X MyTH4-FERM domain. *The EMBO journal*, 30(13):2734–2747.

Hivert, B., Z. Liu, C.-y. Chuang, and P. Doherty
2002. Robo1 and Robo2 Are Homophilic Binding Molecules That Promote Axonal Growth. *Molecular and Cellular Neuroscience*, 21:534–545.

Hodge, R. G. and A. J. Ridley
2016. Regulating Rho GTPases and their regulators. *Nature reviews. Molecular cell biology*, 17(8):496–510.

Hohenester, E.
2008. Structural insight into Slit-Robo signalling. *Biochemical Society transactions*, 36(Pt 2):251–6.

Hohenester, E., S. Hussain, and J. A. Howitt
2006. Interaction of the guidance molecule Slit with cellular receptors. *Biochemical Society transactions*, 34:418–421.

Howe, K., M. D. Clark, C. F. Torroja, J. Torrance, M. Muffato, J. E. Collins, S. Humphray, K. Mclaren, L. Matthews, S. Mclaren, I. Sealy, M. Caccamo, C. Churcher, J. C. Barrett, R. Koch, G.-j. Rauch, S. White, B. Kilian, L. T. Quintais, J. A. Guerra-assunção, Y. Zhou, Y. Gu, J. Yen, J.-h. Vogel, T. Eyre, S. Redmond, R. Banerjee, B. Fu, E. Langley, S. F. Maguire, G. K. Laird, D. Lloyd, E. Kenyon, S. Donaldson, H. Sehra, J. Almeida-king, S. Trevanion, M. Jones, M. Quail, D. Willey, A. Hunt, J. Burton, S. Sims, K. Mclay, B. Plumb, J. Davis, C. Clee, R. Clark, C. Riddle, D. Eliott, G. Threadgold, G. Harden, D. Ware, B. Mortimer, G. Kerry, P. Heath, B. Phillimore, N. Corby, M. Dunn, C. Johnson, J. Wood, S. Pelan, G. Griffiths, M. Smith, R. Glithero, P. Howden, N. Barker, C. Stevens, J. Harley, K. Holt, J. Lovell, H. Beasley, C. Henderson, D. Gordon, K. Auger, D. Wright, J. Collins, C. Raisen, L. Dyer, L. Robertson, K. Ambridge, D. Leongamornlert, S. Mcguire, R. Gilderthorp, C. Griffiths, D. Manthravadi, S. Nichol, G. Barker, S. Whitehead, M. Kay, J. Brown, C. Murnane, E. Gray, M. Humphries, N. Sycamore, D. Barker, D. Saunders, J. Wallis, A. Babbage, S. Hammond, M. Mashreghi-mohammadi, L. Barr, P. Wray, A. Ellington, N. Matthews, M. Ellwood, G. Clark, J. Cooper, A. Tromans, D. Grafham, R. Pandian, R. Andrews, E. Harrison, A. Kimberley, S. Palmer, I. Gehring, A. Berger, and C. M. Dooley
2014. The zebrafish reference genome sequence and its relationship to the human genome. *Nature*, 496(7446):498–503.

Hu, H.
1999. Chemorepulsion of Neuronal Migration by Slit2 in the Developing Mammalian Forebrain. *Neuron*, 23:703–711.

Hu, H.
2001. Cell-surface heparan sulfate is involved in the repulsive guidance activities of Slit2 protein. *Nature Neuroscience*, 4(7):695–701.

Hu, H., J. Columbus, Y. Zhang, D. Wu, L. Lian, S. Yang, J. Goodwin, C. Luczak, M. Carter, L. Chen, M. James, R. Davis, M. Sudol, J. Rodwell, and J. J. Herrero
2004. A map of WW domain family interactions. *Proteomics*, 4(3):643–655.

Hu, H., M. Li, J.-P. Labrador, J. McEwen, E. C. Lai, C. S. Goodman, and G. J. Bashaw
2005. Cross GTPase-activating protein (CrossGAP)/Vilse links the Roundabout receptor to Rac to regulate midline repulsion. *Proceedings of the National Academy of Sciences of the United States of America*, 102(12):4613–4618.

Hu, Q., D. Milfay, and L. T. Williams
1995. Binding of NCK to SOS and Activation of ras -Dependent Gene Expression. *Molecular and cellular biology*, 15(3):1169–1174.

Huang, G.-H., X.-T. Yang, K. Chen, J. Xing, L. Guo, L. Zhu, H.-J. Li, X.-C. Li, S.-Y. Zhang, and D.-F. Feng
2016. Porf-2 Inhibits Neural Stem Cell Proliferation Through Wnt/β-Catenin Pathway by Its GAP Domain. *Frontiers in cellular neuroscience*, 10(March):85.

Huang, L., C. Wen, X. Yang, Q. Lou, X. Wang, J. Che, J. Chen, Z. Yang, X. Wu, M. Huang, P. Lan, L. Wang, A. Iwamoto, and J. Wang
2018. PEAK1 , acting as a tumor promoter in colorectal cancer , is regulated by the EGFR / KRas signaling axis and miR-181d. *Cell Death and Disease*.

Huang, X., H. J. Cheng, M. Tessier-Lavigne, and Y. Jin
2002. MAX-1, a novel PH/MyTH4/FERM domain cytoplasmic protein implicated in netrin-mediated axon repulsion. *Neuron*, 34(4):563–576.

Huang, Z., P. Wen, R. Kong, H. Cheng, B. Zhang, C. Quan, Z. Bian, M. Chen, Z. Zhang, X. Chen, X. Du, J. Liu, L. Zhu, K. Fushimi, D. Hua, and J. Y. Wu
2015. USP33 mediates Slit-Robo signaling in inhibiting colorectal cancer cell migration. *International Journal of Cancer*, 136(8):1792–1802.

Hubbard, S. R. and W. T. Miller
2007. Receptor tyrosine kinases: mechanisms of activation and signaling. *Current biology : CB*, 19(2):117–123.

Huisken, J. and D. Y. R. Stainier
2009. Selective plane illumination microscopy techniques in developmental biology. *Development*, 136(12):1963–1975.

Huminiecki, L., M. Gorn, S. Suchting, R. Poulsom, and R. Bicknell
2002. Magic roundabout is a new member of the roundabout receptor family that is endothelial specific and expressed at sites of active angiogenesis. *Genomics*, 79(4):547–52.

Hussain, S.-a., M. Piper, N. Fukuhara, L. Strochlic, J. A. Howitt, Y. Ahmed, A. K. Powell, J. E. Turnbull, C. E. Holt, and E. Hohenester
2006. A Molecular Mechanism for the Heparan Sulfate Dependence of Slit-Robo Signaling. *Journal of Biological Chemistry*, 281(51):39693–39698.

Ingham, R. J., K. Colwill, C. Howard, S. Dettwiler, C. S. Lim, J. Yu, K. Hersi, J. Raaijmakers, G. Gish, G. Mbamalu, L. Taylor, B. Yeung, G. Vassilovski, M. Amin, F. Chen, L. Matskova, G. Winberg, I. Ernberg, R. Linding, P. O'Donnell, A. Starostine, W. Keller, P. Metalnikov, C. Stark, and T. Pawson
2005. WW domains provide a platform for the assembly of multiprotein networks. *Mol Cell Biol*, 25(16):7092–7106.

Ingham, R. J., G. Gish, and T. Pawson
2004. The Nedd4 family of E3 ubiquitin ligases: functional diversity within a common modular architecture. *Oncogene*, 23(11):1972–1984.

Ishizaki, T., Y. Morishima, M. Okamoto, T. Furuyashiki, T. Kato, and S. Narumiya
2001. Coordination of microtubules and the actin cytoskeleton by the Rho effector mDia1. *Nature cell biology*, 3(January):8–14.

Isogai, S., M. Horiguchi, and B. M. Weinstein
2001a. The Vascular Anatomy of the Developing Zebrafish : An Atlas of Embryonic and Early Larval Development. *Developmental Biology*, 301(2):278–301.

Isogai, S., M. Horiguchi, and B. M. Weinstein
2001b. The Vascular Anatomy of the Developing Zebrafish: An Atlas of Embryonic and Early Larval Development. *Developmental Biology*, 230(2):278–301.

Jaffe, A. B., P. Aspenstro, and A. Hall
2004. Human CNK1 Acts as a Scaffold Protein , Linking Rho and Ras Signal Transduction Pathways. *Molecular and cellular biology*, 24(4):1736–1746.

Jaffe, A. B. and A. Hall
2005. Rho GTPases : Biochemistry and Biology. *Annu Rev Cell Dev Biol*, 21:247–272.

Jäger, M., H. Nguyen, J. C. Crane, J. W. Kelly, and M. Gruebele
2001. The folding mechanism of a beta-sheet: the WW domain. *Journal of molecular biology*, 311(2):373–393.

Jäger, M., H. Nguyen, M. Dendle, M. Gruebele, and J. W. Kelly
2007. Influence of hPin1 WW N-terminal domain boundaries on function, protein stability, and folding. *Protein science : a publication of the Protein Society*, 16(7):1495–501.

Jay, P. Y., P. A. Pham, S. A. Wong, and E. L. Elson
1995. A mechanical function of myosin II in cell motility. *Journal of Cell Science*, 393(108):387–393.

Jékely, G., H.-h. Sung, C. M. Luque, and P. Rørth
2005. Regulators of Endocytosis Maintain Localized Receptor Tyrosine Kinase Signaling in Guided Migration. *Developmental Cell*, 9:197–207.

Johnson, K. G., A. Ghose, E. Epstein, J. Lincecum, M. B. O. Connor, and D. V. Vactor
2004. Axonal Heparan Sulfate Proteoglycans Regulate the Distribution and Efficiency of the Repellent Slit during Midline Axon Guidance. *Current Biology*, 14:499–504.

Jones, C. A., N. R. London, H. Chen, K. W. Park, D. Sauvaget, R. A. Stockton, J. D. Wythe, W. Suh, F. Larrieu-lahargue, Y.-s. Mukouyama, P. Lindblom, P. Seth, A. Frias, N. Nishiya, M. H. Ginsberg, H. Gerhardt, K. Zhang, and D. Y. Li
2008. Robo4 stabilizes the vascular network by inhibiting pathologic angiogenesis and endothelial hyperpermeability. *Nat Med*, 14(4):448–453.

Jones, C. A., N. Nishiya, N. R. London, W. Zhu, L. K. Sorensen, A. C. Chan, C. J. Lim, H. Chen, Q. Zhang, P. G. Schultz, A. M. Hayallah, K. R. Thomas, M. Famulok, K. Zhang, M. H. Ginsberg, and D. Y. Li
2009a. Slit2-Robo4 signalling promotes vascular stability by blocking Arf6 activity. *Nature cell biology*, 11(11):1325–31.

Jones, C. A., N. Nishiya, N. R. London, W. Zhu, L. K. Sorensen, A. C. Chan, C. J. Lim, H. Chen, Q. Zhang, P. G. Schultz, A. M. Hayallah, K. R. Thomas, M. Famulok, K. Zhang, M. H. Ginsberg, and D. Y. Li
2009b. Slit2-Robo4 signalling promotes vascular stability by blocking Arf6 activity. *Nature cell biology*, 11(11):1325–31.

Kamei, M., W. B. Saunders, K. J. Bayless, L. Dye, G. E. Davis, and B. M. Weinstein
2006. Endothelial tubes assemble from intracellular vacuoles in vivo. *Nature*, 442(7101):453–456.

Kanchanawong, P., G. Shtengel, A. M. Pasapera, E. B. Ramko, M. W. Davidson, H. F. Hess, and C. M. Waterman
2010. Nanoscale architecture of integrin-based cell adhesions. *Nature*, 468(7323):580–4.

Katayama, M., M. Kawata, Y. Yoshida, H. Horiuchi, T. Yamamoto, Y. Matsuura, and Y. Takai
1991. The Posttranslationally Modified C-terminal Structure of Bovine Aortic Smooth Muscle rhoA p21. *Journal of Biological Chemistry*, 266(19):12639–45.

Kaur, S., M. D. Castellone, V. M. Bedell, M. Konar, J. S. Gutkind, and R. Ramchandran
2006. Robo4 signaling in endothelial cells implies attraction guidance mechanisms. *Journal of Biological Chemistry*, 281(16):11347–11356.

Kaur, S., G. V. Samant, K. Pramanik, P. W. Loscombe, M. L. Pendrak, D. D. Roberts, and R. Ramchandran
2008. Silencing of directional migration in roundabout4 knockdown endothelial cells. *BMC cell biology*, 9(1):61.

Kawahara, A. and I. B. Dawid
2001. Critical role of biklf in erythroid cell differentiation in zebrafish. *Current Biology*, 11:1353–1357.

Keleman, K., S. Rajagopalan, D. Cleppien, D. Teis, K. Paiha, L. A. Huber, G. M. Technau, and B. J. Dickson
2002. Comm sorts Robo to control axon guidance at the Drosophila midline. *Cell*, 110(4):415–427.

Keleman, K., C. Ribeiro, and B. J. Dickson
2005. Comm function in commissural axon guidance : cell-autonomous sorting of Robo in vivo. *Nature Neuroscience*, 8(2):156–163.

Kidd, T., K. S. Bland, and C. S. Goodman
1999. Slit Is the Midline Repellent for the Robo Receptor in Drosophila. *Cell*, 96:785–794.

Kidd, T., K. Brose, K. J. Mitchell, R. D. Fetter, M. Tessier-lavigne, C. S. Goodman, and G. Tear
1998. Roundabout Controls Axon Crossing of the CNS Midline and Defines a Novel Subfamily of Evolutionarily Conserved Guidance Receptors. *Cell*, 92:205–215.

Kimura, Y., Y. Hisano, A. Kawahara, and S.-i. Higashijima
2014. Efficient generation of knock-in transgenic zebrafish carrying reporter/ driver genes by CRISPR/Cas9-mediated genome engineering. *Scientific Reports*, 4:1–7.

Koch, A. W., T. Mathivet, B. Larrivée, R. K. Tong, J. Kowalski, L. Pibouin-Fragner, K. Bouvrée, S. Stawicki, K. Nicholes, N. Rathore, S. J. Scales, E. Luis, R. del Toro, C. Freitas, C. Bréant, A. Michaud, P. Corvol, J. L. Thomas, Y. Wu, F. Peale, R. J. Watts, M. Tessier-Lavigne, A. Bagri, and A. Eichmann
2011. Robo4 Maintains Vessel Integrity and Inhibits Angiogenesis by Interacting with UNC5B. *Developmental Cell*, 20(1):33–46.

Koh, W., R. D. Mahan, and G. E. Davis
2008. Cdc42- and Rac1-mediated endothelial lumen formation requires Pak2 , Pak4 and Par3 , and PKC- dependent signaling. *Journal of Cell Science*, 121:989–1001.

Kok, F. O., M. Shin, C.-w. Ni, A. Gupta, A. S. Grosse, A. V. Impel, B. C. Kirchmaier, J. Peterson-maduro, G. Kourkoulis, I. Male, D. F. Desantis, S. Sheppard-tindell, L. Ebarasi, C. Betsholtz, S. Schulte-merker, S. A. Wolfe, and N. D. Lawson
2015. Reverse Genetic Screening Reveals Poor Correlation between Morpholino-Induced and Mutant Phenotypes in Zebrafish. *Developmental Cell*, 32(1):97–108.

Kurosaka, S. and A. Kashina
2008. Cell Biology of Embryonic Migration. *Birth Defects Res C Embryo Today*, 84(2):102–122.

Küssel-Andermann, P., A. El-amraoui, S. Safieddine, J.-p. Hardelin, S. Nouaille, J. Camonis, and C. Petit
2000. Unconventional Myosin VIIA Is a Novel A-kinase-anchoring Protein *. *The Journal of Biological Chemistry*, 275(38):29654–29659.

Laberge, G., M. Douziech, and M. Therrien
2005. Src42 binding activity regulates Drosophila RAF by a novel CNK-dependent derepression mechanism. *The EMBO journal*, 24(3):487–498.

Lanahan, A. A., K. Hermans, F. Claes, J. S. Kerley-hamilton, Z. W. Zhuang, F. J. Giordano, P. Carmeliet, and M. Simons
2010. Article VEGF Receptor 2 Endocytic Trafficking Regulates Arterial Morphogenesis. *Developmental Cell*, 18(5):713–724.

Lanigan, T. M., A. Liu, Y. Z. Huang, L. Mei, B. Margolis, and K.-L. Guan
2003. Human homologue of Drosophila CNK interacts with Ras effector proteins Raf and Rlf. *FASEB journal : official publication of the Federation of American Societies for Experimental Biology*, 17(14):2048–60.

Lauffenburger, D. A. and A. F. Horwitz
1996. Cell migration: A physically integrated molecular process. *Cell*, 84(3):359–369.

Lawson, C. D., K. Burridge, C. D. Lawson, and K. Burridge
2014. The on-off relationship of Rho and Rac during integrin-mediated adhesion and cell migration. *Small GTPases*, 5:e27958–1/12.

Lawson, N. D. and B. M. Weinstein
2002. In vivo imaging of embryonic vascular development using transgenic zebrafish. *Developmental biology*, 248(2):307–318.

Lee, J.-s. and C.-b. Chien
2004. WHEN SUGARS GUIDE AXONS : INSIGHTS FROM HEPARAN SULPHATE PROTEOGLYCAN MUTANTS. *Nature reviews. Genetics*, 5:923–35.

Leslie, J. D., L. Ariza-mcnaughton, A. L. Bermange, R. Mcadow, S. L. Johnson, and J. Lewis
2007. Endothelial signalling by the Notch ligand Delta-like 4 restricts angiogenesis. *Development*, 134:839–844.

Li, X., H. Yang, H. Huang, and T. Zhu
2014. CELLCOUNTER: Novel open-source software for counting cell migration and invasion in vitro. *BioMed Research International*, 2014(Figure 1).

Li, Z., M. Hannigan, Z. Mo, B. Liu, W. Lu, Y. Wu, A. V. Smrcka, G. Wu, L. Li, M. Liu, C.-k. Huang, D. Wu, and N. York
2003. Directional Sensing Requires G beta gamma -Mediated PAK1 and PIX alpha -Dependent Activation of Cdc42. *Cell*, 114:215–227.

Lim, J., D. A. Ritt, M. Zhou, and D. K. Morrison
2014. The CNK2 scaffold interacts with vilse and modulates rac cycling during spine morphogenesis in hippocampal neurons. *Current Biology*, 24(7):786–792.

Liu, D., J. Hou, X. Hu, X. Wang, Y. Xiao, Y. Mou, and H. D. Leon
2006. Neuronal Chemorepellent Slit2 Inhibits Vascular Smooth Muscle Cell Migration by Suppressing Small GTPase Rac1 Activation. *Circulation Research*, 98:480–489.

Liu, J., Y. Zhou, X. Qi, J. Chen, and W. Chen
2017. CRISPR / Cas9 in zebrafish : an efficient combination for human genetic diseases modeling. *Human Genetics*, 136(1):1–12.

Lobov, I. B., R. A. Renard, N. Papadopoulos, N. W. Gale, G. Thurston, G. D. Yancopoulos, and S. J. Wiegand
2006. Delta-like ligand 4 (Dll4) is induced by VEGF as a negative regulator of angiogenic sprouting. *Proc. Natl. Acad. Sci. U.S.A.*, 104:3219–24.

London, N. R., W. Zhu, F. A. Bozza, M. C. P. Smith, D. M. Greif, L. K. Sorensen, L. Chen, Y. Kaminoh, A. C. Chan, S. F. Passi, C. W. Day, D. L. Barnard, G. A. Zimmerman, M. A. Krasnow, and D. Y. Li
2010. Targeting Robo4-Dependent Slit Signaling to Survive the Cytokine Storm in Sepsis and Influenza. *Science Translational Medicine*, 2(23):23ra19 LP – 23ra19.

Lu, P. J., X. Z. Zhou, M. Shen, and K. P. Lu
1999. Function of WW domains as phosphoserine- or phosphothreonine-binding modules. *Science (New York, N.Y.)*, 283(5406):1325–1328.

Lundström, A., M. Gallio, C. Englund, P. Steneberg, J. Hemphälä, P. Aspenström, K. Keleman, L. Falileeva, B. J. Dickson, and C. Samakovlis
2004. Vilse, a conserved Rac/Cdc42 GAP mediating Robo repulsion in tracheal cells and axons. *Genes and Development*, 18(17):2161–2171.

Luo, B.-h., C. V. Carman, and T. A. Springer
2007. Structural basis of integrin regulation and signaling. *Annu. Rev. Immunol.*, 25:619–647.

Machacek, M., L. Hodgson, C. Welch, H. Elliott, O. Pertz, P. Nalbant, A. Abell, G. L. Johnson, K. M. Hahn, and G. Danuser
2009. Coordination of Rho GTPase activities during cell protrusion. *Nature*, 461(7260):99–103.

Macias, M. J., V. Gervais, C. Civera, and H. Oschkinat
2000. Structural analysis of WW domains and design of a WW prototype. *Nature Structural Biology*, 7(5):375–379.

Macias, M. J., S. Wiesner, and M. Sudol
2002. WW and SH3 domains, two different scaffolds to recognize proline-rich ligands. *FEBS Letters*, 513(1):30–37.

Marillat, V., O. Cases, K. T. Nguyen-Ba-Charvet, M. Tessier-Lavigne, C. Sotelo, and A. Chedotal
2002. Spatiotemporal expression patterns of slit and robo genes in the rat brain. *Journal of Comparative Neurology*, 442(2):130–155.

Marlow, R., M. Binnewies, L. K. Sorensen, S. D. Monica, P. Strickland, E. C. Forsberg, D. Y. Li, and L. Hinck
2010. Vascular Robo4 restricts proangiogenic VEGF signaling in breast. *Proceedings of the National Academy of Sciences of the United States of America*, 107(23):10520–5.

Martin, K., A. Reimann, R. D. Fritz, H. Ryu, N. L. Jeon, and O. Pertz
2016. Spatio-temporal co-ordination of RhoA, Rac1 and Cdc42 activation during prototypical edge protrusion and retraction dynamics. *Scientific reports*, 6(October 2015):21901.

Matsuura, R., H. Tanaka, and M. J. Go
2004. Distinct functions of Rac1 and Cdc42 during axon guidance and growth cone morphogenesis in Drosophila. *European Journal of Neuroscience*, 19:21–31.

McConnell, R. E., J. E. V. Veen, M. Vidaki, A. V. Kwiatkowski, A. S. Meyer, and F. B. Gertler
2016. A requirement for filopodia extension toward Slit during Robo-mediated axon repulsion. *Journal of Cell Biology*, 213(2):261–274.

Memon, A. R.
2004. The role of ADP-ribosylation factor and SAR1 in vesicular trafficking in plants. *Biochimica et Biophysica Acta (BBA) - Molecular Cell Research*, 1664:9–30.

Merajver, S. D. and S. Z. Usmani
2005. Multifaceted role of Rho proteins in angiogenesis. *Journal of Mammary Gland Biology and Neoplasia*, 10(4):291–298.

Mertsch, S., N. Schmitz, A. Jeibmann, W. Paulus, and V. Senner
2008. Slit2 involvement in glioma cell migration is mediated by Robo1 receptor. *Journal of Neuro-Oncology*, 87:1–7.

Michaelson, D., J. Silletti, G. Murphy, P. D. Eustachio, M. Rush, and M. R. Philips
2001. Differential Localization of Rho GTPases in Live Cells : Regulation by Hypervariable Regions and RhoGDI Binding 7. *Journal of Cell Biology*, 152:111–126.

Midori Maekawa, T. Ishizaki, S. Boku, N. Watanabe, A. Fujita, A. Iwamatsu, T. Obinata, K. Ohashi, K. Mizuno, and S. Narumiya
1999. Signaling from Rho to the Actin Cytoskeleton Through Protein Kinases ROCK and LIM-kinase. *Science*, 285(August):895–898.

Miki, H., H. Yamaguchi, S. Suetsugu, and T. Takenawa
2000. IRSp53 is an essential intermediate between Rac and WAVE in the regulation of membrane ruf Â¯ ing. *Nature*, 408(December):1–4.

Mittag, T., S. Orlicky, W.-y. Choy, X. Tang, H. Lin, F. Sicheri, L. E. Kay, M. Tyers, and J. D. Forman-kay
2008. Dynamic equilibrium engagement of a polyvalent ligand with a single-site receptor. *PNAS*, 105(46):17772–17777.

Miyamoto, S., S. K. Akiyama, and K. M. Yamada
1994. Synergistic Roles for Receptor Occupancy and Aggregation in Integrin Transmembrane Function. *Science*, 2179(1993):883–885.

Mollica, L., L. M. Bessa, X. Hanoulle, M. R. Jensen, M. Blackledge, and R. Schneider
2016. Binding Mechanisms of Intrinsically Disordered Proteins : Theory , Simulation , and Experiment. *Frontiers in Molecular Biosciences*, 3(September):1–18.

Molnár, G., M. C. Dagher, M. Geiszt, J. Settleman, and E. Ligeti
2001. Role of prenylation in the interaction of RHO-family small GTPases with GTPpase activating proteins. *Biochemistry*, 40(35):10542–10549.

Mooseker, M. S. and B. J. Foth
2008. *Myosins - A superfamily of Molecular Motors*. Springer New York.

Morcos, P. A.
2007. Achieving targeted and quantifiable alteration of mRNA splicing with Morpholino oligos. *Biochemical and Biophysical Research Communications*, 358(2):521–527.

Moskwa, P., M.-H. Paclet, M.-c. Dagher, and E. Ligeti
2005. Autoinhibition of p50 Rho GTPase-activating Protein (GAP) Is Released by Prenylated Small GTPases *. *Th eJournal of Biological Chemistry*, 280(8):6716–6720.

Nagase, T., R. Kikuno, A. Hattori, Y. Kondo, and K. Okumura
2000. Prediction of the Coding Sequences of Unidentified Human Genes . XIX . The complete Sequences of 100 New cDNA Clones from Brain Which Code for Large Proteins in vitro. *DNA Research*, 355:347–355.

Nasevicius, A. and S. C. Ekker
2000. Effective targeted gene â knockdown ' in zebrafish. *Nature genetics*, 26(october 2000):216–20.

Nguyen Ba-Charvet, K. T., K. Brose, L. Ma, K. H. Wang, V. Marillat, C. Sotelo, M. Tessier-Lavigne, and a. Chédotal
2001. Diversity and specificity of actions of Slit2 proteolytic fragments in axon guidance. *The Journal of neuroscience : the official journal of the Society for Neuroscience*, 21(12):4281–4289.

Niclou, S. P., L. Jia, and J. A. Raper
2000. Slit2 Is a Repellent for Retinal Ganglion Cell Axons. *The Journal of Neuroscience*, 20(13):4962–4974.

Nishiya, N., W. B. Kiosses, J. Han, and M. H. Ginsberg
2005. An alpha4 integrin-paxillin-Arf-GAP complex restricts Rac activation to the leading edge of migrating cells. *Nature cell biology*, 7(4):343–352.

Nobes, C. D. and A. Hall
1995. Rho, Rac, and Cdc42 GTPases regulate the assembly of multimolecular focal complexes associated with actin stress fibers, lamellipodia, and filopodia. *Cell*, 81(1):53–62.

Noren, N. K., C. M. Niessen, B. M. Gumbiner, and K. Burridge
2001. Cadherin Engagement Regulates Rho family GTPases *. *The Journal of Biological Chemistry*, 276(36):33305–33309.

Nyborg, J. and B. F. C. Clark
1996. The GTP binding motif : The existence. *FASEB journal : official publication of the Federation of American Societies for Experimental Biology*, 10(12):1347–1368.

Ohtakara, K., M. Nishizawa, I. Izawa, Y. Hata, S. Matsushima, W. Taki, H. Inada, Y. Takai, and M. Inagaki
2002. Densin-180, a synaptic protein, links to PSD-95 through its direct interaction with MAGUIN-1. *Genes to Cells*, 7(11):1149–1160.

Olsen, J. G., K. Teilum, and B. B. Kragelund
2017. Behaviour of intrinsically disordered proteins in protein â protein complexes with an emphasis on fuzziness. *Cellular and Molecular Life Sciences*, 74(17):3175–3183.

Otte, L., U. R. S. Wiedemann, B. Schlegel, J. O. S. É. R. Pires, M. Beyermann, P. Schmieder, G. Krause, R. Volkmer-engert, J. Schneider-mergener, and H. Oschkinat
2003. WW domain sequence activity relationships identified using ligand recognition propensities of 42 WW domains. *Protein Science*, 12:491–500.

Palazzo, A. F., T. A. Cook, A. S. Alberts, and G. G. Gundersen
2001. mDia mediates Rho-regulated formation and orientation of stable microtubules. *Nature cell biology*, 3(August):723–729.

Parent, C. A. and O. D. Weiner
2013. The symphony of cell movement: How cells orchestrate diverse signals and forces to control migration. *Current Opinion in Cell Biology*, 25(5):523–525.

Park, K. W., C. M. Morrison, L. K. Sorensen, C. A. Jones, Y. Rao, C. B. Chien, J. Y. Wu, L. D. Urness, and D. Y. Li
2003. Robo4 is a vascular-specific receptor that inhibits endothelial migration. *Developmental Biology*, 261(1):251–267.

Parsons, J. T., A. R. Horwitz, and M. A. Schwartz
2010. NIH Public Access. *Nat Rec*, 11(9):633–643.

Pertz, O.
2010. Spatio-temporal Rho GTPase signaling - where are we now? *Journal of cell science*, 123(Pt 11):1841–1850.

Pertz, O., L. Hodgson, R. L. Klemke, and K. M. Hahn
2006. Spatiotemporal dynamics of RhoA activity in migrating cells. *Nature Letters*, 440(April):1069–1072.

Philipp, M., V. Niederkofler, M. Debrunner, T. Alther, B. Kunz, and E. T. Stoeckli
2012. RabGDI controls axonal midline crossing by regulating Robo1 surface expression. *Neural Development*, 36(7):1–17.

Phng, L.-k., F. Stanchi, and H. Gerhardt
2013. Filopodia are dispensable for endothelial tip cell guidance. *Development*, 4040:4031–4040.

Piper, M., R. Anderson, A. Dwivedy, C. Weinl, F. Van, K. M. Leung, E. Cogill, and C. Holt
2013. Europe PMC Funders Group Signaling Mechanisms Underlying Slit2-Induced Collapse of Xenopus Retinal Growth Cones. *Neuron*, 49(2):215–228.

Placzek, M. and J. Briscoe
2005. THE FLOOR PLATE : MULTIPLE CELLS ,. *Nature Reviews Neuroscience*, 6(March):230–240.

Planelles-Herrero, V. J., F. Blanc, S. Sirigu, H. Sirkia, J. Clause, Y. Sourigues, D. O. Johnsrud, B. Amigues, M. Cecchini, S. P. Gilbert, A. Houdusse, and M. A. Titus
2016. Myosin MyTH4-FERM structures highlight important principles of convergent evolution. *Proceedings of the National Academy of Sciences*.

Pollard, T. D., L. Blanchoin, and R. D. Mullins
2000. MOLECULARMECHANISMS CONTROLLING ACTIN FILAMENTDYNAMICS INNONMUSCLE CELLS. *Annu. Rev. Biophys. Biomol. Struct.*, 2000(29):545–76.

Prasad, A., Z. Qamri, J. Wu, and R. K. Ganju
2007. Slit-2/Robo-1 modulates the CXCL12/CXCR4-induced chemotaxis of T cells. *Journal of leukocyte biology*, 82(3):465–76.

Qian, L., J. Liu, and R. Bodmer
2005. Slit and Robo control cardiac cell polarity and morphogenesis. *Current Biology*, 15(24):2271–2278.

Qin, F., H. Zhang, L. Ma, X. Liu, K. Dai, W. Li, F. Gu, L. Fu, and Y. Ma
2015. Low Expression of Slit2 and Robo1 is Associated with Poor Prognosis and Brain-specific Metastasis of Breast Cancer Patients. *Scientific Reports*, 5(August):14430.

Rane, C. K., A. Minden, C. K. Rane, and A. Minden
2014. P21 activated kinases: Structure , regulation , and functions. *Small GTPases*, 5:e28003_1–13.

Ranganathan, R., K. P. Lu, T. Hunter, and J. P. Noel
1997. Structural and functional analysis of the mitotic rotamase Pin1 suggests substrate recognition is phosphorylation dependent. *Cell*, 89(6):875–886.

Ridley, A. J.
2001. Rho GTPases and cell migration. *J Cell Sci*, 114(Pt 15):2713–2722.

Ridley, A. J.
2003. Cell Migration: Integrating Signals from Front to Back. *Science*, 302(5651):1704–1709.

Ridley, A. J.
2011. Life at the leading edge. *Cell*, 145(7):1012–1022.

Ridley, A. J.
2015. ScienceDirect Rho GTPase signalling in cell migration. *Current Opinion in Cell Biology*, 36:103–112.

Ridley, A. J. and A. Hall
1992. The small GTP-binding protein rho regulates the assembly of focal adhesions and actin stress fibers in response to growth factors. *Cell*, 70(3):389–399.

Ridley, A. J., H. F. Paterson, C. L. Johnston, D. Diekmann, and A. Hall
1992. The small GTP-binding protein rac regulates growth factor-induced membrane ruffling. *Cell*, 70(3):401–410.

Rodriguez, O. C., A. W. Schaefer, C. A. Mandato, P. Forscher, W. M. Bement, and C. M. Waterman-storer
2003. Conserved microtubule â actin interactions in cell movement and morphogenesis. *Nature cell biology*, 5(7):599–609.

Rondard, P., C. Goudet, J. Kniazeff, J. Pin, and L. Prézeau
2011. The complexity of their activation mechanism opens new possibilities for the modulation of mGlu and GABAB class C G protein-coupled receptors. *Neuropharmacology*, 60:82–91.

Rossman, K. L., C. J. Der, and J. Sondek
2005. GEF means Go: turning on Rho GTPases with guanine nucleotide-exchange factors. *Nature Reviews Molecular Cell Biology*, 6(2):167–180.

Rothberg, J. M., D. A. Hartley, Z. Walther, and S. Artavanis-tsakonas
1988. slit: An EGF-Homologous Locus of D . melanogaster Involved in the Development of the Embryonic Central Nervous System. *Cell*, 55:1047–1059.

Round, J. E. and H. Sun
2011. The adaptor protein Nck2 mediates Slit1-induced changes in cortical neuron morphology. *Molecular and Cellular Neuroscience*, 47(4):265–273.

Rymo, S. F., H. Gerhardt, F. W. Sand, R. Lang, and A. Uv
2011. A Two-Way Communication between Microglial Cells and Angiogenic Sprouts Regulates Angiogenesis in Aortic Ring Cultures. *PLoS Genetics*, 6(1).

Rzadzinska, A. K., M. E. Schneider, C. Davies, G. P. Riordan, and B. Kachar
2004. An actin molecular treadmill and myosins maintain stereocilia functional architecture and self-renewal. *Journal of Cell Biology*, 164(6):887–897.

Sabatier, C., A. S. Plump, L. Ma, K. Brose, A. Tamada, F. Murakami, E. Y. P. Lee, M. Tessier-lavigne, and S. Francisco
2004. The Divergent Robo Family Protein Rig-1 / Robo3 Is a Negative Regulator of Slit Responsiveness Required for Midline Crossing by Commissural Axons. *cell*, 117:157–169.

Salah, Z.
2012. WW domain-containing proteins: Retrospectives and the future. *Frontiers in Bioscience*, 17(1):331.

Schlessinger, A., M. Punta, and B. Rost
2007. Structural bioinformatics Natively unstructured regions in proteins identified from contact predictions. *Bioinformatics*, 23(18):2376–2384.

Schmitz, A. A. P., E.-e. Govek, B. Bo, and L. V. Aelst
2000. Rho GTPases : Signaling , Migration , and Invasion. *Experimental Cell Research*, 12:1–12.

Schuchardt, B. J., V. Bhat, D. C. Mikles, C. B. Mcdonald, M. Sudol, and A. Farooq
2014. Molecular basis of the binding of YAP transcriptional regulator to the ErbB4 receptor tyrosine kinase. *Biochimie*, 101:192–202.

Seabra, M. C.
1998. Membrane Association and Targeting of Prenylated Ras-like GTPases. *Cell Signaling*, 10(3):167–172.

Seiradake, E., A. C. V. Philipsborn, M. Henry, M. Fritz, H. Lortat-jacob, M. Jamin, W. Hemrika, M. Bastmeyer, S. Cusack, and A. A. Mccarthy
2009. Structure and functional relevance of the Slit2 homodimerization domain. *EMBO reports*, 10(7):736–741.

Seth, P., Y. Lin, J. I. Hanai, V. Shivalingappa, M. P. Duyao, and V. P. Sukhatme
2005. Magic roundabout, a tumor endothelial marker: Expression and signaling. *Biochemical and Biophysical Research Communications*, 332(2):533–541.

Sheldon, H., M. Andre, J. a. Legg, P. Heal, J. M. Herbert, R. Sainson, A. S. Sharma, J. K. Kitajewski, V. L. Heath, and R. Bicknell
2009. Active involvement of Robo1 and Robo4 in filopodia formation and endothelial cell motility mediated via WASP and other actin nucleation-promoting factors. *The FASEB journal : official publication of the Federation of American Societies for Experimental Biology*, 23(2):513–522.

Shibue, T. and R. A. Weinberg
2011. Seminars in Cancer Biology Metastatic colonization : Settlement , adaptation and propagation of tumor cells in a foreign tissue environment. *Seminars in Cancer Biology*, 21(2):99–106.

Sit, S.-T. and E. Manser
2011. Rho GTPases and their role in organizing the actin cytoskeleton. *Journal of cell science*, 124(Pt 5):679–683.

Small, E. M., L. B. Sutherland, K. N. Rajagopalan, S. Wang, and E. N. Olson
2010. MicroRNA-218 regulates vascular patterning by modulation of Slit-Robo signaling. *Circulation research*, 107(11):1336–44.

Soderling, S. H., K. L. Binns, G. a. Wayman, S. M. Davee, S. H. Ong, T. Pawson, and J. D. Scott
2002. The WRP component of the WAVE-1 complex attenuates Rac-mediated signalling. *Nature cell biology*, 4(12):970–975.

Sorkin, A. and M. von Zastrow
2009. Endocytosis and signalling: intertwining molecular networks. *Nature reviews. Molecular cell biology*, 10(9):609–622.

Sprang, S. R.
1997. G PROTEIN MECHANISMS : Insights from Structural Analysis. *Annu. Rev. Biochem.*, 66:639–78.

Stanyon, C. and O. Bernard
1999. LIM-kinase1. *International Journal of Biochemistry and Cell Biology*, 31:389–94.

Steigemann, P., A. Molitor, S. Fellert, H. Jäckle, and G. Vorbrüggen
2004. Heparan Sulfate Proteoglycan Syndecan Promotes Axonal and Myotube Guidance by Slit/Robo Signaling. *Current Biology*, 14(3):225–230.

Stein, E. and M. Tessier-Lavigne
2001. Hierarchical Organization of Guidance Receptors: Silencing of Netrin Attraction by Slit Through a Robo/DCC Receptor Complex. *Science*, 291(5510):1928–1938.

Stella, M. C., L. Trusolino, and P. M. Comoglio
2009. The Slit / Robo System Suppresses Hepatocyte Growth Factor-dependent Invasion and Morphogenesis. *Molecular biology of the cell*, 20:642–657.

Suchting, S., C. Freitas, F. Noble, R. Benedito, C. Bre, A. Duarte, and A. Eichmann
2007. The Notch ligand Delta-like 4 negatively regulates endothelial tip cell formation and vessel branching. *Proc. Natl. Acad. Sci. U.S.A.*, 104(9):3225–3230.

Suchting, S., P. Heal, K. Tahtis, L. M. Stewart, and R. Bicknell
2005. Soluble Robo4 receptor inhibits in vivo angiogenesis and endothelial cell migration. *The FASEB journal : official publication of the Federation of American Societies for Experimental Biology*, 19(1):121–123.

Sudol, M.
1996. Structure and function of the WW domain. *Progress in biophysics and molecular biology*, 65(1-2):113–132.

Sudol, M. and T. Hunter
2000. New wrinkles for an old domain. *Cell*, 103(7):1001–1004.

Summerton, J.
1999. Morpholino antisense oligomers : the case for an RNase H-independent structural type. *Biochimica et Biophysica Acta*, 1489(1):141–58.

Summerton, J. and D. Weller
1997. Morpholino antisense oligomers: design, preparation, and properties. *Antisense Nucleic cid rug Dev.*, 7(3):187–195.

Sundaresan, V., A. Heppell-Parton, N. Coleman, M. Miozzo, G. Sozzi, R. Ball, N. Cary, P. Hasleton, W. Fowler, and P. Rabbitts
1995. Somatic genetic changes in lung cancer and precancerous lesions. *Ann Oncol.*, 6:27–31.

Tcherkezian, J. and N. Lamarche-vane
2007. Current knowledge of the large RhoGAP family of proteins. *Biology of the cell*, 99(2):67–86.

ten Klooster, J. P., Z. M. Jaffer, J. Chernoff, and P. L. Hordijk
2006. Targeting and activation of Rac1 are mediated by the exchange factor β -Pix. *Journal of Cell Biology*, 172(5):759–769.

Tompa, P. and M. Fuxreiter
2007. Fuzzy complexes : polymorphism and structural disorder in protein â protein interactions. *Trends in biochemical sciences*, 33(1).

Tsvetanova, N. G. and R. Irannejad
2015. G Protein-coupled Receptor (GPCR) Signaling via Heterotrimeric G Proteins from Endosomes. *Journal of Biological Chemistry*, 290(11):6689–6696.

Vaccari, T., H. Lu, R. Kanwar, M. E. Fortini, and D. Bilder
2008. Endosomal entry regulates Notch receptor activation in Drosophila melanogaster. *The Journal of Cell Biology*, 180(4):755–762.

Valencia, A., P. Chardin, A. Wittinghofer, and C. Sander
1991. The ras protein family: evolutionary tree and role of conserved amino acids. *Biochemstry*, 30(14):4637–48.

van der Lee, R., M. Buljan, B. Lang, R. J. Weatheritt, G. W. Daughdrill, A. K. Dunker, M. Fuxreiter, J. Gough, J. Gsponer, D. T. Jones, P. M. Kim, R. W. Kriwacki, C. J. Old, R. V. Pappu, P. Tompa, V. N. Uversky, P. E. Wright, and M. M. Babu
2014. Classification of Intrinsically Disordered Regions and Proteins. *Chemical Reviews*, 114:6589–6631.

van Nieuw Amerongen, G. P. V. N., P. Koolwijk, A. Versteilen, and V. W. M. V. Hinsbergh
2003. Involvement of RhoA/Rho kinase signaling in VEGF-induced endothelial cell migration and angiogenesis in vitro. *Arteriosclerosis, Thrombosis, and Vascular Biology*, 23(2):211–7.

Vetter, I. R. and A. Wittinghofer
2001. The Guanine Nucleotide â Binding Switch in Three Dimensions. *Science (New York, N.Y.)*, 294(November):1299–1305.

Villasenor, R., Y. Kalaidzidis, and M. Zerial
2016. ScienceDirect Signal processing by the endosomal system. *Current Opinion in Cell Biology*, 39:53–60.

Wang, B., Y. Xiao, B. B. Ding, N. Zhang, X. B. Yuan, L. Gui, K. X. Qian, S. Duan, Z. Chen, Y. Rao, and J. G. Geng
2003. Induction of tumor angiogenesis by Slit-Robo signaling and inhibition of cancer growth by blocking Robo activity. *Cancer Cell*, 4(1):19–29.

Wang, K. H., K. Brose, D. Arnott, T. Kidd, C. S. Goodman, W. Henzel, and M. Tessier-Lavigne
1999. Biochemical purification of a mammalian slit protein as a positive regulator of sensory axon elongation and branching. *Cell*, 96(6):771–784.

Wang, Y., J. a. Kelber, H. S. Tran Cao, G. T. Cantin, R. Lin, W. Wang, S. Kaushal, J. M. Bristow, T. S. Edgington, R. M. Hoffman, M. Bouvet, J. R. Yates, and R. L. Klemke
2010. Pseudopodium-enriched atypical kinase 1 regulates the cytoskeleton and cancer progression [corrected]. *Proceedings of the National Academy of Sciences of the United States of America*, 107(24):10920–10925.

Watanabe, N., T. Kato, A. Fujita, T. Ishizaki, and S. Narumiya
1999. Cooperation between mDia1 and ROCK in Rho-induced actin reorganization. *Nature cell biology*, 1(July).

Wehrle-Haller, B. and B. A. Imhof
2003. Actin, microtubules and focal adhesion dynamics during cell migration. *International Journal of Biochemistry and Cell Biology*, 35(1):39–50.

Wei, Z., J. Yan, Q. Lu, L. Pan, and M. Zhang
2011. Cargo recognition mechanism of myosin X revealed by the structure of its tail MyTH4-FERM tandem in complex with the DCC P3 domain. *Proceedings of the National Academy of Sciences*, 108(9):3572–5377.

Weis, K.
2003. Regulating Access to the Genome : Nucleocytoplasmic Transport throughout the Cell Cycle Macromolecular transport between the cytoplasm and. *Cell*, 112:441–451.

Welch, M. D. and R. D. Mullins
2002. CELLULAR CONTROL OF ACTIN NUCLEATION. *Annu Rev Cell Dev Biol*, 18:247–88.

Wennerberg, K., L. Kent, C. J. Der, K. Wennerberg, K. L. Rossman, and C. J. Der
2005. The Ras superfamily at a glance The Ras Superfamily at a Glance. *Journal of Cell Science*, 2005:843–846.

Wheeler, A. P., C. M. Wells, S. D. Smith, F. M. Vega, R. B. Henderson, V. L. Tybulewicz, and A. J. Ridley
2006. Rac1 and Rac2 regulate macrophage morphology but are not essential for migration. *Journal of Cell Science*, 119:2749–2757.

Wiesner, S., G. Stier, M. Sattler, and M. J. Macias
2002. Solution structure and ligand recognition of the WW domain pair of the yeast splicing factor Prp40. *Journal of Molecular Biology*, 324(4):807–822.

Winckler, B. and I. Mellman
2010. Trafficking Guidance Receptors. *Cold Spring Harbor perspectives in biology*, 2:1–19.

Winograd-Katz, S. E., R. Fässler, B. Geiger, and K. R. Legate
2014. The integrin adhesome : from genes and proteins to human disease. *Mol Cell Biol*, 15:273–288.

Wong, K., X. R. Ren, Y. Z. Huang, Y. Xie, G. Liu, H. Saito, H. Tang, L. Wen, S. M. Brady-Kalnay, L. Mei, J. Y. Wu, W. C. Xiong, and Y. Rao
2001. Signal transduction in neuronal migration: Roles of GTPase activating proteins and the small GTPase Cdc42 in the Slit-Robo pathway. *Cell*, 107(2):209–221.

Wozniak, M. A., K. Modzelewska, L. Kwong, and P. J. Keely
2004. Focal adhesion regulation of cell behavior. *Biochimica et Biophysica Acta (BBA) - Molecular Cell Research*, 1692(2):103–119.

Wright, P. E. and H. J. Dyson
2015. Intrinsically Disordered Proteins in Cellular Signaling and Regulation. *Nature reviews. Molecular cell biology*, 16(1):18–29.

Wu, L., L. Pan, Z. Wei, and M. Zhang
2011. Structure of MyTH4-FERM domains in myosin VIIa tail bound to cargo. *Science*, 331(6018):757–760.

Yamazaki, D., T. Itoh, H. Miki, and T. Takenawa
2013. srGAP1 regulates lamellipodial dynamics and cell migratory behavior by modulating Rac1 activity. *Mol Biol Cell.*, 24:3393–3405.

Yang, L. and G. J. Bashaw
2006. Son of Sevenless Directly Links the Robo Receptor to Rac Activation to Control Axon Repulsion at the Midline. *Neuron*, 52(4):595–607.

Ypsilanti, A. R., Y. Zagar, and A. Chédotal
2010. Moving away from the midline: new developments for Slit and Robo. *Development (Cambridge, England)*, 137(12):1939–1952.

Yuasa-Kawada, J., M. Kinoshita-Kawada, Y. Rao, and J. Y. Wu
2009a. Deubiquitinating enzyme USP33/VDU1 is required for Slit signaling in inhibiting breast cancer cell migration. *Proceedings of the National Academy of Sciences of the United States of America*, 106(34):14530–5.

Yuasa-Kawada, J., M. Kinoshita-Kawada, G. Wu, Y. Rao, and J. Y. Wu
2009b. Midline crossing and Slit responsiveness of commissural axons require USP33. *Nature Neuroscience*, 12(9):1087–1089.

Zabarovsky, E. R., M. I. Lerman, and J. D. Minna
2002. Tumor suppressor genes on chromosome 3p involved in the pathogenesis of lung and other cancers. *Oncogene*, 1234:6915–6935.

Zakrys, L., R. J. Ward, J. D. Pediani, A. G. Godin, G. J. Graham, and G. Milligan
2014. Roundabout 1 exists predominantly as a basal dimeric complex and this is unaffected by binding of the ligand Slit2. *The Biochemical journal*, 461(1):61–73.

Zerial, M. and H. Mcbride
2001. RAB PROTEINS AS MEMBRANE ORGANIZERS. *Nature reviews. Molecular cell biology*, 2(February):107–117.

Zhang, B., U. M. Dietrich, J.-g. Geng, R. Bicknell, J. D. Esko, and L. Wang
2009. Repulsive axon guidance molecule Slit3 is a novel angiogenic factor. *Blood*, 114(19):4300–4310.

Zhang, H., J. S. Berg, Z. Li, Y. Wang, P. Lång, A. D. Sousa, R. E. Cheney, and S. Strömblad
2004. Myosin-X provides a motor-based link between integrins and the cytoskeleton. *Nature cell biology*, 6(6):523–531.

Zhao, M., X. Wan, Y. Li, W. Zhou, and L. Peng
2015. Multiplexed 3D FRET imaging in deep tissue of live embryos. *Scientific Reports*, 5:1–15.

Ziogas, A., K. Moelling, and G. Radziwill
2005. CNK1 Is a Scaffold Protein That Regulates Src-mediated Raf-1 Activation. *The Journal of Biological Chemistry*, 280(25):24205–24211.

A. Appendix

A

chromosome, location	exons	gene	transcript ID	UniProt	length
20: 52,685,996-52,789,070	*11*	*si:ch211-218p13.1*	*ENSDART00000113684.1*	*F1QV51*	*967 aa*
20; 52,542,816-52,564,075	7	CABZ01087448.1	ENSDART00000166651.1	A0A0G2KKK2	660 aa
23; 15,290,361-15,442,072	8	si:ch211-218g4.2	ENSDART00000133624.1	E9QHA2	898 aa
23; 15,290,361-15,442,072	12	si:ch211-218g4.2	ENSDART00000082060.5	E7F9H1	1060 aa
11; 24,757,089-24,804,188	10	zgc:92107	ENSDART00000129211.3	A5WUS3	1067 aa
11; 24,757,089-24,804,188	9	zgc:92107	ENSDART00000167285.1	A0A0R41G34	981aa

B

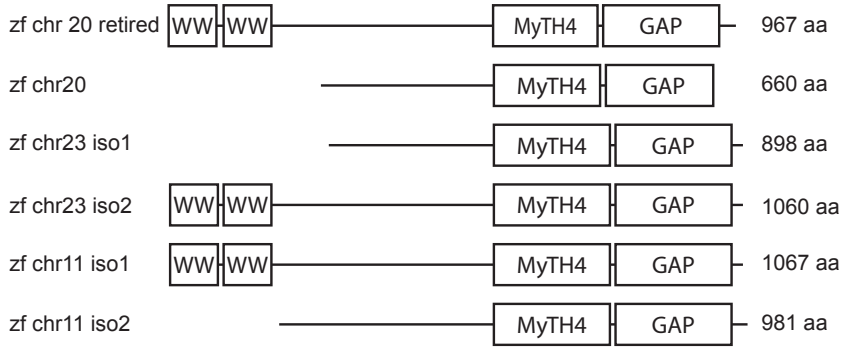

Figure A.1.: Summary of paralogous genes of *arhgap39*
A Table summarizing the the predicted paralogous genes in the zebrafish genome. In the first row depicts the gene, which showed the highest similarity with the human *ARHGAP39* gene and was thus chosen for PCR-primer design. **B** Domain architecture of the predicted Arhgap39 proteins. Order of the table corresponds to order of the illustrated proteins. Abbreviation: zf: zebrafish.

position DNA	change	effect on protein level
243	c to a	no change in amino acid
293-299	deletion	**deletion of 100-101 aa**
546	t to c	no change in amino acid
702	a to g	no change in amino acid
1083	t to a	no change in amino acid
1290	t to c	no change in amino acid
1614	g to c	no change in amino acid
1887	t to c	no change in amino acid
2031	c to a	no change in amino acid
2322	t to g	no change in amino acid

Figure A.2.: The identified zebrafish Arhgap39 transcript only differs in two amino acid residue from its predicted sequence
Six plasmids containing the *arhgap39* gene obtained by PCR-based amplification from zebrafish cDNA were sequenced. All genes showed the same alterations from the predicted sequence at the indicated positions, however the changes in the nucleic acid sequence did not lead to alteration in the amino acid sequence. Only, the deletion of the nucleic acid residues from 293-299 caused the deletion of two amino acids in the identified Arhgap39 transcript.

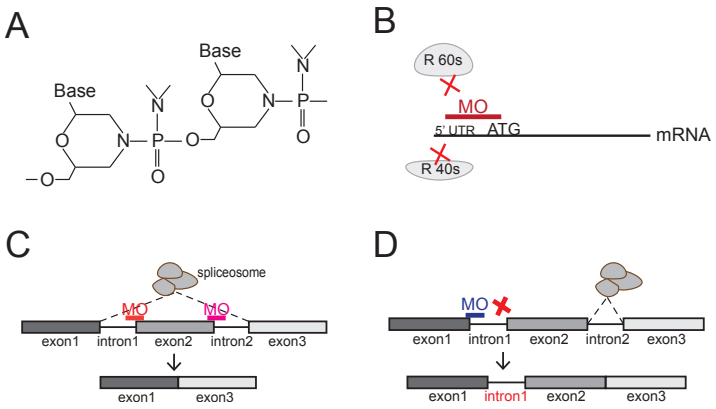

Figure A.3.: General mechanisms of morpholino oligomer function
AStructure of a morpholino oligonucleotide, which consists of a six-membered morpholino ring and a non-ionic phosphorodiamidate link between the two rings. **B** Illustration showing how a translation blocking morpholino (MO) sterically blocks the access of the ribosomal subunits to the translation start of the target mRNA. **C** and **D** Illustration depicting the two typical splice blocking methods that hinder the spliceosome from recognizing the splice site on the pre-mRNA and thus leading to mis-spliced mRNAs. **C** The two MOs target an internal exon by masking one of the two different spliceosomal binding sites, both resulting to the deletion of the internal exon. **D** The MO either targets the first exon-intron boundary, which leads to the insertion of the intron in the mRNA.

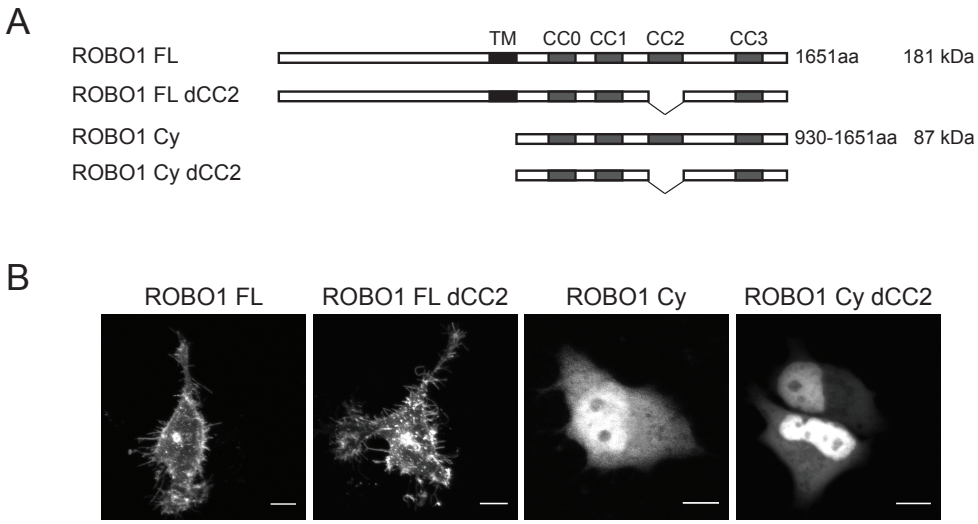

Figure A.4.: Truncated mutants of ROBO1
A Illustration of the generated truncation mutants of ROBO1 in this thesis. **B** Ectopic expression of ROBO1 and its deletion mutants tagged with a YFP-fluorophore in HeLa cells. Abbreviations: Cy: cytoplasmic region, FL: full length. Scale bar: 10 µm

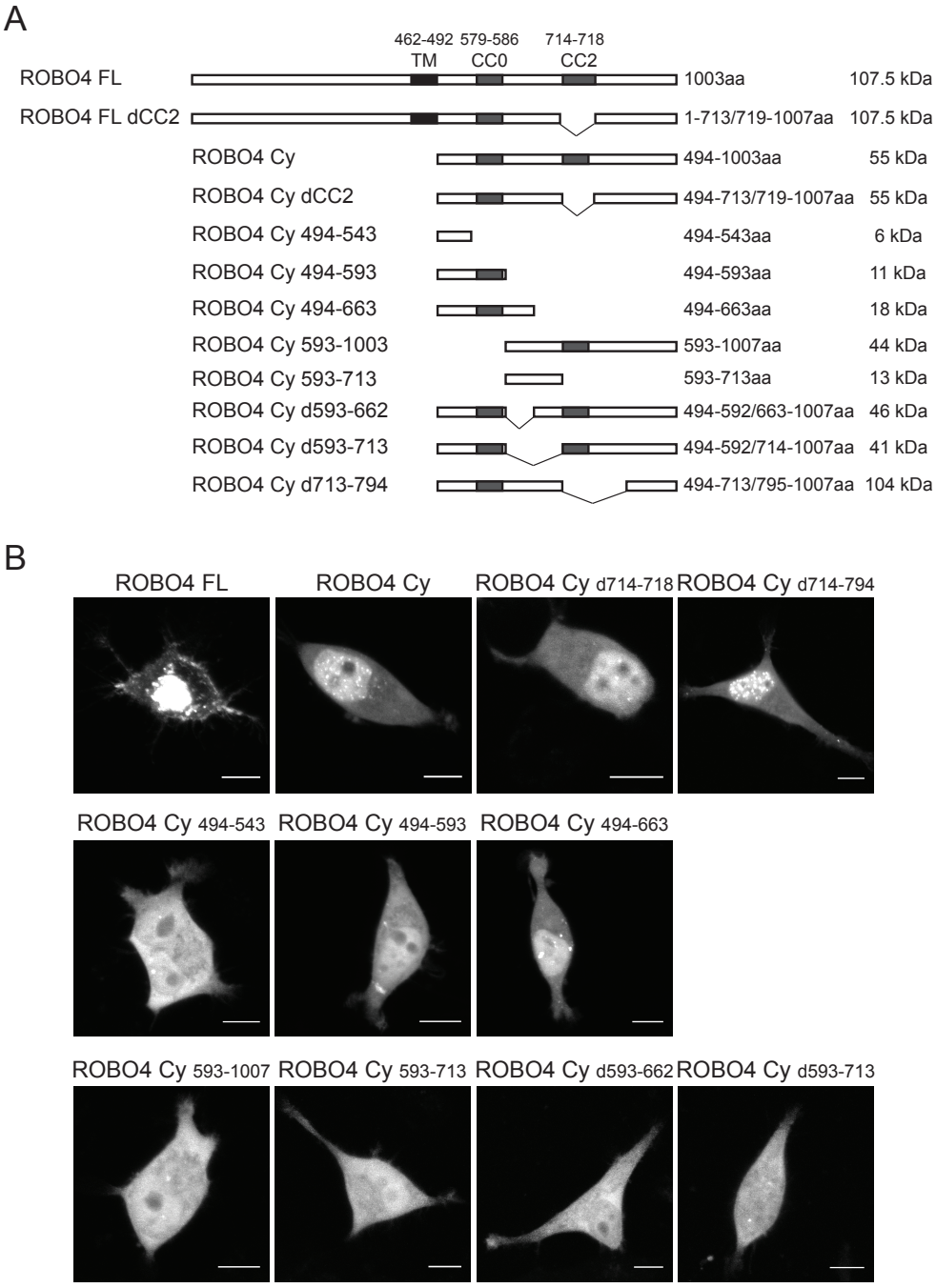

Figure A.5.: Truncated mutants of ROBO4
A Illustration of the generated truncation mutants of ROBO4 in this thesis. **B** Ectopic expression of ROBO4 and its deletion mutants tagged with a YFP-fluorophore in HeLa cells. Abbreviations: Cy: cytoplasmic region, FL: full length. Scale bar: 10 µm

Table A.1.: QuikChange mutagenesis primers

protein	mutation	product	primer sequence	donor
ARHGAP39	Δ890-1114	dGAP	Fw: GCCCGTCCATGTTCGGCTTAATTAACCAGGTAAG Rv: CTTACCTGGTTAATTAAGCCGAACATGGACGGGC	GAP39 FL
ARHGAP39	Δ0-114	dWW	Fw: GGCGCGCCATGTCCCCGCGCGC Rv: GGCGCGCCATGTCCCCGCGCGC	GAP39 FL
ARHGAP39	Δ115-689	dm1	Fw: GAAGCAGAACACGGAGTCGGAGACGGACATCG Rv: CGATGTCCGTCTCCGACTCCGTGTTCTGCTTC	GAP39 FL
ARHGAP39	Δ63-689	dm2	Fw: GGCGTCCGCATCAAGTCGGAGACGGACATC Rv: GATGTCCGTCTCCGACTTGATGCGGACGCC	GAP39 dm1
ARHGAP39	Δ501-114	Cterm1	Fw: GGGCGCGCCATGTGCCAAGCCACC Rv: GGTGGCTTGGCACATGGCGCGCCC	GAP39 dWW
ARHGAP39	Δ689-114	Cterm2	Fw: GGGCGCGCCATGTCGGAGACGGAC Rv: GTCCGTCTCCGACATGGCGCGCCC	GAP39 Cterm1
ARHGAP39	690-910	MyTH4	Fw: GGGCGCGCCATGTCGGAGACGGAC Rv: GTCCGTCTCCGACATGGCGCGCCC	GAP39 $MyTH4_3$
ARHGAP39	882-1114	GAP	Fw: GGGCGCGCCATGTTCAGCCCGTCC Rv: GGACGGGCTGAACATGGCGCGCCC	GAP39 Cterm2
ARHGAP39	1-114	WW	Fw: CGCTGAAGCAGAACACGGAGTTAATTAACCAGGTAAGTTC Rv: GAACTTACCTGGTTAATTAACTCCGTGTTCTGCTTCAGCG	GAP39 shortGAP1
ARHGAP39	115-689	middle	Fw: GGCGCGCCATGTCCCCGCGCGC Rv: GCGCGCGGGGACATGGCGCGCC	GAP39 shortGAP1
ARHGAP39	Δ689-910	dMyTH4	Fw: TGCGCAAGCCCTCCAACGCCGTGTTCAG Rv: CTGAACACGGCGTTGGAGGGCTTGCGCA	GAP39 GAP39 FL
ARHGAP39	1-501	Nterm1	Fw: GCAGAAAGCCCTCTTTGTAGGAGATCCTGGTCAT Rv: ATGACCAGGATCTCCTACAAAGAGGGCTTTCTGC	GAP39 shortGAP1
ARHGAP39	1-400	Nterm2	Fw: GTGCGGCAGCTGGTCTACTTAATTAACCAGGTAAGT Rv: ACTTACCTGGTTAATTAAGTAGACCAGCTGCCGCAC	GAP39 shortGAP1
ARHGAP39	in MyTH4	I749T	Fw: CCTGCGAGCTCTTCAAGCTGACCCAGATGTACATG Rv: CATGTACATCTGGGTCAGCTTGAAGAGCTCGCAGG	GAP39 FL
ARHGAP39	in MyTH4	R781P	Fw: GCAGGGCCTGCCGGACGAGCTCT Rv: AGAGCTCGTCCGGCAGGCCCTGC	GAP39 FL
ARHGAP39	in MyTH4	E783K	Fw: GGGCCTGCGGGACAAGCTCTACATCCA Rv: TGGATGTAGAGCTTGTCCCGCAGGCCC	GAP39 FL
ARHGAP39	in MyTH4	K896W	Fw: CTGACCGGGGCCCAGAAGGGGCTGA Rv: TCAGCCCCTTCTGGGCCCCGGTCAG	GAP39 FL
ARHGAP39	in MyTH4	P901R	Fw: GGGCTGAAGAAGCGCAACGTGGAGGAG Rv: CTCCTCCACGTTGCGCTTCTTCAGCCC	GAP39 FL
ARHGAP39	in WW1	Y43A	Fw: GACCAGGTTGGCGGCCATGCGCTCGCGG Rv: CCGCGAGCGCATGGCCGCCAACCTGGTC	GAP39 FL
ARHGAP39	in WW1	W53A	Fw: GCCGGCGGGTCCGCCACGCACTCACC Rv: GGTGAGTGCGTGGCGGACCCGCCGGC	GAP39 FL
ARHGAP39	in WW2	Y81A	Fw: CCAACACGTCCCGCTTCGCCTACTACAATGCCAGCA Rv: TGCTGGCATTGTAGTAGGCGAAGCGGGACGTGTTGG	GAP39 FL
ARHGAP39	in WW2	Y92A	Fw: CAGCGCACGGTGGCGCACCGGCCGCA Rv: TGCGGCCGGTGCGCCACCGTGCGCTG	GAP39 FL
ROBO1	Δ1186-1196	R1 dCC2	Fw: GAACTGGGCAGACCTGCACAGCAATAGCGAAG Rv: CTTCGCTATTGCTGTGCAGGTCTGCCCAGTTC	ROBO1 FL
ROBO1	Δ1186-1196	R1 Cy dCC2	Fw: GAACTGGGCAGACCTGCACAGCAATAGCGAAG Rv: CTTCGCTATTGCTGTGCAGGTCTGCCCAGTTC	ROBO1 Cy
ROBO4	Δ714-718	R4 dCC2	Fw: AAATGAGCTGGTTACTCGTCATCTCTTTCCTCATGAAACTC Rv: GAGTTTCATGAGGAAAGAGATGACGAGTAACCAGCTCATTT	ROBO4 FL
ROBO4	Δ714-718	R4 Cy dCC2	Fw: AAATGAGCTGGTTACTCGTCATCTCTTTCCTCATGAAACTC Rv: GAGTTTCATGAGGAAAGAGATGACGAGTAACCAGCTCATTT	ROBO4 Cy
ROBO4	494-543	R4 Cy 494-543	Fw: AGCAGCAGCAGCAGCGACCCAGCTTTCTTG Rv: CAAGAAAGCTGGGTCGCTGCTGCTGCTGCT	ROBO4 Cy

ROBO4	494-593	R4 Cy 494-593	Fw: GAGCTGCCCTCCAGTGACCCAGCTTTCTTG Rv: CAAGAAAGCTGGGTCACTGGAGGGCAGCTC	ROBO4 Cy
ROBO4	494-663	R4 Cy 494-663	Fw: GCTCCGGGGCAGCGACCCAGCTTTCT Rv: AGAAAGCTGGGTCGCTGCCCCGGAGC	ROBO4 Cy
ROBO4	593-1007	R4 Cy 593-1007	Fw: CTTCGCCACCATGACCCCAGCCAGGC Rv: GCCTGGCTGGGGTCATGGTGGCGAAG	ROBO4 Cy
ROBO4	Δ593-663	R4 Cy d593-663	Fw: GAGCTGCCCTCCAGTCACTCCTTGGAGCTC Rv: GAGCTCCAAGGAGTGACTGGAGGGCAGCTC	ROBO4 Cy
ROBO4	Δ593-713	R4 Cy d593-713	Fw: GCTGCCCTCCAGTCTCCCTCCAGCAC Rv: GTGCTGGAGGGAGACTGGAGGGCAGC	ROBO4 Cy
ROBO4	Δ714-794	R4 Cy 714-794	Fw: AAATGAGCTGGTTACTCGTCATCTGGGGGAGGAT Rv: ATCCTCCCCCAGATGACGAGTAACCAGCTCATTT	ROBO4 Cy

Table A.2.: Infusion-HD cloning primers

gene	product	primer sequence
ROBO1	Gateway donor	Fw: ATGCCAACTTTGTACAAAAAAGCAGGCTTCGCCACCATGAAATGGAAACATGTTCCT Rv: ATGCCAACTTTGTACAAGAAAGCTGGGTCGCTTTCAGTTTCCTCTAATTCT
ROBO4	Gateway donor	Fw: ATGCCAACTTTGTACAAAAAAGCAGGCTTCGCCACCATGGGCTCTGGAGGA-GACAGC Rv: ATGCCAACTTTGTACAAAAAAGCAGGCTTCGCCACCATGGGCTCTGGAGGAGACAGC
SLIT2	Gateway donor	Fw: ATGCCAACTTTGTACAAAAAAGCAGGCTTCGCCACCATGCGCGGCGTTGGCTG-GCAG Rv: ATGCCAACTTTGTACAAGAAAGCTGGGTCGGACACACACCTCGTACAGCCGC
ROBO1	R1 Cy, 930-1651 aa	Fw: ATGCCAACTTTGTACAAAAAAGCAGGCTTCGCCACCATGAGTACC-TACGCGGGTATCAG Rv: ATGCCAACTTTGTACAAGAAAGCTGGGTCTCAGCTTTCAGTTTCCTCTAATTCT
ROBO4	R4 Cy, 494-1007 aa	Fw: ATGCCAACTTTGTACAAAAAAGCAGGCTTCGCCACCATGCGAGCTAGGGTGCACCTG Rv: ATGCCAACTTTGTACAAGAAAGCTGGGTCTCAAGGAGAAGCACCAGCCTTGG
ROBO2	Creator donor	Fw: TTCCCCAGGGGCGCGCCATGTGGACATGGGCTCCGGGACTG Rv: GAACTTACCTGGTTAATTAATAATTCACCTGTAAACTGTCCTTGACTGTTG
zfArhgap39	Creator donor	Fw: TTCCCCAGGGGCGCGCCATGGCGGAGAGGTTGGAATGG Rv: GAACTTACCTGGTTAATTAACTATAGCACCCCGTCCATGAAG

The following primers were used: 1) for PCR cloning of *arhgap39* from zf-cDNA into the pCS2+ vector; 2) for quantitative-PCR (q-PCR) of human cDNA samples; 3) for sequencing reactions; 4) for TaqMAN based q-PCR of zebrafish cDNA samples.

Table A.3.: Sequences of Primers

	primer	binds	sequence
PCR cloning	zfArhgap39-1	5' UTR/1-2 bp	Fw: TAGGATGTGGATTACTCTCACTGCGTGTTGAAGCGGCAC-CCAGAGGCACCAT
		3' UTR	Rv: CCTAACACTTCTTCAGCGCCCACT
	zfArhgap39-2	5 bp	Fw: CGGAGAGGTTGGAATGGGTGGAGA
		3' UTR	Rv: CACCTAACACTTCTTCAGCGCCCA
q-PCR	ARHGAP39-Fw	198 bp	Fw: GAGTACTGGAAATGGTAACTACATGG
	ARHGAP39-Rv	271 bp	Rv: TCAGGATCAGCTTCTCGATTT
	GAPDH-Fw	83 bp	Fw: AGCCACATCGCTCAGACAC
	GAPDH-Rv	190 bp	Rv: GCCCAATACGACCAAATCC
sequencing	GAP39-1	1900 bp	Fw: TCTCCGTGCAGACCAACCTG
	O19	Creator donor	Fw: TGCTCACATGTTCTTTCCTG
	O20	Creator donor	Rv: TGGATTTGTTCAGAACGCTC
	O21	Creator acceptor	Fw: CAAAATGTCGTAACAACTCC
	O23	Creator acceptor	Rv: TTTATGTTTCAGGTTCAGG
	CMV pCS2+	pCS2+	Fw: GTAAATGGCCCGCGATGGCTGCC
	pCS2+ R	pCS2+	Rv: CTCCCACACCTCCCCCTGAACC
	BGH Reverse	Gateway acceptor	Rv: TAGAAGGCACAGTCGAGG
	EGFP C F	GFP/YFP/CFP tag	Fw: CAACGGGACTTTCCAAAATG
	CMVF pCDNA3	Gateway acceptor	Fw: CAACGGGACTTTCCAAAATG
	M13F	Gateway	Fw: TGTAAAACGACGGCCAGT
	M13R	Gateway	Rv: CAGGAAACAGCTATGACC
TaqMAN	zfArhGAP39-F		Fw: TGGCATCACCCGAACCTTAC
	zfArhGAP39-R		Rv: TGGCCTCGAACTGAGAACATG
	zfArhGAP39-Probe		FAM-5'-TCCCTCTCAGTCGGAGGATCTGGGA-3'-TAMRA

Acknowledgements

First, I would like to thank my supervisor Oliver Rocks, for his guidance and support throughout my PhD, for always having an open ear to trouble shoot any problems I encountered, for having patience with my writing skills and for giving me the freedom to develop as a scientist. For all this I am very grateful. Next, I want to thank Prof. Stephan Sigrist for supervising my thesis at Freie Universität Berlin and Prof. Volker Haucke and Prof. Gary Lewin for helpful discussions in my committee meetings. Additionally, I would like to thank Prof. Ferdinand le Noble for giving me the opportunity to perform the zebrafish experiments in his laboratory.
I would like to greatly acknowledge the support of the following people: Katja Meier, who supervised me in zebrafish care and micro-injection. Dr. Anja Schütz who purified the GST-ARHGAP39 WW domain. Dr. Kerstin Zühlke and Dr. Enno Klussmann who provided the peptide spots. Special thank to Dr. Anup Arumughan for helpful and enthusiastic discussions. Thank you to my AG Rocks family for support and help throughout my PhD. Special thanks to the RockStars Becca, Juliane, Markus and Matti. We just met in the right place at the right time! Thank you for the great time in the lab and for the extensive dancing at beer hours. I also want to thank Dr. Maciej Czajkowski for critically questioning everything and endless discussions about the best coffee places in Berlin. Thank you to Caro, Efraim and Simon for all the help with tricky Co-IP experiments. To all the Rocks lab members past and present, Marlies, Lisa K., Lisa S., Jana, Sebastian, Linda, Lennart, Phillip, Laura R, Moritz, Mackenzie, Kiara, Bella, Vanessa, Denise, Celina and Merve, thank you for making it such a great place to do science.
I would like to thank you, Becca, Vicky and Laura for supporting me in and out of the lab. I learned so much from your everlasting optimism, your critical scientific minds and your crazy time scheduling habits. I am very happy to have you as my friends.
Many thanks to my dear school friends, Evy and Many, for encouraging me to believe in myself. Thank you to my parents and my sisters for their belief in me and their support which made this work possible.

Karl and Lotta, to have got you is the best thing that happened to me. You show me every day what really matters in life.
Last but not least, I thank you, Martin! For your unconditional support and patience with me in the last years. I could not have done it without your encouragement, belief in me and countless coffees made with love. Your love means the world to me!

Declaration

The present thesis ”The Role of ARHGAP39 in Cell Migration” has been composed by myself and describes my own work, unless specifically acknowledged in the text. This thesis is submitted to the Department of Biology, Chemistry and Pharmacy of Freie Universität Berlin to obtain the academic degree Doctor rerum naturalium (Dr. rer. nat.). This work has not been submitted for any other degree.

Berlin, September 2018 Carolin Barth